UNIVERSITY OF READING

Department of Meteorology

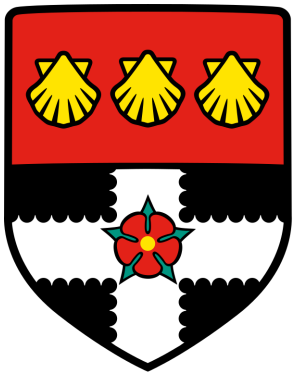

The treatment of vegetation in land surface models: implications for predictions of land-atmosphere exchange

Andrea Manrique-Suñén

A thesis submitted for the degree of Doctor of Philosophy

August 2016

Declaration

I confirm that this is my own work and the use of all material from other sources has been properly and fully acknowledged.

Andrea Manrique-Suñén

The tallest tree begins from a tiny sprout;
the tallest building starts with one shovel of dirt;
a journey of a thousand miles starts with a single foot step

Tao Te Ching

Abstract

Plant processes affect fluxes of energy, moisture and CO_2 between the land and the atmosphere. Land surface models need to correctly represent the vegetation functioning and its response to environmental conditions. Due to anthropogenic carbon emissions rising, and global warming, plant processes are being affected and in turn modulate the terrestrial carbon sink. However, models still disagree on the response of plants to changing conditions. This work analyses how vegetation is treated in two land surface models: the Joint UK Land Environment Simulator (JULES) and Carbon Hydrology Tiled ECMWF Scheme for Surface Exchanges over Land (CTESSEL). The aim is to analyse how environmental variables control the vegetation processes at daily and seasonal timescales at present day climate and the changes that arise in a scenario of double atmospheric CO_2 and higher temperature. The analyses are carried out at the leaf level and at the canopy level. To investigate the responses at the leaf level, the photosynthesis scheme used in each model was extracted, thereby providing a submodel that can be run in stand alone mode. The photosynthesis submodel provides a means to analyse the leaf level response of each photosynthesis model to environment variables as well as the internal model parameters that characterise each plant type. In JULES the environmental controls on photosynthesis are explicitly introduced by three limiting regimes: light, rubisco (carbon) or export limiting regime. In CTESSEL the carbon and light limitations are implicitly represented but there is no export limitation. Due to the lack of export limiting regime, CTESSEL presents higher sensitivity to CO_2 concentration resulting in a stronger CO_2 fertilization effect. The carbon and energy fluxes produced by the full land surface models were tested and compared at 10 European FLUXNET sites. The main differences between modellled carbon fluxes were found to be the treatment of soil moisture stress and the lack of export limiting regime in CTESSEL. The optimum temperature for photosynthesis in models is the result of model parameters' dependence on temperature and the combination of limiting regimes. The optimum temperature for photosynthesis was found to be a determining element in the strength and sign of the vegetation modelled feedback to climate change.

Acknowledgements

I would like thank Gianpaolo Balsamo for inspiring me to embark on this journey and being a reference for me during this time. Thank you to my supervisors, Emily Black and Anne Verhoef who have accompanied me through the ups and downs of the trip. Thank you very much for the discussions, advice and encouragement, I appreciate your time and effort. I would also like to thank Pier Luigi Vidale and Tristan Quaife for their input at my monitoring committees and at various times. Thanks to my ECMWF colleagues, Gianpaolo Balsamo, Souhail Boussetta, Emanuel Dutra and Anton Beljaars for technical help and insightful conversations. Thanks to Gregorio Egea and Cor Jacobs for very fruitful email exchanges, you will never realise how much those encouraged me. Thanks to Javier for plenty of advice in various topics, our coffee breaks and chats but especially thank you for the moral support. Thank you Enza, Giovanna and Francesca for support and wise words. And thanks to all my fellow PhDs for making the Department such a nice place.

Gracias a mis padres y mi hermana por todo el apoyo que siempre me habéis dado y especialmente en esta etapa, vuestros ánimos me han hecho seguir caminando cada día. Gracias a mi tía Carmen, mi prima Alba y la pequeña Mar que se las ha apañado para llegar al mundo antes que esta tesis. Gracias a mis amigas las pajarillas Elena, Gloria, Cris, Blanca, Bea y Noe porque aunque andemos desperdigadas por el mundo y con diferentes ocupaciones os tengo siempre muy cerca. Gracias a mis amigos físicos Laia, Isma, Maru y Álex, por compartir conmigo buenos ratos y esa curiosidad por las cosas.

Contents

Chapter 1

Introduction

1.1 Introduction

Vegetation plays an important role in land-atmosphere interactions. Plant processes are closely linked to their environment, as plants rely on radiation, water, CO_2 and soil nutrients as well as favourable temperature and air humidity to be able to grow and develop. The CO_2 exchange and transpiration through the leaves are key components of the carbon cycle, the water cycle and the energy balance at the surface. Since plants are living organisms, not only do they influence the atmosphere, but also they interact with the environment and adapt to it. The response of vegetation to elevated CO_2 and to associated changes in environmental variables has important consequences for the evolution of the climate system, as it determines the capacity of the biosphere carbon sink.

Land surface models (LSMs) need to represent vegetation to correctly predict turbulent fluxes and carbon fluxes at the land-atmosphere interface. Vegetation function is explicitely reproduced with photosynthesis models, where different plant species are characterised with specific parameters and carbon assimilation is linked to transpiration. Some models used in climate projections include a dynamic representation of the vegetation land cover with the possibility of changing species through competition. However the differences in the modelling still rise questions on the representation of vegetation.

A realistic modelling of the vegetation needs to account for the complex processes that

take place in the plants in order to reproduce the fluxes correctly for the present climate and under climate change conditions. The aim of the thesis is to (i) analyse the representation of vegetation processes in land surface models (photosynthesis, transpiration and respiration); (ii) study how these processes are controlled by environmental factors (atmospheric and soil) in both observations and models, and (iii) study the implications of these controls for plant processes under climate change conditions.

1.2 Background

This section introduces the surface energy balance, terrestrial carbon cycle and hydrological cycle. The main plant processes are then explained as well their interactions with the environment and their role in the energy balance, carbon and water cycles. Figure 1.1 shows a diagram representing the energy, CO_2 and water fluxes between vegetation and its surroundings.

1.2.1 Terrestrial surface energy balance

The source of energy for the Earth system is the sun. A fraction of the solar radiation that reaches the land surface is reflected back. The atmosphere and surface emit thermal radiation in virtue of their temperature. If the surface is assumed to be a very thin layer that does not store energy, the energy fluxes should balance. The energy balance at the surface is given by:

$$NR - G - LE - H = 0 \tag{1.1}$$

where NR is the net radiation, G is the ground heat flux and LE and H are the latent heat flux and sensible heat flux, respectively. In the sign convention used NR and G are positive downward and LE and H are positive upward. Net radiation is the sum of shortwave and longwave downward and upward radiation:

$$NR = R_s \downarrow + R_s \uparrow + R_l \downarrow + R_l \uparrow = R_s \downarrow - \alpha R_s \downarrow + R_l \downarrow - \varepsilon\sigma(T_s)^4 \tag{1.2}$$

$R_s \downarrow$ is the incoming solar radiation, α is the surface albedo, $T_l \downarrow$ is the incoming longwave radiation from the atmosphere and $R_l \uparrow$ is the longwave radiation emitted by the surface at

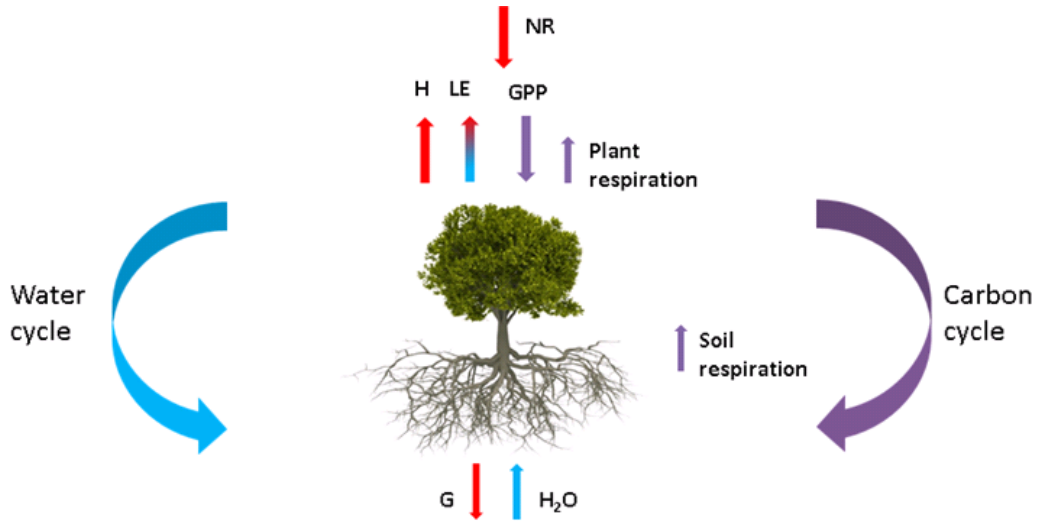

Figure 1.1: Interaction of vegetation with carbon,water and energy cycles. Net radiation (NR), sensible heat flux (H), latent heat flux (LE), ground heat flux (G), gross primary productivity GPP.

a temperature T_s, where σ is the Stefan-Boltzmann constant and ε is the surface emissivity. L, E are the latent heat of vaporisation, evapotranspiration rate. Figure 1.1 represents the components of the energy balance, as well as the connections with the carbon and water cycles. Evapotranspiration includes all evaporation from land surface, i.e., vegetation and soil. All fluxes are positive downwards and have units of W m^{-2}. The term LE, latent heat flux, has a particular role as it establishes the link between energy and water. A certain amount of energy is put into the conversion of liquid water into vapour (given by the latent heat of vaporisation, $L = 2250$ kJ per kilogram of water). Therefore for every kilogram of evaporated water (E), there are LE kilo jules of energy being transported within the vapour into the atmosphere, which will only be released when the vapour condensates, i.e., in cloud formation. The rate of evaporation from the land surface is as well an element of the water cycle.

1.2.2 Terrestrial water cycle

Globally, the amount of precipitating water must equal the evaporating water in order to maintain an equilibrium, precipitation (P) equals evaporation (E):

$$P = E \tag{1.3}$$

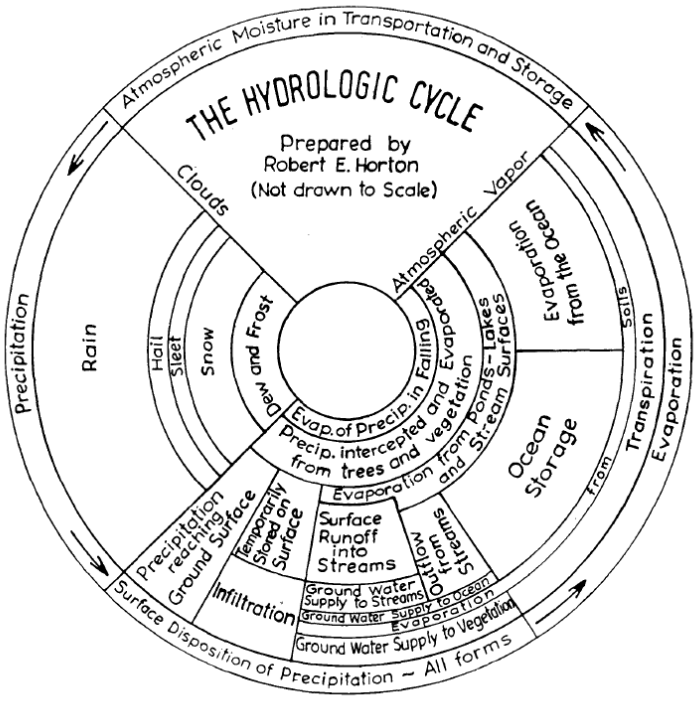

Figure 1.2: Hydrological cycle by Horton (Horton, 1931) from Dooge (1992)

A diagram of the processes involved in the hydrological cycle over land was depicted by Horton (Figure 1.2). The circular shape of the diagram emphasizes the conservation of water. On the external ring the complete cycle is represented. At the top there is the moisture contained by the clouds, which, following the arrow to the left, precipitates towards the ground. When reaching the surface, the different pathways water can encounter are described at the bottom and on the right there is the evaporation of water back to atmospheric vapour. Part of the precipitation evaporates before reaching the surface, part is intercepted by the vegetation and evaporated directly and the rest reaches the ground surface. In the ground, there is storage, infiltration, and there is runoff reaching the ocean. Some of the infiltrated water is used by plants and transpired to the atmosphere. On the land surface, vegetation and soil exert some control over the evaporation, and also water supply might be limited.

The water budget over the land surface can be expressed as:

$$P = E + R + I \tag{1.4}$$

where P is the precipitation, E evapotranspiration, R runoff and I infiltration. Evapotranspiration establishes the link between the energy balance (Eq. 1.1) and the water balance. Evapotranspiration is the total evaporation from the land surface and is the sum of three contributions: interception layer evaporation, soil evaporation and transpiration. As precipitation falls on vegetated areas, some of the rain is intercepted by the canopy leaves. The amount of water that is trapped by leaves depends on their surface, morphology and inclination. This fraction of the water, although small, is important because it is the first to evaporate back to the atmosphere. Because it sits forming a thin layer or as droplets on the leaves, it evaporates as soon as there is atmospheric demand. The rest of the precipitation falls in the ground where part will infiltrate into the ground and when the soil saturates, the excess trickles above the surface (runoff). How the water is partitioned depends on the type of soil, (sandy soils are more permeable and water infiltrates more easily), the slope, and the actual water content of the soil. Soil evaporation happens from the outermost layer of the soil and at a longer timescale than the interception evaporation. Transpiration is the evaporation through the leaves of the water that is absorbed from the roots. The amount of water evaporated through the leaves depends on the type of vegetation, and the depth of the roots. This evaporative process is the one with the longest timescale.

1.2.3 Terrestrial carbon cycle

Carbon is one of the elements forming living organisms. In photosynthesis, atmospheric CO_2 is converted into its organic form and it is allocated in the roots, leaves and stems. It becomes part of the biomass, which is a carbon storage. The amount of carbon assimilated by plants is called gross primary productivity (GPP). Not all the carbon assimilated is converted into plant tissue, some carbon is expelled in the plant respiration, this type of respiration is called autotrophic respiration. The net carbon taken the plants is GPP minus plant (or autotrophic) respiration (R_a), this quantity is called net primary productivity (NPP).

$$NPP = GPP - R_a \tag{1.5}$$

Both NPP and GPP are positive downwards (towards the plant) and respiration is positive upwards (from the plant). All fluxes have units of mass of carbon per unit area and time.

When elements of the vegetation die and fall to the ground, they become part of the litterfall and eventually decompose. The bacterial decomposition in the ground releases CO_2. This process is called soil respiration, and can be higher than plant respiration, especially in highly organic soils. All carbon loss by organisms other than the plants is termed heterotrophic respiration, this includes soil respiration, animals or dead organisms. The net ecosystem exchange (NEE) is the sum of all CO_2 fluxes in the system, the plant exchange and the heterotrophic respiration.

$$NEE = -NPP + R_h = -GPP + R_{eco} \tag{1.6}$$

where the sum of autotrophic (plant respiration in Figure 1.1) and heterotrophic respiration (soil respiration in Figure 1.1) is the ecosystem respiration $R_{eco} = R_a + R_h$. NEE is positive upwards (away from the ecosystem-carbon source) and negative downwards (towards the ecosystem-carbon sink). NEE constitutes a small difference between two very large fluxes; it is on average close to zero in systems at a steady state and it causes seasonal variations on the global CO_2 concentration (Lambers et al., 1998).

1.2.4 Plant processes: photosynthesis, transpiration and respiration

Plants are autotrophic organisms, which means they are able to synthesise organic carbon compounds from the ambient CO_2. This process is called photosynthesis and the energy needed is obtained from solar radiation. CO_2 enters the place of photosynthesis through some specialized pores on the leaves called stomata. While these pores are open, water evaporates through them. Transpiration is thought to be an inevitable consequence of photosynthesis (Lambers et al., 1998), although it has some functions, like cooling the leaves and maintaing the flow of sap through the plant (Section 1.2.4.3). Plant's transpiration contributes to the evapotranspiration term in the energy balance and water cycle. The products of photosynthesis are used to build and maintain the plant's tissues in a process called dark respiration, which produces a release of CO_2 to the atmosphere. The net carbon balance by plants is the difference between the gross rate of carbon fixed in photosynthesis and the rate of carbon lost in autotrophic respiration. This quantity is the net primary productivity (Equation 1.5).

The following sections introduce the plant morphology and physiology, focusing on the

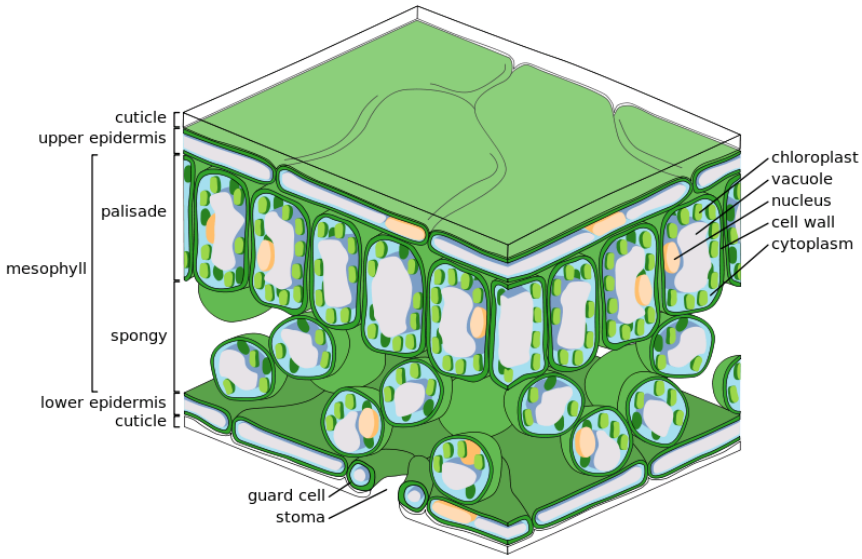

Figure 1.3: Cross section of the leaf tissues. Figure from Wikimedia commons http://en.wikipedia.org/wiki/File:Leaf_Tissue_Structure.svg

processes that take place in the leaves. First of all, the structure of the leaf is described in Section 1.2.4.1, and then the main processes are discussed, photosynthesis (Section 1.2.4.2), transpiration (Section 1.2.4.3) and respiration (Section 1.2.4.4).

1.2.4.1 Leaf anatomy

Leaves are comprised of a set of organised tissues, with specific functions. Figure 1.3 depicts a cross section of a leaf. The most external layer is the epidermis, which has the function of protection and regulation of the gas exchange through the stomata. The stomata play a very important role in photosynthesis and their aperture is controlled by specialised epidermal cells, called guard cells. The aperture of stomata is influenced by external factors. The epidermis is externally coated by the cuticle which prevents water loss. The interior of the leaf is the mesophyll tissue. In the upper part of the mesophyll, cells are elongated and are vertically arranged, forming the palisade layer. These cells are very rich in chloroplasts, which contain the pigments that trap the radiation, mainly chlorophyll, which is also responsible of the green colour. Under the palisade layer, in the spongy layer the mesophyll cells have a round shape and are quite loosely packed leaving intercellular spaces amongst them. Most processes of photosynthesis take place inside the chloroplasts.

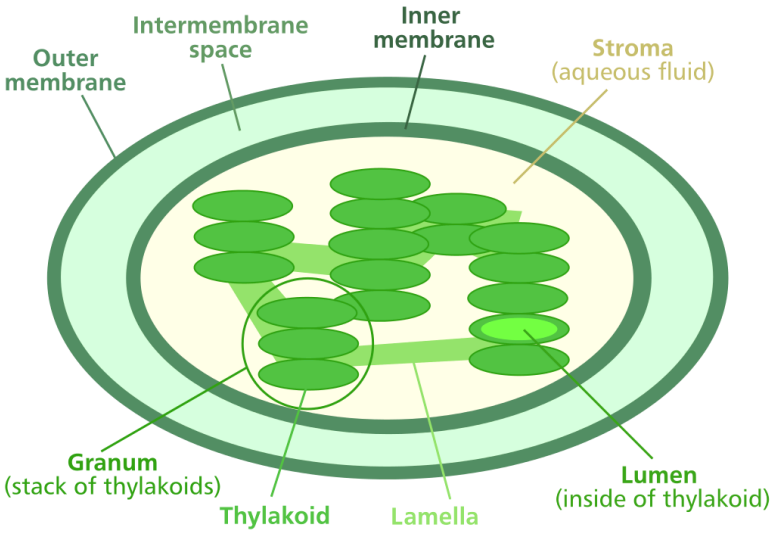

Figure 1.4: Chloroplast. Figure from Wikimedia commons http://commons.wikimedia.org/wiki/File:Chloroplast_diagram.svg

The chloroplasts are constituents of the plant cells. They are enveloped by a double membrane as shown in Figure 1.4. The inside is composed of vesicles called thylakoids sometimes arranged in stacks forming grana. The network of thylakoids is embedded in a fluid called stroma. The epidermis cells do not have chloroplasts, and therefore the epidermis is transparent, allowing the sunlight to reach the mesophyll cells.

The morphology described above corresponds to C_3 plants which represent the majority of the plants, like most shrubs and trees. However there is another type of plants, called C_4, which use a different pathway for photosynthesis and therefore have a different distribution of organs. C_4 species includes some kinds of grasses and sedges, especially in tropical ecosystems but also crops. Instead of the two distinct layers in the mesophyll, C_4 species have some special photosynthetic cells called bundle sheath cells distributed within the mesophyll cells. C_4 plants are believed to be an evolution from C_3 plants because they are more efficient under low CO_2 concentrations (Ehleringer et al., 1997).

Across the spongy layer of the mesophyll there are two networks of vascular tissue. The xylem which has the purpose of providing the cells with water and minerals from the root zone and the phloem which distributes the sap with dissolved sugar to other parts of the plant.

1.2.4.2 Photosynthesis

The process of photosynthesis consists of the fixation of carbon into complex organic compounds that can be used by the plant. The energy used comes from the solar radiation. The overall reaction of photosynthesis is given by:

$$CO_2 + 2H_2O + light \rightarrow (CH_2O) + H_2O + O_2 \tag{1.7}$$

The process can be separated in two parts: i) light reactions, in which photons are trapped by the pigments and used to synthesise high energy compounds; ii) light-independent (or dark) reactions in which the biochemical reduction of CO_2 takes place using the energy compounds created in the light reactions. Both reactions occur at day time, but the latter does not require solar radiation to occur.

Light reactions

These are the mechanisms which allow the absorption of energy from incoming solar radiation and the synthesis of ATP (Adenosin triphosphate) and NADPH (Nicotinamide adenine dinucleotide phosphate), which are the molecules that carry the energy. Only light of wavelengths between 400-700 nm is useful for photosynthesis, this part of the spectrum is called Photosynthetically Active Radiation (PAR). The light reactions take place in the thylakoid membranes inside the chloroplast. The main pigment is the chlorophyll which has absorption peaks in the red and blue, but there are also other pigments such as carotenoids. The chlorophyll is held in three chlorophyll-protein complexes: the light harvesting complex (LHC), the photosystem I antenna complex (PS I) and the photosystem II antenna complex (PS II). The pigments in LHC are excited by the light photons and the energy is passed to the photosystems. In PS II chlorophyll loses an electron, which is passed to a chain of electron acceptors (quinone, plastoquinone etc.). This way, electrons are channelled towards PS I. The electron flow creates a proton gradient across the membrane which is used by ATP synthase to phosphorylise ADP into ATP. In PS I, light absorption again excites an electron, ultimately leading to the reduction of $NADP^+$ to NADPH. Some energy might be lost in re-radiation producing fluorescence, especially from PS II. The oxidised chlorophyll at PS II recovers electrons from the photolysis of water. The described pathway is called non-cyclic, only ATP is created whereas in the cyclic pathway electrons displaced from PS I are recaptured by the electron acceptor molecules, returning to PS I.

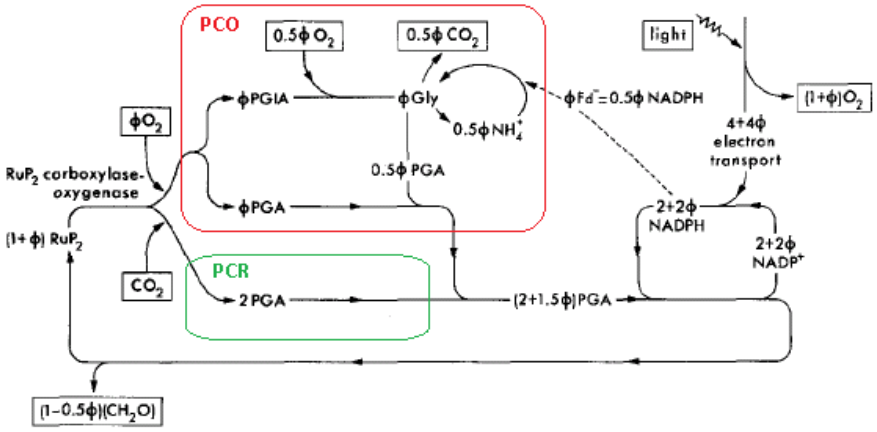

Figure 1.5: Diagram of photosynthetic carbon reduction cycle (in the green rectangle) and photorespiratory carbon oxidation cycle (in the red rectangle). For each carboxylation ϕ oxygenations occur. Figure from Farquhar et al. (1980).

Light-independent reactions

These reactions are responsible for the fixation of CO_2. C_3 and C_4 plants use different pathways. In C_3 plants the first product of the reactions forms a 3-carbon compound while in C_4 plants it is a 4-carbon compound. In C_3 plants, the biochemical reactions take place in the mesophyll cells. Figure 1.5 shows a diagram of the light independent reactions. One molecule of CO_2 from the atmosphere is combined with a molecule of ribulose biphosphate (RuBP) in presence of the enzyme ribulose biphosphate carboxylase-oxygenase (rubisco), to produce 2 molecules of the 3-carbon compound phosphoglyceric acid (PGA). This is known as the photosynthetic carbon reduction cycle (PCR). The PGA is then converted to triose phosphate (triose-P, not shown in Figure 1.5) using ATP and NADPH created in the light reactions. Most of this product is then used in the Calvin cycle, which requires further ATP to regenerate the substrate of the initial carboxylation reaction (RuBP). Part of the triose phosphate is transformed into hexose phosphate, which ultimately yield the final products of photosynthesis, the organic carbon compounds (CH_2O), bottom left in Figure 1.5.

As well as catalysing the carboxylation of RuBP when CO_2 is present (PCR), the enzyme rubisco is also capable of catalysing the oxygenation of RuBP in presence of O_2. This process is known as photorespiration or photosynthetic carbon oxidation (PCO). Its purpose is still unknown. It has been thought to act as a regulator of CO_2 concentration and to be

a waste of energy. While PCR produces 2 molecules of PGA, PCO produces one molecule of PGA and a molecule of phosphoglycollate (PGIA) which eventually leads to the release of CO_2. The activity of rubisco depends on the ratio $[CO_2]/[O_2]$ and on leaf temperature (Lambers et al., 1998).

Although the C_3 photosynthetic pathway is predominant for most terrestrial ecosystems, C_4 is important for certain agricultural and tropical environments. Many common crops use the C_4 mechanism, like corn, sorghum, sugar cane and pasture grasses. C_4 photosynthesis is also common amongst tropical and subtropical species, but is rare amongst tree species. The C_4 pathway presents a biochemical and morphological adaptation to C_3 photosynthesis, providing significant advantage over C_3 plants under low atmospheric CO_2 (Ehleringer et al., 1997). The emergence of C_4 photosynthesis is believed to have occured globally, possibly as a response to deacresing values of CO_2 and increasing temperature in the late Miocene, 6-8 M ago. Ehleringer et al. (1997) used variations in the carbon isotope ratio found in the enamel of teeth fossils to determine the changes in the vegetal intake of some animals in this era. This type of photosynthesis shows how biological systems adapt to the the environment.

C_4 photosynthesis has two carboxylation processes, making it more efficient in low CO_2 environments. In the mesophyll CO_2 is initially carboxylated by a more active enzyme phosphoenolpyruvate (PEP) carboxylase, producing oxaloaceatate, a 4-carbon acid. This compound is transferred from the mesophyll cells to the specialized bundle sheath cells, where it is decarboxylated to supply CO_2 for rubisco. The CO_2 released enters the same pathway used by C_3 plants, but within the bundle sheath cells. The initial carboxylation in the C_4 pathway induces a concentration of CO_2 in the area where rubisco is present, increasing the ratio $[CO_2]/[O_2]$ and therefore leading to higher efficiency of the carboxylation process and virtually no photorespiration. However, the regeneration of PEP yields an additional ATP cost in C_4 photosynthesis. Overall, C_4 photosynthesis is favoured at high temperatures and low atmospheric CO_2, however the extra energetic cost is not worthwile under certain environments. The differences in the metabolic process result in different sensitivities of net photosynthesis to environmental conditions, including CO_2.

There is also a third group of plants with a crussalean acid metabolism (CAM). They use a pathway similar to C_4 plants with the peculiarity that the carboxylation by PEP

takes place at night. This mechanism allows the plant to keep the stomata closed during the day, when the highest water vapour deficit occurs, and hence reducing the water lost in transpiration and increasing water-use efficiency. CAM plants have derived as an adaptation to drought (Lambers et al., 1998).

1.2.4.3 Transpiration

Transpiration is the loss of water vapour from the plant. Most of the vapour is diffused through the stomata but some evaporation happens through the cuticle. Water is pulled up from the roots and moves through the xylem. Most of the water molecules evaporate at the leaves through the stomata, but some of them (10%) are used in photosynthesis. The inflow and outflow of water controls the turgor pressure and allows the movement of nutrients within the plant, although it has been suggested that transport in the xylem also occurs in the absence of transpiration (Lambers et al., 1998). Transpiration also has a cooling effect as the water evaporates from the leaf, and in fact this may be its main purpose, avoiding leaves from overheating while trapping radiation needed for phosynthesis. Brown and Escombe (1905) conducted a very exhaustive analysis on the energy balance in sunflower leaves. They derived that of the incoming radiant energy on a leave less than 1% is used for photosynthesis and up to 80% energy is dissipated in transpiration. They considered transpiration as a safety-valve to avoid over-heating of leaves. Although their values for transpiration might have been overestimated because they ignored the leaf boundary layer conductance (Jarvis and McNaughton, 1986).

1.2.4.4 Respiration

The consumption of the organic compounds to create the plant structure, maintain the existing tissue and ion transport is known as dark respiration. The proportion of photosynthates that goes into these three processes depends on the age of the plant. The older it is the more energy is required for maintenance. The pathways included in dark respiration are glycol's, the exudate pentose phosphate oxidation, tricarboxylic acid (Krebs cycle). These processes produce a release of CO_2 and a consumption of O_2 and occur in roots, stem and leaves.

Photorespiration is the process of oxygenation of RuBP which is catalysed by rubisco (PCO cycle in Figure 1.5). CO_2 and O_2 compete for rubisco, consequently photorespiration inhibits photosynthesis and releases previously fixed CO_2. Photorespiration is virtually absent in C_4 plants, which is why they are more efficient. Photorespiration rate increases with temperature, therefore C_4 photosynthesis becomes advantageous in warm conditions, as well as in environments with low CO_2. However, due to the extra energetic cost of CO_2, with increasing CO_2 concentrations and decreasing temperatures C_3 becomes more efficient.

1.2.5 Vegetation's interaction with the environment

The described plant processes entail gas exchange between plants and the environment, which sustains interactions in both ways. The evolution of the atmosphere's composition has been linked to the biosphere activity (as well as to geological and chemical processes), and vegetation is affected by anthropogenic changes to the environment.

The function of the stomata is to regulate the intake of CO_2 and the release of water vapour. Plants have control of the stomatal openings via the guard cells, and operate them to their benefit according to the external conditions. High light intensity and reduced CO_2 concentration tend to cause stomatal opening. Increased water vapour deficit in the leaf surface and lack of soil water available to the roots both tend to close the stomata. Stomatal movements are controlled by changes in turgor pressure inside the guard cells and adjacent epidermal cells (Jones, 1992). The behaviour of stomata is analysed in detail in Meidner and Mansfield (1968). There is consensus amongst studies about the response of stomata to a single environmental factor, but it less known how a response is conditioned by other factors. It is still uncertain how the plant senses the environment, i.e. where the actual sensors are located.

The environmental factors that are known to influence plant growth and development are sunlight, temperature, CO_2, humidity, soil moisture and nutrients. The response of plants and more precisely stomatal responses found in laboratory experiments are described in the next sections. Endogenous rhythms also affect the stomatal opening, forcing the pattern of diurnal opening even in continuous darkness (McClung, 2006).

1.2.5.1 Radiation

The opening of stomata in sunlight drives the uptake of carbon dioxide during the day. Stomata are highly responsive to sunlight, and this response is independent of the photosynthetic activity, with its own photoreceptors being involved, one sensitive to red and far red and another one to blue and ultraviolet. Maximum aperture is usually achieved with irradiances greater than about a quarter of full summer sun (i.e. about 200 W m^{-2} (total shortwave) or 400 μmol m^{-2} s^{-1}(PAR)) (Jones, 1992). CAM plants exhibit the opposite behaviour, with their stomata opening at night.

1.2.5.2 CO_2

Stomata have been found to respond to the carbon concentration, particularly to the CO_2 concentration in the intercellular spaces (Mott, 1988). Stomata tend to reduce their aperture as intercellular carbon concentration increases and conversely tend to open as it decreases. However, there is an indirect effect as well, an increase in CO_2 enhances photosynthesis which affects stomatal conductance. CO_2 concentration in the intercellular spaces is generally kept constant owing to the correlation between photosynthetic assimilation and stomatal conductance. Stomatal sensitivity to CO_2 has been found to be higher in greenhouse grown plants than in the field, and this has been attributed to the effect of water stress through absorbic acid ABA (Raschke 1979). The mechanisms that control the response of stomatal pores to CO_2 have been revised by Mansfield et al. (1990). They point out the concentration of calcium ions as the trigger for guard cells response.

1.2.5.3 Temperature

The speed of the photosynthesis reaction depends highly on temperature. The optimal leaf temperature for photosynthesis is in the range 15-30 °C for C_3 plants and 35-45 °C for C_4 plants. At high temperatures, the limitation to photosynthesis comes from the transfer of CO_2 from the intercellular airspaces to the chloroplasts, rather than by the rubisco capacity (Bernacchi et al., 2002). To attain the optimum metabolic processes, the

plant is capable of regulating its temperature. In hot environments leaf temperature is reduced to avoid overheating. Leaf temperatures can be very different to the soil temperature underneath the vegetation. The main cooling mechanism is transpiration, but this requires an abundant source of water which might not always be guaranteed in arid regions. Plants have also developed other strategies to lower the leaf temperature. They avoid sun interception at peak insolation by positioning leaves vertically (*Larrea divaricata*) or rolling them (*Graminae*). Temperature, together with radiation regulates the seasonal cycles of plants, and influences the the beginning of the growing season as well as interannual differences.

1.2.5.4 Air humidity

The water vapour in the air is strongly linked to vegetation, as already seen most of the energy trapped by leaves is returned in the form of latent heat by transpiration. Meidner and Mansfield (1968) believed that stomata were unaffected by changes in humidity. Now most studies suggest that stomata respond to drying air, by closing when vapour pressure deficit increases. Mott and Parkhurst (1991) suggested that the response of stomata was a consequence of a change in transpiration rather than of humidity. The stomatal sensitivity to air humidity is conditioned by the soil moisture availability, so there is interaction between soil and atmospheric water stress. These interactions are pointed out in a study by Calvet (2000) with observational data from 63 case studies. This study also finds a large variability within the same plant species while trying to fit parameters of photosynthesis response to air humidity. It is suggested that cultivar or growing conditions may contribute to how plants respond to humidity.

1.2.5.5 Soil Moisture

Water is fundamental for the functioning of the plant. It plays a role on the physiological mechanisms and acts as the carrier of metabolites dissolved in it. The high concentration of solutes exerts a positive pressure (turgor) against the cell walls, which is responsible for the structural support in herbaceus plants. Larger plants have lignified tissues to provide a more solid structure. Turgor pressures are of the order of 1.0 - 5.0 MPa (Lambers et al.,

1998). When plants lose turgor, by lack of water or minerals, their physiologic functions become limited, and if maintained for a long time they wilt. Water and soil minerals are absorbed from the soil by roots. Therefore the soil moisture content in the soil and its profile are crucial for plant survival. The distribution and depth of the rooting systems varies amongst species, and also depends on external factors such as soil texture and structure, aeration, moisture, temperature, pH and salinity (Kramer and Boyer, 1995). Root hairs facilitate the absorption by increasing the contact surface.

Water availability is the major factor limiting plant growth in ecosystems at a global scale. In dry climates, plants have evolved to survive during periods of drought. Moreover, losses in crop yield due to water stress exceed losses due to all other biotic and environmental factors combined. The response of vegetation to water deficit is one of the least understood in plant physiology. Plants have developed several mechanisms, to either avoid or tolerate water stress. Drought avoiding strategy is adopted by saving water by regulating transpiration and reducing photosynthesis. For example some desert annuals remain dormant until water arrives. On the other hand, a tolerant strategy is associated with less or no regulation on transpiration, keeping photosynthetic activity. This risky behaviour is compensated with growing deeper roots to reach for underground water or with a rapid reproductive cycle. The response of vegetation varies across species, and many plants exhibit intermediate strategies. Also the strategy adopted might depend on the stage of the plant cycle, water may be saved during vegetative stages in favour of reproductive stages. In one way or another, lack of availability of soil moisture in the root zone affects photosynthesis and transpiration as well as the plant growth (Tardieu et al., 2014). A reduction of transpiration rate can be achieved by closing the stomata or by reducing the leaf area, i.e. reducing the leaf growth. The former entails an increase in leaf temperature while the latter has the drawback of a reduction in carbon gain. The closure of stomata is thought to be controled by a hormone called abscisic acid (ABA) and is also related to other factors like air humidity. A large genetic variability has been found in the controls of the different reponses (Tardieu et al., 2014).

Two stomatal control strategies have been identified associated to the two drought responses. Plants with an avoiding strategy present isohydric behaviour, and plants with a tolerant strategy present anisohydric behaviour. The isohydric behaviour attempts to maintain a constant midday leaf water potential (ψ_{leaf}) when water is abundant and under

stressed conditions, by reducing the stomatal opening to reduce transpiration. Conversely, plants with anisohydric behaviour allow for a more variable ψ_{leaf} and keep the stomata open and photosynthetic rates high for longer periods. This is considered as a risky behavior, which might be beneficial under moderately stressful conditions, but can endanger the plant if the water stress becomes severe or prolonged in time. The water-use strategy is not a unique characteristic of the species, but instead it is a consequence of the vegetation's adaptation to the environmental and climatic conditions. This implies that the plant-environment relations influence what the plant becomes. An example of different behaviours for the same species is found in Schultz (2003). They categorize two varieties of *Vitis vinifera* cultivated in different regions as isohydric and anisohydric. The sensors to moisture stress are thought to be located in the roots, and transmitted to the shoots by a chemical signal. When exposed to insufficient water, ABA is synthesised in the roots and transported in the sap to the leaves. The increase in ABA concentrations is believed to be responsible for the closure of stomata in water stress conditions as deducted by Tardieu et al. (1992) in experiments with maize. Anisohydric behaviour has been considered as an advantage for agriculture as anisohydric plants are more productive than isohydric plants under mild water stress (Sade et al., 2012). Moreover, anisohydric plants are believed to present a higher resistance to biotic stress such as fungus or bacteria. Advances in genetic research are allowing to include anisohydric characteristics to crops (Sade et al., 2009).

1.2.5.6 Nutrients

Mineral nutrients are a fundamental element for plant processes. They are mostly absorbed through the root system as ions dissolved in the water, and distributed in the xylem flow. However plants are also capable of acquiring nitrogen and sulfurous compounds from the air through the stomata. The elements most needed by the plant are N, P, K, Ca, Mg and S which are known as macronutrients, while those required in less quantities are known as micronutrients: Fe, B, Mn, Cu, Zn, S. The nutrients that most frequently limit plant growth are N, P, K, which are the ones involved in metabolic processes. Each element has a specific role in the plant. Salts dissolved in water produce an increase of the osmotic potential which controls the movement of water and is a regulator of different mechanisms. Some provide elemental constituents of macromolecules, enzymes and compounds that are

synthesized by the plant, as well as the vegetal tissue. The availability of nutrients depends on the soil type, and the limiting nutrient tends to be N in younger soils and P in older, weathered soils.

1.2.6 Climate change effects on photosynthesis and transpiration

With the increasing anthropogenic emissions of CO_2, the atmospheric CO_2 concentration is increasing. From the biochemical point of view, an increase in ambient CO_2 provides more product for the photosynthesis reaction, thus photosynthesis activity is stimulated. This process is known as CO_2 fertilisation effect. At the same time, the stomata react to regulate the ratio of intercellular to ambient CO_2 by a partial closing. The closure reduces the water vapour lost in transpiration. The combined increase in carbon assimilation and reduction of transpiration results in an increase of the water use efficiency or the rate of carbon uptake per unit of water lost. Keenan et al. (2013) analysed the climatic drivers behind the Northern Hemisphere forest water use effiency rise and concluded that the most plausible cause is a strong fertilisation effect of the increased CO_2 concentrations. They also report that this effect is typically underestimated by biosphere models. The effect also has an impact on the water cycle, as water savings from reduced transpiration result in an increase in continental runoff (Gedney et al., 2006; Betts et al., 2007).

Along with the increased CO_2 there are other aspects of climate change, like global warming, changes in precipitation patterns, global dimming due to increased clouds and aerosols (Mercado et al., 2009) etc. that can affect vegetation. Determining the effects of climate change on vegetation is crucial to predict the behaviour of the terrestrial carbon sink as CO_2 emissions continue to rise.

Several observational techniques show the increase in water use efficiency, although the magnitude of the effect is still unknown. Changes in water use efficiency at the plant level have been observed by carbon isotope discrimination (Saurer et al., 2004). At the ecosystem level, the effects can be measured by carbon and water fluxes from with eddy-covariace instruments (Keenan et al., 2013). Finally, for a global coverage, satellite imagery has proven an invaluable tool, measuring the absorbed radiation for photosynthesis and other plant parameters. Combining observations with models, global trends in net primary

productivity can been computed. Nemani et al. (2003) reported an overall increase in the land carbon sink for the period 1982-1999, due to the ease of climatic constraints on plant growth. For the later period 2000-2009, Zhao and Running (2010) only obtained a slight increase in NPP in the Northern Hemisphere, outweighted by a drought induced decrease in NPP in the Southern Hemishere, resulting in a slight reduction in the global carbon sink for the studied decade. These results show the complexity of the ecosystems response to climate change and the myriad of factors driving this response. On the other hand, the physiological response of vegetation to CO_2 contributes to climate change; Sellers and Bounoua (1996) highlighted that the warming effect over the continents was increased due to reduced evapotranspiration.

The factors responsible for the increase in the CO_2 assimilation are both environmental and biotic. Amongst the environmental factors there is the increase in average temperatures, the rise in atmospheric carbon dioxide and global dimming. It is difficult to disentangle the effects of each factor as there are highly interative. Moreover, the biotic or biophysical properties of vegetation are likely to change and acclimate to the environmental conditions.

1.2.7 Key aspects of modelling plant processes

LSMs aim to reproduce the interactions between surface and atmosphere. For this purpose they need to solve the surface energy balance (Eq. 1.1) and the water budget (Eq. 1.4) which are affected by vegetation processes in various ways. The representation of vegetation functioning in LSMs is carried out at different levels: first plant processes are represented at the leaf level, then scaled up to canopy level and finally to the ecosystem level. The processes at the leaf level (photosynthesis, transpiration and respiration) are represented by a photosynthesis model and a gas exchange formulation for the stomatal aperture. These typically take a semi-empirical approach. The equations for vegetation modelling have been derived based on measurements taken in the field or in laboratory experiments. Some attempts have been made to describe physiological processes in order to produce mechanistic models, but many parts remain empirical. This is partly due to the immense complexity of the biochemical reactions that occur inside the plants, but also the interactions that occur amongst the responses of plants to diverse factors.

The carbon assimilation rate is calculated as a combination of the potential limitations to the photosynthesis biochemical reaction (Farquhar et al., 1980). These are typically rubisco availability, light and in some models the triose phosphate utilization. The main limitation controlling photosynthesis influences its response to environmental variables.

In a LSM the interest is in the canopy level moisture, energy and carbon fluxes which interact with the atmosphere as well as a correct derivation of the prognostic variables. To scale to the canopy level, a good representation of the vegetation structure is needed. Many assumptions have to be made about the vegetation height and shape of the trees and biomass density. Moreover, vegetation grows and there are also seasonal changes in the biomass.

Finally the ecosystem level requires knowledge of the vegetation's spatial distribution. Land cover maps are used to identify the distribution of species. Most models represent diversity by binning plant species into several plant functional types with common characteristics with a set of specific parameters each. However, due to acclimation, same species will present different traits depending on the geographic region. Model development is pushing towards splitting PFT's into climatic regions. Dynamic vegetation models allow for competition amongst species resulting in changes in the vegetation distribution.

There are many challenges in the modelling of vegetation. As seen in Section 1.2.5, plants respond to several environmental and soil conditions. However, all stimuli happen simultaneously and they are closely linked, therefore it is difficult to attribute the plant's response to a single stimulus. This synergy amongst environmental factors poses a problem for modelling, as not all the relations are still well understood.

Moreover, plants are living organisms, they grow, feed, reproduce and as such are able to adapt to change. Vegetation is constantly exposed to stress from environmental factors that reduce the maximum growth it could sustain. Lambers et al. (1998) classify the response from vegetation to stress depending on the time scale. The adaptation of a single plant to compensate for a declining performance due to changing conditions is termed *acclimation*. It involves morphological and physiological adjustments, and happens in the lifetime of an individual. As a consequence, plants of the same species develop different characteristics depending on where they grow. At longer timescales, the traits

become inherited and this evolutionary response is called *adaptation*. It involves several generations. The vegetation existing today comes from the adaptation during some billion years, from photosynthesising organisms that first lived on Earth.

Because of the adaptation of plants to the climatic conditions, they present a major challenge in climate models (De Kauwe et al., 2013). Photosynthesis and respiration determine the gross primary productivity which plays a major role in the carbon cycle. Changes in plant water use efficiency affect the water cycle (Betts et al., 2007). It is therefore crucial to understand the physiological trade-offs plants processes entail to deduct the adaptations that the vegetal kingdom will undergo.

There is a need to improve the representation of carbon cycling in Earth Models, and carbon assimilation by the process of photosynthesis a a key component, linking the carbon cycle to energy and water cycles. Photosynthesis is controlled by biotic and environmental factors, and therefore sensitive to changes in climate conditions. This thesis aims to analyse the biochemical representation of plant processes in two land surface models and their response to environmental factors.

1.3 Research questions and organization of the thesis

The aim of this project is to analyse how current LSMs incorporate vegetation modelling and what assumptions are made in the parameterizations. For this purpose two LSMs are studied: (a) The Joint UK Land Environment Simulator (JULES) and (b) Carbon Hydrology tiled ECMWF (European Centre for Medium-Range Weather Forecasts) Scheme for Surface Exchanges over Land (CHTESSEL). Special interest is put on the modelled response of plants to environmental factors. Soil water, atmospheric CO_2 and light are fundamental for photosynthesis. In most photosynthesis parameterizations, the influence of these components is introduced through the limiting regimes: typically CO_2 or light limiting regime. A good representation of the response of plants to environmental factors allows a model to correctly estimate seasonal and interannual variation, as well as the projected response of plants to a changing climate. The increase of CO_2 and temperature might change the limitations that control plants behaviour, and vegetation is an important feedback in climate. The research questions for the project are as follows:

RQ1. When do the limiting regimes determining photosynthetic activity occur?

RQ2. What are the most important driving variables and model internal parameters during each regime?

RQ3. What differences are there in the carbon uptake-water use relation in models?

RQ4. How well do models capture the interannual variability in vegetation fluxes?

RQ5. What are the assumptions in photosynthesis models that mainly affect their response to CO_2 increase and to the associated changes in climate change?

Chapter 2 describes LSMs, and the most used photosynthesis and stomatal conductance models. In particular the treatment of vegetation in the two studied LSMs is explained. Then, in Chapter 3 the photosynthesis schemes from both LSMs are analysed and compared at the leaf level. This approach provides a theoretical framework to test the sensitivity of the leaf level schemes. The differences in the responses of photosynthesis to environmental variables are highlighted; these are relevant for the representation of vegetation in LSMs and can be hidden in the upscaling process or due to different degrees of canopy-atmosphere coupling when using the full LSM. The occurrence of the limiting regimes of photosynthesis at the leaf level will be explored in JULES. In Chapter 4 the models are tested at the canopy level. The representation of energy and carbon fluxes is compared with eddy covariance measurements from 10 European FLUXNET sites representative of diverse ecosystems and climates. Interannual variability in observations and in models is analysed. The occurrence of the limiting regimes is again explored under realistic conditions. In Chapter 5, an idealised climate change experiment is conducted by testing the LSMs at the same sites under conditions of double atmospheric CO_2 and increased temperature. The effects on carbon fluxes and the limiting regimes are explored and related to each model's assumptions. Finally, in Chapter 6 the main findings are summarised and discussed.

Chapter 2

Land Surface Models

2.1 Introduction

Land Surface Models (LSMs) represent the energy, water and carbon fluxes at the interface between the atmosphere and the land that were described in Chapter 1. The energy, water and carbon balances are affected by the surface and soil characteristics as well as the processes taking place at the surface. The surface processes are fueled by the sun's radiative energy and affected by the atmosphere's general circulation (e.g. advection, precipitation events). LSMs are important for a number of reasons: firstly, they calculate the fluxes of heat, moisture and momentum which provide the boundary condition from the land for numerical weather prediction (NWP) models as well as general circulation models (GCMs). LSMs also provide prognostic variables at the surface Moreover, the surface has to provide the correct feedback mechanisms to the physical processes in the atmosphere (Viterbo, 2002). The partitioning between sensible and latent heat flux is one of the factors determining soil moisture content, which acts as one of the forcings of low frequency atmospheric variability. Lastly, LSMs are increasingly being used to represent the biological processes in the ecosystems determining fluxes of CO_2 and other gases and to predict the response of land-atmosphere interactions to climate change (Prentice et al., 2014). A good representation of physiological and biological processes is crucial for a realistic prediction of changes in the carbon and water cycles (Sellers et al., 1996; Betts et al., 2007).

The land surface cover is very diverse, ranging from vegetated areas to bare ground (fallow, deserts) and can also vary seasonally, e.g. land covered by snow in winter. The type and state of the land affects directly the energy partition, so the land surface has to be well characterised. One of the difficulties when describing the land surface is its spatial heterogeneity. Diverse types of surfaces with different characteristics can coexist in one single model gridbox. The most common method to represent this diversity is the tiling approach, by which each land surface type is assigned a fraction of the total gridbox area and processes are solved separately. The resulting variables and fluxes are then combined together to provide the state of that gridbox and total fluxes towards/from the atmosphere.

Vegetation interacts with the atmosphere in many ways. The tree canopy presents an obstacle to the wind, which is quantified via roughness length; it also intercepts rainfall, preventing part of it from reaching the ground and instead evaporating directly from the leaves. In addition to these physical interactions, plants carry out biological processes for their development which play an important role in energy, water and carbon cycles. Photosynthesis and respiration control the CO_2 flux balance and water vapour loss as transpiration. These processes related to vegetation function were described in Chapter 1. The gas exchange with the atmosphere occurs through the stomatal pores which are controlled by physiological mechanisms and are highly sensitive to environmental variables (Mansfield et al., 1990). It is believed that stomata perform in such a way as to minimise the water loss from the leaf mesophyll while allowing the necessary carbon for photosynthesis (Cowan and Farquhar, 1977; Wong et al., 1979). The stomatal opening is determined by the stomatal conductance, and controls the intake of carbon by the plant as well as the loss of water, therefore establishing a fundamental link between the carbon and water balances.

Photosynthesis models calculate the carbon assimilation by the vegetation given environmental variables, such as radiation, ambient CO_2, temperature and humidity, for given plant specific characteristics. They have been developed from studies of plant physiology based on measurements collected both in laboratories and in the field, (Badger and Collatz, 1977; Wong et al., 1978). The biochemical models derived (e.g. Farquhar et al. (1980)) are considered semi-empirical as, although they make some attempt to describe the biochemical processes, there are parameters that are adjusted from correlations of net assimilation or stomatal conductance to environmental variables. This approach means

that the adjusted parameters make the parametrization specific to a vegetation-climate system and need empirical re-adjusting for other vegetation systems (Collatz et al., 1991).

Photosynthesis models are embedded in LSMs and coupled to a gas-exchange scheme, linking net assimilated carbon (A_n) to the stomatal conductance (g_s). This relationship, originally deduced by Ball et al. (1987), takes slightly different forms in models. It typically varies with air humidity and atmospheric CO_2, and it has been argued that soil moisture content varies the relationship as well (Egea et al., 2011). Since transpiration is controlled by stomatal conductance (when canopy and atmosphere are well coupled) the different assumptions made by models in the description of plant processes result in large variance in the response of transpiration to increased atmospheric CO_2 concentration (De Kauwe et al., 2013). The response of ecosystems to climate change diverges across models (Friedlingstein et al., 2006). With the increasing complexity of ecosystem models, it becomes crucial to understand the assumptions implied in the basic mechanisms of plant processes of each model.

In this chapter different aspects of land surface parametrization are described, with particular focus on the formulation of gas exchange through the canopy. Section 2.2 presents a general description of LSMs. Section 2.2.2 introduces the two LSMs that are used throughout the thesis. The following sections present the main equations used to solve the energy balance at the surface (Section 2.2.4), the partition of precipitation (Section 2.2.5) and terrestrial carbon balance (Section 2.2.6), as implemented in the two LSMs. The role of the vegetation in these processes is emphasized. In Section 2.3 the canopy gas exchange parameterization is explained. The main biochemical photosynthesis models for C_3 (Section 2.3.1) and C_4 (Section 2.3.2) photosynthesis are described. The conductance system that regulates the flow of both carbon and water are described at the leaf level (Section 2.3.3) and at the canopy level (Section 2.3.4). Then two alternative formulations to derive stomatal conductance are described: Jarvis model (Section 2.3.5) and A-g_s (Section 2.3.6). Section 2.4, explains how the gas exchange and photosynthesis schemes from the previous sections have been implemented in the LSMs used in this thesis as well as other model specific aspects related to the vegetation processes, such as soil moisture stress (Section 2.4.6) and the upscaling from leaf to canopy (Section 2.4.7). Finally, the main differences found between the two LSMs are summarised in Section 2.5.

2.2 Land surface parameterization

2.2.1 Introduction

The importance of land surface processes for the atmospheric models was already envisaged in the early 1920s by Richardson (Richardson, 2007). Most of the approaches used by current land surface models were initiated by his pioneering work. While solving the turbulent motion of air he acknowledged the effects of the land surface on the lower atmosphere. He studied the flux of heat from the surface as well as the the flux of heat into the subsoil, quantifying the fluxes with a partition coefficient and analysed its variations. He introduced a sub-surface parameterization by solving the coupled equations of the transfer of heat and water, by differential equations using finite differences and dividing the ground into layers. He also recognised the importance of transpiration from vegetation to the total evaporation and introduced the stomatal control on transpiration, based on work from Brown and Escombe (1905) on plant physiology. He even accounted for the limitation of evaporation by the soil moisture availability.

2.2.2 LSMs in this study: JULES and CTESSEL

Throughout this thesis two land surface models are analysed, tested and compared. The models are:

a) JULES: The Joint UK Land Environment Simulator. (Best et al., 2011; Clark et al., 2011). JULES is the land surface component of UK MetOffice Unified Model, evolved from the Met Office Surface Exchange Scheme (MOSES). It is also part of the Hadley Centre Climate models. HadCM family uses MOSES and the more recent HadGEM family uses JULES. These models have contributed to the physical understanding of the Earth's climate system and their projections have been included in the IPCC assessment reports, including the latest IPCC (Stocker et al., 2013), with contributions from HadGEM3-ES and HadCM2. JULES is also the land surface model in the first generation of UK Earth system model (UKESM).

b) CTESSEL/CHTESSEL: Carbon Hydrology tiled ECMWF (European Centre for Medium-Range Weather Forecasts) Scheme for Surface Exchanges over Land (Viterbo and Beljaars, 1995; Balsamo et al., 2009; Boussetta et al., 2013b). CHTESSEL is part of the European Centre for Medium Range Weather Forescasts (ECMWF) operational model, the Integrated Forecast System (IFS). The Copernicus Atmosphere Monitoring Service (CAMS) uses the CTESSEL biogenic fluxes in their near-real time global CO2 analysis and forecast (Agustí-Panareda et al., 2014). CHTESSEL is also the land component used in ERA-Interim and ERA-Clim reanalyses. The difference between CTESSEL and CHTESSEL is that CHTESSEL incorporates a carbon module but photosynthesis is not linked to transpiration which is calculated with the Jarvis approach; whereas CTESSEL has coupled photosynthesis and transpiration (Boussetta et al., 2013b). For the purpose of analysing the vegetation-transpiration link and comparing it with JULES, throughout this thesis the coupled version CTESSEL is used.

2.2.3 Land classification

The models analysed represent the variety of land surfaces found in a model gridbox with the tiling method. This means that each gridbox is characterised by fractions of land types or tiles; these fractions are not spatially located within the gridbox. The energy balance is then computed for each tile and the total surface fluxes are an average of all tile contributions. An alternative approach to address land heterogeneity is the aggregated method in which the properties of the different surfaces are averaged and the energy balance is computed once. The tiling method however allows a correct characterisation of contrasting surfaces, where fluxes can even have opposite signs (Manrique-Suñén et al., 2013). The tiling method does not allow for interaction amongst surfaces, neither horizontally (local advection), or vertically (grasses under high vegetation). To account for this, dual or multiple source models have to be implemented (Blyth et al., 1999; Verhoef and Allen, 2000).

JULES has 5 types of vegetation, denominated as Plant Functional Types (PFTs); these are broadleaf trees, needle leaf trees, C_3(temperate) grasses, C_4 (tropical) grasses and shrubs. It is possible to simulate crops in JULES (Osborne et al., 2015); however in this

study crops are not considered. There other 4 tiles corresponding to non vegetated areas are urban, lake, soil and ice. Every land gridbox is composed of a fraction of each of these 9 surface types; these fractions can also be 0 if a surface type is not present in a particular gridbox. In the CTESSEL model, the tiles are also used to represent dynamic features of the land surface, such as the presence of snow and the intercepted water by the canopy. The tiles for land gridboxes are high vegetation, low vegetation, interception reservoir, snow on top of low vegetation, snow on top of high vegetation and bare ground. Both high vegetation and low vegetation can represent different species, with the limitation that only one high and one low vegetation type (the dominant biome) can be accounted for in each gridbox. A lake tile is also added in LAKEHTESSEL, a version of the model which resolves inland water (Dutra et al., 2010b).

2.2.4 Surface energy balance

The energy balance presented in Chapter 1 (Equation 1.1) is the key equation in land surface parameterization. It represents the conversion of radiative energy to other forms of energy and it is solved numerically to derive the surface temperature. LSMs solve the energy balance at each tile representing each land surface type and then compute the fluxes and state variables as a weighted average of the tiles of a gridbox.

In JULES the equation takes the form shown in Eq. 2.1. All fluxes are positive downward execept for sensible and latent heat fluxes, which are positive upward. The energy balance is solved at the surface and the term on the left represents the excess of energy. This energy varies the surface temperature T_* accordingly with the surface heat capacity C_s.

$$C_s \frac{\delta T_*}{\delta t} = (1-\alpha)R_s\downarrow + R_l\downarrow - \varepsilon\sigma(T_*)^4 - H - LE - G \tag{2.1}$$

where $R_s\downarrow$ and $R_l\downarrow$ are the incoming shortwave and longwave radiations, α the surface albedo, ε the canopy emissivity, σ the Stefan Boltzmann constant. The sensible heat flux (H) is a function of the gradient of temperature between the surface (T_*) and the lowest layer of the atmosphere (T_1), regulated by the aerodynamic resistance r_a, specific heat capacity c_p, and density ρ of air.

$$H = \frac{\rho c_p}{r_a}(T_1 - T_*) \tag{2.2}$$

The latent heat flux (LE) is the energy consumed in evaporation (E). L is the latent heat of vaporisation (J kg^{-1}) and evaporation E is a function of the gradient of moisture between the saturated specific humidity at the surface temperature and the specific humidity at the lowest layer of the atmosphere (q_1). The flux is regulated by the air density, the aerodynamic resistance and the surface resistance, which can be that of soil or vegetation.

$$E = \frac{\rho}{r_a + r_s}\big(q_1 - q_{sat}(T_*)\big) \tag{2.3}$$

The aerodynamic resistance used in the computation of the turbulent fluxes depends on atmospheric stability via exchange coefficients, which take into account roughness lengths and windspeed.

The ground heat flux (G) in JULES is expressed as follows:

$$G = \nu\left\{\sigma\varepsilon\varepsilon_s\big((T_*)^4 - (T_{s1})^4\big) + \frac{\rho c_p}{r_{a_{can}}}(T_* - T_{s1})\right\} + (1-\nu)\lambda_{soil}(T_* - T_{s1}) \tag{2.4}$$

It is composed of three channels for energy transmission towards the ground: radiative, turbulent, and conductive. The transmission in the vegetated (ν represents the vegetated fraction) part has a radiative component for the radiative loss from the first layer of soil, at temperature T_{s1}, and its reflection in the canopy and the radiative emission from the canopy, at temperature T_*, and its reflection in the first layer of soil. ε is the canopy emissivity and ε_s the soil emissivity. The second component is the turbulent transmission of energy from the canopy to the ground, with $r_{a_{can}}$ representing an aerodynamic resistance between the canopy and the soil. The last term accounts for the thermal conduction within the soil, only in the non vegetated area (1-ν) with λ_{soil} being the thermal conductivity.

CTESSEL uses an energy balance equation similar to Eq. 2.1, but the equation is solved at the skin layer, defined as the interface between land and atmosphere. The temperature at this layer is the skin temperature (T_{sk}).

$$0 = (1 - f_{Rs})(1-\alpha)R_s\downarrow + \varepsilon(R_l\downarrow) - \varepsilon\sigma(T_{sk})^4 + H + LE - G \tag{2.5}$$

Contrary to JULES there is no term for surface thermal inertia ($C_s = 0$ in Eq. 2.1). However, CTESSEL accounts for a small fraction of net shortwave energy transmitted directly to the soil or snow, (f_{Rs}). This fraction is tile dependent and is only transmitted in the low and high vegetation tiles, interception reservoir and snow on high vegetation.

The latent heat and sensible fluxes are calculated similarly to JULES but making use of the skin temperature.

$$E = \frac{\rho}{r_a + r_s}\big(q_1 - q_{sat}(T_{sk})\big) \tag{2.6}$$

$$H = \frac{\rho c_p}{r_a}(T_{s1} + gZ_L/C_p - T_{sk}) \tag{2.7}$$

where the extra term contains g for the acceleration of gravity and is Z_L the lowest atmospheric model level.

Finally, the ground heat flux represents the flux of energy from the skin layer to the top soil layer.

$$G = \Lambda_{sk}(T_{sk} - T_{s1}) \tag{2.8}$$

The ground heat flux is only described with a conduction term determined by the temperature difference between the skin layer and the top soil layer. The skin conductivity Λ_{sk} establishes the thermal connection between the skin level and the soil or snow deck. It varies for stable or unstable stratification of the temperature gradient in the case of high vegetation. This difference is considered to represent the asymmetric coupling between the ground surface and the tree canopy layer: an effective convective transport within the tree trunk space for unstable conditions, and a limited turbulent exchange for stable stratification (ECMWF, 2015). Although there are no explicit terms for radiative or turbulent transfer as in JULES (Eq. 2.4), this transmission is implicitly accounted for.

Subsoil heat transfer

The transfer of heat vertically through the soil is described by the Fourier law of diffusion with an additional term to account for the thermal effects related to phase changes of water.

$$C_{soil}\frac{\partial T}{\partial t} = \frac{\partial}{\partial z}\left[\lambda_T \frac{\partial T}{\partial z}\right] + L_{fus}\rho_w \frac{\partial \theta_I}{\partial t} \tag{2.9}$$

C_{soil} is the volumetric soil heat capacity (J m^{-3} K^{-1}), T is the soil temperature, z is the vertical coordinate and λ_T is the thermal conductivity, which depends on the soil water content. The last term represents thermal effects of latent heat of fusion or freezing. L_{fus} is the latent heat of fusion, ρ_w is the density of water and θ_I is the volumetric ice water content which depends on temperature and soil moisture content. The energy used to melt the frozen soil in spring delays the surface warming and the freezing of the soil in autumn

or winter delays soil cooling (Viterbo et al., 1999). JULES solves a similar equation for the soil heat transfer. The effects of the water phase changes are accounted for using an apparent capacity, and additional term accounts for the transfer of heat via the water flow (Cox et al., 1999). This transfer is neglected in CTESSEL.

To solve this differential equation the soil is discretised into horizontal layers. Both JULES and CTESSEL divide the soil into four layers with exponentially increasing depths. JULES layers are 0.1, 0.25, 0.65 and 2 m thick and CHTESSEL layers are 0.07, 0.21, 0.72 and 1.89 m thick; adding up to a total depth of 3 and 2.89 m respectively. This depth allows to capture the seasonal signal in temperature variation (Deardorff, 1978).

Although at the surface the gridbox is divided into several tiles, the subsoil is described as a single type. At the top, the boundary condition is the soil heat flux at the surface computed as a weighted average over the tiles, plus, in the case of CTESSEL, the fraction of solar radiation which was transmitted directly (f_{Rs} in Equation 2.5) and snow basal flux when present. At the bottom, the boundary condition is of zero heat flux, to ensure conservation of energy.

2.2.5 Surface water balance

Land surface models have precipitation given as an input and need to correctly distribute the water over the surface. Some of the precipitation is intercepted by the canopy structure before reaching the ground. The fraction of water that falls on the ground is denominated throughfall. Upon reaching the ground, part of the throughfall infiltrates into the permeable unsaturated soil and part can flow above the surface as runoff. The equation representing the water balance at the surface is:

$$T + M = E + I + R \tag{2.10}$$

where T, throughfall is precipitation minus intercepted water, M is the available water from melting snow. On the right hand side, E is the water lost via evaporation, I is the infiltration into the first soil layer and R is the surface runoff.

Canopy interception

Depending on the type of leaves, droplets can aggregate as a thin film. This layer of

water will evaporate more easily back to the atmosphere, as there is no stomatal or soil resistance involved. The amount of intercepted water is a very uncertain quantity, as its measurement presents many challenges. It depends on the type of leaf, leaf angle, type of precipitation, and the presence of wind. Horton (1919) conducted a very meticulous study on this subject in his own hydrologic laboratory.

In JULES the water intercepted by the canopy is calculated as a linear function of the leaf area index (LAI), with a maximum capacity. In CTESSEL the intercepted water is considered as an extra tile, the interception reservoir. It has its own water balance equation accounting for rainfall interception, loss by evaporation (or gain by dew collection) as well as dew deposition from other tiles. In both models there is a maximum capacity that can be held on leaves; if it is reached, the exceeding water will fall down to the ground.

Infiltration and runoff

The water reaching the soil surface is then split into infiltration when the soil is unsaturated and lateral runoff of the excess water. The way this division is done varies from model to model. CTESSEL hydrology uses a variable infiltration capacity based on orography and soil type (Balsamo et al., 2009). The orographic complexity of the terrain reduces the infiltration and more water is left for surface runoff. JULES calculates the infiltration based on a typical surface infiltration rate (infiltration enhancement factors (Best, 2009) averaged for the tiles. Runoff is the remaining water, with adjustments to account for the finite timestep.

Subsoil water transfer

The vertical movement of water in the unsaturated zone obeys the following equation (Richards, 1931) for the volumetric water content θ:

$$\rho_w \frac{\partial \theta}{\partial t} = -\frac{\partial F}{\partial z} + \rho_w S_\theta \tag{2.11}$$

where soil moisture θ is defined for each soil layer, ρ_w is the density of water (kg m^{-3}), F is the downward water flux into the next layer (kg m^{-2} s^{-1}) and S_θ is a volumetric sink term associated with the root uptake (m^3 m^{-3} s^{-1}), which depends on the surface energy balance and root profile (Viterbo and Beljaars, 1995). The equation is solved for the same four layers as the energy transfer, with top layer's flux being the infiltration and a bottom boundary condition of free drainage.

The flux of water is described using Darcy's law:

$$F = -\rho_w \Big[\lambda \frac{\partial \theta}{\partial z} - \gamma\Big] \tag{2.12}$$

where λ is the hydraulic diffusivity ($m^2\ s^{-1}$) and γ is the hydraulic conductivity (m s^{-1}). Both parameters control the flow of water through the porous medium and are a function of the soil moisture and the soil texture. The functional relationship of these parameters with soil moisture is of an empirical nature, based on observational studies. In some formulations (Clapp and Hornberger, 1978; Cosby et al., 1984) hydraulic diffusivity and hydraulic conductivity are calculated as a function of the volumetric soil content (θ). However, it has been argued that, instead of using θ as the variable to link the soil moisture content to the soil properties, the matric potential, ψ, represents better the pressure that the droplets experience within the soil pores. The matric potential depends on the soil water content as well as on the soil texture. Van Genuchten (1980) formulation uses the matric potential, ψ, or the related pressure head ($h = -\psi/(\rho_w \cdot g)$) to determine the water flow. The hydraulic diffusivity in Van Genuchten (1980) formulation as a function of the pressure head h (m) is:

$$\gamma = \gamma_{sat} \frac{\big[(1+\alpha h^n)^{1-1/n} - \alpha h^{n-1}\big]^2}{(1+\alpha h^n)^{(1-1/n)(l+2)}} \tag{2.13}$$

where α, n and l are soil texture dependent parameters which are related to the soil composition of sand, silt and clay through pedotransfer functions (Wösten et al., 1999).

JULES allows the use of either Brooks and Corey (1964) or Van Genuchten (1980) formulations. CTESSEL switched from Clapp and Hornberger (1978) formulation, used in its previous model version TESSEL, to Van Genuchten (1980) with the revision of the hydrology (Balsamo et al., 2009).

The pressure head is related to the volumetric soil water content via the water retention curve, which varies with the soil texture class:

$$\theta(h) = \theta_r + \frac{\theta_{sat} - \theta_r}{(1+(\alpha h)^n)^{1-1/n}} \tag{2.14}$$

where θ_r represents a soil moisture residual.

Some aspects of the land parameterization still make use of significant water content quantities in volumetric unit, in particular the soil moisture stress on vegetation growth (Eq.

2.76). The permanent wilting point is the level of soil moisture below which vegetation cannot survive. Soil moisture at field capacity is the amount of water that can be held by the soil against gravity, and soil moisture at saturation is the maximum soil moisture that the soil can hold. These levels of soil moisture are defined in terms of the matric potential as:

$$\begin{aligned} \psi(\theta_{pwp}) &= -1500kPa \\ \psi(\theta_{cap}) &= -10kPa \\ \psi(\theta_{sat}) &= -33kPa \end{aligned} \tag{2.15}$$

Soil water uptake by roots

The soil moisture stress on vegetation is calculated as a function of the water availability in the root zone, which is determined by a root fraction at each layer. The fraction of roots in the soil layers follows an exponential distribution and is plant dependent. The soil moisture stress factor is averaged across the soil layers. The equations describing the root density at each layer are for JULES Eq. 50 in Best et al. (2011) and Eq. 8.13 in ECMWF (2015).

2.2.6 Carbon balance

A full representation of the carbon cycle requires several carbon pools and a correct modelling of the processes that produce an exchange of carbon amongst these pools. Because of the different timescales of the processes, some of them being 100 to 1000 years, an equilibrium state requires a long spin up.

JULES has a carbon module based on the RothC carbon scheme for organic carbon turnover (Jenkinson et al., 1990). It consists of 4 pools: decomposable plant material, resistant plant material, biomass, and humus, and a specific respiration rate for each pool. The rate of carbon respiration or decomposition is modified by soil temperature and moisture. JULES can be run without the organic carbon module, in which case only one carbon pool is accounted for (soil). Similarly, CTESSEL does not include a carbon module, accounting only for CO_2 exchange between the ecosystem and the atmosphere via photosynthesis and respiration both autotrophic and heterotrophic. The CO_2 gas

exchange is given by:

$$NEE = -GPP + R_a + R_h = -GPP + R_{eco} \tag{2.16}$$

where the sum of autotrophic and heterotrophic respiration is the ecosystem respiration R_{eco}. NEE is positive upward (away from the ecosystem-carbon source) and negative downward (towards the ecosystem-carbon sink).

2.2.7 Vegetation as a link between water and carbon

Vegetation is a key element in linking water and carbon cycles. First, via the interception layer, a portion of the precipitation that falls on vegetation is evaporated directly to the atmosphere. Secondly, water loss takes place through the leaves stomata as the carbon dioxide enters for photosynthesis. Finally, the roots absorb subsoil water by differences in osmotic pressure which is subsequently transpired into the atmosphere. This process makes it possible to evaporate subsoil water that otherwise would not be accessible via direct soil evaporation (Lambers et al., 1998).

The ratio of lost water per assimilated carbon is called intrinsic water use efficiency. It gives an idea of how efficient the plant is at transforming CO_2 into organic compounds in terms of water cost. Plants that live in a very dry environment need a better water use efficiency to maintain their functions.

The link established by the double gas exchange through the stomata has important consequences for vegetation's response to the increasing levels of atmospheric CO_2 concentration. It has been demonstrated that an increase in atmospheric CO_2 has an impact both on photosynthesis and transpiration (Lambers et al., 1998). As the substrate for photosynthesis reaction, high CO_2 concentration tends to enhance the photosynthetic activity. A high concentration of CO_2 also means that the plant's stomata do not need to open up as much and hence less water escapes. This response of the plant leads to an increase in water use efficiency (Keenan et al., 2013).

The next section explains in detail the modelling of photosynthesis and of the stomatal conductance which controls the exchange of both CO_2 and water vapour.

2.3 Canopy gas exchange

The rate of photosynthetic carbon assimilation is determined by the supply of CO_2 from the atmosphere and demand of CO_2 by the plant. The supply is controlled by the diffusion of CO_2 from the free atmosphere to the sites of carboxylation and limited by a set of conductances. The demand function is determined by photosynthetic activity in the chloroplasts, governed by the biochemistry. Figure 2.1 illustrates this situation: the photosynthetic rate is represented as a function of partial pressure of CO_2 in the inside of stomata, $p(CO_2)$. The demand function is portrayed by the ascending curve, initially with a steep increase with CO_2 (RuBP saturated), and a subsequent diminishing of the slope at higher CO_2 levels, when photosynthesis is limited by RuBP regeneration (RuBP limited). The supply function is represented by a straight dashed line with negative slope; the slope represents the total conductance (or inverse of the resistance) that CO_2 has to overcome to enter the chloroplasts from the free atmosphere.

The present section describes the parameterization of these functions and the elements involved. Sections 2.3.1 and 2.3.2 describe the demand function, based on the biochemical functioning of photosynthesis and the regimes regulated by the availability of substrates for the chemical reaction. The system of conductances that regulates CO_2 and water vapour exchanges is described, at the leaf level (Section 2.3.3), and at the canopy level (Section 2.3.4). The integration from leaf to canopy accounts for the influence of the rest of the leaves/canopy. Finally, two typical formulations used for stomatal conductance are described: the Jarvis approach (Section 2.3.5) and A-g_s approach (Section 2.3.6). A-g_s is the scheme used by most models and is based on the combination of both demand and supply functions to derive the stomatal conductance and photosynthesis rate. It has the advantage that it allows for synergistic interactions between environmental factors affecting the opening of the stomata unlike the Jarvis method. It also allows to introduce in the parameterization the link between the carbon and the water fluxes.

2.3.1 Biochemical model for C_3 photosynthesis

The photosynthetic rate at the leaf level can be derived from the environmental conditions and physiological considerations. Most models are based on the formulation developed by

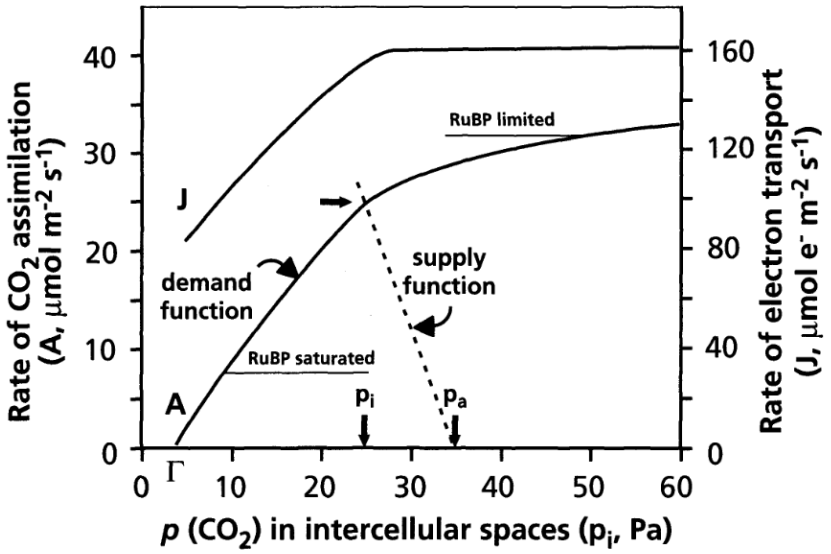

Figure 2.1: Supply and demand functions for CO_2. The demand function is the rate of carboxylation (A) as a function of intercellular CO_2 partial pressure, $p(CO_2)$. The concentration at which $A = 0$ is the CO_2 compensation point Γ. The linear region at low values of $p(CO_2)$ corresponds to CO_2 limited (or RuBP saturated) photosynthesis. At higher levels of $p(CO_2)$ photosynthesis is light limited (or RuBP limited). J is the rate of electron transport. The supply function is a straight line (dashed line) with slope equal to the stomatal conductance. The intersection of the supply function with the demand function is the actual rate of net CO_2 assimilation (indicated by a horizontal arrow) at a value of p_i (indicated by a vertical arrow) for a CO_2 atmospheric partial pressure of p_a. Figure from Lambers et al. (1998) First edition.

Farquhar et al. (1980). This model combines various aspects of the biochemistry of photosynthesis at organelle level gathered by physiologists with gas exchange measurements at the leaf level. The model includes ribulose-1,5-biphosphate carboxylase/oxygenase (rubisco) kinetics and takes into account the dependence of the reactions on temperature. The stoichiometric relations of both carboxylase and oxygenase activities and the regeneration of RuBP were depicted in Figure 1.5. The enzyme rubisco catalyses the carboxylation of Ribulose-1,5-biphosphate (RuBP) in the presence of CO_2 (photosynthetic carbon reduction cycle, PCR in Figure 1.5), as well as its oxidation in the presence of O_2 (photorespiratory carbon oxidation cycle, PCO in Figure 1.5). Farquhar et al. (1980) model uses the stoichiometric relations between the PCR and PCO to determine the rate of phosphoglyceric acid (PGA) production. Because carboxylation and oxidation are competing reactions, the presence of O_2 inhibits photosynthesis, and the ratio of partial pressures of O_2 and CO_2 determine the rate of photosynthesis. The model includes a dependence of electron transport on photon flux.

Depending on the availability of RuBP for carboxylation/oxygenation there are two different situations, (i) there is abundant RuBP and consequently rubisco or CO_2 become the limiting factors, (ii) there is shortage of RuBP, so its concentration is the limiting factor, and therefore the speed of its regeneration.

(i) RuBP saturated rate (rubisco or CO_2 limited): at low CO_2 at the site of carboxylation, the enzyme rubisco is saturated with respect to the substrate RuBP. The concentration of RuBP is higher than the rubisco concentration. The effect of increasing the $p(CO_2)$ is the activation of the enzyme, consequently an almost linear response in assimilation rate to $p(CO_2)$. This corresponds to the first part of the curve in Figure 2.2, with the slope being proportional to the maximum activity of rubisco in the leaf. The equation proposed by Farquhar et al. (1980) for the rate of carboxylation in this region is given by:

$$A_c = V_{cmax} \frac{C_c - \Gamma^*}{C_c + K_c(1 + \frac{O}{K_o})} - R_d \tag{2.17}$$

where V_{cmax} is the maximum velocity of carboxylation, a parameter that has to be fitted to each specific plant species. C_c is the partial pressure of carbon dioxide in the chloroplasts. The inhibitory effect of the photorespiratory reaction is included

in this equation through the partial pressure of oxygen, O, determining the ratio of the carboxylase-oxygenase reactions. K_c and K_o are the Michaelis-Menten constants for CO_2 and O_2. These are related to the enzyme kinetics and have an exponential dependence on temperature (Eq. 2.23).

(ii) RuBP limiting (Electron transport or light limited): when the concentration of RuBP is lower than that of rubisco, then the carboxylation reaction becomes limited by the rate of regeneration of RuBP. This depends on the activity of the Calvin cycle, which is fueled by the energy carriers, NADPH and ATP, generated by the photon flux from sun's radiation. The rate of regeneration of RuBP is virtually independent of $p(CO_2)$; however, assimilation rate still increases somewhat with $p(CO_2)$, as RuBP is increasingly diverted from oxygenation to carboxylation (Farquhar and Sharkey, 1982). Photosynthesis limited by this regime is labelled RuBP regeneration limited in Figure 2.2. In the Farquhar et al. (1980) original formulation this carboxylation rate allowed by the speed of the electron transport was calculated as:

$$J' = \frac{0.5(1-f)I}{2(2+2\phi)} \tag{2.18}$$

where the term in the numerator is the potential rate of electron transfer, f is defined by Farquhar et al. (1980) as the light lost as absorption by other than the chloroplast lamellae and I is the absorbed photon flux. ϕ is the ratio of oxygenation to carboxylation. However, this formulation was abandoned for a simpler one which relates the RuBP regeneration rate to the electron transport rate (Von Caemmerer, 2000).

$$A_j = J\frac{(C_c - \Gamma^*)}{4C_c + 8\Gamma^*} - R_d \tag{2.19}$$

and the the electron transport rate is represented by non-rectangular hyperbola (Farquhar and Wong, 1984).

$$J = \frac{\alpha PPFD + J_{max} - \sqrt{(\alpha PPFD + J_{max})^2 - 4\alpha\delta PPFD J_{max}}}{2\delta} \tag{2.20}$$

where PPFD is the photosynthetic photon flux density, α is the initial quantum yield or efficiency and δ is the curvature of the light response. At high light intensities, J saturates at J_{max}, which depends on temperature. This equation is responsible for the characteristic shape of the light limited photosynthetic rate as a function of light.

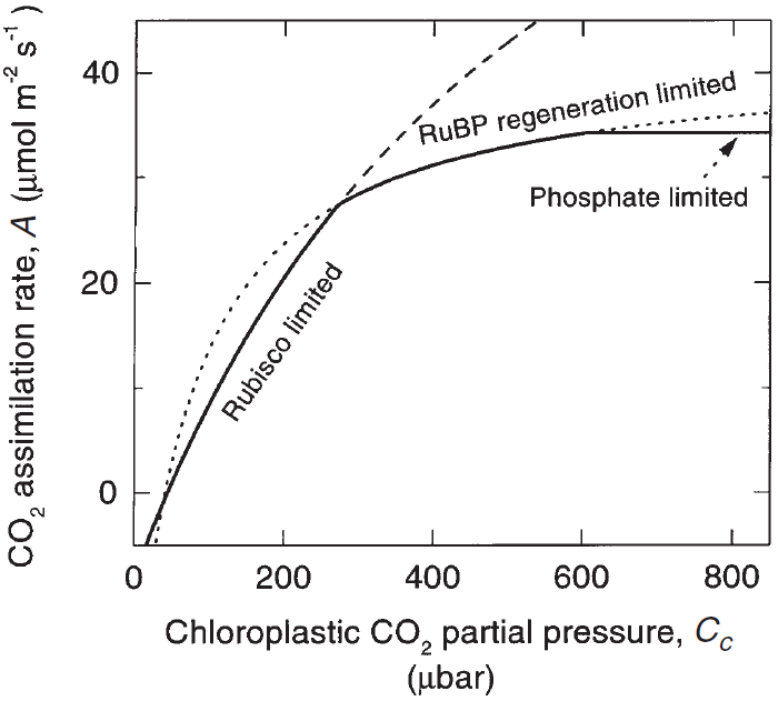

Figure 2.2: Modelled rate of the CO_2 assimilation for the three limiting regimes as a function of chloroplast CO_2 partial pressure. Figure from Von Caemmerer (2000).

Rubisco limited photosynthesis happens at low CO_2 concentrations, typically <20 Pa (~200 ppm); while RuBP regeneration limited photosynthesis occurs for >30 Pa (~300 ppm). For 20-30 Pa there is a transition from one limitation to the other (Sharkey et al., 2007). Although the original Farquhar et al. (1980) formulation only considered these two limiting regimes, a third regime was included later, triose phosphate utilisation (Sharkey, 1985) also known as export limited regime.

(iii) Export limited regime or triose phosphate utilisation (TPU): the photosynthetic rate can be limited by the rate at which triose phosphates are used in the synthesis of starch and sucrose. It occurs at high chloroplastic CO_2 partial pressures as shown in Figure 2.2. The TPU limitation is of great interest since it is the limitation that will reflect the short term interactions between photosynthesis and the physiology of the plant, i.e. the stage of chloroplast developments, changes in enzyme activities, size of metabolite pools as well as the demand from non-photosynthetic parts of the plant 'sinks' (Herold, 1980). This limitation is found at high CO_2 partial pressure, in particular in combination with high irradiance or at low temperatures. The equation

used to model TPU limitation is based on triose phosphate utilisation being required at one third the rate of CO_2 fixation (Sharkey, 1985).

$$A_e = 3T_p - R_d \tag{2.21}$$

where T_p is the rate of triose phosphate export from the chloroplast. When photosynthesis is export limited, both rubisco activity and the rate of RuBP regeneration must be reduced to match the capacity for TPU. This means that some of the rubisco is wasted and there could be light damage of electron transport components (Sharkey, 1985). Under these conditions, A is insensitive to changes in CO_2.

Figure 2.2 shows the three regimes limiting photosynthesis as a function of the carbon concentration at the sites of carboxylation. The rate of photosynthesis is a function of the three photosynthetic levels, carbon limited, light limited and export limited.

$$A = f(A_c, A_j, A_e) \tag{2.22}$$

As the speed of the reaction is constrained by the slowest of the 3 processes, Farquhar et al. (1980) original formulation suggested to use the minimum of the three. In practice a quadratic combination is applied to assure a smooth transition between the limiting regimes. ; the rate of photosynthesis in this case is determined by the minimum of the three rates.

For a compendium of typical values for V_{cmax}, V_{omax}, Michaelis-Menten parameters, J_{max}, Γ, diffusive g_m and R_d see Von Caemmerer (2000).

Temperature dependencies

There is typically an optimum temperature for leaf photosynthesis. Below this optimum the enzymatic reactions are temperature limited. The reaction of carboxylation of RuBP and its competing oxygenation reaction are controlled by the enzyme rubisco, whose activity is highly dependent on temperature. Therefore the velocities of the reactions vary with temperature. Interestingly, these responses to temperature have been known to be different in both reactions (Badger and Andrews, 1974). At high temperatures the rate of the oxygenation reaction of rubisco increases more than that of the carboxylation reaction,

resulting in a decrease of net carbon assimilation. This is partly because the solubility of CO_2 declines with increasing temperature more strongly than does that of O_2, but also due to the kinetic properties of rubisco as demonstrated by Badger and Andrews (1974) in spinach leaf RuBP. This effect is introduced in models by adjusting the temperature dependent parameters.

There are mainly two formulations to represent the parameters variation with leaf temperature. One is based on the Arrhenius functions for enzymatic activity from findings by Badger and Andrews (1974); Badger and Collatz (1977) and used by Farquhar et al. (1980) for rubisco kinematics:

$$Parameter = Parameter(25^{\circ}\mathrm{C})exp\left\{\frac{(25-T)\Delta H_a}{298R(T+273)}\right\} \tag{2.23}$$

where ΔH_a (J mol^{-1}) is the activation energy of the parameter and R is the universal gas constant. The activation energy represents the kinetic energy of substrate required for the reaction to proceed and can be derived from the slope of Arrhenius plot as calculated by Badger and Collatz (1977). This equation is monotonically increasing; therefore it does not impose limitation on photosynthesis for high temperatures apart from the effect of oxygenase-carboxylase competition. There are variations of this function that include more fitting parameters as well as the the energy of activation ΔH_a (Sharkey et al., 2007):

$$Parameter = Parameter(25^{\circ}\mathrm{C})exp\left\{c-\frac{\Delta H_a}{RT}\right\} \tag{2.24}$$

where c is a scaling constant. To represent the decline at high temperatures a denominator in the last equation can include a parameter representing the energy of deactivation ΔH_d (J mol^{-1}), and entropy ΔS (Harley et al., 1992; Bernacchi et al., 2002; Sharkey et al., 2007):

$$Parameter = Parameter(25^{\circ}\mathrm{C})\frac{exp\left\{c-\frac{\Delta H_a}{RT}\right\}}{1+exp\left\{\frac{(\Delta ST-\Delta H_d)}{RT}\right\}} \tag{2.25}$$

The other formulation used is based on Q_{10} parameters. The Q_{10} value represents the relative increase in reaction for a 10 °C temperature change and is specified at a particular temperature.

$$Parameter = Parameter(25^{\circ}\mathrm{C})Q_{10}^{(T-25)/10} \tag{2.26}$$

The Q_{10} formulation has also been further adjusted with inhibition functions that place lower and upper limits on the parameter (Berry and Bjorkman, 1980; Collatz et al., 1992)

$$Parameter = Parameter(25°\mathrm{C})\frac{Q_{10}^{(T-25)/10}}{\left(1+e^{0.3(T_{low}-T)}\right)\left(1+e^{0.3(T-T_{upp})}\right)} \tag{2.27}$$

Vegetation models typically use Equations 2.25 or 2.27 for photosynthesis parameters that decline after the optimum temperature. Many experimental studies have worked on determining the necessary parameters to characterise rubisco kinematics dependence to temperature *in vitro* laboratory experiments. Bernacchi et al. (2001) derived the parameters *in vivo* and argued that *in vitro* conditions might not be representative of the natural environment, due to assumptions made on pH and on the CO_2 diffusion to the site of carboxylation (mesophyll conductance).

2.3.2 Biochemical model for C_4 photosynthesis

C_4 plants use a different metabolic pathway for photosynthesis, which entails different response to environmental factors. C_4 plants are found in tropical and agricultural ecosystems. The C_4 pathway has an initial carboxylation in the mesophyll cells catalysed by PEP carboxylase. This process acts as a metabolic pump of CO_2 for the final carboxylation by rubisco in the chloroplasts of the bundle sheath. C_4 photosynthesis models are therefore based on both the capacity of PEP-carboxylase and rubisco activities. The large CO_2 gradient between the CO_2 repleted bundle sheath cell and the mesophyll cell induces a small CO_2 leakage against the pump direction. The intercellular transport model (Berry and Farquhar, 1978) is a very detailed reproduction of rubisco and PEP carboxylase kinetics. The gross photosynthesis is the PEP carboxylation velocity minus the leaked CO_2, and carboxylation at the bundle sheath is based on rubisco kinetics. Although this model gives good estimates, it is too complex and has a high number of adjustable parameters. Collatz et al. (1992) developed a simplified version of the model that reduced the number of factors. As in C_3 photosynthesis modelling, three limiting situations are determined and combined to yield the photosynthetic rate, which is simultaneously coupled with the A-g_s model for stomatal conductance

(i) Light limited. At low light intensities, photosynthetic activity is determined by the quantum yield, which for C_4 photosynthesis is a rather constant value.

$$J_i = \alpha f Q_p \tag{2.28}$$

α the quantum yield, f fraction of absorbed photons and Q_p is the incident quantum flux.

(ii) CO_2 limited (or PEP carboxylase). At very low CO_2 concentrations, photosynthesis increases linearly from the compensation point to a carbon saturated rate at carbon partial pressure of about 10 Pa (Collatz et al., 1992). This process is related to carboxylation in the mesophyll.

$$J_c = \left(k_p - \frac{L}{p_i}\right)\frac{p_i}{Patm} \tag{2.29}$$

k_p is a factor accounting for PEP carboxylase activity L represents the CO_2 leakage.

(iii) When light and carbon are not limiting, the rate of assimilation approaches the rate J_e and becomes independent of CO_2 and light.

$$J_e = V_{cmax} \tag{2.30}$$

This rate is parameterized as the maximum carboxylation velocity. As at this stage carbon concentration in the bundle sheath is high; it is the rubisco activity that imposes the upper limit. There might be other subsequent reactions limiting the carbon assimilation process, similarly to the export limit in C_3 photosynthesis, but experimental studies are not conclusive as they cannot discern what imposes the limitation.

The combination of the three limiting regimes is obtained in an analogous way to C_3, by a set of nested quadratic equations.

$$A = f(J_i, J_c, J_e) \tag{2.31}$$

2.3.3 Conductances at the leaf level

The stomatal pores located in the leaves are the pathway for CO_2 to enter the carboxylation sites for photosynthesis. At the same time water vapour is lost to the atmosphere

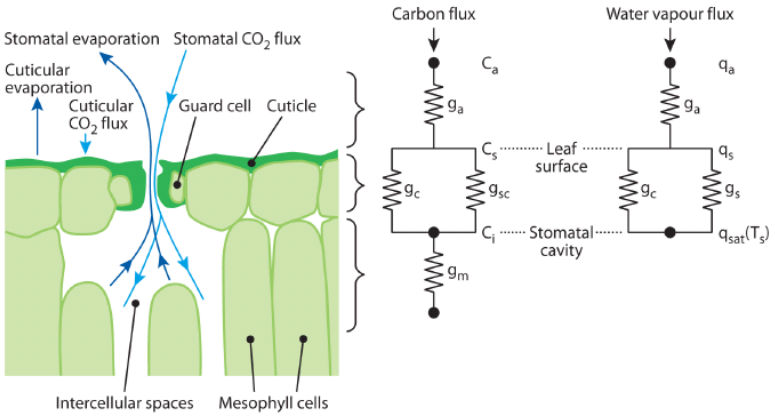

Figure 2.3: Cross section of an open stoma and related conductances diagram; C_a, C_s, C_i, are the carbon concentrations in the free atmosphere, leaf surface and internal space of stomata; g_a, g_{sc}, g_c, g_m are the aerodynamic, stomatal, cuticular and diffusive mesophyll conductances for carbon; q_a, q_s, $q_{sat}(T_s)$ are the specific humidities at the free atmosphere, leaf surface and saturated specific humidity at the stomatal cavity temperature (assumed equal to leaf surface temperature T_s); g_a, g_s, g_c are the aerodynamic, stomatal and cuticular conductances for water vapour. Figure from Boussetta et al. (2013b).

through these pores. Figure 2.3 shows a cross-section of a leaf with the stomatal cavity and pore on the left and a diagram of conductances for carbon and water vapour fluxes on the right. The mechanism by which the gases cross the stomatal pore is diffusion. The diffusion coefficient of a gas is inversely proportional to the square root of its molecular weight. For this reason, water vapour (molecular weight = 18) diffuses more easily than carbon dioxide (molecular weight = 44). In vegetation models this transport through the stomata is controlled by the **stomatal conductance**. The higher the conductance the easier it is for the gas to go through the stomata. The stomatal conductances for water vapour and CO_2 are denoted as g_s and g_{sc} respectively. They are related by:

$$g_s = 1.6 g_{sc} \tag{2.32}$$

The factor 1.6 is the ratio of diffusivities of water vapour and CO_2. The stomatal openings are very sensitive to both environmental factors and internal physiological factors, allowing plants to optimise the balance between CO_2 and water vapour loss.

Although most of the gas exchange occurs through the stomata, some water molecules

can leave the plant through the cuticle; CO_2 can also enter this way. This transport is accounted for via a conductance in parallel to the stomata conductance called the **cuticular conductance** (g_c) (Figure 2.3). The cuticle presents a waxy barrier, which hampers diffusion; in fact cuticular conductance is very small and almost negligible. However, when stomata are nearly closed, stomatal and cuticular conductances become comparable.

In some models, an additional step is included to represent the diffusion of CO_2 from the substomatal cavity (C_i) to the site of carboxylation or chloroplasts (C_c). This is represented by the diffusive **mesophyll conductance**, it does not apply to water vapour, as the transpiration occurs directly from the saturated substomatal cavities. The mesophyll conductance varies widely amongst species and correlates with the photosynthetic capacity (Lambers et al., 1998; Evans and Von Caemmerer, 1996). It is closely linked to physiological processes and it involves diffusion of CO_2 through the cell walls in the gas phase as well as in the liquid phase. The carbon isotope discrimination technique has been used to measure this diffusion an thus the value of the mesophyll conductance (also called internal conductance). It was thought to be constant for a leaf because it is largely related to the leaf anatomy (Evans and Von Caemmerer, 1996) and therefore omitted in many models. More recent physiological research shows that mesophyll conductance is dynamic and has a faster response than stomatal conductance (Flexas et al., 2008). Therefore mesophyll conductance plays an important role in limiting photosynthesis especially at high temperatures (Bernacchi et al., 2002) or due to soil moisture stress (Egea et al., 2011). Despite this evidence, most photosynthesis models in LSMs do not represent it explicitly. Unfortunately, the term mesophyll conductance is also used to refer to a parameter that regulates photosynthetic rate (Goudriaan et al., 1985; Jacobs, 1994). Throughout this thesis the mesophyll conductance referring to the regulation of CO_2 flux entering the chloroplasts, as described here, will be denominated diffusive mesophyll conductance, reserving the term mesophyll conductance for the model parameter.

The leaf boundary layer represents the surrounding of the leaf surface up to which the leaf gas exchange exerts an influence (Figure 2.4). Outside this layer the temperature or humidity of the air are not affected by the leaf, and are those of the free atmosphere (this is not strictly true if we consider the whole canopy). Water vapour, heat and carbon fluxes are regulated by the the **leaf boundary layer conductance**. The factors defining the boundary layer conductance are the leaf morphology (small versus big leaves) and

the wind. g_b is directly proportional to the square root of the windspeed and inversely proportional to the square root of the thickness of the leaf boundary layer. Leaves in well ventilated spaces have thinner boundary layers (higher g_b) than those sitting in still air. Small leaves tend to form thinner boundary layers. The leaf boundary layer conductance can be calculated as (Jacobs, 1994):

$$g_b = k\sqrt{\frac{u}{W_l}} \tag{2.33}$$

where u is the wind speed and W_l is the leaf's width in the direction parallel to the windspeed. Its counterpart for carbon diffusion is related to it as follows:

$$g_b = 1.37 g_{bc} \tag{2.34}$$

The factor used to relate leaf boundary layer conductance for water vapour and CO_2 is 1.37, this is because in this case both diffusion and turbulence influence the fluxes. Under most conditions the stomatal conductance is considerably less than the boundary layer conductance. g_b can reach up to 10 mol $m^{-2}s^{-1}$ at wind speeds up to 5 m s^{-1} while g_s has values up to 1 mol $m^{-2}s^{-1}$ for widely open stomata (Lambers et al., 1998). Therefore the control on gas exchange is typically exerted through the stomata. However, in some cases (still humid air, big leaves) the boundary layer can be thicker, hence g_b values become small and therefore more constraining. The importance of the leaf boundary layer was highlighted by Collatz et al. (1991), who analysed its interaction with the regulatory properties of stomatal conductance. The degree to which stomata control the transpiration rate (or CO_2 assimilation rate) depends on the coupling between the leaf and the atmosphere, which is given by how closely the saturation deficit at the leaf surface, D_s, is linked to that of the air outside the leaf boundary layer, D_a, as explained by Jarvis and McNaughton (1986). They define a decoupling coefficient Ω_l to account for the ratio of leaf boundary layer conductance to stomatal conductance.

Under well coupled conditions and neglecting g_m and g_c, the transpiration and CO_2 intake are controlled by stomatal conductance as shown by the following expressions:

$$E = \rho_w g_s D \tag{2.35}$$

in this expression ρ_w density of water is in kg m^{-3}, g_s is in m s^{-1}, and D in kg kg^{-1},

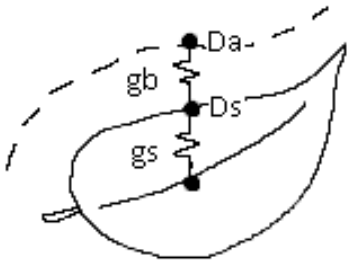

Figure 2.4: A single leaf and its boundary layer (dashed line). Stomatal conductance is denoted by g_s and leaf boundary layer by g_b which are conductances for water vapour. Inside the stomata air is saturated, $D = 0$. D_s is the specific humidity deficit at the leaf surface and D_a the specific humidity deficit at the leaf boundary layer. Cuticular conductance has been omitted.

yielding transpiration as kg of water m^2 s^{-2}.

$$A = \frac{g_s}{1.6}(C_c - C_i) \tag{2.36}$$

in this expression g_s is in m s^{-1}, C_s and C_i are in kg C m^{-3} yielding photosynthesis rate A in kg C m^2 s^{-2}. Stomatal behaviour has been typically represented in models by two approaches, Jarvis (1976), described in section 2.3.5 and A-g_s (Ball et al., 1987) described in 2.3.6.

2.3.4 Conductances at the canopy level

The system of conductances described up to now defines the pathway for water vapour (or CO_2) through a single stoma, across the chloroplast, through the stomatal pore and across the leaf boundary layer. However the bigger picture is formed by clusters of leaves forming a plant, and groups of plants forming the canopy. Jarvis and McNaughton (1986) made a detailed analysis of the process of upscaling from a single pore, to a leaf, plant and canopy. In the case of a single leaf, the humidity deficit just outside the leaf boundary layer is unaffected by the leaf's transpiration. However in the case of the whole canopy, the joint transpiration from all the surrounding leaves affects the environment and the reference level has to be raised. The level at which the humidity deficit is unaffected by

the canopy and can be considered meteorologically driven, defines the surface layer. The height of this level depends on factors such as atmospheric stability. The conductance linking the immediate outside of the canopy (big-leaf boundary layer) with the surface layer is the **aerodynamic conductance**. The aerodynamic conductance accounts for the stability of the atmosphere and the roughness length. In models it controls the evaporation rates from other surfaces as well, like bare soil or ocean. Its importance when including vegetation processes in the atmosphere was already recognised by Richardson (2007) in what he defined as a 'film of vegetation'. Figure 2.3 shows the conductance diagram for carbon: from the atmosphere to the carboxylation sites; and for water vapour: from the substomatal cavity the atmosphere. Note that boundary layer conductance is missing in this diagram (it would be between g_c and g_{sc} and g_a) as some models do not include it.

2.3.5 Jarvis model for stomatal conductance

The Jarvis model for stomatal conductance was developed by analysing the correlation of stomatal conductance to environmental factors (Jarvis, 1976). The variables considered to have an effect on stomatal aperture in the original study were: quantum flux density (radiation), ambient CO_2 concentration, leaf-air humidity deficit, leaf temperature and leaf water status (leaf water potential). The mathematical expression of the Jarvis model is given by a maximum stomatal conductance (or minimum stomatal resistance) multiplied by several stress functions, one for each variable. The maximum stomatal conductance depends on the species, the leaf age etc. Each of the stress functions represents the effect of an environmental factor. The shape of these functions is derived from experimental measurements. The expression for stomatal conductance under the influence of variables $x_1 ... x_n$ would be:

$$g_s = g_{max} \cdot f_{x1} \cdot ... \cdot f_{xn} \tag{2.37}$$

Where $f_{x1}, ..., f_{xn}$ are normalised stress functions. Their values range from 0 to 1; 0 meaning complete restriction on the stomatal conductance and therefore no gas exchange, and 1 meaning no effect on the conductance by the corresponding variable.

An underlying assumption inherent in this method is that there are no synergistic interactions amongst the environmental factors. This is not true in nature, as the response of stomata to a stimulus is conditioned by the levels of other factors. On the contrary, the

A-g_s model is able to account for the interaction of the external factors in the response of stomata.

ECMWF's operational land surface model, CHTESSEL, uses this formulation to calculate the stomatal conductance for leaf evaporation. It uses stress functions for shortwave radiation, soil moisture, and atmospheric humidity deficit. In the coupled version CTESSEL, stomatal conductance for evaporation is derived from the photosynthetic rate (A-g_s formulation). Transpiration and photosynthesis become coupled in this version, as occurs in JULES. The coupled veresion, CTESSEL, has been used in the next chapters.

2.3.6 A-g_s model for stomatal conductance

With the implementation of photosynthesis modules in vegetation parameterization, a new way of calculating stomatal conductance was introduced. Most vegetation models now use the A-g_s photosynthesis scheme. It is based on the observed correlation between net carbon assimilation by the plant and the stomatal conductance (Cowan and Farquhar, 1977; Wong et al., 1978). This relation recognises that stomatal function has evolved to maximise carbon gain while minimising water loss.

Ball et al. (1987) developed this idea and analysed the relation between the stomatal conductance and the CO_2 assimilation under changing environmental factors. When radiation was varied, A and g_s showed a linear correlation, but changing values of humidity and carbon lead to a less straight forward relationship. Increases in CO_2 were followed by an increase in A but a reduction in stomatal conductance, and decreases in humidity made the stomata close with no change in A. These observations led to the development of the basic equation relating the stomatal opening to net carbon assimilation, humidity and CO_2:

$$g_s = kA\frac{h_s}{C_s} \tag{2.38}$$

where A is the CO_2 assimilation rate, h_s is relative humidity at the leaf surface, C_s is CO_2 concentration at the leaf surface, and k is a constant representing the sensitivity of stomatal conductance to assimilation, CO_2 concentration, humidity and temperature. This is known as the 'Ball-Woodrow-Berry' model (BWB). Unlike the Jarvis model, this expression combines together several of the factors known to affect stomatal conductance.

The use of relative humidity implies a dependence with temperature as well (for a fixed specific humidity). In this expression g_s is implicitly dependent on radiation, temperature and CO_2 concentration inside the stomata through the dependence of A on these variables. However it has been found that the slope k varies under soil moisture stress (Egea et al., 2011).

In A-g_s models the photosynthetic rate is calculated with a dedicated model for photosynthesis (e.g. Farquhar et al. (1980)). This model, although still empirical with regards to environmental variables on stomata, introduces the possibility of including a biochemical component to the derivation of stomatal conductance.

The BWB model has seen some if its terms being further revised and adjusted following laboratory experiments that added knowledge about plant's physiological processes. Experiments by Mott (1988) showed that stomata respond to CO_2 concentration at the intercellular spaces inside the chloroplast (C_i) rather than to that at leaf surface (C_s). C_s was replaced by C_i, and the CO_2 compensation point, Γ, was included to improve the behaviour at low values of C_i (Leuning, 1990).

$$g_s = kA\frac{h_s}{C_i - \Gamma} \tag{2.39}$$

The carbon dioxide compensation point is the concentration to which CO_2 has to be lowered so that respirative flux balances with photosynthetic intake, and the net flux is null (See Figure 2.1). Its value is mainly determined by the rate of photorespiration, for C_3 plants it ranges between 40-60 μmol mol^{-1} at 25°C and O_2 concentration of 210 mmol mol^{-1} (Canvin, 1979, 1990). It increases with increasing O_2 concentration and with temperature. In C_4 plants Γ has values below 5-10 μmol mol^{-1}, because of their insignificant photorespiration and their ability to photosynthesise at low concentrations of CO_2. The use of relative humidity at the leaf surface ($h_s = \frac{e_s}{e_{sat}(T_s)}$) in the BWB model has been modified in some cases to water vapour deficit ($D_s = e_{sat}(T_s) - e_s$). Both variables are related as follows:

$$h_s = 1 - \frac{D_s}{e_{sat}(T_s)} \tag{2.40}$$

Both variables include a dependence with (surface) temperature through the saturated water vapour. The use of D_s to represent air humidity has become widely adopted in

models. Studies by Mott and Parkhurst (1991) argued that in fact stomata respond to the actual rate of transpiration rather than to humidity.

Most models now determine the stomatal conductance for carbon from the net photosynthetic rate crossing the stomata and the CO_2 gradient from outside the stomata towards the inside (C_s-C_i).

$$g_s = 1.6 g_{sc} = \frac{1.6 A_n}{C_s - C_i} \tag{2.41}$$

Note that the net CO_2 flux crossing the stoma is the gross flux uptake for photosynthesis minus the leaf dark respiration ($A_n = A_g - R_d$).

The difference in CO_2 concentration outside and inside the stomata becomes a crucial value. Stomata are believed to behave in such way to maintain a rather constant ratio of carbon dioxide concentration outside and inside the pore (Wong et al., 1979). The carbon concentration inside the stoma is estimated based on the ambient humidity. Jacobs (1994) introduced a parametrization of the humidity control on stomata through the effect of humidity deficit on the ratio C_i/C_s. Jacobs's expression offers a closure to Equation 2.41 which is used by most models. The C_i/C_s ratio can be expressed as:

$$\frac{C_i}{C_s} = f + (1 - f)\frac{\Gamma}{C_s} \tag{2.42}$$

where Γ is the CO_2 compensation point and f is defined as:

$$f = \frac{C_i - \Gamma}{C_s - \Gamma} = f_o\Big(1 - \frac{D_s}{D_{max}}\Big) + f_{min}\frac{D_s}{D_{max}} \tag{2.43}$$

Parameters f_0, D_{max} and f_{min} are species specific. The term f ranges from f_{min} to f_0 as a function of D_s, the specific humidity deficit at the surface. Parameter f_{min} determines the C_i/C_s ratio when the stomata are closed ($D_s = D_{max}$), allowing a residual carbon flux representing imperfect stomatal closure or CO_2 absorption via the cuticula. Parameter f_0 is the value of f at saturation ($D_s = 0$). Variations in humidity are scaled by the parameter D_{max} which represents the maximum specific humidity that can be tolerated by the stomata (beyond which they close) and by the parameter f_0. In the most models, there is no variable to represent carbon concentration just outside the stomata (C_s) and the ambient CO_2 concentration (C_a) is used instead.

2.4 Implementation of gas exchange schemes in the models of this study

The next sections will describe gas exchange and photosynthesis parameterizations used in these schemes. The calculation of stomatal conductance is based on the already described A-g_s approach, with the exception of one version of ECMWF's model where carbon and transpiration are not coupled. In CHTESSEL the stomatal conductance for carbon is derived from photosynthetic rate calculations (A-g_s) while stomatal conductance for water vapour is calculated with the Jarvis approach (Boussetta et al., 2013b).

2.4.1 Implementation of photosynthesis model

Photosynthesis parameterization in models is based on observed processes at the leaf scale which are then scaled up to canopy level. These processes depend on solar radiation, soil moisture availability, CO_2 concentrations, temperature and physiological internal factors. The gas exchange formulation in JULES and CTESSEL is based on some of the aspects already described in the previous sections with particularities of each model. Table 2.1 presents a comparison summary of the main features of the photosynthesis schemes of models used in this thesis.

Table 2.1: Summary of JULES and CTESSEL models' characteristics

	JULES	**CTESSEL**
Model name	The Joint UK Land Environment Simulator	Carbon Hydrology Tiled ECMWF Scheme for Surface Exchange over Land
References	Best et al. (2011); Clark et al. (2011)	Viterbo and Beljaars (1995); Balsamo et al. (2009); Boussetta et al. (2013b)
Classification of vegetation	Broadleaf trees Needleaf trees C_3 grass C_4 grass Shrubs	High vegetation Low vegetation
Stomatal conductance	$g_s = \frac{1.6A}{1-f_0(1-\frac{D}{D_{crit}})} f_{CO_2}$	$g_s = \frac{1.6A}{1-[f_0(1-\frac{D_s}{D_{max}})+f_{min}(\frac{D_s}{D_{max}})]} f_{CO_2}$
CO_2 function	$f_{CO_2} = \frac{1}{C_s-\Gamma}$	$f_{CO_2} = \frac{1}{C_s-\Gamma}$
Soil moisture stress	Beta function applied to leaf level photosynthesis (Eq. 2.76)	Applied to g_m, D_{max} for low vegetation and g_m and f_0 for high vegetation. (See Tables 2.3 and 2.4)
Scaling from leaf level photosynthesis to canopy photosynthesis	Big leaf approach Multi-layer approach	Big leaf approach with differentiation between direct and diffuse radiation

2.4.2 Gross photosynthesis

In JULES the photosynthesis module (Clark et al., 2011; Cox et al., 1998) establishes the 3 limiting regimes for the leaf-level potential (unstressed by water) gross photosynthetic rate: (i) Rubisco-limited rate, (ii) Light-limited rate and (iii) Export limited (Sections 2.3.1 for C_3 photosynthesis and 2.3.1 for C_4).

There is a different formulation for C_3 (Farquhar et al., 1980) and C_4 photosynthesis (Collatz et al., 1992). The value of internal carbon concentration used to calculate the limited photosynthesis values is obtained with a simplified version of the Jacobs (1994) closure (Equation 2.43 with the f_{min} term neglected). The limiting regimes are given by:

(i) Rubisco limited rate (W_c)

$$W_c = \begin{cases} V_{cmax}\left(\frac{C_i - \Gamma}{C_i + K_c(1+O_a/K_o)}\right) & \text{for } C_3 \text{ plants} \\ V_{cmax} & \text{for } C_4 \text{ plants} \end{cases} \tag{2.44}$$

This equation is the same as proposed by Farquhar et al. (1980) (Eq. 2.17) with the addition of Γ, the CO_2 compensation point in the numerator. The CO_2 flux released by photorespiration is already subtracted from the gross photosynthesis in this expression. O_a, the partial pressure of atmospheric oxygen, is a constant fraction of the total atmospheric pressure. The different behaviours of carboxylation and oxygenation with temperature are represented through the dependencies with temperature of the Michaelis-Menten parameters for CO_2 and O_2, K_c and K_o. V_{cmax} (mol CO_2 $m^{-2}s^{-1}$) the maximum rate of carboxylation of rubisco is a parameter that can be adjusted for each plant functional type. For C_4 photosynthesis the limitation imposed here (J_e in Collatz et al. (1992), see Eq. 2.30) corresponds to the carboxylation process by rubisco in the bundle sheath cells. Because the carbon at these sites is already at high concentration thanks to the pumping mechanisms, photorespiration is inhibited, and does not depend the on the concentrations of CO_2 or O_2. The C_4 photosynthetic rate under this limitation only depends on temperature through V_{cmax}.

(ii) Light limited rate (W_j)

$$W_j = \begin{cases} \alpha \left(\frac{C_i - \Gamma}{C_i + 2\Gamma} \right) (1-\omega) I & \text{for } C_3 \text{ plants} \\ \alpha (1-\omega) I & \text{for } C_4 \text{ plants} \end{cases} \tag{2.45}$$

The light limited rate in JULES differs to the Farquhar and Wong (1984) formulation in its dependence with radiation. Instead of using an hyperbolic relation (Eq. 2.20), it presents a linear dependence with the absorbed radiation, which resembles the original equation in Farquhar et al. (1980) (Eq. 2.18). α is the maximum quantum efficiency of photosynthesis, which is regulated by the effect of photorespiration, as it is multiplied by the term in brackets to give the effective quantum efficiency. I is the PAR radiation and ω is the leaf scattering coefficient; the product $(1-\omega)I$ is the absorbed PAR radiation. In the case of C_4 photosynthesis, Γ is close to 0 and the quantum efficiency is independent of intercellular carbon concentration, being equal to its maximum value.

(iii) Export limited regime (W_e)

$$W_e = \begin{cases} 0.5 V_{cmax} & \text{for } C_3 \text{ plants} \\ 2 \times 10^4 V_{cmax} \frac{C_i}{P_{atm}} & \text{for } C_4 \text{ plants} \end{cases} \tag{2.46}$$

For C_3 plants, it represents the rate at which photosynthetic products are distributed from the chloroplast to other parts of the plant. The equation used in JULES does not resemble the one described in Sharkey et al. (2007). It determines a rate which is half the maximum rate of photosynthesis. In the case of C_4 plants it represents the process of the initial carboxylation by PEPCarboxylase, with dependence on C_i and air pressure, P_{atm}. This limitation could be considered as the carbon limitation in C_4 plants, since it is the process that depends on carbon availability and only becomes limiting at very low carbon concentrations.

The photosynthetic rate is dependent on the maximum rate of carboxylation of rubisco, V_{cmax} (mol CO_2 m^2 s^{-1}), under regimes (i) and (iii) for all plants. V_{cmax} is calculated from its value at 25 °C, V_{cmax25}, using a temperature dependence equation based on Equation 2.27:

$$V_{cmax} = \frac{V_{cmax25} Q_{10}^{0.1(T_c - 25)}}{\left[1 + e^{0.3(T_l - T_{upp})}\right] \left[1 + e^{0.3(T_{low} - T_l)}\right]} \tag{2.47}$$

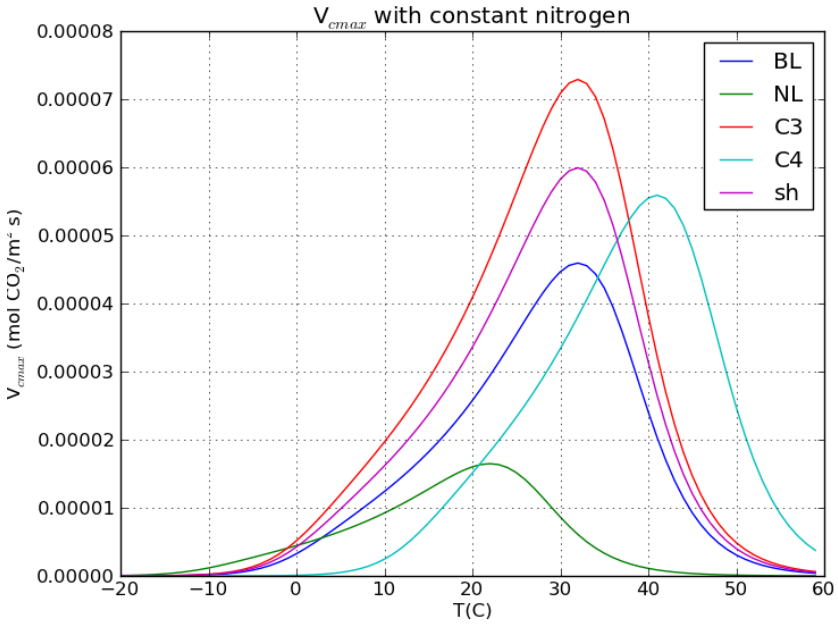

Figure 2.5: V_{cmax} in JULES as a function of temperature for a constant nitrogen content; shows an exponential increase towards an optimum temperature and decrease beyond this temperature.

the temperature dependence is regulated by PFT-specific parameters, T_{upp} and T_{low}. V_{cmax25} is linearly dependent on the leaf's nitrogen content, n_0 (kg N (kg C)$^{-1}$)

$$V_{cmax25} = n_0 \cdot n_{eff} \tag{2.48}$$

with n_{eff} a constant with values of 0.0008 and 0.0004 mol CO_2 m^{-2} s^{-1} (kg C (kg N)$^{-1}$ for C_3 and C_4 plants, respectively. Figure 2.5 shows V_{cmax} as a function of temperature for each PFT in JULES.

The CO_2 compensation point included in the rubisco limited rate (Eq. 2.44) is given by:

$$\Gamma = \begin{cases} \frac{O_a}{2\tau} & \text{for } C_3 \text{ plants} \\ 0 & \text{for } C_4 \text{ plants} \end{cases} \tag{2.49}$$

with τ the rubisco specificity for CO_2 relative to O_2, which varies with temperature according to:

$$\tau = 2600 Q_{10rs}^{0.1(Tc-25)} \tag{2.50}$$

with $Q_{10rs} = 0.57$.

The Michaelis-Menten parameters are also temperature dependent:

$$\begin{aligned} K_c &= 30 Q_{10Kc}^{0.1(T_c-25)} \\ K_c &= 3 \cdot 10^4 Q_{10Ko}^{0.1(T_c-25)} \end{aligned} \tag{2.51}$$

with $Q_{10Kc} = 2.1$ and $Q_{10Ko} = 1.2$.

The rate of gross photosynthesis is then calculated from the three limiting regimes with a set of quadratic equations, which assure a gradual transition from one limitation to another.

$$\begin{aligned} \beta_1 W_p^2 - W_p(W_c + W_l) + W_c W_l = 0 \\ \beta_2 W^2 - W(W_p + W_e) + W_p W_e = 0 \end{aligned} \tag{2.52}$$

where W_p is the smooth minimum of W_c and W_l. Finally, W is the gross photosynthetic rate. This smoothing is argued to represent a co-limitation amongst rates. The values of the co-limitation coefficients are empirically determined (Collatz et al., 1990), in JULES the values $\beta_1 = 0.83$ and $\beta_2 = 0.93$ are used.

The photosynthesis formulation in CTESSEL is based on Goudriaan et al. (1985) as modified by Jacobs (1994); Jacobs et al. (1996). Its performance once embedded has been tested in Boussetta et al. (2013b). This photosynthesis scheme is also used by ISBA-A-gs land surface model (Interactions between Soil, Biosphere and At-mosphere, CO2-reactive), see Calvet et al. (1998). The model distinguishes between the two first limiting situations: CO_2 as the limiting factor (for relatively high light intensity) and light as the limiting factor (at relatively high CO_2 concentrations). Both cases are combined smoothly to yield a net photosynthesis rate, without calculating them separately. The export limiting regime is not taken into account explicitly in CTESSEL. The same formulation is used for both C_3 and C_4 photosynthetic pathways, with specific parameters for each case.

(i) CO_2 limiting regime.

At high light intensities net assimilation acquires the value of A_m (mg CO_2 m^{-2} s^{-1}), which is defined as the photosynthetic rate at saturating light intensity. It is given by:

$$A_m = g_m(C_i - \Gamma) \tag{2.53}$$

here, g_m (mm s^{-1}) is the mesophyll conductance, a parameter that quantifies the slope of the CO_2 response curve at high light intensity, so has an equivalent role to

V_{cmax} in JULES. It must be noted that although g_m has the units of conductance, it does not represent a conductance in the sense that it does not directly regulate the CO_2 flux between stoma and mesophyll as described in Section 2.3.3. The light saturated photosynthesis rate, A_m, has an absolute maximum related to biochemical limitations, imposed by $A_{m,max}$. The value for A_m is thus expressed with an asymptotic exponential function of C_i reaching $A_{m,max}$ for high values of C_i.

$$A_m = A_{m,max}\left[1 - e^{\frac{-g_m(C_i-\Gamma)}{Am,max}}\right] \tag{2.54}$$

$A_{m,max}$ is defined as the absolute limit to photosynthetic rate in full sunlight and non-limiting CO_2 concentration. It is a plant specific parameter that depends on the ability of plants to regenerate RuBP. For saturating values of solar radiation the photosynthetic rate is A_m, for lower radiation, light becomes limiting and the rate of photosynthesis will stay below A_m.

[ii) Light limiting regime.

At very low light intensities photosynthetic rate has the well known linear dependency with absorbed PAR, I_a:

$$A_j = \epsilon I_a \tag{2.55}$$

The slope of the light response curve is the quantum efficiency, ϵ (mg CO_2 (J PAR)$^{-1}$), which varies with CO_2 concentration at the leaf surface and has a maximum value ϵ_0.

$$\epsilon = \epsilon_0 \frac{C_s - \Gamma}{C_s - 2\Gamma} \tag{2.56}$$

where Γ is the CO_2 compensation point. The formulation for the CO_2 assimilation under light limiting regime shown here is the same as the one used in JULES (Eq. 2.45). The absorbed PAR, I_a is equivalent to $I(1-\omega)$ and ϵ_0 is equivalent to α.

The CO_2 and radiation limiting regimes (Eqs. 2.54 and 2.55) are combined in a smooth exponential transition:

$$A_g = (A_m + R_d)\left[1 - e^{\frac{-\epsilon I_a}{A_m+R_d}}\right] \tag{2.57}$$

For high enough radiation (saturation levels), $A_n = A_g - R_d = A_m$, and the photosynthesis is defined by the mesophyll conductance (Eq 2.53).

In CTESSEL some parameters are not independent, and relationships have been established between them, following analyses conducted by Calvet (2000) and Calvet et al. (2004). For low vegetation or herbaceous species, Calvet (2000) analysed 63 datasets of gas exchange measurements for various species in well watered conditions both at the leaf level and field scale. The data were fit using the ISBA A-g_s model to derive the maximum unstressed leaf-to-air saturation deficit, D^*_{max}, and the unstressed mesophyll conductance at 25°C g^*_{m25}, for each data set. The asterisk denotes unstressed conditions. They found a logarithmic relation between D_{max} and g_m for the herbaceous species of both C_3 and C_4 plant types.

$$ln(g^*_m) = a - b\ ln(D^*_{max}) \tag{2.58}$$

where a has values of 5.32 and 2.38, and b has values of 0.89 and 0.61, respectively for C_3 and C_4 plant types. This equation also plays a role in the soil moisture stress formulation in CTESSEL because g_m and D_{max} vary but remain correlated according to Eq. 2.58 also in the case of drying conditions. Equation 2.58 was not able to describe the behaviour of woody species. Calvet et al. (2004) further explored the model parameters for trees. In this case, 32 datasets of measurements of woody species were gathered. The parameters derived were g^*_{m25}, D^*_{max} and f^*_0 (maximum value of f in Jacob's Equation 2.43). A correlation between the mesophyll conductance and f^*_0 was identified in both coniferous and broadleaf trees.

$$ln(g^*_m) = a_w - b_w\ f^*_0 \tag{2.59}$$

where $a_w = 4.7$ and $b_w = 7$, the subscript w denotes woody. This relationship can be applied in stressed conditions with lower intercept $a_w = 2.8$.

CTESSEL applies these constraints to its plant parameters, reducing the number of adjustable parameters. In the case of low vegetation, D_{max} is derived from the prescribed g_m according to Eq. 2.58. For high vegetation, f_0 is derived from g_m according to Eq. 2.59. The soil moisture stress effect on photosynthesis is applied via these parameters and is explained in more detail in Section 2.4.6.

The temperature dependent parameters in CTESSEL are the Γ, $A_{m,max}$ and g_m. The temperature dependence is described making use of the Q_{10} parameters (Eq. 2.26) and with inhibition modification in the case of $A_{m,max}$ and g_m (Eq. 2.27). The formulations

are as follows:

$$\Gamma = \Gamma(25°\mathrm{C})Q_{10\Gamma}^{(T-25)/10} \tag{2.60}$$

$$g_m = \frac{g_m(25°\mathrm{C})Q_{10gm}^{(T-25)/10}}{\left(1+e^{0.3(T_{1gm}-T)}\right)\left(1+e^{0.3(T-T_{2gm})}\right)} \tag{2.61}$$

$$A_{m,max} = \frac{A_{m,max}(25°\mathrm{C})Q_{10Am,max}^{(T-25)/10}}{\left(1+e^{0.3(T_{1Am,max}-T)}\right)\left(1+e^{0.3(T-T_{2Am,max})}\right)} \tag{2.62}$$

where $Q_{10\Gamma}$, Q_{10gm}, $Q_{10Am,max}$, T_{1gm}, T_{2gm}, $T_{1Am,max}$ and $T_{2Am,max}$ are constants affecting the sensitivity to the leaf temperature.

The adjustable parameters have been adapted to each functional type. JULES has five plant functional types and CTESSEL has 20 surface types (also including deserts or inland water). Table 2.2 contains the vegetation specific parameters for JULES five PFTs; broadleaf trees, needle leaf trees, C_3 grasses, C_4 grasses and shrubs. From CTESSEL vegetation types, only the most comparable to JULES PFTs are shown in Table 2.2; deciduous broadleaf, evergreen needle leaf, short grass, tall grass and deciduous shrubs. The nomenclature and units shown follow each model's documentation, for coherence with literature. In the next chapters, these are the parameters used by default by each model for each vegetation type, both at the leaf level (Chapter 3) and at the canopy level (Chapters 4 and 5).

Relating JULES's V_{cmax} to CTESSEL's g_m and $A_{m,max}$

V_{cmax} is proportional to both g_m and $A_{m,max}$. The role played by g_m in CTESSEL is to regulate the radiation saturated rate of photosynthesis. It determines the slope of the CO_2 response curve of photosynthesis at low C_i and high light intensities. It can be related to parameters of the Farquhar et al. (1980) formulation by evaluating the slope of C_3 carbon limited photosynthesis (Eq. 2.44) at $C_i = \Gamma$, and doing the same for CTESSEL formulation (Eq. 2.68), thus relating mesophyll conductance with V_{cmax} and the Michaelis-Menten parameters (Jacobs, 1994).

$$\frac{dA_n}{dC_i} = g_m = \frac{V_{cmax}}{C_i + K_c(1+O_a/K_o)} \tag{2.63}$$

Table 2.2: Models vegetation parameter values

Parameter	Description (Units)	BL	NL	C3	C4	Sh
JULES						
α	Quantum efficiency (mol CO_2 (mol photons)$^{-1}$)	0.08	0.08	0.12	0.060	0.08
D_{crit}	Maximum specific humidity deficit (kg kg^{-1})	0.09	0.06	0.1	0.075	0.1
f_0	Factor related to C_i/C_a (-)	0.875	0.875	0.9	0.8	0.9
n_0	Top leaf nitrogen concentration (kg N (kg C)$^{-1}$)	0.046	0.033	0.073	0.06	0.06
n_{eff}	Constant related to V_{cmax}(mol CO_2 m^{-2} s^{-1} kg C (kg N)$^{-1}$)	0.008	0.008	0.008	0.004	0.008
T_{low}	Lower temperature parameter (°C)	0	-10	0	13	0
T_{upp}	Upper temperature parameter (°C)	36	26	36	45	36
f_{dr}	Dark respiration coefficient (-)	0.015	0.015	0.015	0.025	0.015
CTESSEL						
ϵ_0	Quantum efficiency (mg CO_2 (J PAR)$^{-1}$)	0.0142	0.0142	0.0142	0.0117	0.0142
D_{max}	Maximum specific humidity deficit (kg kg^{-1})	0.109	0.124	Eq.2.58	Eq.2.58	Eq.2.58
f_0	Factor related to C_i/C_a (-)	Eq. 2.59	Eq. 2.59	0.65	0.7	0.72
g_m	Mesophyll conductance (m s^{-1})	1.4	0.8	1.3	2.3	0.9
$A_{m,max}$	Upper limit on carbon limited assimilation (mg CO_2 m^{-2} s^{-1})	1.83	2.2	0.2	0.2	0.15
T_{1gm}	Lower temperature parameter for g_m (°C)	5	5	5	13	5
T_{2gm}	Upper temperature parameter for g_m (°C)	36	36	36	36	36
$T_{1m,max}$	Lower temperature parameter for $A_{m,max}$ (°C)	8	8	8	13	8
$T_{2m,max}$	Upper temperature parameter for $A_{m,max}$ (°C)	38	38	38	38	38

Alternatively, JULES's V_{cmax} can also be related to $A_{m,max}$ (Collatz et al., 1991), instead of g_m:

$$V_{cmax} = 2A_{m,max} \tag{2.64}$$

This relation was used in a comparison between MOSES and a A-g_s scheme (Steeneveld, 2002). However, it should be noted that these two relationships are not unequivocal, making it impossible to directly relate model parameters. Although in reality this occurs even between models that use apparently the same parameter (e.g. V_{cmax} has lower values in models that contain a diffusive mesophyll conductance than in those that do not).

2.4.3 Net photosynthesis

The gross photosynthetic rate, A_g, is the amount of CO_2 taken up by the plant for photosynthesis. The outgoing CO_2 fluxes at the leaf are are photorespiration, R_p, and leaf dark respiration, R_d. The CO_2 loss via photorespiration has already been accounted for in the calculation of gross photosynthesis. The net flux of CO_2 through the stomatic pores is the difference between the incoming or gross photosynthesis minus what is lost by leaf dark respiration.

$$A_n = A_g - R_d \tag{2.65}$$

A_n at the leaf level is the flux which passes through the stomata, and it is directly linked to the stomatal conductance via Equation 2.41.

In JULES the net photosynthetic rate is therefore:

$$A_n = W - R_d \tag{2.66}$$

with leaf dark respiration as a fraction of V_{cmax}:

$$R_d = f_{dr} V_{cmax} \tag{2.67}$$

where f_{dr} is 0.015 for C_3 and 0.025 for C_4.

In CTESSEL net photosynthesis is expressed by:

$$A_n = (A_m + R_d)\left[1 - e^{\frac{-\epsilon I_a}{A_m + R_d}}\right] - R_d \tag{2.68}$$

leaf dark respiration is a fraction of the CO_2 limited assimilation rate:

$$R_d = \frac{A_m}{9} \tag{2.69}$$

Consequently, in both models, leaf dark respiration is a function of temperature through V_{cmax} (Eq. 2.67) or A_m (Eq. 2.69).

2.4.4 Stomatal conductance

Once the net leaf photosynthesis that enters through the stomata for photosynthesis is known, the stomatal aperture can be calculated with Eq. 2.41, if the carbon concentrations inside and outside the leaf are known. It is assumed that the CO_2 just outside the stoma, C_s, is equal to the atmospheric CO_2, C_a. The carbon concentration inside the stomata is derived from C_a and the specific humidity deficit with Jacob's closure Equation 2.43. This step is effectively where the demand and supply functions introduced in Figure 2.1 are combined.

There are some differences between the models in this calculation. To calculate C_i JULES does not include the term f_{min} in Eq. 2.43. Stomatal conductance in JULES takes the form:

$$g_s = \frac{1.6A_n}{\left[1 - f_0(1 - \frac{D}{D_{crit}})\right]} \frac{1}{C_s - \Gamma} \tag{2.70}$$

In the case of CTESSEL the term f_{min} is the value of f when D_s=D_{max} and is given by:

$$f_{min} = \frac{g_c}{g_c + g_{min}} \tag{2.71}$$

A minimum photosynthetic rate is subtracted to the net photosynthetic rate before dividing by the gradient of carbon concentrations. This minimum photosynthetic rate, A_{min}, is related to the CO_2 diffusion inwards via the cuticle, represents the residual photosynthesis rate (at full light intensity) when stomata are closed:

$$A_{min} = g_m(C_{min} - \Gamma) \tag{2.72}$$

It is associated to a minimum CO_2 concentration, C_{min} corresponding to a minimum value of f, f_{min}. It is calculated at full light intensity, assuming carbon limitation and stomatal

closure, therefore A_{min} and C_{min} are assumed to be in the linear part of the C_i response curve, as explained in Jacobs (1994). C_{min} is defined by:

$$C_{min} = \frac{g_c C_s + g_m \Gamma}{g_c + g_m} \tag{2.73}$$

Finally, the net photosynthetic rate is modified for the limiting cases of very dry air and the carbon flux low light. The stomatal conductance in CTESSEL takes the form:

$$g_s = \frac{1.6\left[A_n - A_{min}\left(\frac{D_s}{D_{max}}\frac{A_n+R_d}{A_m+R_d}\right) + R_d\left(1 - \frac{A_n+R_d}{A_m+R_d}\right)\right]}{C_s - C_i} \tag{2.74}$$

Equations 2.70 and 2.74 are solved via an iterative process. The calculated stomatal conductance is used to correct the humidity deficit at the canopy level. This ensures consistency of humidity and transpiration. The corrected humidity is then taken into account and the internal carbon modified accordingly, and photosynthesis rates recalculated.

2.4.5 Plant respiration

The leaf dark respiration is only one part of the total plant respiration, that which occurs through the leaves, the roots and stems may also contribute. In JULES plant respiration is split in two terms: growth respiration and maintenance respiration. Growth respiration is a fixed fraction of the net primary productivity. Maintenance respiration is divided in terms from the leaves, stem and roots. The maintenance respiration from the leaves is what has already been described as leaf dark respiration (Eq. 2.67). Maintenance respiration depends on temperature and nitrogen contents, equations can be found in Best et al. (2011).

In CTESSEL all respiration from other parts of vegetation, apart from leaf dark respiration, is included in a term called heterotrophic respiration. Heterotrophic respiration depends on soil temperature, soil moisture, snow depth and vegetation type (ECMWF, 2015).

2.4.6 Soil moisture stress

The are several formulations employed by land surface models to represent the limitation on photosynthesis and transpiration exerted by the availability of soil moisture in the root zone. The most straight forward approach is a multiplicative factor scaled linearly by the volumetric soil moisture. This concept of soil moisture content as a limitation to evaporation dates back to the first land surface models (Manabe, 1969). When soil moisture falls below a certain threshold the rate of evaporation stays below the potential evaporation and scales linearly with soil moisture.

When applied to vegetation, the upper limit was initially set to field capacity. However, for moisture levels near field capacity plants do not generally decrease photosynthesis. The water limitation occurs for lower levels of moisture in plants than it does in bare soil. Therefore a lower threshold (critical point) was used as upper limit. The multiplicative factor ranges from 0 (wilting plants) to 1 (non stressed plants). This stress factor can be applied to different variables of the photosynthesis model: to the gross photosynthesis directly (Cox et al., 1999) or to mesophyll conductance (Calvet et al., 1998). Because the linear dependence with soil moisture seems to underestimate transpiration, non-linear relations have been tested (Ronda et al., 2001; Egea et al., 2011).

The use of leaf water potential as a variable for the response of A and g_s has been tested; for example Jarvis (1976) used a multiplicative factor on g_s with an exponential dependence on ψ_l. However this approach seems to be less appropriate than using soil water indicators because of isohydric plants whose leaf water potential tends to stay rather constant despite moderate dry conditions, as opposed to anhisohydric behaviour (Egea et al., 2011). On the contrary, soil matric potential seemed to outperform volumetric soil moisture as the driving variable for transpiration reduction due to water scarcity, as it was better able to capture the shape of relative transpiration as a function of the fraction of transpirable soil water (Verhoef and Egea, 2014).

In JULES soil moisture stress is applied to the net photosynthesis rate by multiplying the potential photosynthetic rate by the stress function β (Cox et al., 1998) calculated as a combination of all the soil layers.

$$\beta = \sum_{k=1}^{4} \beta_k r_k \tag{2.75}$$

where r_k is the root density at each soil layer and the stress functions are calculated as:

$$\beta_k(\theta_k) = \begin{cases} 0 & \theta_k \leq \theta_{pwp} \\ \frac{\theta_k - \theta_{pwp}}{\theta_c - \theta_{pwp}} & \theta_{pwp} < \theta_k \leq \theta_c \\ 1 & \theta_k > \theta_c \end{cases} \tag{2.76}$$

where θ_k (m^3 m^{-3}) is the unfrozen soil moisture content in layer k and θ_{pwp} (m^3 m^{-3}) and θ_c (m^3 m^{-3}) are the volumetric soil moisture contents at the permanent wilting point and a critical soil moisture content. The water availability to roots is largely determined by how tightly the water is held by the pores in the solid phase of the medium and this is quantified by the matric potential (see Equations 2.15). Permanent wilting point corresponds to a matric potential of ψ = -1500 kPa, and the critical point to ψ= -33 kPa. The critical point is between permanent wilting point and field capacity (ψ = -10 kPa) to maintain stress-free transpiration at values below field capacity. The volumetric values of θ_{pwp} and θ_c vary with the soil texture. Although a fine soil medium having large specific surface area may hold more water than a course medium, less water may be available for the roots.

The soil moisture stress applied in CTESSEL follows a more complex parameterization as proposed by Calvet (2000) and Calvet et al. (2004). The parameterization combines the effect of soil moisture with the sensitivity of stomata to air humidity, recognising the interaction between soil and atmospheric water stresses. It predicts different behaviour for high (Calvet et al., 2004) and low vegetation (Calvet, 2000) and offers defensive and offensive strategies. The defensive and offensive strategies could be associated to the isohydric and anisohydric behaviours described in Chapter 1.

The parameters directly affected are (D_{max}-g_m) in the case of herbaceous species and (g_m-f_0) in the case of woody species (low vegetation and high vegetation in CTESSEL, respectively). The mesophyll conductance g_m is related to the the photosynthetic capacity at high light intensities. D_{max} and f_0 are parameters that control the sensitivity of stomatal aperture to air humidity by modulating the internal CO_2 concentration in Jacob's humidity equation (Equation 2.43). The lower D_{max}, the higher the sensitivity of stomata

Table 2.3: Herbaceus species soil moisture stress parameterization from Calvet (2000)

Vegetation	**Strategy**	**Stress**	$\mathbf{D}_{max}$	$\mathbf{g}_m$
Low vegetation	Defensive strategy	$f_2 \geq f_{2c}$	$D_{max} = D^N_{max} + (D^*_{max} - D^N_{max})\left(\frac{f_2 - f_{2c}}{1 - f_{2c}}\right)$	$g_m = exp\{a - b\ ln(D_{max})\}$
		$f_2 < f_{2c}$	$D_{max} = D^N_{max}$	$g_m = exp\{a - b\ ln(D^N_{max})\}$
	Offensive strategy	$f_2 \geq f_{2c}$	$D_{max} = D^X_{max} + (D^*_{max} - D^X_{max})\left(\frac{f_2 - f_{2c}}{1 - f_{2c}}\right)$	$g_m = exp\{a - b\ ln(D_{max})\}$
		$f_2 < f_{2c}$	$D_{max} = D^N_{max} + (D^X_{max} - D^N_{max})\left(\frac{f_2}{f_{2c}}\right)$	$g_m = exp\{a - b\ ln(D^X_{max})\}$

a = 2.38 for C_3 species and 5.323 for C_4 species, and b = -0.6103 for C_3 species and -0.8929 for C_4 species. CTESSEL uses f_{2c} = 0.3, D^N_{max} = 0.03 kg kg^{-1}, D^X_{max} = 0.3 kg kg^{-1}

Table 2.4: Woody species soil moisture stress parameterization from Calvet et al. (2004)

Vegetation	**Strategy**	**Stress**	$\mathbf{g}_m$	$\mathbf{f}_0$
High vegetation	Defensive strategy	$f_2 \geq f_{2c}$	g_m=g^*_m	$f_0 = f^N_0 + (f^*_0 - f^N_0)\left(\frac{f_2 - f_{2c}}{1 - f_{2c}}\right)$
		$f_2 < f_{2c}$	$g_m = g^*_m\left(\frac{f_2}{f2c}\right)$	$f_0 = \Big[a_{ws} - ln(g_m)\Big]/b_w$
	Offensive strategy	$f_2 \geq f_{2c}$	g_m=$g^N_m + (g^*_m - g^N_m)\left(\frac{f_2 - f_{2c}}{1 - f_{2c}}\right)$	$f_0 = f^*_0$
		$f_2 < f_{2c}$	$g_m = g^N_m\left(\frac{f_2}{f_{2c}}\right)$	$f_0 = \Big[a_{ws} - ln(g_m)\Big]/b_w$

a_{ws} = 2.8 and b_w = 7

to air specific humidity deficit (through more variability of internal carbon). The same applies to f_0, the higher this value, the more variability of internal carbon for the same change in humidity deficit. The effect of soil moisture stress on these parameters depends on the degree of the water stress; evaluated with a soil moisture stress index, f_2, calculated as in Eq. 2.76. Soil moisture stress is considered moderate when f_2 is above the critical value f_{2c} and it becomes severe when it falls below the critical value f_{2c}.

For low vegetation the relationship found for unstressed herbaceous plants relating mesophyll conductance with D_{max} (Equation 2.58) is maintained under moderate stressed conditions. For a moderate soil moisture stress in the defensive strategy D_{max} diminishes; in the offensive case D_{max} increases linearly with f_2. This tendency is maintained until the critical stress is reached. For moderate stress, the defensive strategy implies an increase in sensitivity to air humidity (enhanced stomatal closure due to dry air conditions) but at the same time an increase in photosynthetic capacity via the increase in g_m. By contrast, in the case of the offensive strategy, the increase in D_{max} induces a decrease in sensitivity to air humidity and a decrease in photosynthetic capacity. For more pronounced water stress, in the defensive case D_{max} stays at a minimun constant (D^N_{max}) while g_m decreases linearly with the stress function. In the offensive case D_{max} drops for severe stress while g_m remains constant.

As a summary Calvet's defensive and offensive strategies can be related to the drought avoiding and tolerant water management strategies as follows:

- For moderate soil moisture stress the defensive strategy reduces D_{max}, increasing stomata sensitivity to air humidity, which is asociated to drought avoiding strategy. Conversely, the offensive strategy tolerates drought by increasing D_{max}.
- For severe soil moisture stress the value of g_m can be related to the plant strategy. A rapid decrease in the defensive case could correspond with a dormant state, characteristic of a drought avoiding strategy. Conversely, the constant rate maintained in the offensive case can be related to the mechanisms of growing deeper roots or developing a rapid life cycle.

In the case of high vegetation, the lack of soil moisture will cause g_m to vary and/or f_0 while D_{max} has a constant tabulated value. The relationship found for unstressed

conditions between g_m and f_o (Equation 2.59) will still hold for severe stress but with a lower value of a:

$$ln(g_m) = a_{ws} - b_w \ f_0 \tag{2.77}$$

with a_{ws}=2.8, where the subindex stands for woody and stressed. For moderate soil moisture stress g_m remains unaffected while f_0 decreases linearly with soil moisture until the soil moisture critical value, where f_0 reaches a minimum value (f_0^N). For more pronounced water stress g_m is reduced linearly to zero and scaled by the soil moisture content while f_0 increases according to Equation 2.77. In the offensive strategy, for moderate water stress g_m is initially reduced until g_m^N while f_0 maintains its unstressed value. In both cases f_0 for very low water contents is limited to a certain value (Calvet et al. (2004) proposed 0.99). Increases in f_0 have a similar effect on photosynthesis as reductions in D_{max}, as can be deducted from Jacobs Equation (Eq. 2.43); the variation of carbon internal concentration due to air humidity is regulated by f_0.

2.4.7 Upscaling from leaf to canopy

The photosynthetic rate described so far, A_n, represents the net carbon flux at the leaf level, thus the μmol of CO_2 assimilated per leaf area and per unit of time for known conditions in the leaf environment (incident PAR, leaf temperature and humidity, etc.). For application within a LSM, the carbon fluxes and stomatal conductance need to be scaled up to the canopy level. The total CO_2 exchange by a vegetated surface requires information about canopy structure and radiation profile. The upscaling method uses a canopy radiative transfer formulation. The biochemical properties of vegetation are either assumed to be vertically constant (big-leaf) or to vary with height (multi-layer).

Big-leaf

The simplest method is to assume that leaf biochemical properties do not vary with height within the canopy. This is called the big-leaf approach, since the canopy is considered as one single layer with identical properties. The only variable allowed to vary is radiation, which decreases as it is scattered and absorbed on its way down the canopy. There are different formulations for the attenuation of radiation by the canopy, as explained later. The total amount of CO_2 capture and evapotranspiration depend on the total area of leaves. Therefore the leaf area index (LAI) is a crucial parameter in the upscaling process.

Beers law

The solar wavelengths that are useful for plant photosynthesis (PAR) are between 400-700 nm, and this band is considered to be 48% of the total incoming solar radiation. The within canopy radiation scattering and absorption depend on the abundance, size and position of leaves, as well as the intensity of the radiation itself. Beer's law (Monsi and Saeki, 2005) is frequently used to describe solar radiation's (or PAR's) attenuation by the vegetation. It assumes an exponential decay of radiation with depth from the top of the canopy, described by:

$$I(z) = I_0(h)e^{-K_{ext}L} \tag{2.78}$$

where $L = LAI(h - z)/h$ is the cumulative leaf area index above the point in question (0 at the top of the canopy, LAI at the bottom), K_{ext} the extinction coefficient and I_0 the incoming short-wave radiation at the top of the canopy. The value of K_{ext} is related to the leaf angle and leaf transmittance; grasses and inclined leaves produce low extinction (K_{ext} = 0.3-0.5), whereas broadleaf trees with typically big and horizontal leaves produce high extinction (K_{ext} = 0.7), values from Monsi and Saeki (2005).

JULES

In JULES there are multiple options to upscale leaf photosynthesis to the canopy level as well as the big-leaf method. Several multi-layer canopy methods have been developed; these introduce more complex radiative interactions within the canopy, a vertical gradient of V_{cmax}, inclusion of respiration inhibition, separate photosynthesis for direct and diffuse radiation, or inclusion of sunflecks, (Mercado et al., 2007). Next, the different scaling options in JULES are reviewed:

Big-leaf (Switch `can_rad_mod =1` in JULES settings).

Leaf photosynthesis is supposed to vary proportionally with the vertical distribution of irradiance (Sellers et al., 1992) based on Beer's law (Monsi and Saeki, 2005). Photosynthesis at a certain level is the leaf level photosynthesis at the top of the canopy (A_n, calculated for the light intensity reaching the top of the canopy), attenuated exponentially by the accumulated LAI (L) and the PAR extinction coefficient (K_{ext}).

$$A_l = A_n e^{-K_{ext}L} \tag{2.79}$$

The photosynthesis of the entire canopy is calculated as the integral over the leaf area

index represented by the variable L which takes the value LAI.

$$A_c = \int_0^{LAI} A_l dL = A_n \frac{\left[1 - e^{-K_{ext} LAI}\right]}{K_{ext}} \tag{2.80}$$

Equivalent equations are used to upscale stomatal conductance and dark leaf respiration. Default JULES settings use $K_{ext} = 0.5$ for all PFTs. Hence the big-leaf upscaling method in JULES (Sellers et al., 1992) calculates canopy photosynthesis by multiplying the leaf photosynthesis at the top of the canopy by a factor that depends exponentially on LAI. This is a simple computationally efficient method as it only requires the solution of the A-g_s leaf level model for a single leaf (or layer). However, it assumes that W_c, W_l, W_e all vary in the same way down through the canopy and the limiting regime for photosynthesis at the top of the canopy prevails throughout the canopy. This is certainly not true in dense forests, where the top has enough light but the lower branches are light limited.

JULES run with the big-leaf option presents light saturation of photosynthesis at low levels of radiation (Clark et al., 2011). The model fails to reproduce correctly the diurnal cycle for photosynthesis showing an underestimation with a flat evolution at midday in temperate forest (Clark et al., 2011) and in a tropical forest (Mercado et al., 2007). The diurnal cycle reproduced in Mercado et al. (2007) with the big-leaf approach also presents an overestimation of photosynthesis in the morning and dawn, resulting in a rather flat cycle. This coincides with Jogireedy et al. (2006) findings that Beer's law attenuates too little for low solar angles and diffuse radiation. However it should be noted that these shortcomings, although attributed to the big-leaf approach, come from the missrepresentation of the PAR absorption profile. It is the assumption of a constant attenuation throughout the canopy in Beer's law, rather that the assumption of constant photosynthetic properties throughout the canopy in the big-leaf method, that is flawed in JULES.

Multilayer approach (Switch `can_rad_mod =2-5` in JULES settings).
To overcome the lack of skill to reproduce the diurnal cycle and to avoid the early light saturation of photosynthesis, a more complex upscaling was introduced. The two-stream radiation model of Sellers et al. (1992) is used to calculate the radiation interception in the canopy. The vertical profiles (upward and downward) of direct and diffuse PAR radiation are solved separately as a function of incident direct and diffuse radiation at the top of the canopy, solar zenith angle and leaf radiative properties. Beer's attenuation law agrees with

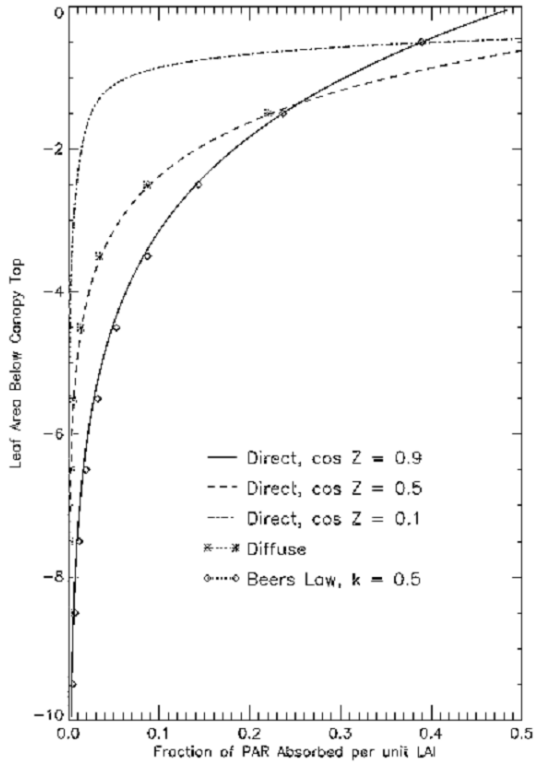

Figure 2.6: Vertical profiles of fraction of absorbed PAR, using Beer's law and the two-stream method. Beer's law agrees with the two-stream method for high solar angles Z (cos Z = 0.9) but underestimates the attenuation at the top of the canopy for low solar angles (cos Z = 0.1). Figure from Jogireedy et al. (2006).

the two-stream approach when the solar radiation comes from a high solar zenith angle (vertical beam), but differs markedly for low angles as shown in Figure 2.6 (Jogireedy et al., 2006). The two-stream approach is highly dependent on the solar angle, presenting a very strong attenuation in the higher layers of the canopy when the sun is low, whereas Beer's exponential law, as implemented in JULES (with $K_{ext} = 0.5$), yields the same profile independently of the solar zenith angle. The canopy is divided into n horizontal layers (typically 10) of equal LAI increments. The leaf level photosynthesis model is then computed for each layer with the corresponding incident PAR for each level from the two-stream profile. The total photosynthesis and stomatal conductance are calculated as the average of the value at each layer, multiplied by the LAI increment. The V_{cmax} was initially kept constant for all layers to avoid spurious big-leaf behaviour if applying Beer's law to V_{cmax} (Jogireedy et al., 2006).

Another approach, using two layers, aims to separate the canopy into non-light limited at the top and light limited at the bottom and calling the leaf level model for the average radiation of these two classes. The idea of separating into sunlit leaves (non-light limited) and shaded leaves (light limited) was also developed by De Pury and Farquhar (1997). In JULES, the level below which leaves are light limited is defined by a radiation threshold (PAR_{crit}), which is the PAR radiation for which light limiting photosynthesis is reduced to the level of the minimum of carbon limited and export limited photosynthesis, $Wl(PAR_{crit}) = min\{W_c, W_e\}$. In JULES the n layers are scanned and aggregated into a sunlit layer and a shaded layer, for which photosynthesis is calculated and scaled by the corresponding differential of LAI. This method corresponds to `can_rad_mod = 3`. However, because the V_{cmax} profile is kept constant and the canopy environment conditions (leaf temperature, humidity) are the same for each canopy level, the radiation threshold will be the same for all layers at a given timestep. Jogireedy et al. (2006) found that the 10-layer and 2-layer upscaling methods yielded very similar results with MOSES (earlier version of JULES). The key element for the canopy level photosynthesis is the absorbed PAR of the entire canopy, (i.e. it is not the multilayering that makes the improvement but the better radiation attenuation and total PAR reaching the canopy). Only in the case of biochemical properties for photosynthesis (i.e. V_{cmax}) varying across the canopy, the improved accuracy of the 10 layer vertical profile is beneficial.

Options `can_rad_mod =2-3` have a constant nitrogen content profile (and therefore V_{cmax}), however JULES has the option of an exponential nitrogen decrease down through the canopy (`can_rad_mod =4-5`). Mercado et al. (2007) found that a decreasing leaf nitrogen profile in conjunction with JULES multilayer upscaling method, did not have much impact on the photosynthesis in comparison with using a contant profile. However, because the site in question was a tropical forest, mainly light limited, not much response of photosynthesis to V_{cmax} was expected, therefore further research on nitrogen distribution within canopies was recommended.

The multi-layer options in JULES also account for inhibition of dark leaf respiration in light. Atkin et al. (1998) and Atkin (2000) have reported that the rate of leaf respiration in daylight is less than at night. Respiration inhibition is included in JULES via options `can_rad_mod` = 4 and 5 with different formulations. Option 4 uses inhibition of respiration for PAR above 10 μmol m^{-2} s^{-1} (2.19 W m^{-2} s^{-1}) from Lloyd et al. (1995). It was

tested by Mercado et al. (2007), who associated the underestimation of photosynthesis at midday at a tropical forest site, Manaus (Brazil), with an excessive daytime respiration. The inhibition of respiration improved the diurnal cycle at that site. Option `can_rad_mod =5` is based on Atkin (2000) and simulates 30% inhibition of leaf dark respiration for PAR radiance levels above 10 μmol m^{-2} s^{-1} (2.19 W m^{-2} s^{-1}).

CTESSEL

In CTESSEL scaling up from leaf to canopy is done with the big-leaf method, assuming leaf parameters constant throughout the canopy. However, scattering and absorbance of PAR within the canopy is described following Roujean (1996) which provides a more realistic profile of absorbed PAR than Beer's law with fix attenuation coefficient (JULES `can_rad_mod =1`). The attenuation is computed using Beer's law with different extinction coefficients for direct and diffuse radiation. The incoming radiation is partitioned into diffuse and direct according to the solar zenith angle. Moreover, and more importantly, the extinction coefficient for direct radiation depends on the solar zenith angle, thus the attenuation increases as the sun lowers in the horizon. This avoids attenuation being too small for low solar angles as calculated by Beer's law (Figure 2.6), allowing a better representation of the diurnal cycle.

The attenuation of radiation as explained in ECMWF (2015) follows:

$$I = I_0\Big[\delta(\mu_s)e^{-0.8bL} + (1-\delta(\mu_s))e^{-\frac{G_l bL}{cos\mu_s})}\Big] \tag{2.81}$$

where b is the foliage scattering coefficient, G_l is a parameter that describes the distribution of leaves (spherical angular distribution is assumed with $G_l = 0.5$), L = LAI $(h-z)/h$ is the cumulative LAI, μ_s is the solar zenith angle and $\delta_s(\mu_s)$ is the the ratio of diffuse to total radiation solar calculated as:

$$\delta(\mu_s) = \frac{0.25}{0.25 + cos(\mu_s)} \tag{2.82}$$

The foliage scattering coefficient b is calculated from the leaf single scattering albedo ω:

$$b = 1 - \frac{1-\sqrt{1-\omega}}{1+\sqrt{1-\omega}} \tag{2.83}$$

Then, assuming a homogeneous leaf vertical distribution, the integrated canopy net CO_2 assimilation is computed as :

$$A_c = LAI \int_0^1 A_n d(z/h) \tag{2.84}$$

The integrals are solved with a three-point Gaussian quadrature method following Goudriaan (1986).

$$A_c = LAI \sum_{i=1}^{3} W_i A_n(z_i) \tag{2.85}$$

where W_i and z_i are the Gauss weights and levels respectively. Equivalent equations are used to upscale dark respiration and stomatal conductance.

2.5 Summary

This chapter describes how JULES and CTESSEL represent the main aspects of the land surface. Particular emphasis has been placed on the parameterization of vegetation processes. JULES photosynthesis model is based on Farquhar et al. (1980), and calculates the leaf net photosynthetic rate as a co-limited function of the three limiting regimes (carbon, light and export). CHTESSEL/CTESSEL photosynthesis model is based on Goudriaan et al. (1985) as modified by Jacobs (1994); Jacobs et al. (1996). This formulation does not calculate separate limiting regimes but does account for carbon and light limitation. It does not explicitly account for the export or phosphate limitation, although it could be argued that a parameter $A_{m,max}$ could play the role of a physiological limitation by imposing a maximum carboxylation rate attainable by each plant species. JULES and CTESSEL calculate the stomatal conductance based on the A-g_s relationship that correlates the photosynthetic rate with the stomatal aperture. CHTESSEL however uses the Jarvis approach to determine the stomatal conductance. In the rest of the thesis, the coupled version CTESSEL, is used for comparison with JULES. Furthermore, both models calculate the C_i/C_a ratio as a function of air humidity based on Jacobs (1994) closure equation, although JULES neglects the term associated to transport through the cuticula when stomata are closed.

The treatment of the soil moisture stress is quite different in both models. While JULES uses a simple linear scaling of the photosynthetic rate based on volumetric water content, CTESSEL uses a complex parameterization based on Calvet (2000) and Calvet et al. (2004), that affects g_m and f_0 or D_{max}. It provides the choice of offensive or defensive water strategies and has different formulation for low and high vegetation. In the next

chapters, CTESSEL uses the offensive strategy.

JULES provides a variety of methods to upscale the leaf level photosynthesis to the canopy level. The most advanced version divides the canopy into several layers. CTESSEL uses the simple big-leaf approach but introduces a radiative transfer through the canopy with different attenuation coefficients for direct and diffuse radiation.

One potential shortcoming of both formulations is the treatment of the leaf temperature. The leaf temperature for the whole canopy is the tile's surface temperature. A dedicated canopy/leaf energy balance could provide a more accurate temperature to regulate the photosynthesis reaction.

In the next chapter the photosynthesis schemes of both models are isolated, in order to be tested against leaf level measurements and to compare their response to environmental variables.

Chapter 3

Leaf level photosynthesis

3.1 Introduction

In this chapter the focus is on the photosynthesis schemes at the leaf level. Photosynthesis is a key process in the modelling of carbon cycle, and one that is prone to variations in a changing climate due to its direct dependence on environmental factors such as temperature, radiation, humidity, soil moisture and ambient CO_2 (Nemani et al., 2003). The trade off between carbon assimilation and transpiration is also affected by climatic changes (Keenan et al., 2013; De Kauwe et al., 2013). Model intercomparison studies have revealed uncertainties in the response of modelled carbon absorption to climate change (Cramer et al., 2001; Friedlingstein et al., 2006). Vegetation models are becoming increasingly complex, with parameters describing traits such as leaf nitrogen concentration or leaf lifespan, and upscaling methods with multiple canopy layers and different treatments for diffuse radiation. However, the core of the photosynthesis activity and its dependence on the environment variables remain dictated by the the leaf level processes. Consequently, the equations at the leaf level are of primary importance in determining how the projected increase in temperature and CO_2 will affect vegetation. These equations are based on biochemical photosynthesis models (Farquhar et al., 1980; Goudriaan et al., 1985) and the empirical A-g_s relationship (Ball et al., 1987; Leuning, 1995) and were described in Chapter 2. In this chapter, the sensitivity of leaf level photosynthesis (and stomatal conductance) to environmental factors as modelled in JULES and CTESSEL is assessed. In particular,

the fertilisation effect on photosynthesis due to enhanced atmospheric CO_2 as reproduced by each model is compared as well as the effects that temperature and radiation exert on it. Each model's photosynthesis scheme at the leaf level has been isolated from the rest of the land surface model in order to reproduce the direct response of photosynthesis to ambient factors at the leaf environment. This analysis leads to a better understanding of how differences in photosynthesis parameterization translate in terms of vegetation's modelled climate response. The variation across the different plant functional types that are represented by land surface models has also been explored. The different species are represented by the same functional relationships and characterised by specific values of the model parameters, except C_4 grasses which possess differentiated formulation for some processes.

The three limiting situations for photosynthesis described in Chapter 2 play an important role in determining the photosynthesis sensitivity to environmental factors. The influence of the limiting regimes on CO_2 fertilisation has been analysed in JULES. The main limiting factors for plant growth are CO_2, even with the increasing levels of this atmospheric molecule, and RuBP regeneration, related to light absorption and patent at low radiation intensities. JULES also incorporates an export limiting regime. The limiting factor for photosynthesis reaction varies throughout the day and geographically and is determined by the combined levels of incoming radiation and temperature, as well as CO_2 concentration.

An increase in atmospheric CO_2 affects the three potential photosynthetic rates to different degrees or has no effect for export limiting regime. The rise in atmospheric CO_2 enhances plant productivity, and the enhancement is more pronounced if carbon is the limiting factor. However, as the CO_2 supply increases, photosynthesis will reach other limitations. Due to these heterogeneous responses, the actual effect of CO_2 on carbon assimilation is not easy to infer directly. Since stomatal conductance is linked to photosynthetic activity, variations in gas exchange due to enhanced CO_2 also depend on the limiting factor on photosynthesis. Using JULES photosynthesis model, the conditions that determine each limiting regime have been analysed and the modifications that a changing climate might bring.

Section 3.2 describes the stand alone versions of the photosynthesis schemes. In Section 3.3, the leaf photosynthesis schemes from both models are validated for present day cli-

mate by comparing with field measurements of photosynthesis and stomatal conductance from vineyards (Jacobs, 1994). These data provide insight into the diurnal dependence of photosynthesis on leaf level incident radiation, temperature and humidity for a particular field site. The occurrence of the limiting regimes in this set of observations has been identified (as modelled by JULES). The remainder of the Chapter considers the photosynthesis response to the whole environment including atmospheric CO_2 concentration. In Section 3.4 the photosynthesis CO_2 fertilisation effect at the leaf level as reproduced by JULES and CTESSEL is analysed, as well as photosynthesis responses to changes temperature and radiation. These results can be related to the climate projections derived from models induced by vegetation's response to enhanced CO_2, increasing temperatures or changes in radiation levels. The underlying assumptions in plant modelling described in Chapter 2 are linked in this chapter to the CO_2 assimilation response to the main drivers. Using the JULES photosynthesis model, the conditions of radiation and temperature that foster each limiting regime have been identified as well as the changes that enhanced CO_2 inflict on these conditions. In Section 3.5 the responses of stomatal conductance are analysed. Finally, in Section 3.6 a global sensitivity analysis using the Extended Fourier Amplitude Sensitivity Test (FAST) is performed on the leaf level photosynthesis schemes. This analysis determines the relative importance of each input variable and the models parameter on the photosynthesis model output.

3.2 Isolation of the leaf level photosynthesis schemes

With the purpose of analysing the leaf level representation of photosynthesis, the corresponding part of the code has been extracted from the two models of study, JULES and CTESSEL. It includes the biochemical representation of photosynthesis coupled with the gas exchange scheme via the stomatal conductance. The details of each model's parameterization were described in Section 2.4 of Chapter 2. JULES leaf level biochemistry representation is based on Farquhar et al. (1980) for C_3 and Collatz et al. (1992) for C_4 photosynthesis while CTESSEL uses Goudriaan et al. (1985). The A-g_s relationship in both models is based on Ball et al. (1987); Leuning (1995) with closure determined by Jacobs (1994) relationship with small differences as described in Table 2.1.

The upscaling process is not considered here to allow us to concentrate on the leaf level response to incident radiation, CO_2 and temperature in the leaf environment; neither are other types of respiration from plant parts other than the leaf. The leaf level photosynthesis values presented troughout this chapter correspond to net assimilation at the leaf level, the difference between gross assimilation and leaf dark respiration.

The subroutines that have been used in the computation of the leaf level output variables are described in Appendix A. The model parameters are those used by each model to describe each plant functional type (Table 2.2).

3.2.1 Input variables

The leaf level input variables that need to be fed into the photosynthesis models along with their units are summarised in the first section of Table 3.1. LSMs use the the skin temperature of the gridbox as leaf temperature to compute photosynthesis, and similarly for surface pressure and specific humidity. Specific humidity deficit is initially calculated from the input specific humidity and later adjusted according to the loss of water through the stomata.

In terms of radiation, the variable used by the photosynthesis code is the photosynthetically active radiation (PAR). Of the total incoming solar radiation only light within 400-700 nm is useful for plants. PAR represents 48% of the global radiation (emitted in the full spectrum). Typically, irradiance is measured as the power of the electromagentic radiation incident on a surface (W m^{-2}). For photosynthesis, the effect of radiation is more dependent on the total number of photons absorbed than on their energy (Jones, 1992). Therefore it is common in photosynthesis models to use Photosynthetic Photon Flux Density (PPFD) which determines the number of photons reaching a surface per unit of time whose wavelenths are within PAR (μmol photons m^{-2} s^{-1}). The energy of a photon depends on its wavelength and is calculated as ($E = hc/\lambda$) where h is the Plank constant, c is the speed of light and λ is the light wavelenght.

The soil water availability is provided as the normalised moisture factor f (or β), ranging between 0 and 1 (as explained in Chapter 2 Section 2.4.6). Aerodynamic conductance, represents the leaf boundary layer conductance (Chapter 2 Section 2.3.3), which charac-

Table 3.1: Input and output variables of the leaf photosynthesis models

Variable	Units	Description
INPUT VARIABLES		
T_l	°C	Leaf temperature
P	Pa	Surface pressure
PPFD	μmol photons m^{-2} s^{-1}	Photosynthetic Photon Flux Density
q	kg $(kg)^{-1}$	Specific humidity
f	-	Soil moisture factor
g_a	m s^{-1}	Aerodynamic (leaf boundary layer) conductance
C_a	ppm	Atmospheric CO_2 concentration
OUTPUT VARIABLES		
A_n	μmol CO_2 m^{-2} s^{-1}	Leaf net photosynthesis
g_s	m s^{-1}	Stomatal conductance
R_d	μmol CO_2 m^{-2} s^{-1}	Leaf dark respiration
C_i	ppm	Intercellular CO_2 concentration
W_c†	μmol CO_2 m^{-2} s^{-1}	Carbon limited photosynthetic rate
W_j†	μmol CO_2 m^{-2} s^{-1}	Light limited photosynthetic rate
W_e†	μmol CO_2 m^{-2} s^{-1}	Export limited photosynthetic rate

† Only in JULES

Table 3.2: Vegetation types used in this study, as named and numbered in each model's documentation.

	JULES	CTESSEL
	Plant functional type (PFT)	Vegetation type
Broadleaf tree	PFT 1 - Broadleaf tree	5 - Deciduous broadleaf
Needle leaf tree	PFT 2 - Needle leaf tree	3 - Evergreen needle leaf
C_3 grass	PFT 3 - C_3 grass	2 - Short grass
C_4 grass	PFT 4 - C_4 grass	7 - Tall grass
Shrubs	PFT 5 - Shrubs	16 - Deciduous shrubs

terises the thickness of the leaf boundary layer. Finally, the ambient carbon concentration (C_a) is the amount of carbon dioxide just outside the stomata. The introduction of carbon concentration as an input variable allows for experimentation of the effects of CO_2 rise directly at the leaf level.

3.2.2 Output Variables

The main output variable obtained from the photosynthesis schemes is the net photosynthetic rate at the leaf level, A_n which provides the amount of CO_2 (moles) assimilated by the leaf surface area per unit of time, for any given conditions at the leaf level (photon flux density reaching the leaf, air temperature and humidity surrounding the leaf, etc.). Other output variables returned by the models are the stomatal conductance, leaf dark respiration, intercellular carbon concentration. All output variables are also listed in Table 3.1. In the case of JULES, the intermediate variables corresponding to the values of the photosynthetic rates of the three limiting regimes prior to the calculation of net photosynthesis through the colimitation equation have also been output for analysis of the dominating regime.

3.2.3 Model parameters for vegetation

Most model parameters are adjusted to each vegetation class. In JULES these are the 5 plant functional types (PFTs), needle leaf, broadleaf tree, C_3 grass, C_4 grass and shrubs; while CTESSEL uses 20 vegetation types from the Global Land Cover Characteristics (GLCC) database. From these classification, the most comparable types to JULES 5 PFTs were selected for the comparison analysis. The names and identification of each vegetation type in each model is listed in Table 3.2, and values, description and units of the main vegetation parameters as used by each model for each vegetation type were presented in Table 2.2.

3.3 Leaf level comparison

The leaf level photosynthesis schemes from both JULES and CTESSEL has been tested against photosynthesis and stomatal conductance measurements of grapevines from a field campaign (Bolle et al., 1993). The comparison analyses the error at the leaf level that occurs in land surface models and may be masked by the upscaling process when validating with flux measurements. The dataset presented here enables a comparison of the leaf level photosynthesis schemes responses to environmental factors under realistic conditions. These observations have previously been used to validate an A-g_s model which is the basis of the photosynthesis model in CTESSEL (Jacobs, 1994; Jacobs et al., 1996). For this reason, a proper validation is not possible, as the data are not independent; however, the comparison provides useful results. The data were also employed to analyse stomatal response to ambient humidity and relate the C_i/C_a ratio to specific humidity deficit (Jacobs, 1994).

3.3.1 Field measurements

The observations used for model validation were gathered in Tomelloso, in the Spanish district of Castilla La Mancha (2°55'48" W, 39°08'30" N, 693 m above sea level). Photosynthetic rate and stomatal conductance were measured in leaves of grapevines (*Vitis Vinifera* L. cv. Airen), in June 1991 as part of the EFEDA campaign (Bolle et al., 1993).

At this time of the season, the plants were in their active growth stage and developing fruit. The shrubs are grown in a semi-arid environment and are rainfed; no episodes of rain were observed during the measuring period. Despite the dry environment, Jacobs (1994) argues that there is no evidence of serious drought stress or temperature stress during the experimental period. The lack of soil moisture stress is justified by the deep roots of the grapevines which enable them to reach ground water.

Observations of leaf photosynthetic rate were carried out during daytime at intervals of about two hours during days 17, 19, 21, 23, 25 and 27 June. Data were collected using an open flow differential gas exchange unit, composed of an air supply unit and an Infra Red Gas Analyser (IRGA). The system samples air from a reference height and the air flow is divided into two streams. One of them is pumped to a transparent cuvette which is clamped onto the sample leaf before being directed to the gas analyser. The rest of the air is directly taken to the gas analyser to determine the CO_2 concentration of the reference air. Because of photosynthesis, the level of CO_2 in the first air flow will be depleted as it flows past the leaf surface. The rate of photosynthesis is calculated by measuring the difference of CO_2 concentration in the air going towards the leaf and the air leaving the leaf. The method is roughly described by the following equation (omitting several corrections that need to be applied, see Jacobs (1994)):

$$A_n = \frac{F(C_r - C_o)}{L_a} \tag{3.1}$$

where F represents the air flow through the chamber (mol s^{-1}), C_r (mol CO_2 (mol air)$^{-1}$) is the carbon dioxide concentration of the reference air, C_o (mol CO_2 (mol air)$^{-1}$) is the carbon dioxide concentration of the air which has been in contact with an area L_a (m^2) of the leaf enclosed by the chamber. Several characteristics of each sample were recorded, for instance age of the leaf (young/old), height of the leaf, and whether it was sunlit or shaded. This last type of information has been used in this study, and the data from sunlit and shaded leaves have been analysed separately. Associated with each photosynthesis observation, temperature and humidity of the air inside the chamber were also measured. Leaf temperature was derived from the cuvette temperature via an energy balance equation. Incident photosynthetic active radiation (PAR) was measured by a sensor just outside the cuvette. Stomatal conductance measurements were obtained in two independent ways. The first method uses data from the gas-exchange unit to derive transpiration, and this

water vapour flux is combined with the humidity in the cuvette to derive the stomatal opening assuming saturated sub-stomatal cavities. A second set of stomatal conductance measurements was carried out with a dynamic diffusion porometer on the same days. The porometer directly measures the increment in humidity in a cup clamped to the leaf surface in a certain time period. The measurements performed with the porometer yielded higher values for stomatal conductance compared to the derived values of g_s from the gas-exchange unit. The possible causes for the difference between both datasets are discussed in Jacobs (1994). It is argued that porometer measurements are dynamic measurements, typically lasting ~10 seconds, whereas the gas-exchange measurements are equilibrium measurements lasting 30 seconds to one minute. The longer time of the gas-exchange measurement may induce a change in the leaf environment. The main alteration is the partial blocking of incident light which may cause a slight closure of the stomata. This effect would not occur in the carbon dioxide measurement because the carbon flux is not as responsive as the stomata themselves. Based on these considerations, the porometer measurements have been used for model validation. For a more detailed description of methods and instruments see Jacobs (1994).

3.3.2 Model runs

There were a total of 673 leaf observations, of which 414 were sunlit and 259 were shaded. Both photosynthesis models were run using as input the measurements of temperature, humidity and PPFD particular to each leaf photosynthesis observation.

3.3.2.1 Model driving data

Measurements of leaf temperature, humidity and incident PAR were used as driving variables of the photosynthesis schemes of JULES and CTESSEL. Since the plants are assumed not to suffer from soil water stress, the normalised soil moisture factor in the models has been set to 1 (volumetric soil water above the critical point), so photosynthesis and stomatal conductance are not reduced by water stress. For the atmospheric CO_2 (C_a) a value of 325 ppm was used, which is close to the average of measured CO_2 concentration of the reference air (C_r) (Jacobs, 1994). The leaf boundary layer conductance, g_b, was set to a

fixed value calculated using Equation 2.33 assuming an average windspeed of 2.5 m s^{-1} and leaf width of $W_l = 0.075$ m as used in Jacobs (1994). The derived value for the CO_2 flow in the leaf boundary layer is $g_b = 0.0323$ m s^{-1}.

3.3.2.2 Model parameters

Initially, model parameters were set to the default model characterization for a grapevine, broadleaf tree model settings (PFT 1) in JULES and deciduous broadleaf tree (vegetation type 5) in CTESSEL. These settings underestimate leaf photosynthesis, highlighting the drawbacks of using a single plant functional type to characterise biomes inhabiting different climatic zones. The work by Jacobs (1994) derived specific parameters for the grapevine, which have also been tested. The photosynthesis model used in Jacobs (1994) is fundamentally similar to CTESSEL photosynthesis scheme; they both derive from Goudriaan et al. (1985). Consequently, in CTESSEL the adjusted parameters could be directly introduced but some transformations were required to derive the corresponding parameters for JULES. Both sets of parameters are presented in Tables 3.3 and 3.4.

Although the model parameters in CTESSEL correspond to the adjusted parameters in Jacobs (1994), CTESSEL's formulation introduces some relationships between parameters, which were described in Chapter 2. Specifically, in tree species parameters f_0 and g_m are not independent: f_0 is derived from the g_m according to Equation 2.59 following Calvet et al. (2004). This coupling was removed to be able to prescribe f_0 and g_m simultaneously; introducing one extra degree of freedom. The use of adjusted parameters yields an increase in the photosynthesis capacity in carbon limited situations (higher g_m and $A_{m,max}$ in Equation 2.54). CTESSEL's default value for the parameter ϵ (Equation 2.55) related to the response to radiation in light limiting situations, does not vary; it is the same as derived by Jacobs (1994). The temperature limits in the temperature dependence (Equations 2.61 and 2.62) are shifted upwards, yielding a higher optimum temperature. The increase of the humidity parameter f_0 enhances the sensitivity of C_i to changes in specific humidity deficit (Eq. 2.43) and consequently stomatal conductance and photosynthesis. The maximum specific humidity deficit vegetation can cope with (D_{max}) is reduced, as an adaptation to a dry environment. In the case of JULES, to be able to adjust the model parameters consistently, some relationships that link the main param-

Table 3.3: CTESSEL model settings

CTESSEL	Deciduous broadleaf	Grapevine
$g_m(25)$ (mm s^{-1})	1.4	2
g_c (mm s^{-1})	0.25	0
$A_{m,max}$ (mg CO_2 m^{-2} s^{-1})	1.83	2.2
D_{max} (kg kg $^{-1}$)	0.109	0.0582
f_0	0.623†	0.916
$\Gamma(25)$ (ppm)	42	45
[T_{1gm}-T_{2gm}] (°C)	[5-36]	[0-42]
[$T_{1Am,max}$-$T_{2Am,max}$] (°C)	[8-38]	[15-42]
ϵ_0 (mg CO_2 J^{-1}PAR)	0.017	0.017

† (Eq.2.59 in Chapter 2)

Table 3.4: JULES model settings

JULES	Broadleaf	Grapevine
n_0 (kg N (kg C)−1)	0.046	0.125
D_{crit} (kg kg $^{-1}$)	0.09	0.0582
f_0	0.875	0.916
[T_{low}-T_{upp}] (°C)	[0-36]	[0-42]
α (mol CO_2 (mol PAR photons)$^{-1}$)	0.08	0.0846

eters from both models were explored. There is not an unequivocal conversion between parameters from different models. Moreover, there is not necessarily a direct match between the same parameter used in two different models. This is because the other parts of the model may exert another type of control on photosynthesis. For example, the widely used maximum velocity of carboxylation, V_{cmax}, presents a lower value in models that contain a diffusive mesophyll conductance than in those which do not. Bearing this consideration in mind, two approaches were followed to find 'equivalent' parameters to the grapevine settings suggested by Jacobs (1994) for the JULES model. Both relationships are described in the appendixes in Jacobs (1994). The first attempt is to relate mesophyll conductance to V_{cmax} by making use of the relationship obtained by deriving photosynthetic rate with respect to intercellular carbon concentration, as described in Chapter 2 (Equation 2.63). With the default settings, broadleaf trees have V_{cmax} of 35 μmol CO_2 m^{-2} s^{-1}, derived from leaf nitrogen content (Equation 2.48, Chapter 2). The resulting V_{cmax}, using Equation 2.63 in Chapter 2 and persevering through some unit conversions, is 45 μmol CO_2 m^{-2} s^{-1}. This value increased slightly JULES photosynthesis, but there was still a significant underestimation. The second approach relates V_{cmax} to $A_{m,max}$, instead of g_m:

$$V_{cmax} = 2A_{m,max} \tag{3.2}$$

This relation was used in a comparison between MOSES and a A-g_s scheme (Steeneveld, 2002). The V_{cmax} derived from $A_{m,max}$ was much higher, V_{cmax} = 100 μmol CO_2 m^{-2} s^{-1} which corresponds to a leaf nitrogen content (n_0) of 0.125 kg N (kg C)$^{-1}$. This value has been chosen to be used in JULES for the grapevine settings since the leaf level photosynthesis values resulting from it, although above observations, were closer than when using V_{cmax} from the first method (Equation 2.63). It should be noted than this V_{cmax} is more than double the values used in JULES for any PFT. However, other modelling studies have also suggested higher values of nitrogen content in JULES (den Hoof et al., 2013).

In terms of temperature settings, the parameters derived by Jacobs (1994) for g_m have been used for temperature dependent parameters in JULES (T_{low} and T_{upp}). As in CTESSEL, the modifications applied for grapevines tend to increase photosynthesis especially in the carbon limited regime (V_{cmax} in Equation 2.44 is almost tripled) and also less significantly in the light limited regime (α increases in Equation 2.45). The grapevines settings also

increase the sensitivity to ambient humidity (via increased f_0 in Equation 2.43) and the resilience to the dry (decreased D_{max}) and hot environment (increased T_{low} and T_{upp} in Equation 2.47).

3.3.3 Effect of environmental factors

The relation between leaf level photosynthesis and incident PAR, leaf temperature and humidity has been plotted in Figure 3.1 for broadleaf settings and 3.2 for grapevine settings. Each subfigure contains all 673 single measurements with sunlit leaves and shaded leaves marked with different colours. The root mean squared error for sunlit shaded and total leaves is presented in Table 3.5.

Although modelled photosynthesis with default broadleaf settings becomes insensitive to radiation at high light intensities, there is no evidence of light saturation in the observed data. This behaviour is rectified with the grapevine settings due mainly to the higher values of g_m in CTESSEL and n_o (hence V_{cmax}) in JULES (Table 3.3 and Table 3.4). The initial linear response of photosynthesis to low radiation shows a steeper slope in JULES, even when the same maximum quantum efficiency is imposed with the grapevine settings runs (ϵ_0 in CTESSEL and α in JULES, due too higher values of C_i modelled by JULES resulting in higher effective quantum efficiency (Equation 2.45). The high value for V_{cmax} introduced in JULES (about double of the highest V_{cmax} used by the default PFTs) has some additional effects by increasing the dark leaf respiration rate, as can be seen by some negative values especially towards the high temperatures.

With regards to temperature, both models experience a shift towards higher temperatures when using grapevine settings, yielding a better match with the observed optimum temperature. In the case of specific humidity, the observations show a clear relationship with steeper slope for sunlit than for shaded. In the models with broadleaf settings, this relationship was only correctly achieved for shaded leaves. With the modified settings sunlit photosynthesis values increase presenting a more similar slope to the observed one. JULES shows more scattering whereas CTESSEL imposes some restriction on the higher photosynthesis values.

In general models represent best the photosynthesis in the shaded leaves (for low radiation

Table 3.5: Leaf photosynthesis root mean squared error for each model against observations (μmol CO_2 m^{-2} s^{-1})

	JULES		CTESSEL	
	Broadleaf	Grapevine	Broadleaf	Grapevine
Sunlit leaves (n=414)	6.68	7.22	5.48	2.94
Shaded leaves (n=259)	1.12	2.30	0.92	1.24
All leaves (n=673)	5.29	5.84	4.34	2.43

values) than in the sunlit leaves as can be seen by the lower RMSE in Table 3.5. The introduction of the adjusted parameters for grapevines has a greater effect on the sunlit model predictions than on the shaded. The difference found in RMSE between sunlit and shaded leaves is greater than the difference in RMSE between models. Overall CTESSEL shows a slightly better performance (lower RMSE in Table 3.5).

3.3.3.1 Limiting regimes in the observations

The difference in model performance found for sunlit and shaded leaves can in fact be related to the limiting factor for the photosynthesis reaction. In order to relate the measurements of leaf photosynthesis with the limiting regimes, we made use of the model runs performed with JULES. Each observation was classified as carbon, light or export limited according to the minimum potential photosynthetic rate (W_c, W_j or W_e) as calculated by JULES for the corresponding PPFD, T_l and humidity. Of a total of 673 measurements, 400 were carbon limited, 272 were light limited and only one was export limited. Interestingly, the division between carbon and light limitation is strongly related to whether the leaf was sunlit or shaded. Of all the sunlit photosynthesis observations (n = 414), 379 (91.55%) were limited by carbon, 34 (8.21%) were light limited and 1 (0.24%) was export limited. In the case of observations on shaded leaves (n = 259), 21 (8%) were carbon limited and 238 (92%) were light limited. The distribution of this classification with respect to the magnitude of photosynthesis and PPFD, T_l and specific humidity is illustrated in Figure 3.3 with limiting regimes determined by the colour. Shaded and sunlit measurements have

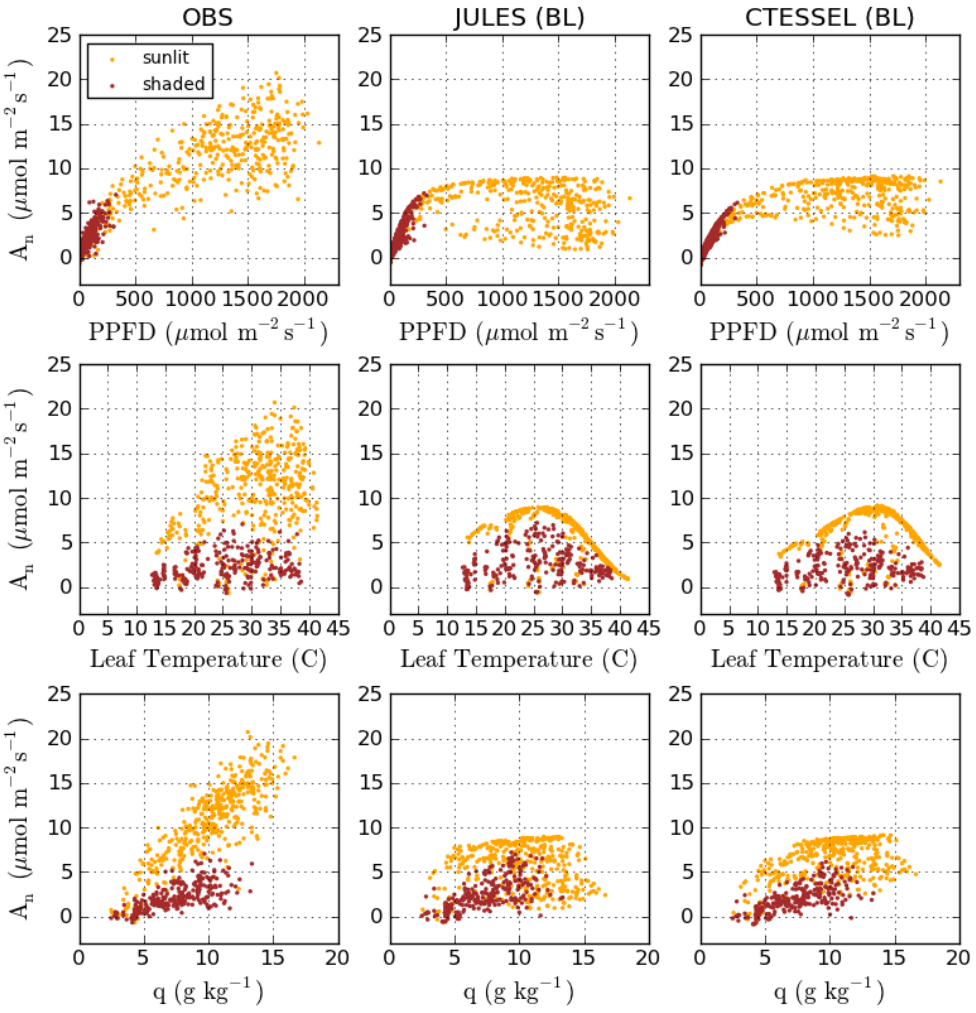

Figure 3.1: Observed (first column) leaf photosynthesis and modelled leaf photosynthesis with broadleaf settings (JULES second column and CTESSEL third column) against radiation, temperature and humidity. Colour indicates whether leaves were sunlit or shaded.

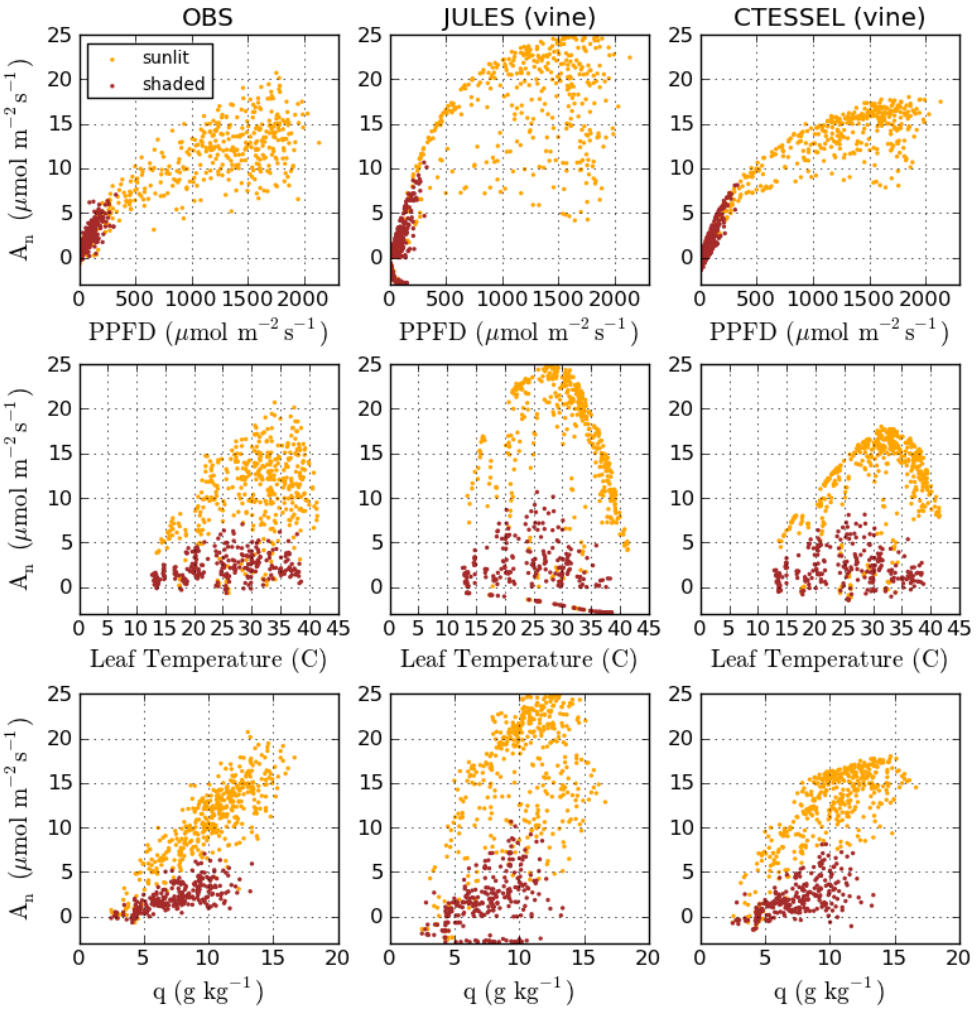

Figure 3.2: Observed (first column) leaf photosynthesis and modelled leaf photosynthesis with grapevine settings (JULES second column and CTESSEL third column) against radiation, temperature and humidity. Colour indicates whether leaves were sunlit or shaded.

been plotted separately. In terms of radiation intensity, light limitation is associated to low incident radiation and carbon limitation is associated to higher radiation. The threshold radiation is around 200 μmol photon m^{-2} s^{-1} (as will be addressed in Section 3.4.3), which is a consequence of JULES parameterization (and might be too low). Both light and carbon limited processes occur at all temperatures. In this set of measurements only one case of export limitation was identified, occurring at the lower end of the temperature range. In a colder climate or time of the year however, export limitation would be more significant. Concerning humidity, carbon limited photosynthesis was only found to occur for specific humidity values above 5 g kg^{-1}.

The identification of limiting regimes performed here is limited to this set of observations relevant to a hot and dry climate and CO_2 concentration of 325 ppm. For higher ambient CO_2 the number of export limitated cases might be increased. The influence of a broader set of temperatures, radiation and changes in CO_2 on the limiting regimes of the JULES model net photosynthesis will be explored in Section 3.4.4.

3.3.4 Diurnal cycles

To visualise the diurnal cycle, the measurements obtained for different leaves of the same plant and in the same time window have been averaged together. At least two single measurements were required to compute the average. The magnitude of the sunlit leaves photosynthesis is consistently higher than the shaded leaves photosynthesis, hence sunlit and shaded leaves have been analysed and plotted separately. Figure 3.4 shows diurnal net photosynthesis, as reproduced by both models (JULES and CTESSEL) using both parameter settings (broadleaf and grapevine). Observations are grouped by plant. The vertical bars in the observations are the standard deviation of the cluster of measurements combined for each value, and indicate the natural variability. The model output was averaged per plant in the same manner as the observations. Figure 3.5 is analogous for the shaded leaves.

Despite the differences in their parameterization both models show a similar behaviour when using the default broadleaf settings (solid lines); they underestimate photosynthesis by about half for the sunlit leaves in the middle of the day (Figure 3.4) and they reproduce

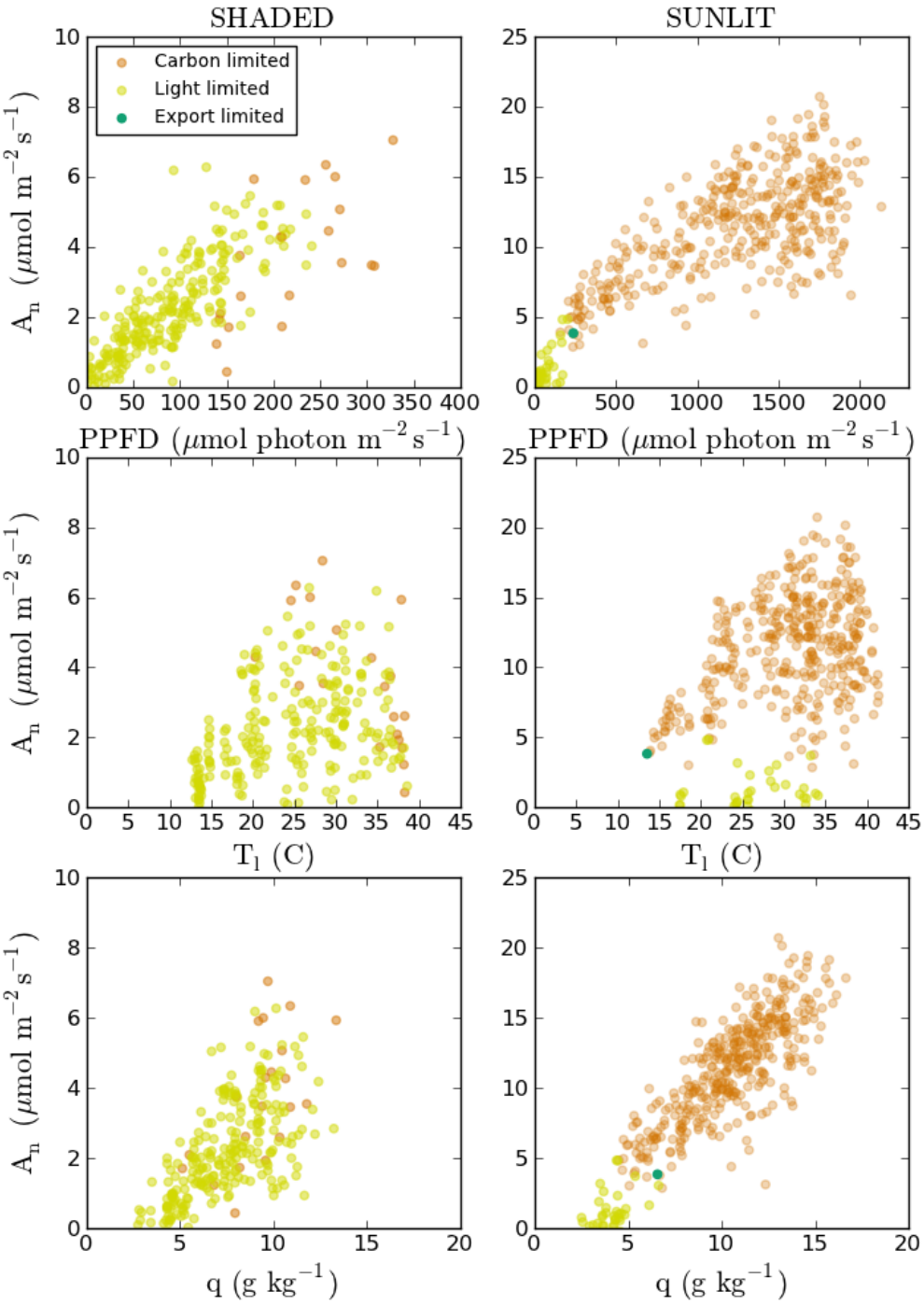

Figure 3.3: Limiting regimes in the observations. The limiting regime is derived from the JULES photosynthesis model.

well photosynthesis for the shaded leaves (Figure 3.5). The low values for sunlit leaves compared to observations are expected given that the model settings concern a generic broadleaf tree, whereas these grapevines are grown in a hot and dry environment and probably well adapted to this particular climate. Nevertheless, it is remarkable how well the two models represent photosynthesis for the shaded leaves even with 'untuned' model parameters.

When modifying model parameters to the specific settings derived for grapevines (dashed lines in Figures 3.4 and 3.5) the estimated photosynthesis increases in both models. The increase is more pronounced for the sunlit leaves, whereas for the shaded leaves the predicted photosynthesis with adjusted settings are close to the predicted photosynthesis with default settings. The reason why the change in parameters primarily affects the sunlit leaves is because photosynthesis in the sunlit leaves is carbon limited (as shown in Section 3.3.3.1) and the modified parameters are related to carbon limited photosynthesis. The photosynthesis modelled by CTESSEL sees an improvement in the diurnal evolution with the adjusted set of model parameters. This is to be expected since the photosynthesis model used by Jacobs (1994) to derive the plant parameters is conceptually similar to CTESSEL's photosynthesis model. In the case of JULES, the adjusted parameters also increase the photosynthetic rate. However the increase in leaf photosynthesis in the morning for the sunlit leaves is exaggerated, producing a severe overestimation especially in the early mornings. Although generally afternoon values agree better (days 21, 23, 25 and 28). Overall, JULES performs in average worse with the grapevine settings than with the default settings, as shown by RMSE values, due to the large overestimation in the first two days. For the sunlit leaves, both models with default settings reproduce the increase of photosynthesis at the early hours of the day with increasing levels of sunshine and temperature. However on some days, after the initial increase there is a drop at around 9 UTC, this can be interpreted as a midday stomatal closure related to a drop in the air humidity. This behaviour is exhibited by both models for days 21, 23, 25, 27 and 28 in Figure 3.4, moreover JULES also shows a drop in photosynthesis for days 17 and 19 although this drop is less dramatic. Thereafter, models consistently underestimate sunlit photosynthesis during the hottest, driest and more intensely radiated hours of the day. This drop in photosynthesis may be related to an increase in the specific humidity deficit during the day, controlling C_i. However it is not seen in the observations.

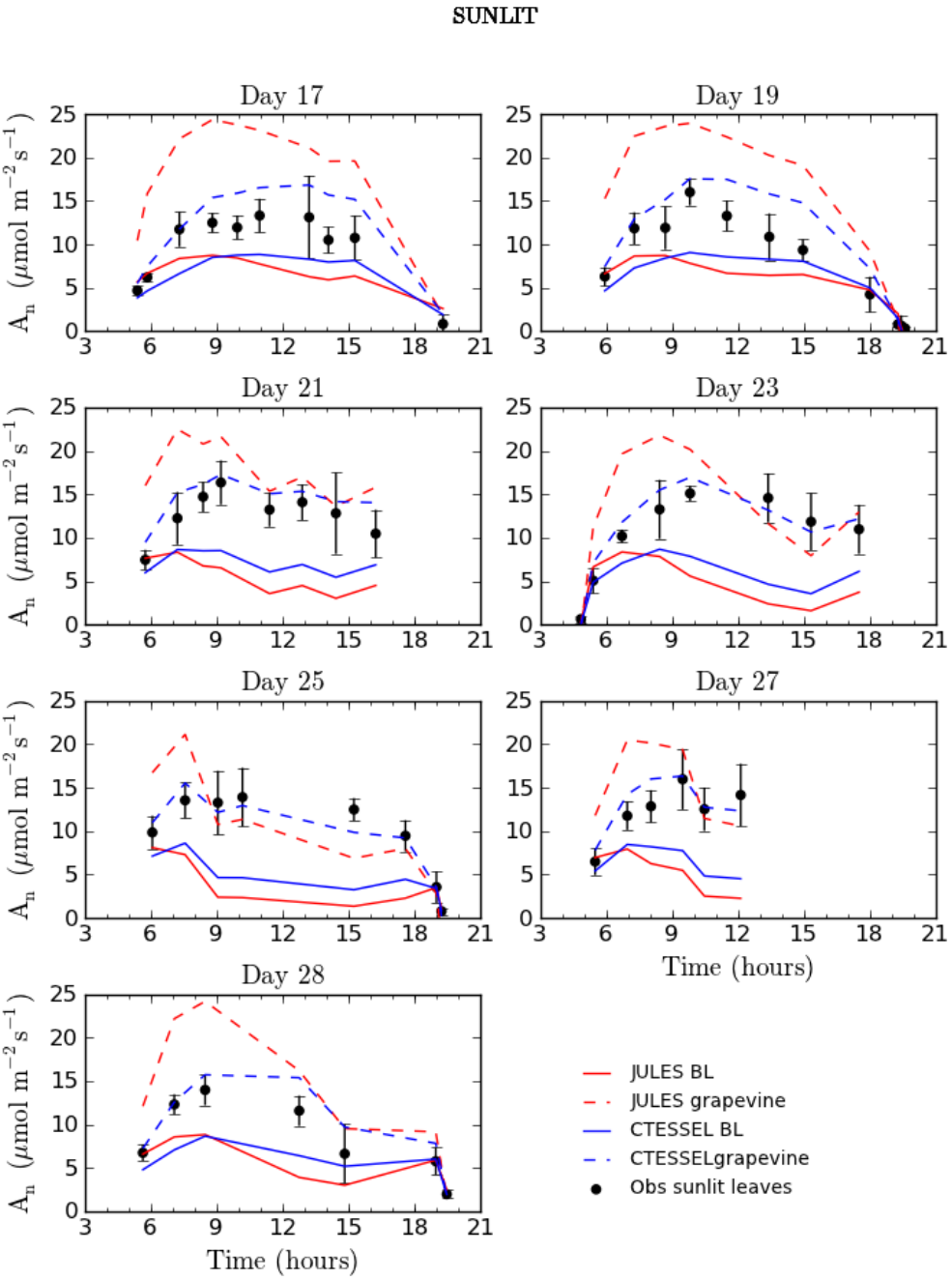

Figure 3.4: Diurnal cycle of leaf photosynthesis, averages per plant sunlit leaves only. Time is UTC.

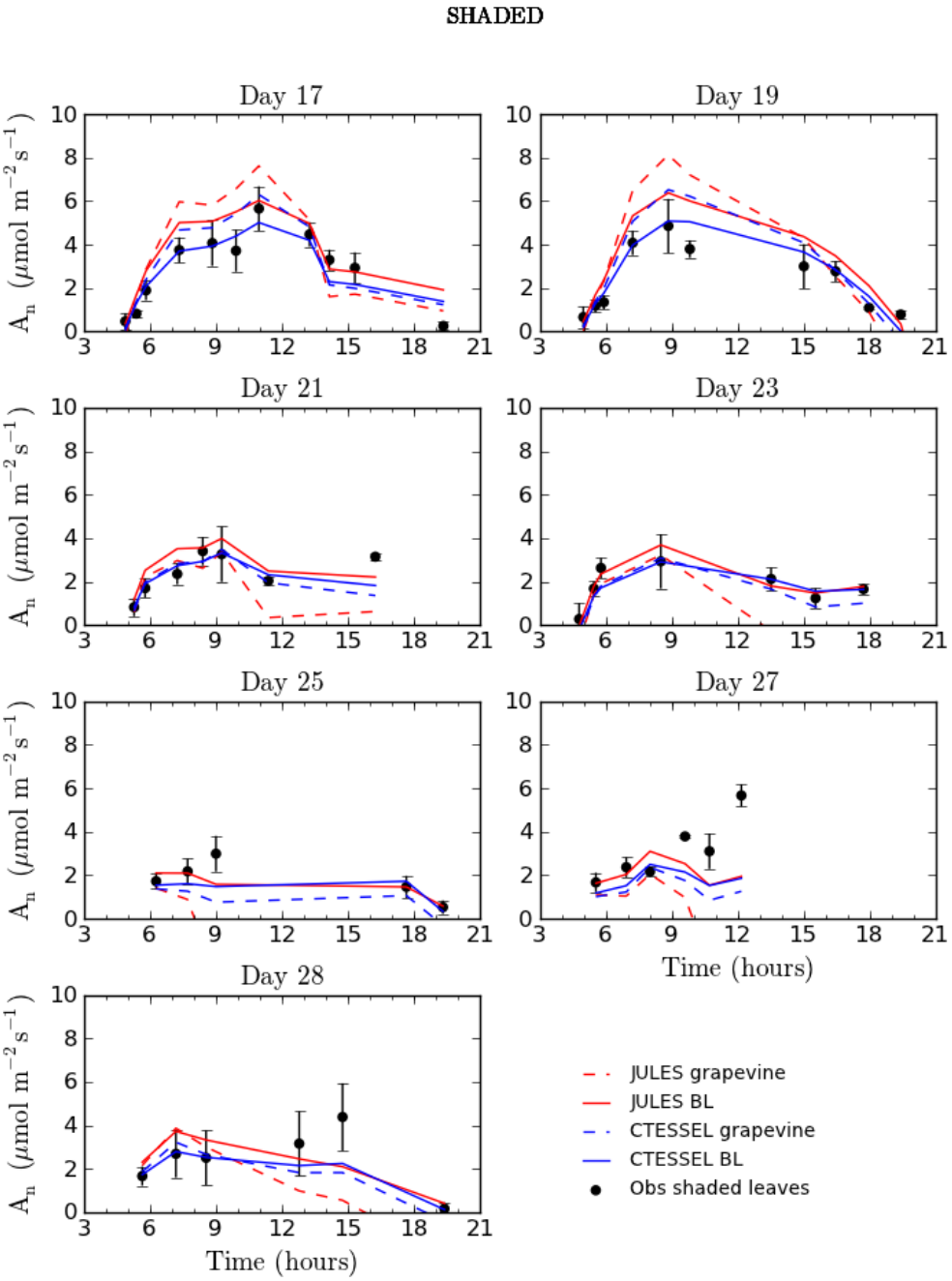

Figure 3.5: Diurnal cycle of leaf photosynthesis, averages per plant shaded leaves only. Time is UTC.

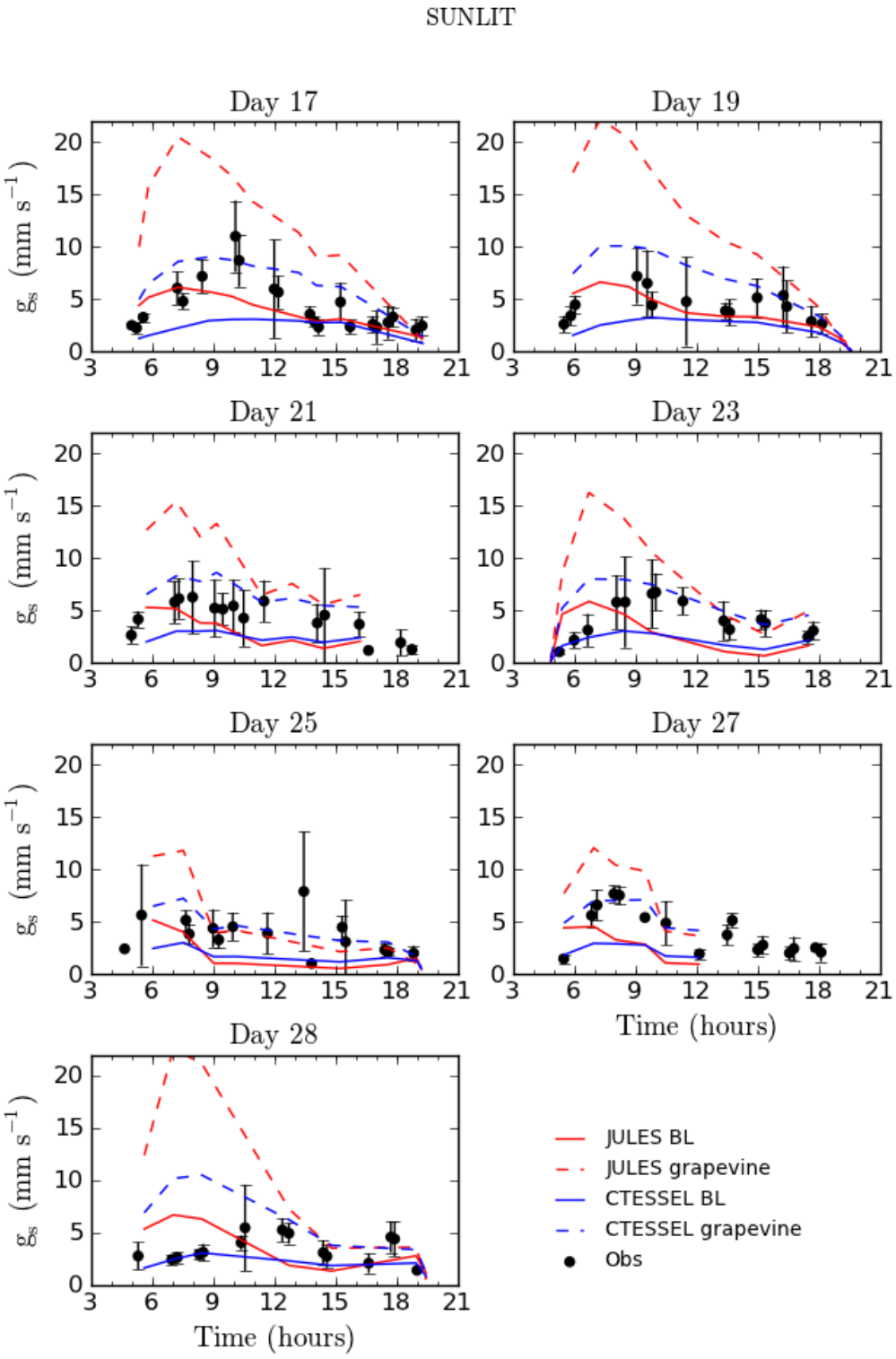

Figure 3.6: Diurnal cycle of leaf stomatal conductance, independent observations from porometer. Averages per plant sunlit leaves only. Time is UTC.

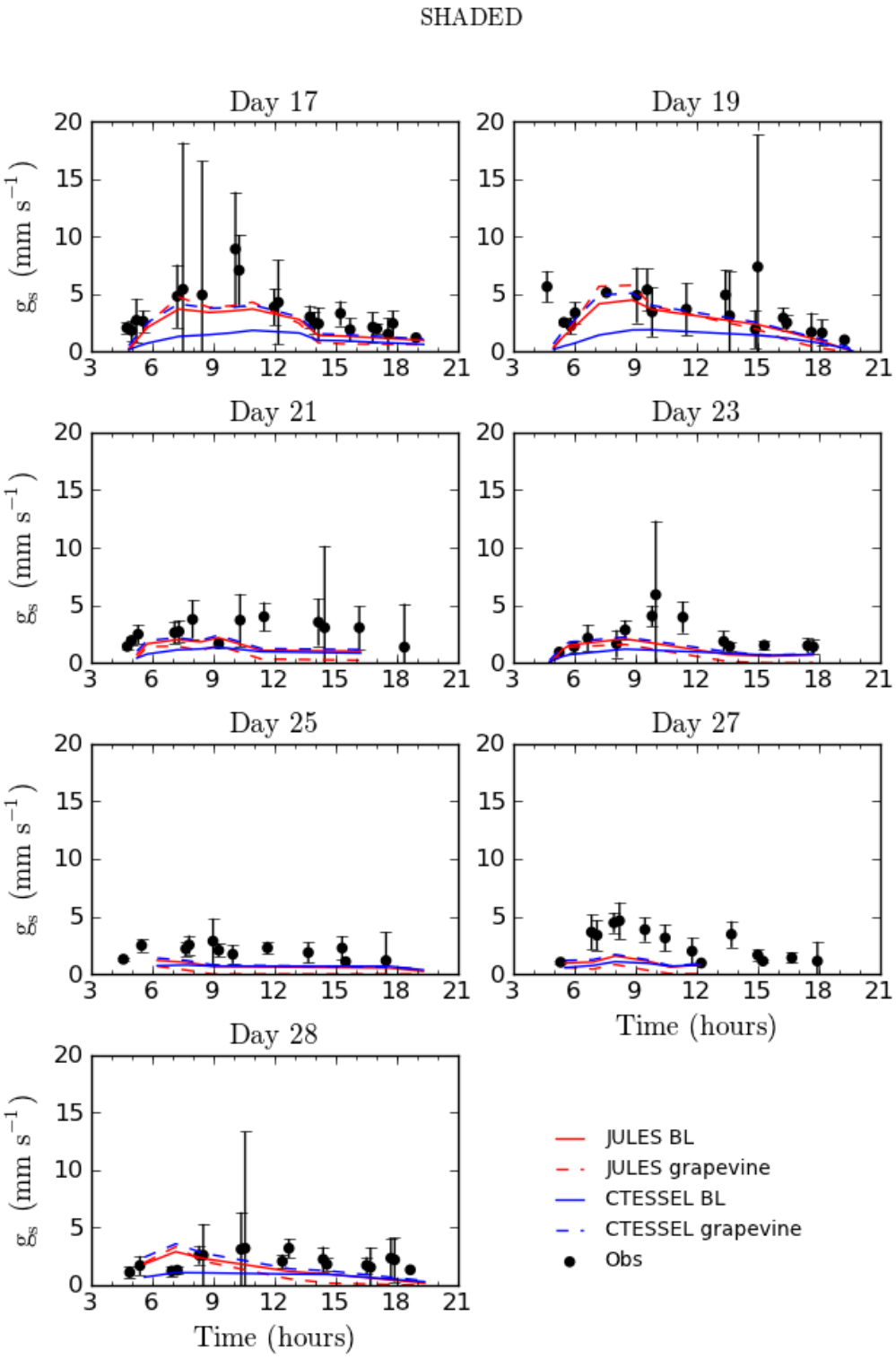

Figure 3.7: Diurnal cycle of leaf stomatal conductance, independent observations from porometer. Averages per plant shaded leaves only. Time is UTC.

In CTESSEL the adjusted parameters for grapevines correct this drop. But in the case of JULES the drop in the morning is still present (days 21, 23, 25, 27 and 28).

Stomatal conductance measurements were obtained independently on the same days with a porometer. The diurnal evolution of the observations, and model estimations, is shown in Figure 3.6 for sunlit leaves and in Figure 3.7 for the shaded leaves. The modelled points do not correspond exactly to the g_s measurements, but both sets are for the same days, so they have been plotted together. Equally to A_n, measurements on leaves of the same plant were grouped together and the standard deviation has been included as an indication of the natural variability, which in this case is quite large. Despite this, a diurnal cycle can be identified with the maximum values in the first half of the day. Sunlit and shaded observed values do not show the marked differentiation found for A_n values, although sunlit leaves tend to present slightly higher g_s. The model runs with the broadleaf settings underestimate g_s, although the estimation in most cases overlaps with the high variability of the observations. JULES presents a peak of g_s in the mornings, higher for the sunlit leaves, followed by a drop or midday stomatal closure, as seen for A_n. CTESSEL shows too little diurnal variation for sunlit leaves due to the small sensitivity to humidity (low f_0). The grapevine settings improve model performance, the higher f_0 increases g_s and the diurnal amplitude. However for JULES the increased f_0 for the sunlit leaves, enhances the morning peak well above observed values making the drop even larger. As seen for A_n the change in models settings has more impact in the sunlit leaves (carbon limited) than in the shaded leaves.

It is interesting that although the grapevine model parameters have been chosen to be equivalent in both models, the model output actually differs more than with the out-of-the-box broadleaf settings for each model. This illustrates how challenging it is to relate model parameters.

3.3.4.1 Humidity and C_i

The diurnal cycle of specific humidity deficit in the environment surrounding the leaf (calculated from observed leaf temperature and leaf humidity as $D_s = q_{sat}(T_l)$-q) is shown in Figure 3.8. In the early mornings, humidity deficit is at its lowest value. As temperature

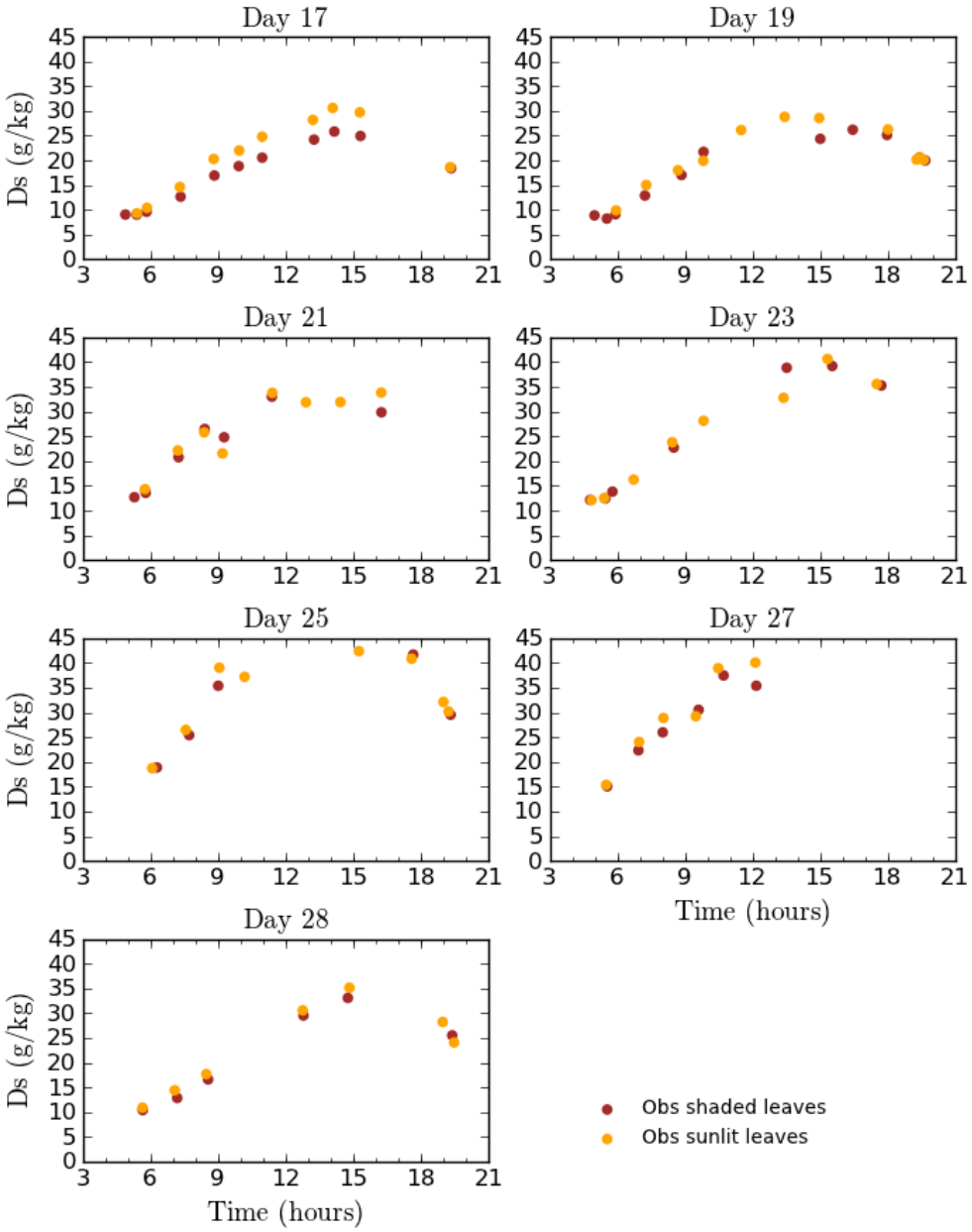

Figure 3.8: Diurnal specific humidity deficit derived from observations.

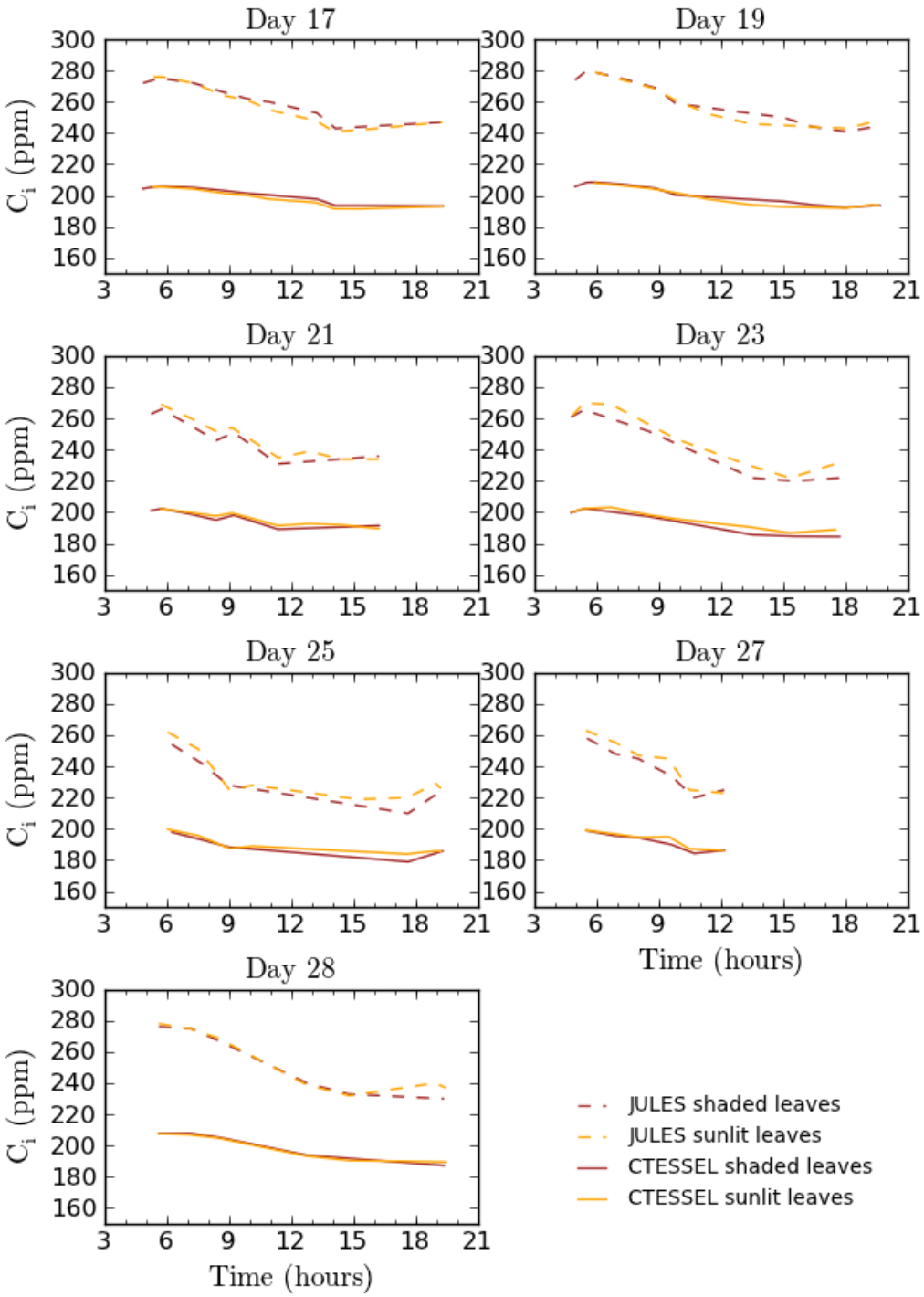

Figure 3.9: Diurnal intercellular carbon concentration in models (broadleaf settings).

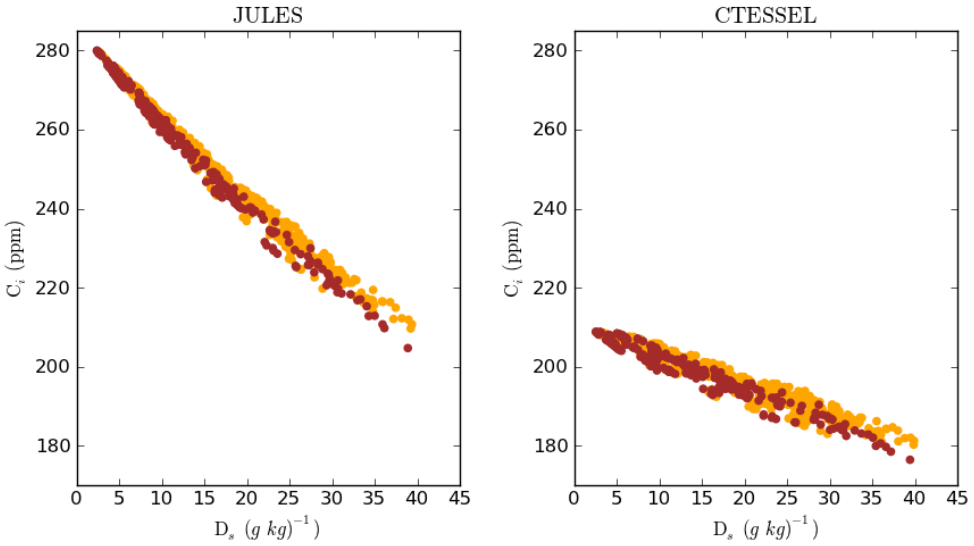

Figure 3.10: Intercellular carbon concentration against specific humidity deficit in models (Broadleaf tree settings). The slopes are dictated by f_0 in Jacobs (1994) equation (f_0 = 0.875 in JULES and $f_0 = 0.623$ in CTESSEL)

increases, the humidity deficit also increases. At around 15h, D_s it at its maximum, marking the moment when the humidity demand around the stomata is highest. The diurnal variation of C_i in the models when broadleaf settings are used is depicted in Figure 3.9. JULES values of C_i are systematically higher than those found for CTESSEL, and present more variation during the course of the day. In the mornings, JULES C_i is high, corresponding with the time of the day when the air is most humid (Figure 3.8). As the air becomes drier JULES C_i decreases. CTESSEL presents a similar cycle, although the amplitude is smaller. In both models C_i is strongly driven by the changes in D_s via Jacobs (1994) closure equation (Equation 2.43) and regulated by the values of the f_0 parameter. Figure 3.10 depicts the relation between the ratio C_i/C_a and D_s for both models with broadleaf settings. The slope of the line is dictated by the value of f_0, being steeper for JULES (f_0 = 0.875) than for CTESSEL (f_0 = 0.623). The sensitivity of C_i to changes in humidity is responsible for the drops both in g_s and A_n, more apparent in JULES due to higher sensitivity (higher f_0). When prescribing the grapevine settings (f_0 = 0.916), the sensitivity increases for both models, and the same relationship between D_s and C_i is present, yielding the same C_i values for both models. However, although with the grapevine settings models have the same values of C_i, these result in more divergent photosynthetic rates, as seen in Figures 3.4 and 3.6. In JULES, the high C_i values cause

an increase in the morning A_n. The diurnal variations in C_i affect net photosynthesis more in JULES than in CTESSEL possibly because JULES iterates C_i in the photosynthesis calculations. The C_i diurnal variation has an effect on A_n mainly on the sunlit leave, where photosynthesis is carbon limited and therefore dependent on C_i.

3.4 Leaf level CO_2 fertilisation effect

In the previous section the photosynthesis schemes embedded in JULES and CTESSEL were validated with observations of leaf level photosynthesis and stomatal conductance in present day levels of atmospheric CO_2. In this section, the schemes are tested for variations in environmental factors through sensitivity studies that also include changes in atmospheric CO_2 .

The biochemistry of photosynthesis is such that an increase in available CO_2 leads to an enhancement in the carbon assimilation. This effect is believed to be accompanied by a partial closure of the stomata to maintain near constant CO_2 concentration in the intercellular spaces, resulting in reduced transpiration. The combined effect is an increase in water use efficiency (carbon uptake per water lost). The increased carbon uptake at the leaf level (also called direct effect) will result in plant growth, and an increase in the plant's biomass through carbon allocation. The expansion of leaf surface will in turn enhance the capacity of the plant for even more CO_2 sequestration (indirect effect). The photosynthesis parameterization in models reproduces the fertilisation effect, although they tend to fall short when reproducing changes in WUE (Keenan et al., 2013) and sometimes disagree (De Kauwe et al., 2013).

To analyse the response of carbon assimilation to environmental factors, photosynthesis schemes were run for a range of conditions. The variation of atmospheric CO_2 allows to characterise the CO_2 fertilisation effect at the leaf level, as reproduced by both models. When treating with the JULES model, emphasis is put in interpreting the results based on the underlying limiting regimes on photosynthesis. The environmental variables of interest are PAR radiation, leaf temperature and atmospheric CO_2:

- Photosynthetic photon flux density (PPFD). PPFD was varied from 0 to 1600 μmol

photons m^{-2} s^{-1} in intervals of 100 μmol photons m^{-2} s^{-1}. The maximum value in units of energy flux is about 350.4 W m^{-2} s^{-1} in the PAR spectrum, and 730 W m^{-2} s^{-1} of global radiation (assuming λ = 546.32 nm and PAR = 0.48 SW).

- Leaf temperature (T_l). It was varied from 0 to 50°C in intervals of 2°C.
- Atmospheric CO_2 (C_a). The units are μmol CO_2 (mol air)$^{-1}$ or ppm. It was varied from 200 to 800 ppm in intervals of 50 ppm. This range allows to analyse model response under conditions of low carbon dioxide all the way to a double CO_2 climate scenario (present level of atmospheric CO_2 is 400 ppm).

The rest of input parameters were set to reasonable values. Specific humidity was varied with temperature in order to maintain a constant relative humidity of 50%. The leaf boundary layer was set to a high value (g_b = 0.07 m s^{-1}) to represent fully coupled conditions between the leaf and the atmosphere. It is assumed that the soil water supply is not limiting photosynthesis.

The simulations were performed for each of the five plant functional types in JULES and for 5 vegetation types from the 20 possible vegetation types in the case of CTESSEL. The selected vegetation types for CTESSEL were chosen as the most comparable to JULES PFTs. The specific names and numbers of the vegetation types used are listed in Table 3.2 and their associated model parameter values are presented in Table 2.2. In what follows, fertilisation will refer to the CO_2 enhancement of photosynthesis at the leaf level only. This excludes effects derived from an increased leaf area index. The fertilisation effect is represented with plots depicting the response of CO_2 assimilation to atmospheric CO_2 concentration from 200 ppm to 800 ppm (A-C_a plots). These plots are related to A-C_i curves described in Chapter 2 (See Figure 2.2), due to the almost linear relationship between C_a and C_i (C_i/C_a~0.8). A-C_i curves are one of the main diagnostic tools in the study of photosynthesis (Von Caemmerer, 2000). Enhanced carbon dioxide concentrations slightly decrease the C_i/C_a ratio, resulting in increased difference outside (C_a - C_i) and therefore a reduction in stomatal conductance. The A-C_i curves for the different vegetation types shown in Table 3.2 are included in Appendix B.

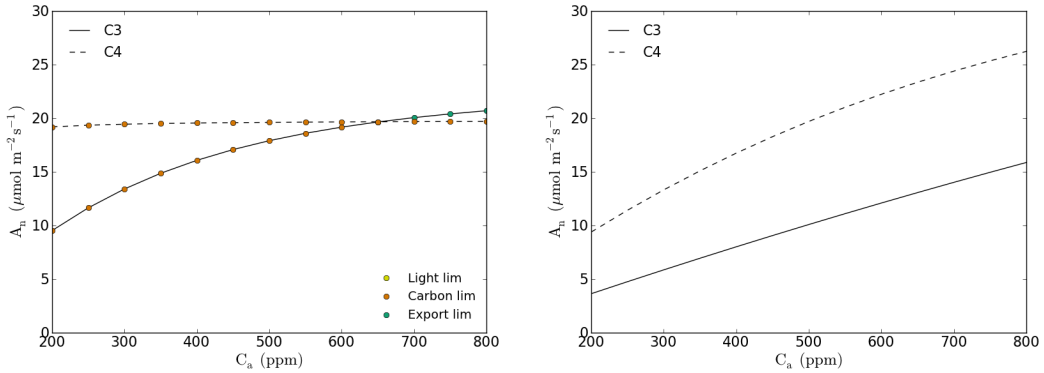

(a) JULES (b) CTESSEL

Figure 3.11: CO_2 response curve for C_3 grasses and C_4 grasses; leaf T =24°C, PAR=1600 μmol photon m^{-2} s^{-1}

3.4.1 C_3 and C_4 photosynthesis

The differences in the metabolism of C_3 and C_4 plants and how they incorporate CO_2 to the photosynthesis reaction lead to different sensitivities to increased atmospheric CO_2 concentration (Ehleringer et al., 2002). The C_4 photosynthetic pathway has the ability to concentrate CO_2 in the initial PEP carboxylation process. The carbon dioxide for rusbisco carboxylation is pumped from the chloroplasts, maintaining a constant high concentration, resulting in C_4 plants being less sensitive to CO_2 changes. C_4 photosynthesis is advantageous under low atmospheric CO_2 and high temperatures (Ehleringer et al., 2002).

Figure 3.11 shows A-C_a curves for C_3 grass and C_4 grass, as reproduced by JULES and CTESSEL's photosynthesis models. The leaf level response of each plant to ambient CO_2 is reflected by the slope of the curves, revealing the fertilisation effect or lack thereof. In JULES, for C_3 photosynthesis the curve's slope at low C_a and the magnitude of photosynthesis is determined by the value of V_{cmax}, the maximum rate of carboxylation. C_3 grass is shown as representative of the C_3 family, the other PFTs that also employ the C_3 pathway (shrubs, broadleaf trees and needle leaf trees) show a similar behaviour with lower slopes and lower photosynthetic rates (due to their lower V_{cmax}). JULES different formulation for C_4 pathway results in a minimal response of C_4 photosynthesis to CO_2. This lack of fertilisation effect has been corroborated by laboratory experiments (Collatz et al., 1992; Von Caemmerer, 2000) and is attributed to the initial carbon carboxylation process. C_4

photosynthesis is only sensitive to carbon at very low concentrations. The way this lack of fertilisation effect is reproduced with JULES formulation is by photosynthesis being limited by rubisco (Equation 2.44). W_c in the C_4 case represents rubisco carboxylation in the bundle sheath cells and is determined by the value of V_{cmax}, therefore not affected by changes in C_i, responding only to temperature variations. The limiting regime for photosynthesis has been highlighted on the curves in Figure 3.11a to identify the main drivers of photosynthesis. For the C_3 curve, rubisco limits the reaction for most C_a, except for the highest concentrations, when the export of photosynthesis products becomes limiting. There is no limitation from light in Figure 3.11a because these values are for high radiation (PAR = 1600 μmol photon m^{-2} s^{-1}). In the case of C_4, for all studied concentrations, the reaction is limited by rubisco, thus independent of CO_2. PEPcarboxylase limitation, occurs only for very low internal carbon concentrations (Partial pressure of CO_2, p_i ~5 Pa), beyond the range shown here. At these concentrations A_n increases abruptly with CO_2 and then stabilises in the range shown here (see Figure 1 in Collatz et al. (1992)).

CTESSEL however does not exhibit the different behaviour for each type of photosynthesis, at least not when using the default parameters for each plant type. Rather, all vegetation types present some fertilisation effect due to increased CO_2. Although the parameterization used in CTESSEL is the same for both metabolic pathways, it is possible to reproduce the C_4 photosynthesis lack of sensitivity to CO_2 change by imposing a high mesophyll conductance, as shown in other simulations using a similar photosynthesis model (Jacobs, 1994), with g_m = 17 mm s^{-1} (In Fig. 3.11b C_4 grass uses g_m = 2.3 mm s^{-1}).

In terms of climate change effects on vegetation, the lack of fertilisation in C_4 plants makes them less competitive against the thriving C_3 species in a high CO_2 scenario. However, the biochemical impact of CO_2 via the fertilisation is only one of the factors at stake. The influence of temperature, as will be discussed later, plays an important role.

3.4.2 Effect of temperature on fertilisation

In this section, the combined effect of temperature and CO_2 is explored. Only one plant type is shown, namely broadleaf trees as both models show good agreement for the photo-

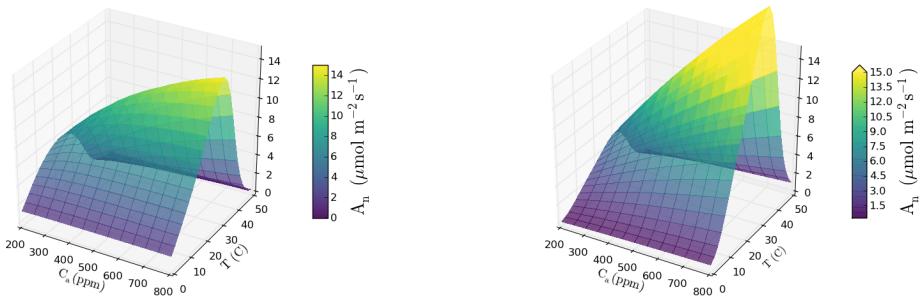

(a) JULES (b) CTESSEL

Figure 3.12: CO_2 response curve (C_a) with varying temperatures for broadleaf trees, PPFD = 1600 μmol photon m^{-2} s^{-1}

synthetic rates of this species, providing a better comparison. In Figures 3.12a and 3.12b the photosynthesis rate is shown (color and z-axis) as a function of both atmospheric CO_2 and leaf temperature. The lines across y-axis represent the effects of temperature on the kinetic activity behind photosynthesis. Initially there is a steady increase in photosynthesis rate with temperature, reaching a maximum at the optimum temperature and a steep drop thereafter, when high temperatures hamper plant activity. The fertilisation effect can be seen along the other axis (x-axis), from left to right. The slope of these lines is modulated by temperature dependence (y-axis), being virtually flat at low temperatures, and increasing slope and therefore fertilisation effect with temperature up to the optimum, after which the slope is reduced again. A more pronounced fertilisation effect is found for CTESSEL for the middle range of temperatures.

In Figure 3.13, the A-C_a curves introduced in Figure 3.12 are shown for three temperatures: 6°C, 18°C and 30°C, all below the optimum temperature, and at low radiation. It is evident how the fertilisation effect is greater at higher temperatures, as long as temperature remains below the optimum temperature (once past the optimum the slopes would be reduced again as seen in Fig. 3.12). Figure 3.14 also shows the fertilisation effect for the same temperatures but in this case for high radiation intensity PPFD = 1600 μmol photon m^{-2} s^{-1}. Again the higher temperatures foster the CO_2 fertilisation effect and CTESSEL presents the strongest CO_2 effect, with an almost linear increase with CO_2.

There is a clear relation between the magnitude of the fertilisation effect and the limiting

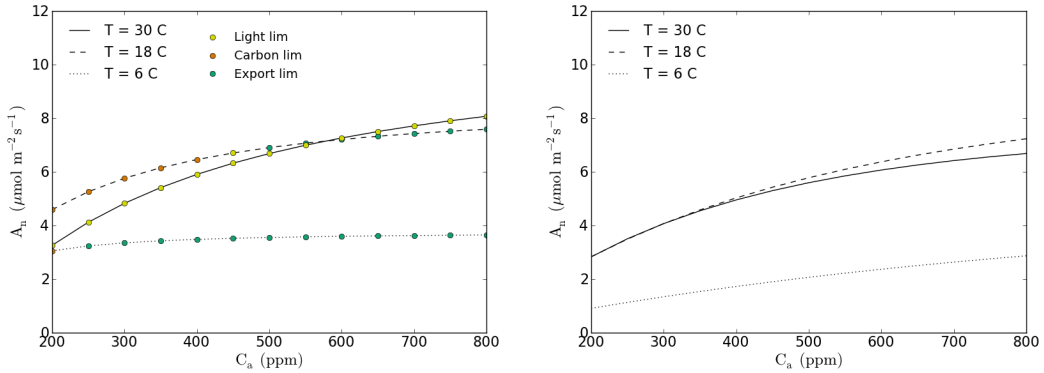

(a) JULES (b) CTESSEL

Figure 3.13: CO_2 response curve (C_a) with varying temperatures, for broadleaf trees, PPFD = 200 μmol photon m^{-2} s^{-1}.

factor on photosynthesis, as shown for JULES in Figures 3.14a and 3.13a, where the main limitation on photosynthesis has been indicated with coloured circles. To exemplify how the three photosynthetic rates (W_c in Equation 2.44, W_j in Equation 2.45 and W_e in Equation 2.46) respond to increased CO_2 and how they are combined together to yield the leaf net photosynthesis via a co-limitation quadratic equation (Eq. 2.52), their values are shown in Figure 3.15. Specifically, these values correspond to Figure 3.13a for T = 18°C. The carbon limiting regime has the strongest dependence with CO_2. The light limiting regime has weaker dependence and the export limiting regime is independent of CO_2. For this case (as was shown by the dashed line in Figure 3.13a) carbon limits the reaction when the C_a is up to 400 ppm, then there would be light limitation for C_a = 450 ppm and finally it is the export limitation that dominates, reducing the fertilisation effect as C_a increases. Due to the co-limitation there is still a subtle slope in A_n at the higher C_a, although W_e is flat.

At low irradiance, as can be seen in Figure 3.13a (PPFD = 200 μmol photon m^{-2} s^{-1}), export is the sole limitation for temperatures below 6°C and there is virtually no fertilisation effect. For temperatures between 6-36 °C the limitation comes from either CO_2 or light (or RuBP regeneration); there is therefore CO_2 fertilisation effect which is eventually reduced at higher C_a when export dominates. At high irradiance (Figure 3.14a) the light limitation plays no direct role. In this case, again export is the dominating regime at low temperatures (up to 6°C) hampering the fertilisation. For moderate temperatures (18-

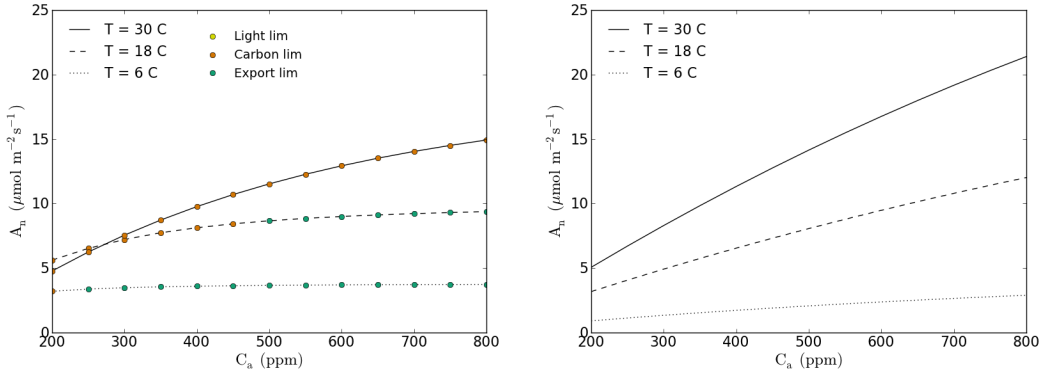

(a) JULES (b) CTESSEL

Figure 3.14: CO_2 response curve with varying temperatures for broadleaf trees, PPFD = 1600 μmol photon m^{-2} s^{-1}. In (a) the regime limiting photosynthesis is shown by the coloured circles.

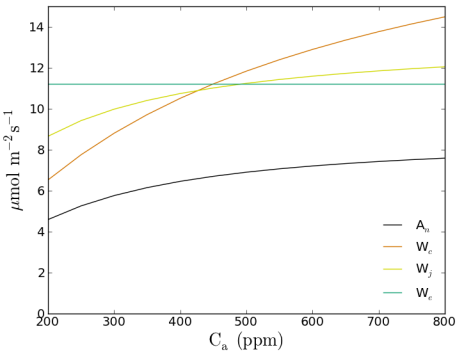

Figure 3.15: Dependence with ambient carbon of the three limiting photosynthetic regimes in JULES and the resulting leaf net photosynthesis. Broadleaf trees, PPFD = 200 μmol photon m^{-2} s^{-1} and T = 18 °C.

26°C) there is a combination of carbon at low C_a and export at high C_a, and for higher temperatures only CO_2 dominates.

At low temperatures, under export limiting regime, there is hardly any increase in photosynthetic rate with enhanced ambient carbon. This represents the lack of demand of carbon compounds from other organs of the plant, as the low temperatures reduce all physiological activity. Therefore enhanced CO_2 does not translate into increased photosynthetic activity. Export limiting regime in JULES is only dependent on temperature (via V_{cmax}, see Equation 2.45 in Chapter 2), and it is independent of carbon dioxide and radiation. As temperatures increase, some carbon limitation appears at the lower ambient carbon dioxide levels, combined with export for higher C_a. When carbon limits the photosynthesis reaction, the curve starts to show some steepness, to then flatten as it reaches the export limitation. The C_a value at which the shift from carbon to export limiting regime occurs increases rapidly with temperature. On the other hand, for temperatures above 28°C the limitation is entirely by carbon or light.

CTESSEL shows a similar behaviour at low radiation (Figure 3.13b), except for the coldest case, with a slightly steeper curve at 6°C. The fertilisation effect in CTESSEL diminishes for low temperature, but is not suppressed as in JULES, as this model has no export limitation. At low radiation both models exhibit similar predictions, as in CTESSEL the light limits photosynthesis at high C_a. At high radiation however, with no limitation from light in CTESSEL, there is a steady increase in photosynthesis in response to a carbon dioxide rise, with the fertilisation rate maintained up to the double CO_2 levels. This linear fertilisation is a consequence of the lack of export limiting regime. Although the highlighted limitation for JULES at high C_a in Figure 3.14a is carbon, the effect of export is manifested as a saturation through the co-limitation.

3.4.2.1 Effect of CO_2 on optimum temperatures for photosynthesis

The temperature at which the photosynthetic rate is maximum is determined by the combined temperature dependencies of the regimes in JULES, or temperature dependent parameters in CTESSEL. In JULES each limiting regime has a distinct temperature dependency. The export limiting regime presents a temperature optimum corresponding to

the V_{cmax} temperature optimum, whereas the carbon limiting regime presents an optimum for temperatures a few degrees lower, due to the effects of the other temperature dependent parameters. The light limited regime, although not directly affected by changes in temperature, can experience indirect variation via changes in humidity. If D_s is reduced due to an decrease in temperature, C_i increases following the Jacobs (1994) closure, increasing the apparent quantum efficiency (Eq. 2.45 and Eq. 2.56). The temperature at which each PFT is able to assimilate the maximum amount of carbon is the result of the co-limitation between the three situations. The effect of temperature is ultimately regulated by the T_{upp} and T_{down} parameters that regulate all temperature dependent parameters in JULES. These parameters are PFT dependent. In CTESSEL there are two pairs of parameters T_1 and T_2, one pair for mesophyll conductance and one pair for $A_{m,max}$. However these parameters are the same for all C_3 species and only vary for C_4 species (see Table 2.2).

The leaf net photosynthesis as a function of temperature for each plant type in both models is shown in Figure 3.16. The effect that CO_2 increase has on the response of photosynthesis to temperature is shown by the different colour lines, indicating the atmospheric CO_2 from 200 ppm to 800 ppm. As well as an increase in the photosynthetic rate due to fertilisation, the optimum temperature for photosynthesis sees an increase in a few degrees °C towards higher temperatures. The shift is particularly evident in JULES, although also found in a more reduced amount for some low vegetation plant species in CTESSEL (shrubs and C_3 grasses). Table 3.6 shows the values for the optimum temperatures for photosynthesis for each species and model for present day CO_2 (400 ppm) and doubled CO_2 (800 ppm). JULES shows an increment of 2°C on average by a doubling of present day atmospheric CO_2 concentrations. There is an exception: the optimum temperature for C_4 photosynthesis is not altered by CO_2 increase in neither model. Because of the PFT dependence of the T_{upp} and T_{down} parameters in JULES, the optimum temperatures for different species are more varied, from 20°C for needle leaf trees to 41°C for C_4 species. In CTESSEL, the optimum temperatures are more similar for all plant types.

The reason for the shift in the optimum temperature for photosynthesis is a consequence of the uneven response of the different limiting regimes to CO_2 increase in JULES. The CO_2 induced photosynthesis increase is more pronounced if the process is carbon limited. If the limit is on the triose phosphate (export), then there is only a slight fertilisation

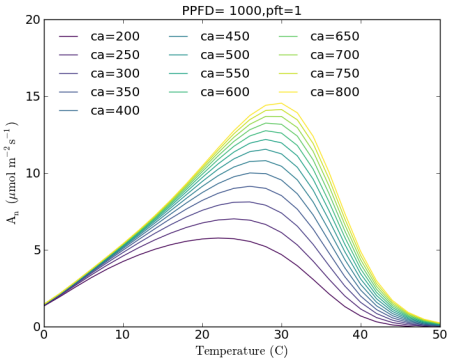

(a) JULES, Broadleaf trees

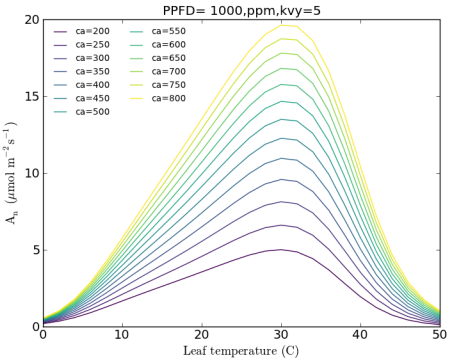

(b) CTESSEL, Broadleaf trees

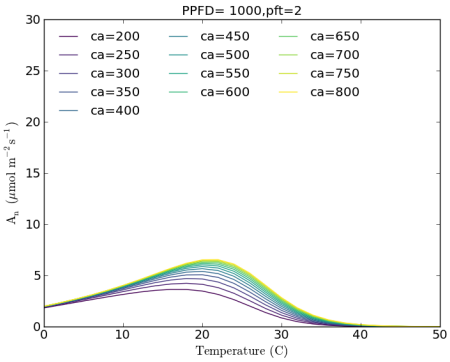

(c) JULES, needle leaf trees

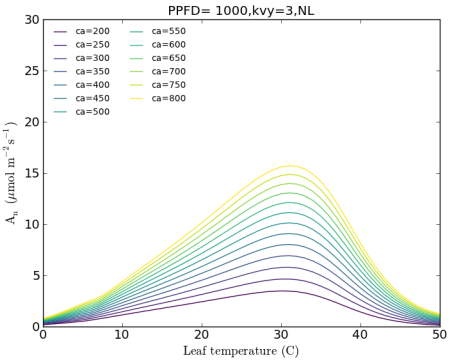

(d) CTESSEL, needle leaf trees

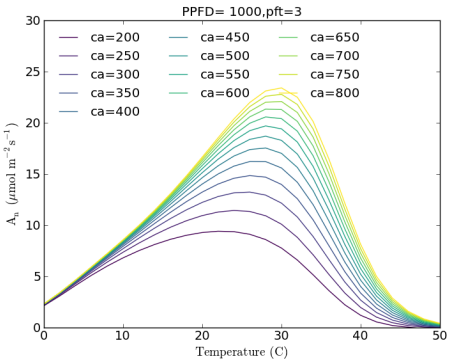

(e) JULES, C_3 grasses

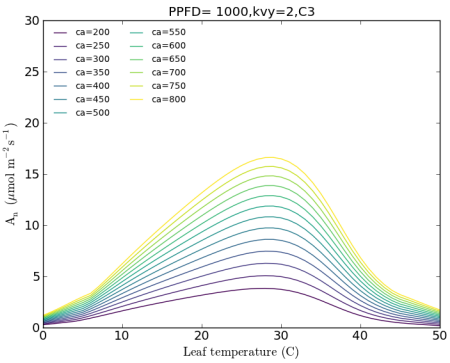

(f) CTESSEL, C_3 grasses

Figure 3.16: Leaf level photosynthesis as a function of leaf temperature for each PFT, with varying ambient CO_2 indicated by colour. PPFD = 1000 μmol photon m^{-2} s^{-1}.

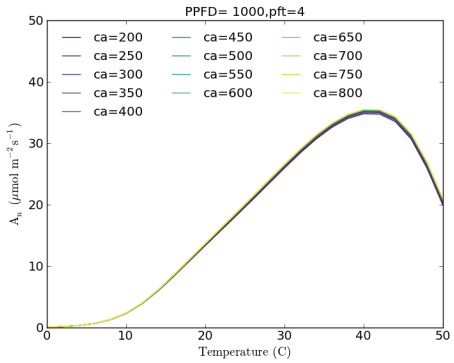

(g) JULES, C_4

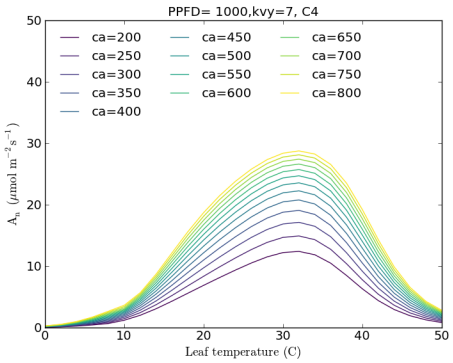

(h) CTESSEL, C_4

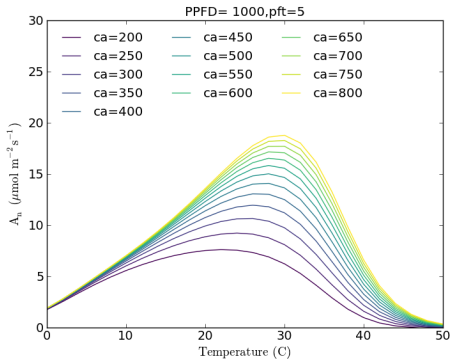

(i) JULES, shrubs

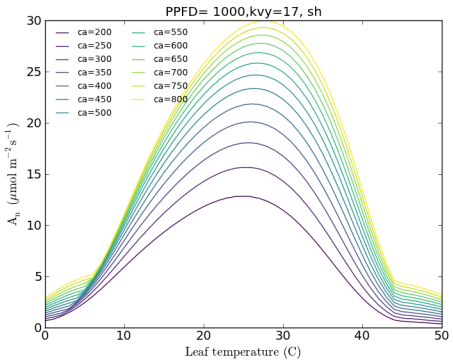

(j) CTESSEL, shrubs

Figure 3.16: (Cont.) Leaf level photosynthesis as a function of leaf temperature for each PFT, with varying ambient CO_2 indicated by colour. PPFD = 1000 μmol photon m^{-2} s^{-1}.

Table 3.6: Optimum temperature (°C) for photosynthesis, at C_a = 400 ppm and 800 ppm PPFD = 1000 μmol photon m^{-2} s^{-1}

PFT	JULES		CTESSEL	
	400 ppm	800 ppm	400 ppm	800 ppm
Broadleaf trees	27	29	31	31
Needle leaf trees	20	21	31	31
C_3 grasses	27	30	28	29
C_4 grasses	41	41	32	32
Shrubs	27	29	26	28

effect (from the co-limitation).

In JULES at relatively high radiation (1000μmol photon m^{-2} s^{-1}) photosynthesis is increasingly less carbon and export limited as CO_2 levels rise; since the export limited regime has its optimum at a higher temperature, the actual photosynthesis peaks at temperatures closer to the export limit optimum. At low light, the effect of optimum temperature shift is less severe. The *A-T* curve is more blunt around the maximum, due to the light limitation, which only has an indirect dependence on temperature through possible changes in humidity. Although CTESSEL's parameterization presents differences in the way the limitations of photosynthesis are brought together, there is also a slight increase of the optimum temperature. In this case the shift is more subtle, and not appreciated in the plots.

There are some differences in how this effect appears in the different PFTs in JULES. C_3, shrubs and broadleaf trees show a similar response to enhanced CO_2, a substantial increment in photosynthesis and 2-3°C increment in the optimum temperature for a doubling in the atmospheric CO_2. Needle leaf trees are less responsive to the CO_2 increase and show a 1°C shift. On the other hand, C_4 plants are virtually insensitive to the carbon increase (as seen in Figure 3.11a) and show no shift in the optimum temperature for photosynthesis. In CTESSEL there is less variation in the behaviour of the different PFTs. C_4 plants photosynthesis also see a photosynthesis increase with enhanced CO_2 but no variation on the optimum temperature. The effective increase in the optimum temperature for photosynthesis can be interpreted as an acclimation of the plants. However, the driver of the acclimation is not the temperature itself but the enhanced CO_2. This is an interesting result that emerges in a implicit way from the construction of photosynthesis models, and is in agreement with observations/predictions of acclimation (Yamori et al., 2005).

3.4.3 Effect of radiation on fertilisation

In this section the response of photosynthesis to increasing radiation levels in JULES and CTESSEL is explored, as well as the effect radiation has on fertilisation by enhanced CO_2.

Figures 3.17a and 3.17b show the combined effects of ambient CO_2 and incident photon

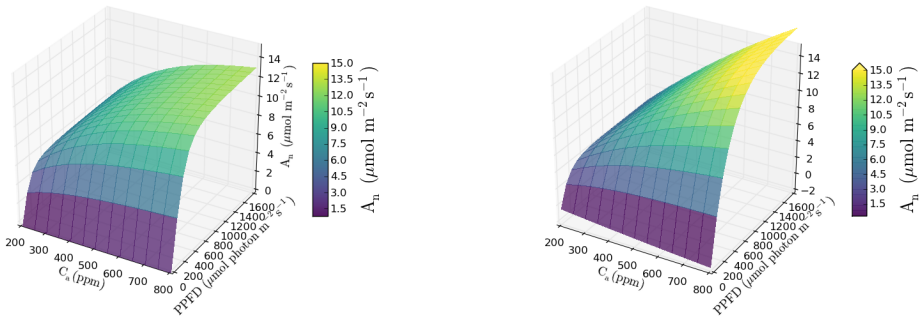

(a) JULES (b) CTESSEL

Figure 3.17: CO_2 response curve with varying irradiances, for broadleaf trees (vegetation type = 5), leaf T = 24°C.

flux on photosynthesis rate. The photosynthesis values shown represent the steady-state response, i.e. the rate that would be attained after exposure of a leaf to a constant level of irradiance. Temperature is fixed to 24°C and the plant type is broadleaf tree. Along the y-axis the effect of light on photosynthesis is reproduced. Initially, for low radiation intensities, there is a steep linear increase in photosynthesis governed by the quantum efficiency. The quantum efficiency (ϵ_0 or α) measures the effectiveness in transforming radiant energy to fixed carbon. During the linear increase photosynthesis is light limited (or RuBP regeneration limited). Under these conditions of low light, CO_2 assimilation is highly sensitive to radiation. At a certain level of radiation, the photosynthetic system becomes light saturated, and an increase in radiation will no longer increase the photosynthetic rate because it becomes limited by carbon or the consumption of the photosynthetic products. The CO_2 fertilisation effect is influenced by radiation levels, being greater at high radiation. However, the effect of radiation on the CO_2 fertilisation effect (slope of the A-C_a curves) is not as strong as the effect of temperature (Figures 3.12a and 3.12b).

Figure 3.18 shows the A-C_a curves projected on the z-x plane to illustrate the influence of varying radiation on photosynthesis and the CO_2 fertilisation. In the case of JULES (Figure 3.18a), again the limiting regime has been highlighted to be able to interpret the results in the light of the limiting regimes. For radiation levels below 200 μmol photon m^{-2} s^{-1}, light is the limiting factor. The sensitivity to light at low radiation is very high (as shown by the wider separation between 200 μmol photon m^{-2} s^{-1} and 500 μmol photon

m^{-2} s^{-1} and the progressive approaching of lines for higher radiation). This enhances the importance of a correct radiative transfer representation inside the canopy, since although the magnitude of photosynthesis for little light intensity is low, the accumulated effect after upscaling can be important. As radiation increases the limiting regime switches from light to carbon, and photosynthesis progressively becomes less sensitive to radiation. Both carbon and export limiting regimes are dominating and are independent of radiation, but due to the co-limitation, some radiation dependence is still apparent. At the highest radiation levels, the curves stack together: an increase in radiation does not result in an increase in carbon assimilation and photosynthesis becomes light saturated. Experimental studies support this lack of response to light when CO_2 assimilation is RuBP saturated (Sage et al., 1990) but generally for higher radiations than the ones seen in JULES.

In terms of the fertilisation effect seen for the various radiative levels shown in Figure 3.18, it can be seen how, as seen with varying temperatures in the previous section, the limiting regime has an influence on the magnitude of the fertilisation. At low radiation levels when light limits the speed at which RuBP regeneration can occur, the photosynthetic process becomes RuBP-limited, i.e. there is not enough RuBP for carboxylation, then photosynthesis rate is less affected by enhanced CO_2. This is reflected by the smaller slope of the A-C_a curves in Figure 3.18 for PPFD = 200 μmol photon m^{-2} s^{-1}. On the other hand, for high levels of radiation, when carbon is the limiting factor, RuBP is present in saturating quantities and any increase in CO_2 molecules will find substrate for carboxylation, resulting in increased net photosynthesis. When carbon limits photosynthesis and with temperature near the optimum the strongest fertilisation effect is achieved. In JULES, the curves for PPFD = 500, 1000 and 1500 μmol photon m^{-2} s^{-1} only show a slight difference in slope compared to PPFD = 200 μmol photon m^{-2} s^{-1} and this is due to the influence of the export limiting regime. When photosynthesis is limited by triphosphate utilisation it is insensitive to changes in CO_2. Again CTESSEL shows a more steady increase in photosynthesis as a response to enhanced CO_2. The main difference when comparing Figures 3.18a and 3.18b appears at high radiation and high ambient CO_2 concentrations. CTESSEL presents a more steady fertilisation effect than JULES. The slope of CTESSEL's A-C_a curves is maintained for all the range of CO_2 levels (Figure 3.18b), whereas JULES curves experience a levelling off at high CO_2 associated to the export limiting regime. (Figure 3.18a). This difference is a consequence of the lack of

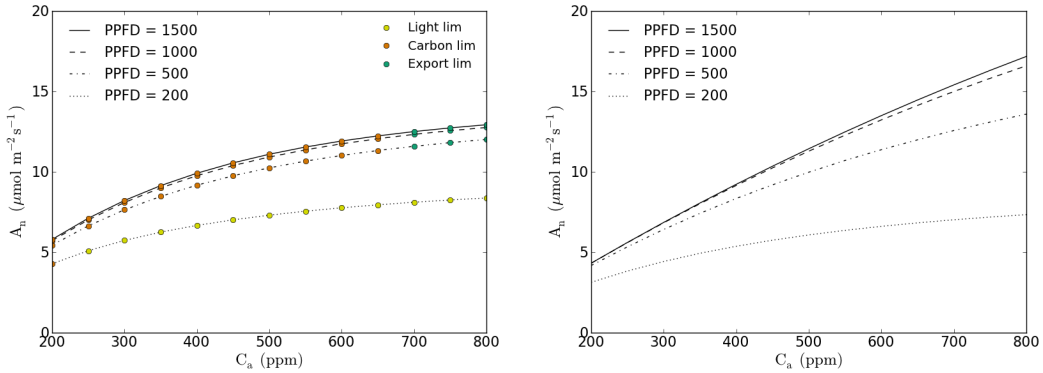

(a) JULES (b) CTESSEL

Figure 3.18: CO_2 response curve (C_a) with varying irradiances for broadleaf trees, leaf T = 24°C. In (a) the regime limiting photosynthesis is shown by the symbols.

export limiting regime in CTESSEL. At normal temperature and conditions both models behave similarly; however, the fertilisation effect reproduced by CTESSEL is greater, especially when combined with high radiation levels and around the optimum temperature for photosynthesis. This difference is a consequence of the lack of export limiting regime in CTESSEL.

3.4.3.1 Effect of CO_2 on light saturating values

As a consequence of the dissimilar response to CO_2, depending on the limiting factor, the level of radiation at which the photosynthesis reaction shifts from being RuBP limited (light limited) to RuBP saturated (carbon/export limited) has been found to increase with enhanced CO_2 if the transition is made to carbon limited.

Figure 3.19 depicts the dependence of photosynthesis on radiation and the effect of increasing CO_2 (shown by the colour lines). The enhanced CO_2 increases primarily the carbon limited photosynthetic rate, and therefore the value of photosynthesis at light saturation (flat part of the curves). It also affects the light response (slope at low radiations) but to a lesser extent. The export limited regime is independent of carbon concentrations; therefore while the other carbon rates increase driven by carbon, the export limit slows the photosynthetic rate and becomes the limiting factor at higher CO_2 concentrations. These changes result in higher levels of photosynthesis at saturating radiation levels and

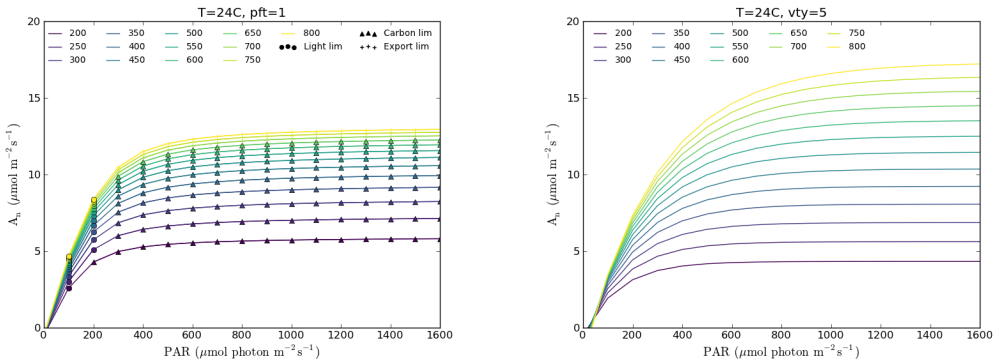

(a) JULES (b) CTESSEL

Figure 3.19: Leaf level photosynthesis as a function of PAR irradiance for broadleaf trees; colour indicates the CO_2 concentration, leaf T = 24°C

Table 3.7: PPFD (μmol photon m^{-2} s^{-1}) at which photosynthesis becomes light saturated, JULES model for broadleaf trees for different temperatures and atmospheric CO_2.

	200 ppm	400 ppm	800 ppm
T_l = 6 °C	80	80	80
T_l = 18 °C	160	200	200
T_l = 30 °C	220	260	300

a more acute response to irradiance for low levels of radiation as a response to increasing levels of CO_2. The fertilisation effect on the A-PPFD curves in CTESSEL's photosynthesis model is greater than in JULES, as seen in previous sections, related to the lack of export limitation and can be seen in Figure 3.19b by the larger spread of the curves.

The values of radiation at which photosynthesis becomes light saturated are presented in Table 3.7, for three leaf temperatures, 6°C, 18°C and 24°C and for broadleaf trees in the JULES model. The radiation indicated is that for which photosynthesis is no longer under light limiting regime, and becomes carbon limited or export limited at very high CO_2 concentrations (the transition is to export at low temperatures and/or high CO_2 concentrations). The progressive increase of the radiation level at which the transition from light limiting to rubisco limitation occurs has been acknowledged before (Von Caemmerer, 2000). This effect has been identified in the leaf level modelled experiments; however it has been found that when the transition occurs from light limiting regime to export limiting

regime (at colder temperatures) the threshold radiation does not change (will be addressed in Section 3.4.4). In Table 3.7 the values for 6°C correspond to light saturation towards export limiting regime. Similarly to JULES, the progressive increase of the radiation at which photosynthesis becomes light saturated also occurs in CTESSEL simulations, with the difference that saturation levels are generally higher.

The increased difference between light limited photosynthesis and light saturated photosynthesis with elevated CO_2 could enhance the effect of global dimming on increasing photosynthesis reported by Mercado et al. (2009). If diffuse radiation increases as a result of increased clouds and aerosols, more light can reach canopy layers that are limited by light and therefore have potential to increase their photosynthesis rate. Figure 3.19 shows that the effect of CO_2 is to increase the difference between light limited photosynthesis and light saturated photosynthesis, allowing a greater response to light in the light limited regime.

3.4.4 Effects of CO_2 on limiting regimes

In the previous sections the interaction of temperature and radiation with the CO_2 leaf level fertilisation has been analysed. It has become evident how the limiting regime governing photosynthesis plays an important role in determining the magnitude of the fertilisation effect. In this section the focus is not on the magnitude of photosynthesis but on the changes in the occurrence of the limiting regimes. Thus, dependence of the limiting regimes (carbon, light and export) on incoming radiation and temperature is analysed, as well as potential changes that a doubling of atmospheric CO_2 would have on when the limiting factors occur.

For this purpose the JULES model is used, since in its calculation process the 3 limiting regimes are derived beforehand in order to obtain the actual photosynthesis. The minimum of the limiting regimes for each combination of photosynthetic photon flux density, leaf temperature and atmospheric CO_2, is identified as the dominating regime. The increase in atmospheric CO_2 affects the three potential photosynthetic rates in a different manner. In C_3 plants the carbon limiting regime is significantly increased by enhanced CO_2, the light limiting regime is increased at a lesser rate and the export limiting regime is not affected

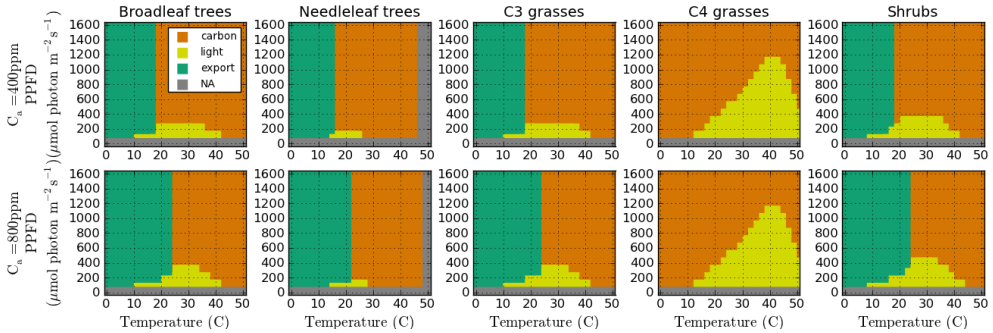

Figure 3.20: Dominating limiting regime as a function of leaf temperature and PPFD, for 400 ppm and 800 ppm, and for each PFT.

by it. Due to these heterogeneous responses, the distribution of the limiting regimes varies with CO_2 increase. C_4 plants with their photosynthetic process being insensitive to CO_2 (at least at the studied concentrations) show no change with increasing CO_2. These effects have already been described in previous sections for specific cases; however, in this section the limiting regimes distribution is presented for all PFTs at all temperatures and radiation values studied.

In Figure 3.20 the dominating regimes are presented for the 5 PFTs and the atmospheric CO_2 concentrations of 400 ppm and 800 ppm. The carbon limited regime is represented by the orange area, the export limiting regime is represented by the green area and the light limiting regime is represented by the yellow area. Grey indicates that net photosynthesis is below zero, which means that leaf dark respiration offsets the carbon uptake. The resolution is 2°C for temperature and 100 μmol photons m^{-2} s^{-1} for radiation.

In the case of C_3 species, the general picture is set by carbon limited conditions at higher temperatures and export limited regime at lower temperatures. Light is the limiting factor when radiation is low (up to 200-400 μmol photons m^{-2} s^{-1}) and around the optimum temperature for photosynthesis. Although it might appear as the area corresponding to light limited regime is rather small, it should be noted that daily radiation varies from zero before dawn to a maximum at midday and down to zero after sunset. Moreover, the light limited areas correspond to more common temperatures.

There are two main effects on the regime distribution as a consequence of double CO_2 concentrations: (i) the temperature threshold between export and carbon limitations becomes

higher and (ii) the radiation threshold between light and carbon limitation is increased. The first effect is the precursor of the shift seen in optimum temperatures described in Section 3.4.2.1 while the second determines the radiation at which photosynthesis becomes light saturated, as described in Section 3.4.3.1.

For an atmospheric CO_2 concentration of 400 ppm, for broadleaf trees, C_3 grasses and shrubs, the temperature beyond which photosynthesis is carbon limited is similar (approximately 18°C), whereas for needle leaf trees it is slightly lower, since coniferous species are typically adapted to lower temperatures. In a scenario of double atmospheric CO_2 (bottom row of Figure 3.20), the boundary temperature between export and carbon regimes is pushed towards higher temperatures by several degrees in all C_3 species. This implies that, in a scenario with double atmospheric CO_2 concentration, export will be the limiting regime under conditions that were before limited by carbon. Contrary to the carbon and light limiting regimes, the photosynthetic rate associated with the export limiting regime does not increase with a rise in carbon; becoming limiting in areas where CO_2 is no longer limiting. The photosynthetic rate determined by the export limitation is independent of atmospheric carbon or radiation, being only related to the plant biochemical capacity and therefore temperature. This result suggests that, the physiology of the C_3 vegetation will play a bigger role in determining the rate of the vegetation carbon sink. Although the parameterization of the export limiting regime in JULES is rather crude, the underlying assumptions have a reasonable basis (Sharkey, 1985). Further model development should incorporate potential plant acclimation either through the export limiting regime or by establishing physiological constraints between the carbon gain and other plant processes.

The different functioning of C_4 photosynthesis results in different limitations on photosynthesis. Carbon limitation in Figure 3.20 corresponds to rubisco (final carboxylation) and export corresponds to PEP carboxylase (initial carboxylation). Under the studied conditions, C_4 photosynthesis is limited either by light or by rubisco kinetics, with no limitation by PEP carboxylase. The partial CO_2 pressure required for PEP carboxylase to be limiting in JULES would be 5 Pa (taking P_{atm}~10^5 Pa in Equation 2.46). This value is extremely low and only obtained in laboratory experiments. It would correspond to an ambient CO_2 concentration of $C_a = 70$ ppm (assuming C_i/C_a ratio of 0.7). This value is in accordance with Collatz et al. (1992) who assign PEP carboxylase limitation for values of intercellular carbon partial pressures below 10 Pa. The JULES photosynthesis

model shows no response to increases in atmospheric CO_2 for C_4 vegetation. There is no increased assimilation via a fertilisation effect and no change in the limiting factors. The only regime sensitive to CO_2 is PEP carboxylase limitation, and an effect could be manifested via the co-limitation; however the photosynthetic rates from a supposed PEP carboxylase limitation are extremely high and therefore have no effect in the total net photosynthesis. The light limitation in C_4 grasses is more common than in C_3 species. The range of temperatures for which the light limitation dominates decreases as radiation increases, but it persists until higher radiation levels than those seen for C_3. The distribution of limiting regimes for C_4 plants has virtually no variation with an increase in ambient CO_2, as the only regime with dependence on C_i is the carboxylation catalysed by PEP carboxylase.

The distribution of limiting regimes presented here for broadleafs at 400 ppm in Figure 3.20 can be related to the identification of limiting regimes conducted in the model validation using field observations in Section 3.3.3.1, (Figure 3.3). However, from 3.20, one would have expected export limitation to occur more often in the observations (for any temperature below 18°C). One reason why there are less observations limited by the export regime is that in that case ambient CO_2 was 325 ppm (reference value measured at the site). The lower atmospheric CO_2 lowers the limiting temperature between export and carbon, the same way that the doubled CO_2 raises it. Moreover the fact that there is not a strict delimitation between regimes in Figure 3.3 with respect to temperature, light and PPFD as seen in Figure 3.20 is because of the variations in humidity.

3.5 Stomatal conductance

The stomatal conductance for water vapour is very closely linked to photosynthesis. Stomata behave in such way to maintain a rather constant ratio of carbon dioxide concentration outside and inside the pore (Wong et al., 1979). In the studied photosynthesis models, and A-g_s models in general, the C_i/C_a ratio regulates the coupling between photosynthesis and stomatal aperture (Eq. 2.41). This relationship is the basis of the A-g_s schemes, which establish a connection between the carbon and water exchanges. The stomatal conductance controls the transpiration from the leaf, which is fueled by the water uptake

from the roots, and conditions the soil moisture content, affecting hydraulic conductivity and surface runoff. In this section the stomatal conductance's response to CO_2 and air humidity, as reproduced by JULES and CTESSEL, is compared, as well as the intrinsic water use efficiency.

3.5.1 Effect of CO_2

The stomatal conductance is the result of the ratio of photosynthetic rate A_n and the (C_a - C_i) difference (scaled by the factor 1.6). Therefore the effect of CO_2 on stomatal conductance depends on the response of these two terms to increased CO_2. The effect of increased ambient CO_2 on photosynthesis is of enhancement (fertilisation), which results in an increase in g_s (numerator in Eq. 2.41). On the other hand, intercellular CO_2 also increases with increased ambient CO_2 but at a lower rate than C_a itself, resulting in a increase of (C_a - C_i) (denominator in Eq. 2.41). This effect outweights the A_n increase, hence the net effect of a CO_2 increase on stomata is to reduce the stomatal conductance. The stomatal closure reduces transpiration from the leaves, consequently increasing the water use efficiency (WUE), or water transpired per unit of carbon assimilated.

To illustrate the effect of CO_2 increase on the C_i/C_a ratio, their dependence is shown in Figure 3.21 for the five PFTs represented in JULES and their corresponding plant types in CTESSEL. To focus on the influence of CO_2 on C_i/C_a, relative humidity has been kept constant. Both models calculate the intercellular carbon concentration with Jacobs (1994) closure (Eq. 2.43); however, the C_i estimates from both models are different, with CTESSEL having lower intercellular carbon concentration (also seen in Section 3.3.4.1, Figures 3.9 and 3.10).

Overall CTESSEL presents lower C_i/C_a ratios for all plant types, due to the lower values for f_0 used in CTESSEL (Tables 3.4 and 3.3). In JULES, shrubs and C_3 grasses present the highest ratio, with $f_0 = 0.9$. Broadleaf trees have a higher ratio than needle leaf trees. Although both have $f_0 = 0.875$, the difference in this case relays in the higher D_{crit} of broadleaf trees. C_4 plants present the lowest ratio, which agrees with experimental data Jacobs (1994). In CTESSEL, shrubs have the highest C_i/C_a ratio corresponding to the highest f_0 (0.95). Next are needle leaf trees, C_4 plants, broadleaf tress and C_3 grasses which

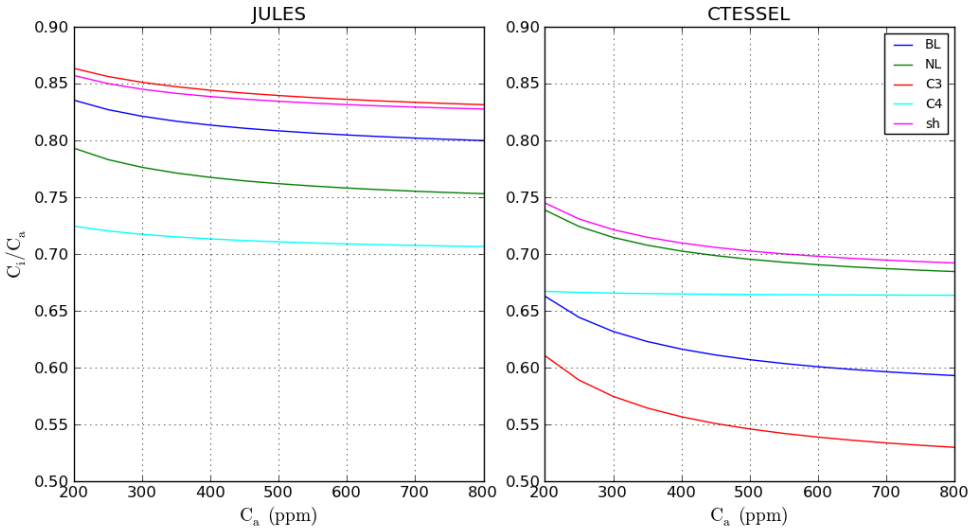

Figure 3.21: C_i/C_a ratio dependence on C_a for all PFTs. Leaf temperature = 24°C, relative humidity = 50%, PPFD = 1600 μmol photon m^{-2} s^{-1}.

present the lowest ratio given its low value of f_0 (0.65). The f_0 values for high vegetation are derived from mesophyll conductance by the relation stated by Calvet (2000). The ratio shown for C_4 plants is higher than reported by experimental data (about 0.4) in Wong et al. (1979). The insensitivity shown to the increase of ambient CO_2 is achieved by a very low CO_2 compensation point of Γ = 2.6 ppm (see Equation 2.42), while all other C_3 species have 42 ppm and therefore show a more marked decrease in C_i/C_a with increased C_a.

The higher C_i/C_a ratios found in JULES are associated with higher stomatal conductances. Figure 3.22 shows the stomatal conductance for broadleaf trees as produced by each model as a function of C_a. The effect of temperature is shown by three cases. This figure depicts the g_s associated to the leaf level net photosynthesis values showed in Figure 3.14. It is interesting to compare these two figures: although CTESSEL showed more sensitivity on A_n due to increased C_a; in terms of g_s, it is JULES that shows more sensitivity due to increased C_a. The relation between A_n and g_s is determined by the intrinsic WUE, which is simply the ratio A_n/g_s, a leaf level equivalent of WUE (Egea et al., 2011). In fact, the intrinsic WUE is by definition the difference C_a - C_i as deduced from Equation 2.41. Figure 3.23 shows the intrinsic WUE of both models calculated by dividing the values of g_s and A_n presented in Figures 3.22 and 3.14. JULES has lower WUE and presents less

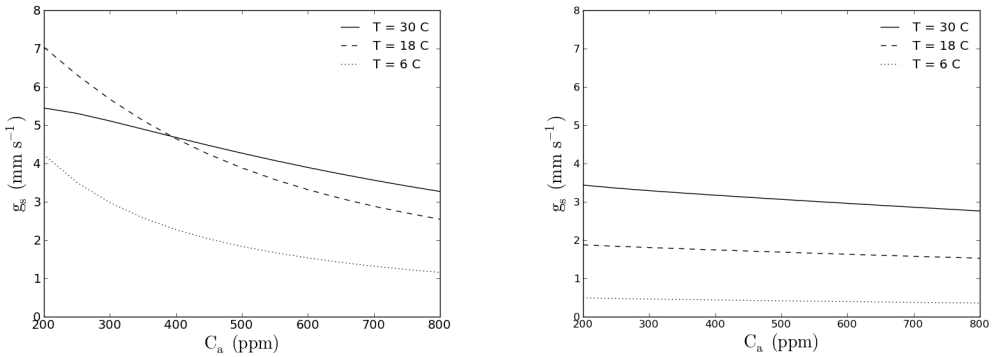

(a) JULES (b) CTESSEL

Figure 3.22: Stomatal conductance as a function of atmospheric CO_2 for broadleaf trees; PPFD = 1600 μmol photon m^{-2} s^{-1}

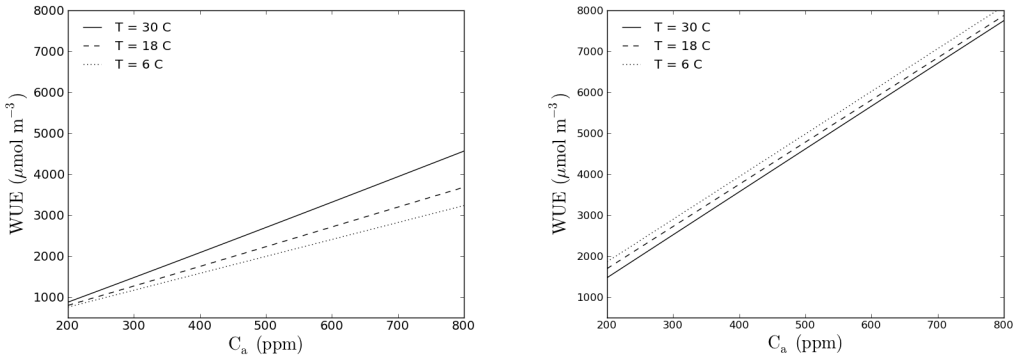

(a) JULES (b) CTESSEL

Figure 3.23: Intrinsic WUE as a function of atmospheric CO_2 for broadleaf trees; PPFD = 1600 μmol photon m^{-2} s^{-1}

variation with CO_2.

The higher sensitivity of JULES' g_s to CO_2 has implications for the hydrological cycle in climate change simulations. Under well coupled conditions, a reduction in g_s driven by an increase in atmospheric CO_2 will reduce transpiration more than in other models.

3.5.2 Effect of air humidity

Air humidity plays an important role in determining C_i and the stomatal aperture. Similarly to the effect of CO_2, it is through the Jacobs (1994) closure equation (Eq. 2.43) that

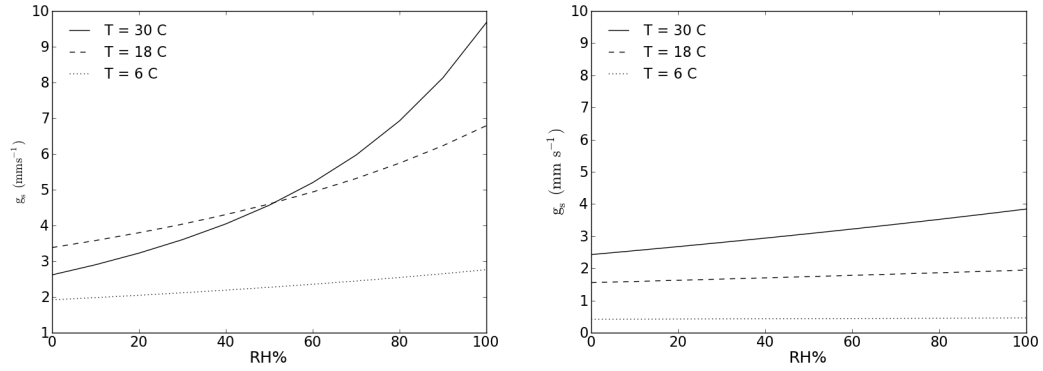

(a) JULES (b) CTESSEL

Figure 3.24: Stomatal conductance as a function of relative humidity for broadleaf trees; PPFD = 1600 μmol photon m^{-2} s^{-1}

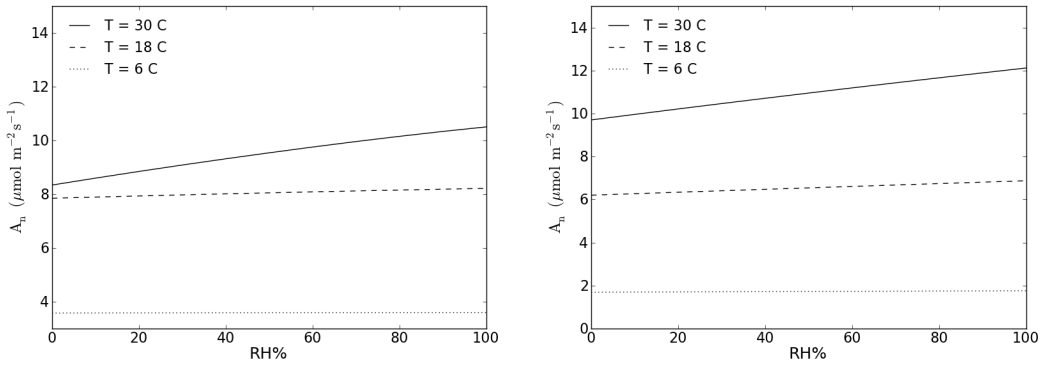

(a) JULES (b) CTESSEL

Figure 3.25: Net leaf photosynthesis as a function of relative humidity for broadleaf trees; PPFD = 1600 μmol photon m^{-2} s^{-1}

humidity, or more specifically humidity deficit (D_s) regulates the stomatal aperture.

Figure 3.24 shows g_s for broadleaf trees as a function of relative humidity for 3 different temperatures. JULES values for g_s are higher than those is CTESSEL. More importantly, JULES presents a higher stomatal sensitivity to humidity and temperature. As indicated in light of the high sensitivity to atmospheric CO_2 showed by JULES, in the case of humidity it is again the higher values of f_0 in Jacobs (1994) closure equation that are behind the high sensitivity. This high sensitivity explains the rapid stomatal closure highlighted in the models validation for JULES at the sunlit leaves (Figure 3.6). A benchmarking study using JULES by Blyth et al. (2010) also reported an exaggerated drop in modelled

diurnal evaporation at two dry sites compared to observations.

The sensitivity does not translate to the photosynthesis values as illustrated by Figure 3.25 which shows the leaf net photosynthesis associated to the cases presented in Figure 3.24. Both models show comparable estimates of A_n despite their difference in g_s. This is because the differences in g_s are compensated by the differences in intrinsic WUE (or C_a-C_i).

3.6 Global sensitivity analysis

In the previous sections the effects of environmental variables on photosynthesis have been analysed by varying each factor and the emphasis was put into explaining the differences based on the limiting regimes. The differences amongst PFTs via model parameters have also been explored within each model and across the two models. However due to the complexity and non-linearity of the modelled photosynthesis, a more comprehensive and robust sensitivity analysis is needed to identify the key environmental drivers for photosynthesis and the model parameters to which photosynthesis is most sensitive and underpin the interactions amongst them.

3.6.1 Introduction

A global sensitivity analysis allows to ascertain the individual influence of each input parameter in a particular model output of a system or numerical model. With the increasing complexity of land surface models, sensitivity analysis are a valuable tool to highlight relevant parameters for certain model output (e.g. energy fluxes). Several land surface models have been previously studied using sensitivity analysis (Collins and Avissar, 1994; Rodríguez-Camino and Avissar, 1998). More recently, Alton et al. (2007) conducted a sensitivity analysis on JULES model for several biomes. The information provided by sensitivity analyses is useful for calibration purposes as well as providing a better understanding of the model processes. Consequently, sensitivity analyses have also been applied to ecological models (Raj et al., 2014; Verrelst et al., 2015).

Due to the non-linearity and complexity of the photosynthesis models, global sensitivity

methods for uncertainty and sensitivity analysis are required instead of local methods that vary one factor at the time (Saltelli et al., 2006). Global methods are model independent, whereas methods based on correlation analysis give information about the linear representation of the model (Saltelli et al., 1999). Global methods search parameter space by varying all parameters simultaneously, therefore exploring interactions amongst the dimensions. Consequently, they are able to determine not only the main effect (first order term) of a given parameter, but also the total variability attributable to the parameter via its interactions with other parameters (total sensitivity indices). These methods are based on variance decomposition of model output and include Sobol' (Sobol', 2001) and Extended Fourier Amplitude Sensitivity Test (FAST) (Saltelli et al., 1999).

In this section, the sensitivity of JULES and CTESSEL photosynthesis models to both the driving variables and the model parameters is analysed. Sensitivity analyses of land surface models have revealed that stomatal conductance is a key parameter affecting energy fluxes (Collins and Avissar, 1994; Orth et al., 2016). In this study, a further step is taken to reveal the influence of photosynthesis on stomatal conductance and analyse what environmental factors (driving variables) and plant specific model parameters most influence the variance of the stomatal conductance. As well as stomatal conductance, other output variables are analysed: leaf level photosynthesis (A_n), intercellular carbon concentration (C_i) and leaf dark respiration (R_d).

3.6.2 Method

The most common variance based methods that compute total sensitivity indices are Sobol' and Extended Fourier Amplitude Sensitivity Test (FAST). Although their numerical approach varies, they have shown to give similar results for the main effect of the input variables (Saltelli and Bolado, 1998). Sobol' has proved more accurate when higher order terms are important, however it is more dependent on sample size. The advantages of FAST are its robustness and its computational efficiency (Saltelli and Bolado, 1998).

The mechanism of FAST (or any quantitative methods for sensitivity analysis) is shown in the schematic in Figure 3.26 extracted from Saltelli et al. (1999). The theoretical basis behind FAST and its extended version is described in Appendix A and a summary is

introduced here.

The system or model f returns an output y for a given set of n input parameters x_i:

$$y = f(x_1, x_2, ...x_n) \tag{3.3}$$

Each of the input parameters is sampled from its characteristic probability distribution. A number of samples N_s is created combining values of each input parameter. The model is run for each sample, and the variance of the output is analysed and explained in terms of the variance of each input parameter. The method assigns to each input factor a first order effect index S_i (from 0 to 1) that indicates the influence it has on model output.

$$S_i = \frac{Var_i(y)}{Var(y)} \tag{3.4}$$

The extended version also computes an index to quantify the total influence attributable to each input parameter, in this case accounting for interactions amongst parameters, the total effect index is:

$$S_{Ti} = Var(y) - Var_{(\sim i)}(y) \tag{3.5}$$

where $\sim i$ means variance by all factor except for factor i.

An input factor is considered 'very important' if its S_{Ti} is above 0.8 , 'important' if 0.8 $>S_{Ti}$ >0.5, 'unimportant' if 0.5 $>S_{Ti}$ >0.3 and 'irrelevant' if less than 0.3.

3.6.2.1 Extended FAST - SimLab

The photosynthesis models of JULES and CTESSEL were analysed with the Fourier extended Amplitude Sensitivity Test (FAST) method (Saltelli et al., 1999), as implemented in the SimLab software package, developed by the Joint Research Centre of the European Commission (`https://ec.europa.eu/jrc/en/samo/simlab`). As well as FAST, SimLab provides a myriad of methods for uncertainty and sensitivity analysis.

The analysis will ascertain how important the ambient conditions (driving variables) are compared to the plant type characteristics (model parameters) in regulating each of the analysed output variables: leaf photosynthesis (A_n), stomatal conductance (g_s), intercellular carbon (C_i) and leaf dark respiration (R_d). The analysis was performed with other

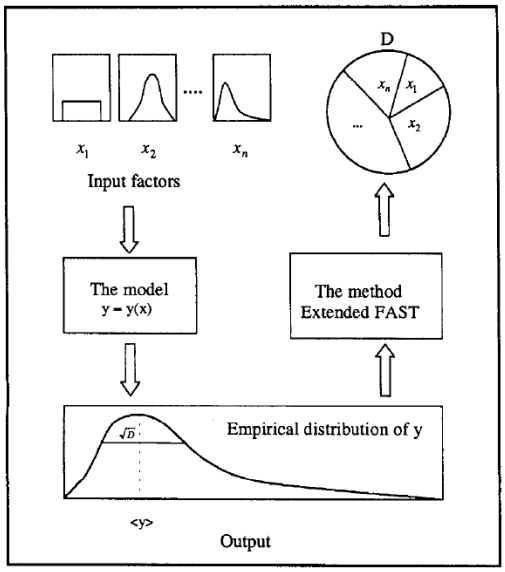

Figure 3.26: General scheme of a quantitative Sensitivity Analysis method. Figure from Saltelli et al. (1999). D is the output variance.

model outputs (limiting photosynthesis rates W_c, W$_j$ and W_e in the case of JULES) which reveals the importance of both groups of input parameters (ambient conditions and model parameters) during each limiting regime.

SimLab's procedure consists of 3 stages: (i) Generation of N_s samples from the input factors, (ii) Model execution for the N_s combinations of input factors, (iii) Uncertainty and sensitivity analyses.

The input variables (x_i) include both the driving variables and internal model parameters, which are typically specific to each PFT. The set of input factors is provided by the user along with a probability distribution for each of them. Once the factors are defined, the sampling is performed by the software with a technique that is defined by the preferred analysis method. In the case of FAST, an appropriate set of frequencies ω_i is selected. The number of samples N_s is chosen by the user but a minimum number related to the number of factors is required (Equation C.10). The combinations of input factors are then used to run the model N_s times and the output variable(s) y is returned to the package to be analysed in the last stage.

The probability distribution and ranges of each input variable used in the study are dis-

Table 3.8: Probability distribution of input parameters for FAST sampling (JULES)

Parameter	Units	Description	Probability Distribution
DRIVING VARIABLES			
T_l	°C	Leaf temperature	Normal (μ=15, σ=10)
P	Pa	Surface pressure	Normal (μ=101000, σ=2000)
PPFD	μmol photons m^{-2} s^{-1}	Photosynthetic Photon flux density	Beta (α=1, β=2.5, a=0, b=2000)
q	kg (kg)$^{-1}$	Specific humidity	Beta (α=2, β=5, a=0, b=0.025)
f	-	Soil moisture factor	Uniform (0,1)
g_a	m s^{-1}	Aerodynamic conductance	Normal (μ=0.03, σ=0.006)
C_a	ppm	Atmospheric CO_2 concentration	Uniform (400, 800)
MODEL PARAMETERS			
α	mol CO_2 (mol photons)$^{-1}$	Quantum efficiency	Uniform (0.06,0.12)
D_{crit}	kg (kg)$^{-1}$	Maximum specific humidity deficit	Uniform (0.06,01)
f_{dr}	-	Dark respiration coefficient	Uniform (0.015,0.025)
f_0	-	Factor related to C_i/C_a	Uniform (0.8,0.9)
n_0	kg N (kg C)$^{-1}$	Top leaf nitrogen concentration	Uniform (0.33,0.73)
n_{eff}	mol CO_2 m^{-2} s^{-1} kg C (kg N)$^{-1}$	Constant related to V_{cmax}	Uniform (0.004,0.008)
T_{low}	°C	Lower temperature parameter	Uniform (-10,13)
T_{upp}	°C	Upper temperature parameter	Uniform (26,45)

Table 3.9: Probability distribution of input parameters for FAST sampling (CTESSEL)

Parameter	Units	Description	Probability Distribution
DRIVING VARIABLES			
T_l	°C	Leaf temperature	Normal(μ=15, σ=10)
P	Pa	Surface pressure	Normal(μ=101000, σ=2000)
PPFD	μmol photons m^{-2} s^{-1}	Photosynthetic Photon flux density	Beta(α=1, β=2.5, a=0, b=2000)
q	kg $(kg)^{-1}$	Specific humidity	Beta(α=2, β=5, a=0, b=0.025)
f	-	Soil moisture factor	Uniform(0, 1)
g_a	m s^{-1}	Aerodynamic conductance	Normal(μ=0.03, σ=0.006)
C_a	ppm	Atmospheric CO_2 concentration	Uniform(400, 800)
MODEL PARAMETERS			
ϵ_0	mg CO_2 $(J\ PAR)^{-1}$	Quantum efficiency	Uniform(0.012, 0.024)
D_{max} [a]	kg $(kg)^{-1}$	Maximum specific humidity deficit	Uniform(0.109, 0.124)
f_{dr}	-	Dark respiration coefficient	Uniform(0.099, 0.121)
f_0 [b]	-	Factor related to C_i/C_a	Uniform(0.65, 0.96)
g_m	m s^{-1}	Mesophyll conductance	Uniform(0.0005,0.0023)
$A_{m,max}$	mg CO_2 m^{-2} s^{-1}	Upper limit on carbon limited assimilation	Uniform(1.83,3.00)
T_{1gm}	°C	Lower temperature parameter for g_m	Uniform(-10, 13)
T_{2gm}	°C	Upper temperature parameter for g_m	Uniform(26, 45)
$T_{1Am,max}$	°C	Lower temperature parameter for $A_{m,max}$	Uniform(-10, 13)
$T_{2Am,max}$	°C	Upper temperature parameter for $A_{m,max}$	Uniform(26, 45)

[a] D_{max} is only varied independently in the high vegetation case

[b] f_0 is only varied independently in the low vegetation case

played in Table 3.8 for JULES (n = 15 parameters) and Table 3.9 for CTESSEL (n = 16 parameters). The first 7 input factors in both cases are the driving variables for the leaf level model: leaf temperature (T_l), atmospheric pressure (P), photosynthetic photon flux density (PPFD), specific humidity at the leaf level (q), normalised soil moisture factor (f), aerodynamic conductance (g_a) and atmospheric CO_2 concentration (C_a). The probability distribution of each factor is the same for both models. Temperature, pressure and aerodynamic conductance (associated to the wind speed) have been characterised by a normal distribution around the standard atmospheric values. Radiation and humidity were described by a beta distribution, to avoid zero in the distribution, and in the case of radiation to represent the high probability close to zero. The beta distribution has been found to fit well hourly radiation values (Rahman et al., 1988) and is commonly used in photovoltaic energy analysis (Sulaiman et al., 1999). The soil moisture availability is represented by f, the normalised soil moisture factor, (also known as β), and has been characterised by a uniform distribution ranging from a volumetric soil moisture at the permanent wilting point ($f = 0$) to a soil moisture equal to the critical soil moisture ($f = 1$).

The range covered by the meteorological driving variables is rather broad, spanning all possible values of each variable across the planet. The aim of this study is to fully explore each of the photosynthesis models without constraining the analysis to a certain climatic region. More specific studies could be done by delimiting the ranges for a particular climate. Another limitation of the study arises in that the input variables are treated as independent, and the driving variables are clearly correlated. Despite this limitation, the study will still provide useful information of the influence of the input parameters on the output variables.

The second set of input factors is composed of a series of model parameters. The nomenclature and units of each parameter are those used by each model. Table 3.8 contains the list of model input parameters for JULES. In the absence of information about the probability distribution of model parameters, a uniform distribution is assumed. The range of the distribution is limited by the lowest and highest value used in JULES for each particular parameter across the PFTs. This approach allows to explore the different model configurations related to PFTs. The model parameterization that is being tested is for C_3 photosynthesis, however the parameter range has been chosen to include parameter values of C_4 plants as well (the distribution range is delimited by minimum and maximum values

shown in Table 2.2). The perturbed parameters include quantum efficiency (α), parameters in the Jacobs (1994) closure equation (f_0 and D_{crit}), leaf dark respiration coefficient (f_{dr}), and parameters that determine V_{cmax}, the top leaf nitrogen concentration n_0 and n_{eff}. In fact n_{eff} is a constant that multiplies n_0 to derive V_{cmax}; it has different value for C_3 and C_4 species, so it has been varied between its possible values and treated as a parameter. The last parameters are those that regulate the temperature dependence, T_{low} and T_{upp}.

Some of these parameters have their counterpart in CTESSEL model, like quantum efficiency although denoted by ϵ_0 and with different units, the range of variation has been set to be the same as in JULES. Other common parameters are Jacobs (1994) closure parameters f_0 and D_{max} (the latter being D_{crit} in JULES), and leaf dark respiration coefficient f_{dr}, not exactly equivalent although similar to the one used in JULES. Some other parameters pertaining only to CTESSEL are the mesophyll conductance (g_m), the upper limit on carbon limited assimilation ($A_{m,max}$) and their temperature related parameters (T_{1gm},T_{2gm},$T_{1Am,max}$, $T_{2Am,max}$). The latter have been varied in the same range as the temperature related parameters in JULES.

As detailed in Chapter 2, CTESSEL includes some relationships between parameters, and these differ in the low vegetation (herbaceous) and high vegetation (woody) formulations. In particular for low vegetation, D_{max} is derived from g_m (Calvet, 2000) and regulated by soil moisture stress. For high vegetation f_0 is fixed to it unstressed value or derived from g_m under severe soil water stress conditions ($f < f_{2c}$) (Calvet et al., 2004). Due to these model connections two separate analyses have been conducted for CTESSEL, one for each group of vegetation, low and high vegetation. In the case of low vegetation D_{max} is not included in the set of varying input parameters and is allowed to be computed within the model, similarly for parameter f_0 in the case of high vegetation. The soil moisture strategy in both cases is offensive (see Chapter 2), since this is the setting that is used operationally. Once the input variables are defined, SimLab generates a collection of samples by simultaneously varying each parameter within its own probability distribution, assuring that parameter space is thoroughly explored. Then, in the second stage, each model is run for every sample of input parameters (driving variables and model internal parameters) generated by SimLab. One set of runs is performed with JULES, and two sets of runs with CTESSEL, one using the configuration for low vegetation (LV) and

another one with the configuration of high vegetation (HV). Several sizes for the sample set were tested, finally $N_s = 14992$ assured convergence of the first and total indices of three models. Convergence was defined for a tolerance of 0.01 in the indices. In the third stage, the model output is fed to SimLab, which creates a mapping between the input space and the output space, basis for the sensitivity analysis.

3.6.3 Analysis

The uncertainty analysis consists of an evaluation of the variance of model output, whereas the sensitivity analysis tries to explain that variance in terms of the input variance, allotting sensitivity indices to each input parameter. In the case of FAST, a Fourier analysis is performed on the model output, searching for the frequencies associated to the input parameters in the sampling stage.

3.6.3.1 Uncertainty analysis

The uncertainty analysis consists of an statistical examination of the spread of the model output for the N_s model runs. The boxplots in Figure 3.27 show the span of each model's output, given the meteorological driving variables sampled from the same probability distribution and model parameters sampled from a distribution representative of each parameter's possible values within each model. A summary of the statistics is presented in Table 3.10. Overall the output from both models look comparable. In terms of net photosynthesis and dark respiration ((a) and (d)) JULES values are slightly lower in average and present less spread. The lower photosynthesis values in JULES are in agreement with the extra limitation imposed on photosynthesis by export limiting regime (as seen in Section 3.4). The higher variability in both sets of CTESSEL model runs could be related to the higher sensitivity found in CTESSEL to CO_2 combined with temperature and radiation (Figures 3.12 and 3.17). The output for stomatal conductance differs more amongst models (Fig. 3.27b). In particular, within CTESSEL, g_s presents higher values for the low vegetation runs as well as higher variance. Although the specific influence of parameters will be explored in the sensitivity analysis (Section 3.6.3.2), it is anticipated that the higher variance is most likely related to a higher range of variation of parameter

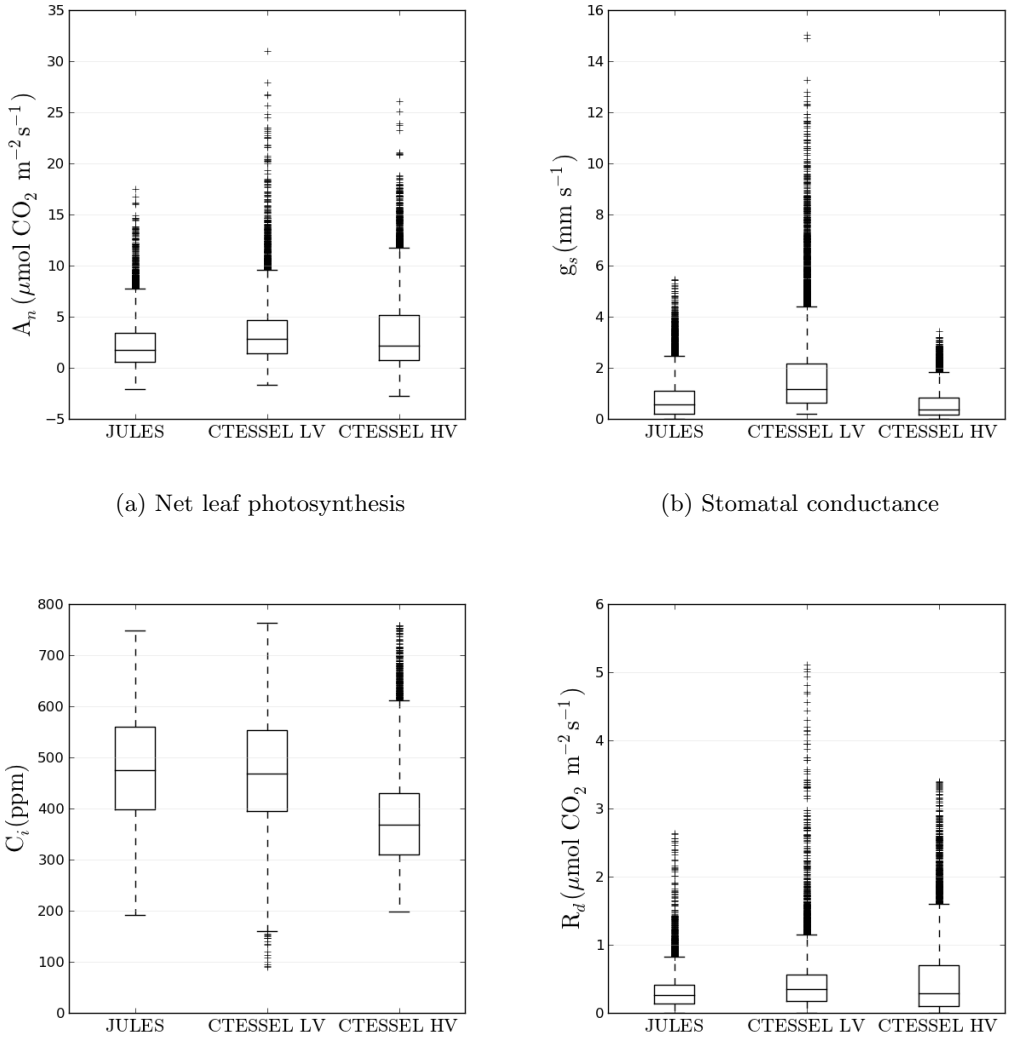

(a) Net leaf photosynthesis

(b) Stomatal conductance

(c) Intercellular CO_2

(d) Leaf dark respiration

Figure 3.27: Boxplots for the model output variables (N_s= 14992 runs). The lower edge of the box represents the 1st quartile (Q1) and the upper edge of the box is the 3rd quartile (Q3). The middle line represents the 2nd quartile (Q2) or median. The vertical lines span the range [(Q1-1.5 IQR),(Q3+1.5 IQR)], with IQR= Q3-Q1 the interquartile range. Points outside this range are plotted as crosses (outliers).

Table 3.10: Statistics for model output, N_s= 14992

		JULES	CT LV	CT HV
A_n (μmol CO_2 m^{-2} s^{-1})	Mean	2.30	3.37	3.31
	Standard deviation	2.21	2.76	3.34
g_s (mm s^{-1})	Mean	0.77	1.70	0.57
	Standard deviation	0.77	1.62	0.55
C_i (ppm)	Mean	480	476	376
	Standard deviation	103	106	86
R_d (μmol CO_2 m^{-2} s^{-1})	Mean	0.30	0.43	0.47
	Standard deviation	0.24	0.40	0.50

f_0 in the LV runs. This effect can also be seen in the higher intercellular carbon concentrations (Fig. 3.27c) found for low vegetation than for high vegetation in CTESSEL.

3.6.3.2 Sensitivity analysis

The sensitivity analysis determines how much of the output variance is due to each of the input parameters. The first order sensitivity indices (Equation 3.4) inform of the influence of the parameter independently while the total influence taking into account interactions is expressed by the total sensitivity indices (Equation 3.5). Both sets of sensitivity indices are shown in Figure 3.28 for A_n, Figure 3.29 for g_s, Figure 3.30 for C_i and Figure 3.31 for R_d. The input parameters have been sorted in order of decreasing importance in each model. The first order indices represent the main effect attributed to each parameter, whereas the total effect indices include the influence of the interactions. Therefore the shaded part of the bars reflects the importance of the interactions amongst the indicated factor and all the others.

The variability in photosynthesis rate is mostly determined by two factors: the soil moisture factor f and the leaf temperature T_l, both with S_{Ti} around 0.5. In JULES and CTESSEL HV, f is the most important factor followed by T_l, in CTESSEL T_l is slightly above f. The significance of the f factor could be exaggerated due to the choice of its

distribution, ($0 < f < 1$). Soil water content is considered to be between wilting point and critical value, therefore the scenarios considered always include some level of water stress. Furthermore, in JULES the moisture stress effect is multiplicative on the potential photosynthesis thereby yielding this high sensitivity. Interestingly, although CTESSEL uses a more complex parameterization for water stress, the value of f also appears to have an important impact.

The high indices associated to leaf temperature provide a more conclusive result. T_l is a key parameter determining the rate of leaf photosynthesis. The amount of incoming PAR radiation PPFD is the fourth (JULES) and third (CTESSEL) parameter in order of importance. The atmospheric carbon dioxide concentration C_a does not appear to contribute significantly to the output variability, ranking 8th for JULES and 5th in both versions of CTESSEL. The reason could be the existence of the export limiting regime; when the level of CO_2 rises, the limitation comes from the own biochemical capacity of the the cells and becomes insensitive to CO_2. The lack of this regime in CTESSEL makes C_a more important in both of its versions, LV and HV. The other meteorological drivers appear to be of minimum importance: humidity, pressure and aerodynamic conductance.

Although all the model parameters have total sensitivity indices values below 0.3, we can still derive useful information. The most important of the internal model parameters is the one that determines the upper limit on the temperature dependent parameters; T_{upp} for JULES controlling V_{cmax} temperature dependence amongst other parametes and T_{2gm} for CTESSEL, controlling g_m. Most of the relevance of T_{upp} and T_{2gm} comes from interactions (presumably with temperature) as can be seen by the low value of their main effect. The large temperature dependence of V_{cmax} and g_m make the parameters that determine the temperature dependence more important than the parameters themselves. In JULES, the next parameters in order of importance are n_0 and n_{eff}, which effectively correspond to V_{cmax} (Equation 2.48). In CTESSEL g_m appears to have very little importance, especially in CTESSEL HV. When comparing the two branches of CTESSEL, it can be noted that low vegetation presents a more balanced distribution of the sensitivity indices. This observation is true for three other model outputs. The sensitivity analysis of stomatal conductance (Figure 3.29) shows some common features with the results described for leaf photosynthesis. Namely, T_l and f also have a clear influence on the output. However, in the case of CTESSEL LV, f_0 overtakes these parameters and becomes the most important

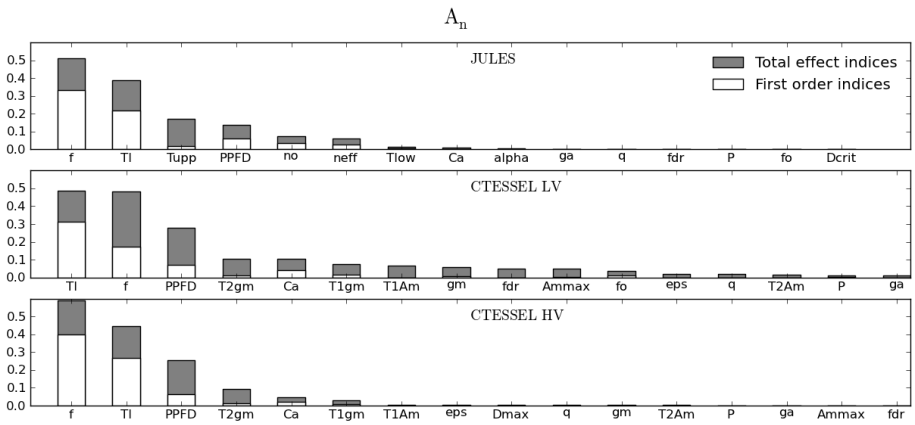

Figure 3.28: FAST indices for model output A_n

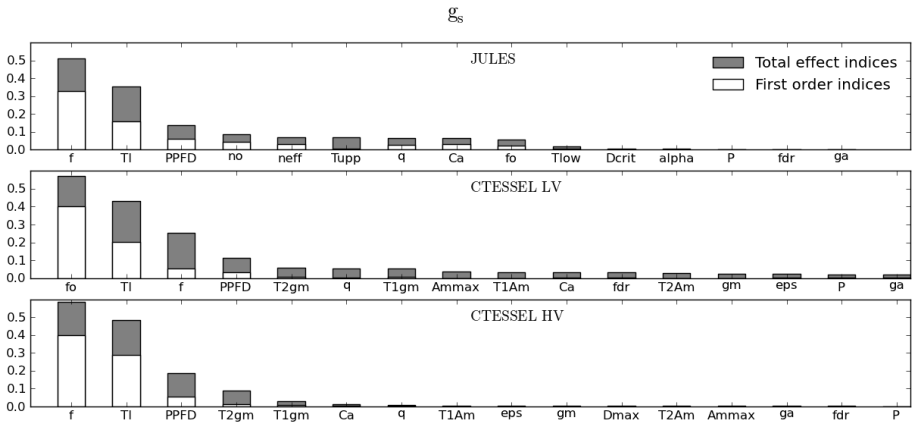

Figure 3.29: FAST indices for model output g_s

factor with $S_{Ti} = 0.58$. As it was noted in the uncertainty analysis, g_s presented more variability in the low vegetation case, where f_0 was varied independently. In the high vegetation formulation, f_0 varies less, as it is fixed to its unstressed value and only changes under severe water stress conditions. This explains the smaller variance in g_s, and the lower influence that f_0 exerts on it.

The most relevant factor determining the carbon dioxide concentration in the intercellular spaces C_i, (Figure 3.30) is the atmospheric carbon dioxide concentration C_a, as expected. Following in importance, there is T_l in JULES, f_0 in CTESSEL LV and f in CTESSEL HV. The rest of the parameters account for very little variance.

For leaf dark respiration, (Figure 3.31) findings are very similar to those of photosynthesis,

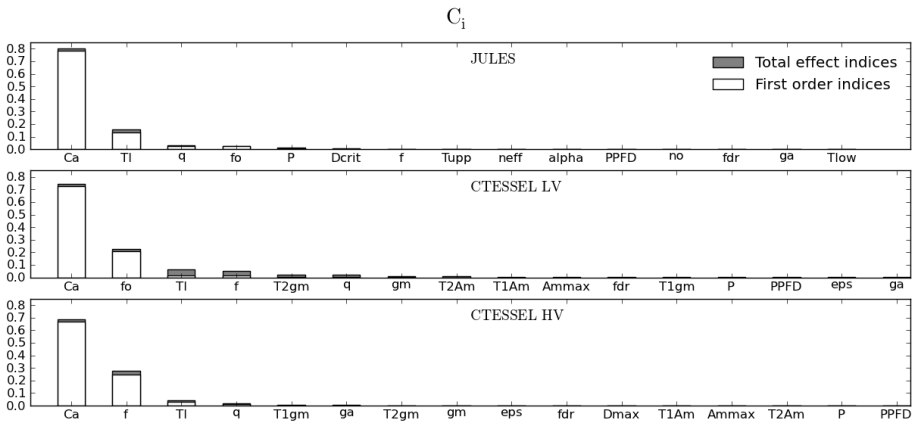

Figure 3.30: FAST indices for model output C_i

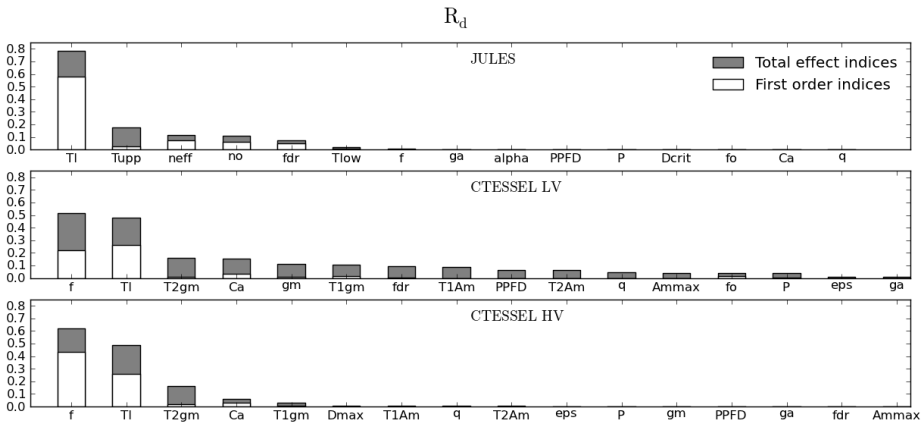

Figure 3.31: FAST indices for model output R_d

with the difference that R_d is not affected by water stress in JULES. However in CTESSEL f continues to be a relevant factor. It is surprising to see that the coefficient for dark respiration f_{dr} has such a small effect for both models.

3.6.3.3 Sensitivity analysis of the photosynthesis limiting regimes in JULES

In this section, the sensitivity analysis has been performed on each of the photosynthetic rates that compose the net photosynthesis. In this way, certain input variables or model parameters can be associated to each limiting regime. In reality, due to the co-limitation equation used to aggregate the three rates, there is an influence from all regimes on the photosynthetic rate, rather than only the limiting one (minimum rate). However the full

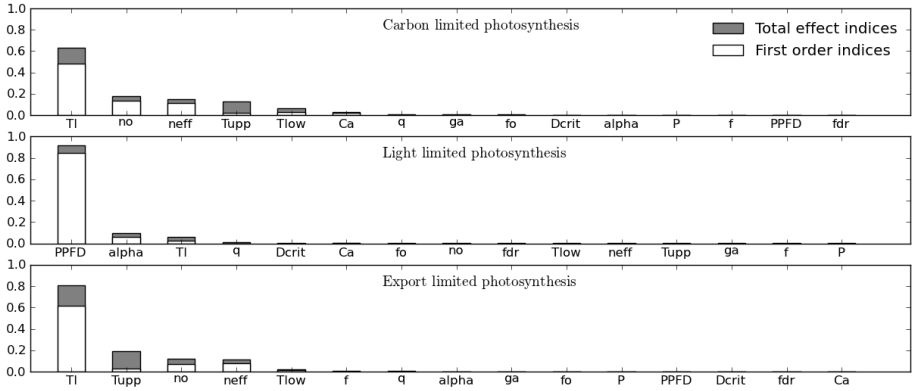

Figure 3.32: FAST indices for carbon, light and export photosynthesis rates from JULES.

complexity was already analysed in A_n. In this part, the photosynthetic rate associated to each limiting regime is analysed separately via a dedicated sensitivity analysis. Figure 3.32 shows the first order and total order indices for the photosynthetic rate associated to carbon, light and export limited regimes (W_c, W_j, W_e).

The most important input parameter for carbon and export regimes remains the leaf temperature. It is followed first by n_0 and n_{eff} (parameters that determine V_{cmax}) and then by T_{upp}, in the case of carbon limited photosynthesis; and in the inverse order for export limited photosynthesis. In the case of light limited photosynthesis, PAR is the most influential factor followed by the quantum efficiency use, α. These results are in agreement with findings of Alton et al. (2007). Their study analysed JULES in three distinct natural biomes. Although their study is at the canopy level, their results for GPP at specific sites can be related with the present results at the leaf level for the limiting regimes. They found quantum efficiency (α) was the most influential model parameter in Manaus, a dense tropical rainforest. At such site, light interception by the canopy is large, therefore photosynthesis is highly light limited, hence α being important. In Harvard forest, a temperate broadleaf site, the most relevant model parameter explaining GPP variability was V_{cmax}. This is expected for a site where photosynthesis is mostly carbon limited. The last site in their analysis is Zotino, a sparse boreal forest, for which the most influential parameter in GPP turned out to be leaf area index, parameter related to the upscaling from leaf to canopy, and therefore not covered by the present analysis.

3.7 Conclusions and discussion

Vegetation modelling in LSMs is rapidly developing with additions that require increasing numbers of adjustable parameters (allocation of the assimilated carbon to specific pools, dynamic vegetation models that predict competition between species etc.). However, the core of the photosynthesis response to environmental variables still relies on equations derived in the early years of plant modelling (Farquhar et al., 1980; Ball et al., 1987). In particular the predicted response of photosynthesis to CO_2 is based on these equations. For this reason the photosynthesis schemes used by JULES and CTESSEL are analysed to characterise the response of photosynthesis to changes in environmental variables, particularly its response to an atmospheric CO_2 increase. The leaf level photosynthesis scheme embedded in each model has been isolated and used to compare model performance, sensitivity to environmental factors and global sensitivity to environmental factors and model parameters combined.

At present day CO_2 both photosynthesis models perform similarly at reproducing leaf level photosynthesis, despite the differences in formulation discussed in Chapter 2. Modelled photosynthesis was contrasted against photosynthesis measurements of grapevines (Jacobs, 1994). Both models show more accuracy for photosynthesis in the shaded leaves, when photosynthetic reactions are light limited and very much conditioned by the incoming radiation. For the sunlit leaves however, when the photosynthesis reactions are carbon limited, the models underestimate photosynthesis. The low photosynthesis reproduced by the models for high radiation levels could be attributed to the model parameters being set for a generic broadleaf tree, while the grapevines are well adapted to the hot and dry environment. To better characterise the grapevines, observation fitted model parameters from Jacobs (1994) were used. CTESSEL's performance of the sunlit photosynthesis was improved. However, JULES performance did not improve, due to the non exact equivalence in the relations between photosynthesis parameters from both models.

The isolated photosynthesis schemes from JULES and CTESSEL are used to compare the leaf level respose to some environmental factors: CO_2 concentration, temperature, radiation and humidity. Photosynthesis response to enhanced levels of atmospheric CO_2 is of particular interest in the light of increasing anthropogenic CO_2 emissions. The fer-

tilisation effect is a negative feedback by which increased atmospheric CO_2 concentration enhances plant activity which in turn is able to absorb more CO_2 from the atmosphere. It is therefore an important effect as a determinant of the net terrestrial carbon sink. The fertilisation effect has been evidenced at the global scale by Earth Observation data combined with models (Nemani et al., 2003).

The leaf level response of photosynthetic rate reproduced by both photosynthesis models diverges at high carbon dioxide concentrations. While CTESSEL predicts a rather linear response to an increase in CO_2, in JULES the export limiting regime restrains C_3 photosynthesis at high CO_2, predicting lower carbon assimilation than CTESSEL for the same atmospheric CO_2 concentration (Figure 3.14). Export limitation in JULES is independent of carbon dioxide, therefore insensitive to ambient CO_2 increase. Export limiting regime is only dependent on temperature (via V_{cmax}, see Equation 2.45 in Chapter 2).

The fertilisation effect explored here is at the leaf level, meaning that it does not comprise the amplification that could occur due to LAI growth driven by an increase in biomass production. Moreover, the fertilisation effect exposed here is the result of the instantaneous response of the model, which does not consider acclimation in time (e.g. as a reduction in the number of stomatal pores per leaf area).

In order to answer the first research question, concerning the conditions under which each limiting regime dominates, JULES photosynthesis regimes were identified for a wide range of leaf temperatures and radiation levels (Figure 3.20). It was found that, while carbon is the most common limitation, export occurs at lower temperatures and light limits at low radiation levels. The effects of enhanced CO_2 on how the limiting regimes affect photosynthesis in JULES were also investigated. Fundamentally two effects were identified when increasing from 400 ppm to 800 ppm: (i) the temperature threshold between export and carbon limitation becomes higher and (ii) the radiation threshold between light and carbon limitation is increased. These effects translate into the export limiting regime becoming limiting for a broader set of environmental conditions at the expense of carbon (or rubisco) limitation, and light limitation becoming dominant at the expense of export and carbon (Figure 3.20). Under current CO_2 concentrations export limits mainly at low temperatures, but JULES predicts that it will increasingly become a major limitation on plant photosynthesis. The export limiting regime represents the capacity of the plant

to incorporate the carbon compounds synthesised in the photosynthesis process. It is therefore deeply connected to the physiology and carbon requirements of the plant organs, relating to its life stage and other intrinsic characteristics. The export limiting regime is the process that is more likely to be specific to each particular species. In this respect, more dedicated physiological experiments are needed to determine how the capacity of plants to assimilate carbon might vary under changing climatic conditions.

As a consequence of the heterogeneous response of the limiting regimes to CO_2 and the changes in their co-limitation, a shift of a few degrees in the optimum temperature for photosynthesis towards higher temperatures was identified when C_a was increased to 800 ppm. A shift of smaller magnitude was also found in CTESSEL for some species. This result emerges from the photosynthesis formulation and is in line with observations of plant temperature acclimation (Yamori et al., 2005).

The different response of C_4 photosynthesis to CO_2 increase seen in both JULES and CTESSEL has consequences for climate change simulations of the CO_2 uptake in C_4 ecosystems. JULES showed virtually no CO_2 fertilisation effect, while in CTESSEL the effect is similar to C_3 species. These results apply to the default model settings; the CTESSEL formulation is also capable of reproducing the insensitivity of C_4 photosynthesis to elevated CO_2 if a higher value of g_m is chosen. The lack of CO_2 fertilisation under climate change might be compensated in C_4 photosynthesis by the temperature effect. As shown in Figure 3.33, both models show a stronger response to temperature increases for C_4 plants. Although anthropogenic increase in CO_2 does not directly affect C_4 plants, the effect of climate change on C_4 plants is to be perceived trough greater sensitivity to temperature increase. C_4 plants find their optimum temperature for photosynthesis at higher temperatures than C_3 plants, and have potential to increase assimilation levels due to increased temperature. However, the extra energetic cost incurred by C_4 photosynthesis in the CO_2 pumping might be counterproductive at high CO_2 concentrations. Ehleringer et al. (1997) predicted that for atmospheric levels greater than 500 ppm C_3 plants are favoured.

Finally, a global sensitivity analysis was conducted to ascertain the importance of each model parameter and each environmental variable in the model output of the leaf photosynthesis models of JULES and CTESSEL. Because of the complexity of the photo-

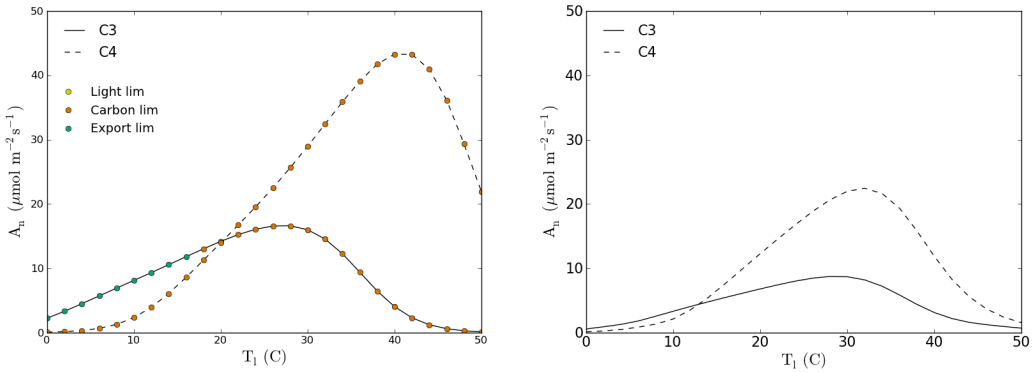

(a) JULES (b) CTESSEL

Figure 3.33: Leaf level photosynthesis as a function of leaf temperature for C_3 grasses and C_4 grasses, C_a= 400 ppm, PAR=1600 μmol photon m^{-2} s^{-1}.

synthesis and stomatal gas exchange computations and the strong interactions amongst parameters, a global sensitivity method is needed. The FAST method (Saltelli et al., 1999) from the SimLab software package, provided by the Joint Research Centre, was used to perform a global sensitivity and uncertainty analysis. The study revealed that the most influential factors for leaf photosynthesis in both JULES and CTESSEL were leaf temperature and the soil moisture factor. The most important model parameters were those related to the maximum velocity of carboxylation (V_{cmax}), particularly the upper limit in the temperature dependence. In the case of CTESSEL, the most important parameter was T_{2gm}, related to the temperature dependence of the mesophyll conductance. The variance in stomatal conductance was explained mostly by the same parameters as leaf photosynthesis. In the case of CTESSEL low vegetation, f_0 becomes the main driver of stomatal conductance's variability. When comparing both formulations used in CTESSEL (low and high vegetation) it is noticed that for the four output variables under study (leaf net photosynthesis, stomatal conductance, intercellular carbon and dark respiration), the variance attributed to each factor is more distributed across parameters, while in the case of high vegetation most of the variance is explained by the first four parameters alone (T_l, f, PPFD, T_{2gm}).

The analysis was conducted for each of JULES limiting regime's photosynthetic rate to determine which factors are more important under each limiting regime (Research Question 2). For carbon and export limited photosynthesis, T_l is the most important driving vari-

able, while for light limited photosynthesis PPFD is the most important driving variable. For carbon limited photosynthesis, leaf nitrogen content is the most important model parameter, for export limited photosynthesis T_{upp}. For the light limiting regime the quantum efficiency is the most important model parameter.

This analysis has attempted to explore the model's response for a wide combination of meteorological conditions by sampling each driving parameter from a realistic probability distribution function (pdf). However, although the individual pdfs are realistic, the sampling from pdfs provides an aleatory combination that might not represent realistic joint conditions, since the correlations amongst model drivers are not taken into consideration. Moreover, the pdfs were designed to span all possible values of each variable across the globe. Some other global sensitivity studies focus on a specific site or climate, therefore restricting the meteorological variables pfds. By limiting the possible values of the meteorological variables (otherwise the most influential), the relevance of the model internal parameters can emerge. In this study, however, there is no focus on a single site or climate; rather, the aim is to identify the most important parameters including environmental variables.

This chapter has analysed the representation of the photosynthesis function in JULES and CTESSEL at the leaf level. The next chapters will present results from the full LSMs, both for present climate and idealised climate change conditions.

Chapter 4

Fluxes at the ecosystem level

4.1 Introduction

The previous chapter analysed the carbon assimilation reproduced by the photosynthesis schemes at the leaf level. In this chapter the exchange of carbon dioxide and water vapour, as predicted by the full land surface models at the ecosystem level, is analysed and compared at 10 vegetated locations. The main purpose is to contrast CTESSEL and JULES'representation of vegetation's exchange of fluxes with the atmosphere, as well as the predicted responses to environmental factors. The values of energy and carbon fluxes have their origin at the leaf level photosynthesis schemes, whose differences were analysed in the previous chapter. At the ecosystem level, another source of dissimilarity is added, the scaling up from the leaf level to canopy level (described in Section 2.4.7). Moreover, the canopy level fluxes are affected by the degree of coupling between vegetation and and the atmosphere (Jarvis and McNaughton, 1986). To validate the models' estimates, eddy covariance measurements of turbulent and carbon fluxes from FLUXNET towers are used (Baldocchi et al., 2001). The analysis provides a sound understanding of the sources contributing to the differences between the models when reproducing gas exchange. The correlation between models, compared to the correlation found between each model and the observations, highlights the similarities between models. The ability of models to reproduce interannual variability is also analysed. The observational data sets have been obtained from the web portal European Fluxes Database Cluster (EFDC)

(http://gaia.agraria.unitus.it/). Ten sites located in Europe were selected: 5 evergreen needle leaf trees, 4 broadleaved trees and one grass site. The models were driven with meteorological data from the sites and using the most similar settings possible, to focus on model output as generated by the the differences in the photosynthesis models.

4.2 FLUXNET tower observations

The FLUXNET network offers a valuable collection of continuous long-term measurements of land-atmosphere fluxes of water vapour, carbon and energy (Baldocchi et al., 2001). Continuous observations of fluxes and key state variables are taken at micrometeorological tower sites situated at diverse locations across the globe, surveying different ecosystems and climates. At some pioneering sites the datasets go back to the early 1990s. The long time series and fine temporal resolution of the measurements (30 minutes) provide invaluable monitoring of land-atmosphere fluxes at sub-daily, seasonal and interannual time scales. Atmospheric fluxes are measured using the eddy covariance technique, which is based on the turbulent motion in the surface layer. Fluctuations in the vertical component of the wind are related with variations in concentrations of water vapour and CO_2 to derive the net vertical transport. The measured fluxes are suited for the study of ecosystem physiology as they capture the response of the whole ecosystem to changes in environmental factors with a minimal disturbance of the canopy environment (Baldocchi, 2003). The representative area or flux footprint is variable and can have a longitudinal direction that spans from a hundred meters to several kilometers (Schmid, 1994). The method is most accurate when atmospheric conditions are steady, the underlying vegetation extends upwind for an extended distance and terrain is flat. Along with the flux measurements, a series of meteorological variables are measured, such as incoming solar radiation, temperature, humidity, net radiation, precipitation and surface pressure. Specific properties of the vegetation and soil are sampled for site characterisation, providing ancillary information to modellers.

The continuous measurement of the interchange of water and CO_2 fluxes between terrestrial biosphere and the atmosphere has different applications and offers valuable information at the different temporal resolutions. At short timescales (sub-daily), it provides

information of physiological processes and fast responses to drivers like temperature, humidity, radiation. At seasonal timescale it reflects the vegetation phenology, driven by the environmental variables as well as each species phenotype. At this timescale vegetation's response to soil moisture can be identified. Interannual timeseries capture the natural variability and the influence of climate on vegetation. With changes in environmental factors due to climate change, a continuous monitoring of ecosystems gas exchange with the atmosphere is crucial, as it can reveal changes in the vegetation phenology and long term variations of the CO_2 terrestrial sink determining the actual amount of CO_2 that resides in the atmosphere at any moment in time.

FLUXNET energy and carbon fluxes are frequently used for the validation and calibration of land surface models (Blyth et al., 2010; Bonan et al., 2011; Boussetta et al., 2013b; Balzarolo et al., 2014; Friend et al., 2007). Carbon fluxes values are also being used to produce credible estimates of annual carbon exchange, with values converging with estimates from independent biomass inventory and soil carbon change studies over multiple years (Baldocchi, 2003; Curtis et al., 2002; Ehman et al., 2002). Although the greatest value of FLUXNET data for carbon cycle modelling is in evaluating process representation (Friend et al., 2007). Other uses include the validation of satellite products used for monitoring terrestrial ecosystems (Running et al., 1999). The available products comprise different levels of data. Level 2 data are directly provided by the PIs of the sites; level 3 data have quality flags added to them and level 4 data have been gap-filled and carbon flux has been partitioned into ecosystem respiration (R_{eco}) and gross primary productivity (GPP). The data used as driving variables and fluxes in this study are level 4, except for windspeed and surface pressure which are level 2.

4.2.1 Eddy covariance measurements

The eddy covariance technique is based on Reynold's decomposition of turbulent vertical motion and the conservation of mass. The typical instrumentation in a FLUXNET tower is a three-dimensional sonic anemometer that measures wind velocity and virtual temperature, and a open path or closed path infrared gas analyser to measure concentration fluctuations in CO_2 and water vapour (Moncrieff et al., 1997). The mean flux densities of CO_2, latent and sensible heat between the vegetation and the atmosphere are proportional

to the mean covariance between the vertical velocity fluctuation (w') and the respective scalar fluctuation c' (CO_2, water vapour or temperature):

$$F \propto \overline{\rho_a}\overline{w'c'} \tag{4.1}$$

ρ_a is the air density and primes represent fluctuations around the mean according to Reynolds decomposition. The covariance term is derived from the sensors measurements by sampling at a frequency of generally 10 Hz to ensure the detection of the smaller scales of motion and averaging over 30-60 minutes periods to capture lower frequency contributions. Despite these efforts some high and low pass filtering is assumed to occur, and the measured flux might be smaller than the true gas exchange. There are different techniques to compensate for these losses (Massman and Lee, 2002). At night, when there is thermal stratification, the flux from the vegetation might not entirely reach the instruments and some storage occurs within the canopy. This produces an underestimation of the nighttime fluxes. At dawn, when the stable nocturnal boundary layer breaks, the accumulated CO_2 is vented and sensors will overestimate the actual flux. For a correct estimation of biosphere-atmosphere exchange the storage term must be accounted for. The detailed methodology to compute the fluxes is described in Aubinet et al. (2000, 2012).

4.2.1.1 Energy balance closure

A long known problem with the eddy covariance method is the lack of closure of the energy balance (Wilson et al., 2002; Franssen et al., 2010). The energy balance at the surface can be represented by:

$$NR - G - \Delta S = LE + H \tag{4.2}$$

The term on the left is the available energy, net radiation (NR) minus ground heat flux (G) and change in heat storage of canopy and air mass (ΔS). The latter corresponds to term $C_s \frac{\delta T_*}{\delta t}$ in Eq. 2.1. For most FLUXNET sites the combined eddy covariance measurements of latent heat (LE) and sensible heat (H) account only for approximately 80% of the available energy. The imbalance between the left and right hand side of Eq. 4.2 could be related to an underestimation of turbulent fluxes with the eddy covariance technique but could also be caused by errors in calculating the available energy terms. Several hypotheses for the lack of closure are discussed by Wilson et al. (2002): (i) sampling errors associated

with the footprint mismatch of the sensors measuring the terms left and right in Eq. 4.2, resulting in different representativeness of the source areas, (ii) systematic errors in instrumentation, (iii) neglected energy sinks, (iv) loss of high/low freqency contributions to the turbulent flux and (v) neglected advection. The greatest imbalance is associated with low friction velocities, and hence the lack of closure is more severe during nighttime, when conditions are typically more stable. Although the closure problem concerns energy fluxes, if the cause of the imbalance is related to the eddy covariance technique (hypotheses (ii), (iv) and/or (v)), then CO_2 flux measurements would be affected as well. Wilson et al. (2002) found lower values of CO_2 fluxes were associated to worse energy balance closure, suggesting CO_2 measurements could be underestimated. Nevertheless, the lack of closure in the energy balance is a fact that needs to be acknowledged when interpreting both energy and carbon fluxes.

4.2.1.2 Carbon fluxes - Net Ecosystem Exchange partition

The eddy covariance instruments measure the total carbon flux, from which net ecosystem exchange (NEE) is derived by taking into account canopy storage terms. The EFDC data portal provides NEE derived from two alternative methods: NEE standardized (calculated using the storage obtained with the discrete approach with the same method for all the sites) and NEE original (calculated using the storage term sent by the PI that can be obtained with the discrete approach or using the profile system). In this study, the standardized NEE has been used for the model validation.

Measured NEE is separated into the components of the carbon balance, gross primary productivity (GPP) and ecosystem respiration (R_{eco}).

$$NEE = R_{eco} - GPP \tag{4.3}$$

The sign convection in 4.3 is the one typically used in the ecology community, NEE and R_{eco} are positive upwards and GPP is positive downwards. The partition into GPP and R_{eco} distinguishes between assimilation and respiratory fluxes which is useful for the purpose of calibration and validation of ecosystem models. However, there is no standard method to partition into GPP and R_{eco}, and due to their dependence, a bias in one will result in a bias in the other. Several algorithms have been proposed to perform the flux

partitioning, for a review see Reichstein et al. (2005). These methods are divided into those that use exclusively nighttime values and those that exploit daytime or both daytime and nighttime data. The methods that use nighttime data derive a direct estimate of R_{eco} at night from the eddy covariance measurements. Then this estimate is extrapolated to daytime based on a relation between respiration and soil temperature (Lloyd and Taylor, 1994), which requires a value for the sensitivity of respiration to temperature. Once R_{eco} is determined, GPP is calculated by substraction in Eq. 4.3. The methods that use both day and nighttime data are able to simultaneously solve the NEE partitioning (Gilmanov et al., 2003), however they rely more heavily on models, particularly of carbon assimilation's light dependence and therefore suffer from potentially poor model assumptions.

In the EFDC dataset, the flux partitioning algorithm proposed by Reichstein et al. (2005) is used. This method uses filtered nighttime values to estimate R_{eco}, which is then extrapolated to day time using short-term temperature sensitivity as opposed to previous calculations (Falge et al., 2002) which used long-term temperature sensitivity. The estimation of temperature sensitivity is based on the same exponential relation (Lloyd and Taylor, 1994) but the regression is performed at shorter periods (15 days) instead of annual. They argue that a long-term sensitivity factor does not reflect the short-term (hour to hour) temperature sensitivity that is effective when extrapolating from night to day, because the annual sensitivity may be contaminated by other seasonally varying factors that co-vary with temperature (e.g. soil moisture, growth effects). They show that the use of long-term sensitivity overestimated respiration (and consequently GPP) in summer-active ecosystems (high latitudes) and underestimated it in summer-passive ecosystems (Mediterranean).

4.2.1.3 Gapfilling

It is inevitable that the flux dataseries contain some gaps. These can be caused by system or sensor breakdown or maintenance, periods when instruments are off-scale, spikes in the raw data or vertical angle of attack by the wind vector is too severe (Baldocchi et al., 2001). For a review on gap filling methods for carbon fluxes see Falge et al. (2001). EFDC datasets provide fluxes processed applying two different gap-filling procedures: marginal distribution sampling (MDS) and artificial neural network (ANN). In the present study

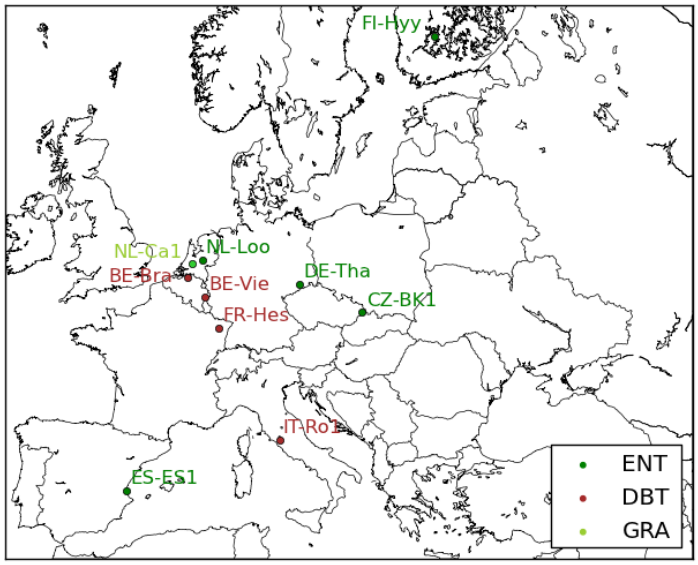

Figure 4.1: FLUXNET sites and their corresponding PFT. ENT: Evergreen needle leaf trees, DBT: deciduous broadleaf trees, GRA: Grass

the carbon fluxes gapfilled with MDS were used.

4.2.2 Sites

Ten sites were selected to represent different vegetation types and climates across Europe. Sites with a long record of meteorological data and eddy covariance fluxes were selected. A description of the sites is given in Table 4.1 and their geographical distribution is shown in Figure 4.1. There are 4 broadleaved or mixed forests, three of them in temperate climate (Hesse Forest-Sarrebourg in France, Vielsalm and Brasschaat in Belgium); and one in Mediterranean climate (Roccarespampani in Italy). Five towers are located in needle leaf forests sampling boreal climate (Hyytiälä in Finland), humid continental conditions in a mountainous region (Bily Kriz-Beskidy Mountains in Czech Republic), temperate climate (Loobos in the Netherlands and Tharandt-Anchor Station in Germany) and Mediterranean climate (El Saler in Spain). Finally, Cabauw in the Netherlands is representative of grasslands under temperate climate conditions.

Table 4.1: Description of the FLUXNET sites. IGPB land classification: MODIS v5 determined IGBP land use designation. DBF: Deciduous broadleaf forest, MF: Mixed forest, ENF: Evergreen needle leaf forest, GRA: Grasslands.

Site	**Site code**	**IGBP land cover**	**Köppen- Geiger Climatic Classification**	**Years of data**
Hesse Forest-Sarrebourg	FR-Hes	DBF	Cfb - Warm temperate fully humid with warm summer	(1998 - 2009)
Vielsalm	BE-Vie	MF	Cfb - Warm temperate fully humid with warm summer	(1998 - 2008)
Brasschaat (De Inslag Forest)	BE-Bra	MF	Cfb - Warm temperate fully humid with warm summer	(2004 - 2010)
Loobos	NL-Loo	ENF	Cfb - warm temperate fully humid with warm summer	(1998, 2012)
Tharandt-Anchor Station	DE-Tha	ENF	Cfb - Warm temperate fully humid with warm summer	(1998 - 2008)
Roccarespampani	IT-Ro1	DBF	Csa - Warm temperate with dry, hot summer	(2000 - 2008)
El Saler	ES-ES1	ENF	Csa - Warm temperate with dry, hot summer	(1999 - 2006)
Bily Kriz- Beskidy Mountains	CZ-BK1	ENF	Dfb - Snow fully humid warm summer	(2004 - 2005)
Hyytiälä	FI-Hyy	ENF	Dfc - Snow fully humid cool summer	(1998 - 2009)
Cabauw	NL-Ca1	GRA	Cfb - Warm temperate fully humid with warm summer	(2003 - 2008)

4.3 Model setup

The model settings have been selected to be as similar as possible in both models to allow for analysis of the differences in the representation of vegetation physiology. Both models are run in coupled mode, so that stomatal conductance obtained from the photosynthesis module is used for transpiration. JULES model is version 4.1 and CTESSEL is version 41r3 version 3. Both models were run offline for the selected sites using the meteorological data collected at each tower, after being gapfilled with climatology (See Section 4.3.1). The length of the simulation varied across sites depending on the data availability. For most cases it was possible to run for several continuous years, thereby providing results that allowed analysis of the interannual variability. The model timestep was 30 minutes, in agreement with the temporal resolution of the observations.

To achieve equilibrium at the soil variables, JULES and CTESSEL were spun up for the first year of each simulation period (except for NL-Ca1 where 2005 was used to avoid 2003, an anomanously hot year). The model was left to run continuously for the same year for as many cycles as needed until soil moisture content and soil temperature reached a stable state, which was defined when the variables varied less than 1 kg m^{-2} and 0.1 K respectively at each of the four soil layers. Each model was initialised from its own equilibrium variables at each site.

4.3.1 Meteorological driving data

The L4 meteorological data available for the sites are: global radiation, net radiation, precipitation, air temperature and vapour pressure deficit. Windspeed and surface pressure were available as L2 or L3 variables. All data have a temporal frequency of 30 minutes, and the model timestep was also 30 minutes. Like the flux data, meteorological data also suffer from some lack of data. To be able to run the models using the in-situ timeseries of observations, the missing data were gapfilled in a simple way. A climatology of 30 minute values was computed with the available data for each site. Then the missing values in the timeseries were replaced by the corresponding value in the climatology.

Vapour pressure deficit (hPa) was converted to specific humidity (kg kg $^{-1}$) using the

surface pressure and air temperature. Specific humidity was forced to stay below the saturation value for each air temperature to ensure there are no saturation events in the models that could result in sudden negative latent heat fluxes.

JULES has more flexibility than CTESSEL in the combinations of meteorological variables that can be used to drive the model. In the case of radiation JULES accepts either short and long wave downwelling fluxes or shortwave downwards and net radiation. Since the available EFDC data contained net radiation, JULES was run in the first place and the modelled downward longwave flux was used to drive CTESSEL.

For precipitation, JULES allows rainfall and snowfall variables to be provided separately or added together as a single precipitation field, leaving the model to make the distinction between liquid and solid precipitation, by using a temperature threshold. The available field from EFDC dataportal was precipitation, so again the snowfall and rainfall partitioned by JULES were used as driving variables in CTESSEL. It was noticed that both models failed to reproduce enough snow accumulation at Hyytiälä in Finland, a site that is snow covered for most part of the winter. The precipitation field downloaded from EFDC dataportal was verified against a daily dataset of liquid water and melted snow provided by the Finnish Meteorological Institute (FMI) for a nearby station Juupajoki Hyytiälä. It was found that the EFDC precipitation only contained rainfall. The FMI daily dataset was disaggregated to 30 minute periods and the EFDC precipitation was subtracted to yield an estimate of the snowfall. These snowfall values were used to drive the models, providing satisfactory snow depths for the site.

The height at which the forcing variables are introduced in the models, or blending height, is set as the difference between tower height and canopy height. The height of each FLUXNET tower varies from site to site (see Table 4.2). In reality, the blending height is where internal boundary layers from the individual subgrid surfaces merge.

4.3.2 Vegetation and snow

The simulations are run for a single point (gridbox). The vegetation type of the whole gridbox has been set to be homogeneous: only one single type corresponding to the representative species of each FLUXNET tower. This allows for a more direct model comparison

and clearer interpretation of results, as they can be related to the leaf level analysis of each vegetation type in Chapter 3. Coniferous forests in Hyytiälä, El Saler, Loobos, Bily Kriz and Tharandt are represented by needle leaf trees (PFT = 2) in JULES and evergreen needle leaf trees in CTESSEL (vegetation type 3). Broadleaf forests in Hesse forest, Roccarespampani, Vielsalm and Brasschaat are modelled with broadleaf (PFT = 1) in JULES and deciduous broadleaf tree (vegetation type 5) in CTESSEL. Finally, Cabauw is represented by C_3 grass (PFT = 3) in JULES and short grass (vegetation type 2) in CTESSEL.

The choice of canopy model in JULES is the most realistic option available: `can_model = 4`, that uses a canopy heat capacity (called surface capacity, C_s, in Eq. 2.1) and radiative coupling between the canopy and the underlying ground (first term in Eq. 2.4). It also enables the representation of snow beneath the canopy. The upscaling method from leaf to canopy in JULES is the most advanced multilayer approach (`can_rad_mod = 4`) in the JULES version being used (v4.1). CTESSEL upscaling uses a single layer and radiation interception is based on Beer's law. See Section 2.4.7 for details on each model's upscaling procedure.

CTESSEL represents snow on the surface with a dedicated dynamic tile that only has a fraction above zero when there is snow on the ground (Dutra et al., 2010a). A multilayer model is used to represent the thermodynamics of the snow pack. In JULES, the snow model was activated, with three snow layers (`nsmax = 3`), snow was allowed underneath canopy (`cansnowpft = True`) and (`l_snowdep_surf = True`). Model defaults were used for snow related parameters (`total_snow = False`).

Table 4.2: Sites characteristics used in models setup

Site	**Vegetation type**	**Tower height (m)**	**Soil type**
FR-Hes	Broadleaf tree	22	Medium
BE-Vie	Broadleaf tree	40	Medium
BE-Bra	Broadleaf tree	39	Coarse
NL-Loo	Needle leaf tree	24	Coarse
DE-Tha	Needle leaf tree	42	Medium
IT-Ro1	Broadleaf tree	20	Medium-Fine
ES-ES1	Needle leaf tree	13	Coarse
CZ-BK1	Needle leaf tree	36	Coarse
FI-Hyy	Needle leaf tree	73	Medium
NL-Ca1	C_3 grass	5	Medium

4.3.3 LAI and surface albedo

Both models were run with the same prescribed monthly leaf area index (LAI). It is derived from ECMWF's 'climate package' to characterise the land surface (ECMWF, 2015) Chapter 11. It is based on MODIS MOD15A2 LAI product, temporally smoothed and disaggregated to high (forest) and low vegetation (grass) components. Because the simulations are run for a single vegetation type, only high or low component was used. The LAI values for each site are shown in Appendix D. The seasonally varying LAI allows for a better representation of plant phenology, which has an impact on the fluxes. Blyth et al. (2010) showed that the use of a fixed annual LAI can result in poorly represented evaporation at sites where vegetation has a marked phenology and Boussetta et al. (2013a) found a positive effect of seasonally varying LAI on forecasts of screen level temperatures through the effect of improved seasonal course of evapotranspiration.

Snow free surface albedo is also prescribed as a monthly climatology derived from MODIS products interpolated for a smooth temporal transition (ECMWF, 2015; Schaaf et al., 2002).

4.3.4 Soil types and hydraulic schemes

The soil type of each site was derived from the FAO Digital Soil Map of the World, by taking the dominant soil texture class for the deep soil layer (30-100 cm) as detailed in Balsamo et al. (2009); the corresponding classes are listed in Table 4.2. There is one exception to this soil selection, El Saler, in Spain is a pine forest located on a narrow land barrier between the Mediterranean and an inland lagoon. It would be allocated 'fine' soil according to the soil map, but was characterised as 'coarse' to better describe the sandy soil at this location as recommended by the site PI.

The soil moisture factor was found to be a key variable for photosynthesis (Section 3.6). Its value is determined by the soil type via the volumetric soil moisture contents at permanent wilting point and critical point. The associated soil moisture contents for each soil type were taken from CTESSEL soils characterisation (ECMWF, 2015) and are those used operationally (Balsamo et al., 2009). The values are listed in Table 4.3 together with field capacity and residual level for each soil type.

Table 4.3: Volumetric soil moisture content values at saturation, field capacity, permanent wilting point and residual level (m^3 m^{-3}). Values correspond to CTESSEL settings and have been used in JULES as well.

Texture	θ_{sat}	θ_{cap}	θ_{pwp}	θ_{res}
Coarse	0.403	0.244	0.059	0.025
Medium	0.439	0.347	0.151	0.01
Medium-Fine	0.430	0.383	0.133	0.01
Fine	0.520	0.448	0.279	0.01
Very fine	0.614	0.541	0.335	0.01
Organic	0.766	0.663	0.267	0.01

The model hydraulic scheme used by both models is Van Genuchten (1980). JULES also offers the use of Clapp and Hornberger (1978). Because CTESSEL uses the Van Genuchten (1980) formulation (Balsamo et al., 2009), this scheme was selected in JULES to keep both models as similar as possible. The hydraulic scheme determines the conductivity

Table 4.4: Van Genuchten hydraulic parameters

Texture	α (m^{-1})	$l^{\dagger}$ (-)	n (-)	γ_{sat} (m s^{-1})
Coarse	3.83	1.25	1.38	6.94 10^{-6}
Medium	3.14	-2.342	1.28	1.16 10^{-6}
Medium-Fine	0.83	-0.588	1.25	0.26 10^{-6}
Fine	3.67	-1.977	1.10	2.87 10^{-6}
Very fine	2.65	2.5	1.10	1.74 10^{-6}
Organic	1.30	0.4	1.20	0.93 10^{-6}

† In JULES l is fixed to 0.5

and hydraulic diffusivity that control the flow of water in the subsoil and condition the soil moisture available for root extraction at the each soil layer. The Van Genuchten parameters (Eq. 2.13) were chosen to yield the soil moisture content values indicated in Table 4.3, and are listed in Table 4.4. The optional schemes for subgrid heterogeneity available in JULES, TOPMODEL and PDM are not activated.

The soil carbon in JULES was set to 5 kg m^{-2} for all sites except for DE-Tha where 10 kg m^{-2} was used. This parameter determines the rate of soil respiration, affecting the total ecosystem respiration (R_{eco}) and ultimately the net ecosystem carbon balance (NEE). It is difficult to determine the value of this parameter which exerts such an important influence in the net carbon balance. When modelling the full carbon cycle, a spin up process can be performed; achieving the equilibrium for all the carbon pools. However, the CTESSEL model does not have a full carbon module and the carbon module in JULES (RothC) is not activated. Therefore, in these simulations only one carbon pool in considered (soil carbon) and no carbon spin up is carried out. Although ecosystem respiration and NEE output will be compared, the main focus will be on GPP, which is not affected by soil carbon.

4.4 Results

JULES and CTESSEL comply to the settings described in previous sections, which were designed to make the simulations as equal as possible, allowing model difference to emerge. The comparison aims to identify differences in the model structure that affect vegetation processes. The focus will be on GPP, but a general comparison of other carbon and energy fluxes against FLUXNET observations is also performed at different timescales.

4.4.1 Monthly validation of fluxes

The monthly means of energy and carbon fluxes from models and observations (when available) are presented for each full period of simulation at each site in Figures 4.2 to 4.11. These fluxes shape the energy (Eq. 4.2) and carbon (Eq. 4.3) balances. The energy fluxes are shown in the top panels (a): net radiation (NR), latent heat (LE), sensible heat (H) and ground heat flux (G); and the carbon fluxes are shown in the bottom panels (b): gross primary production (GPP) ecosystem respiration (R_{eco}) and net ecosystem exchange (NEE). The sign convention used is positive downward for NR and G and positive upward for the turbulent fluxes. In the case of carbon fluxes, GPP is positive downward (i.e. carbon assimilated by canopy) while R_{eco} and NEE are positive upward (i.e. negative NEE indicates ecosystem carbon sink).

The main variable analysed in terms of carbon is GPP; this is because from the model perspective this variable is the one that links more directly with the photosynthesis scheme at the leaf level and reflects the influence of environmetal variables. The NEE gives a more complete representation of the carbon budget, as it includes the respiratory contribution. However, due to the carbon model consisting of a single carbon pool in the soil, the respiration values are not necessarily realistic.

The ecosystem respiration is the sum of the plant respiration and the soil respiration; it is mainly dominated by temperature in models. The soil respiration in JULES has been found to be very sensitive to the magnitude of the carbon soil pool. The modelled net ecosystem exchange suffers from the possible errors in R_{eco} due to an ill characterisation of the soil carbon pool. On the other hand, from the observations perspective, NEE is the

variable that is directly obtained from the sensors, offering the highest value; while GPP and R_{eco} depend on assumptions embedded in the models associated in the partitioning process (Section 4.2.1.2).

The root mean squared error (RMSE) and bias for the monthly values of LE, H and GPP are presented in Tables 4.5, 4.6 and 4.7, respectively. The statistics have also been calculated between both models to compare them directly.

Table 4.5: Latent heat (LE) monthly means root mean squared error and bias for both models with respect to observations and between both models.

Sites	RMSE			Bias		
	JU-Obs	CT-Obs	JU-CT	JU-Obs	CT-Obs	JU-CT
FR-Hes	47.99	25.38	29.35	42.22	21.04	21.18
BE-Vie	41.16	11.89	32.72	35.95	10.24	25.71
BE-Bra	40.16	10.58	33.43	37.08	7.52	29.56
NL-Loo	10.82	18.29	17.93	0.00	-14.76	14.76
DE-Tha	15.99	9.03	17.00	12.76	-2.34	15.11
IT-Ro1	20.96	14.00	13.04	12.26	6.03	5.86
ES-ES1	21.37	19.37	11.51	-6.61	-11.62	4.73
CZ-BK1	37.76	17.79	22.74	27.50	9.13	18.37
FI-Hyy	17.58	9.62	11.27	13.18	4.22	8.97
NL-Ca1	17.51	11.57	25.32	11.60	-8.32	19.92

Table 4.6: Sensible heat (H) monthly means root mean squared error and bias for both models with respect to observations and between both models.

Sites	RMSE			Bias		
	Obs-JU	Obs-CT	JU-CT	Obs-JU	Obs-CT	JU-CT
FR-Hes	17.60	25.34	23.46	-2.80	14.52	-17.32
BE-Vie	18.20	23.71	32.73	-4.31	17.83	-22.14
BE-Bra	24.97	15.12	26.52	-20.68	3.61	-24.29
NL-Loo	24.05	33.19	13.02	18.70	29.21	-10.51
DE-Tha	17.88	11.89	11.95	-12.73	-3.31	-9.42
IT-Ro1	32.43	33.69	13.36	14.57	16.53	-9.70
ES-ES1	28.12	25.32	10.99	5.31	4.42	1.22
CZ-BK1	22.74	27.62	15.69	-6.17	-0.32	-5.85
FI-Hyy	11.47	20.31	17.33	4.67	15.04	-10.38
NL-Ca1	13.43	20.32	16.28	5.46	17.94	-12.48

Table 4.7: Gross primary productivity (GPP) monthly means root mean squared error and bias for both models with respect to observations and between both models.

Sites	RMSE			Bias		
	JU-Obs	CT-Obs	JU-CT	JU-Obs	CT-Obs	JU-CT
FR-Hes	2.20	1.96	1.00	0.60	0.19	0.42
BE-Vie	1.47	1.91	0.66	-0.87	-1.47	0.60
BE-Bra	1.14	0.86	0.67	-0.18	-0.10	-0.08
NL-Loo	2.27	2.23	0.59	-1.67	-1.86	0.19
DE-Tha	3.26	3.12	0.65	-2.34	-2.49	0.15
IT-Ro1	2.90	1.63	2.17	-1.72	0.17	-1.87
ES-ES1	2.40	1.68	1.13	-2.02	-1.43	-0.62
CZ-BK1	2.08	1.74	0.77	-1.16	-1.05	-0.10
FI-Hyy	0.94	0.68	0.54	-0.38	-0.32	-0.05
NL-Ca1	1.82	2.00	2.20	0.10	-1.35	1.44

Net radiation (NR) is the sum of shortwave and longwave net fluxes. It is dominated by

the incoming solar radiation, which is directly obtained from measurements to drive both models. Longwave incoming radiation is calculated by JULES from observed solar and net radiation and is used to drive both models. Because the snow-free albedo is the same in both models, the small difference in net radiation can only be attributed to differences in surface temperature, altering longwave upward radiation. CTESSEL NR values are slightly lower at most sites, revealing slightly stronger longwave upward radiation. This is related to the small differences in the energy balance solved by each model: JULES includes a term to account for the surface's thermal inertia (Equation 2.1), while CTESSEL does not (Equation 2.5). The magnitude of the NR is higher in the Mediterranean sites (ES-ES1 and IT-Ro1), in agreement with stronger insolation at these lower latitudes and in CZ-BK1 during the second year of simulation.

Latent heat flux at the temperate forests presents positive bias (except CTESSEL in DE-Tha and NL-Loo). JULES estimates of latent heat are higher than those predicted by CTESSEL for all sites, as indicated by the positive bias (JU-CT) shown in Table 4.5 and also shown in the plots. CTESSEL seems to have tighter controls on evaporation. The extra energy in CTESSEL is partly put into sensible heat and partly put into ground heat flux. CTESSEL has higher or similar values of sensible heat negative bias (JU-CT in Table 4.6). This energy partition means that CTESSEL usually presents a higher Bowen ratio (H/LE); the only exception occurs during some summers at the Mediterranean sites when the latent heat in JULES is severely restricted by soil moisture, increasing the Bowen ratio. The ground heat flux modelled by CTESSEL presents a larger amplitude than the ground heat flux modelled by JULES, with higher values both in summer and in winter. This translates into more energy being propagated into the ground in summer and being released in winter in CTESSEL. The differences in G relate to the different terms used in the expressions of ground heat flux (Equations 2.4 and 2.8).

With regard to carbon fluxes, both models tend to underestimate the carbon dioxide assimilated by vegetation. This is seen in the GPP negative biases when comparing models against observations in Table 4.7. The temperate broadleaf forest in FR-Hesse is the only site where both models' predictions are slightly above the observed values (Table 4.7). At this site, the small positive bias is dominated by the high values of GPP predicted by both models during winter and early spring. The burst of vegetation as represented by GPP occurs very rapidly between April and May, which is not well reproduced by

models. During summer the GPP is underestimated, in line with the general trend seen for the other sites. In terms of RMSE, CTESSEL exceeds JULES for all the forest sites. The worst model score for carbon occurs at the needle leaf forest in Tharandt, where the models' underestimation of GPP is about half of the measured uptake in summer. The reason behind this poor performance is not clear: excessive soil moisture stress has been discarded (JULES soil moisture factor for all sites is shown in Figure 4.13). A possible explanation is that the models' parameters that apply to needle leaf trees have typically been adjusted for forests in cold environments. This is in agreement with the results at other needle leaf forests: large RMSE is also seen at NL-Loo and ES-ES1, whereas both models perform well at the boreal site FI-Hyy. In general at the temperate and boreal sites the models' predictions for GPP agree better with each other than with observations (see the RMSE between models in Table 4.7).

Despite the underestimation in carbon assimilation, the seasonal cycle at the temperate sites is generally well represented. The main difference between models appears associated with the representation of soil moisture stress, with JULES restricting more the GPP due to scarce levels of soil water, this will be further discussed in Section 4.4.1.1. During the summers 2006 and 2007 at BE-Bra JULES GPP sees a decrease driven by low soil moisture content (4th layer in Figure 4.12a) as revealed by soil moisture factor β values shown in Figure 4.13c. However, observed GPP values do not support this reduction in carbon assimilation.

At the Mediterranean sites, IT-Ro1, Italy and ES-ES1 Spain, there is more model disagreement in the carbon assimilation. Both models fail to correctly reproduce the magnitude and evolution of the GPP seasonal cycle. The observed carbon uptake exhibits more interannual variability in the seasonal cycle, which models have shown trouble reproducing. The RMSE for GPP are higher than the ones for temperate sites for both models, with CTESSEL performing slightly better. For these Mediterranean sites, the RMSE between models is higher than for the other sites, indicating model disagreement. In the case of the Italian site, IT-Ro1, CTESSEL reproduces a fair seasonal cycle, although it predicts a drop around August, followed by a recovery in September for all simulated years. In the observed data this drop is more gradual or it occurs later, and the September recovery is only seen for years 2002, 2003 and slightly for 2008. For some years JULES fails to reproduce a seasonal cycle at this site. GPP estimates are very low due to excessive soil

moisture stress on vegetation (Figure 4.13f). Photosynthesis is restricted by the available soil water during the whole period, especially in the summer time. Winter 2002 and all year 2003 present particularly low values of soil moisture in the deeper layers leading to the low GPP, similarly during the second half of 2007 is GPP severely reduced due to lack of soil moisture. These correspond with the lowest estimates of GPP. These years also coincide with the years where a dip was shown in summer in observations, possibly related with a hot period. Conversely, at the Spanish site the low GPP cannot be fully explained by lack of soil moisture since the soil moisture factor for the last 3 years is above 0.7 (Figure 4.13g) and the model estimates are still too low.

At the boreal site FI-Hyy GPP estimates from both models are very similar and agree well with measurements except for some underestimation during some summers. Both models agree quite well in turbulent fluxes at this site.

At Bily Kriz forest in Czech Republic, the analysis is limited to two years of data. The climate classification of this site is continental. The pattern found is similar to the temperate forests, GPP flux is underestimated and LE is overestimated with both models showing strong agreement between them.

At the grass site, Cabauw, the strongest disagreement between the models is found for GPP. While CTESSEL estimates continue to be lower than observed, JULES overestimates GPP. The higher GPP modelled by JULES is consistent with leaf level photosynthesis findings, larger values of A_n where predicted by JULES for C_3 grasses (Appendix B: Figures B.2 and B.3). JULES predicts a drastic fall during some summers (2003, 2004 and 2006) beginning in June which is not seen in observations. The drop is caused by a reduction of available soil moisture content in the in summer as revealed in Figure 4.12b and reflected in the the soil moisture factor (Figure 4.13j). Short vegetation is strongly affected by low levels of soil moisture content in the top soil layer, due to the fact that roots do not penetrate deep into the soil (high root density in the top layer). CTESSEL tends to maintain higher levels of soil moisture content than JULES in the 4 soil layers.

The ecosystem respiration analysis must be taken with care, as models' formulations are very sensitive to the carbon content of the soil pool (JULES) or the reference ecosystem respiration (CTESSEL). JULES seems to be able to reproduce the observed reduction in

R_{eco} during summer at the Mediterranean sites. This is driven by a reduction in the soil component of the total respiration due to lack of soil moisture. For all forest sites the ecosystem carbon sink (NEE, Eq. 4.3) is underestimated due to the underestimation of carbon assimilation by vegetation (GPP). At NL-Ca1, summer NEE is overestimated, in JULES due to the GPP overestimation an in CTESSEL due to the a low R_{eco}.

Despite a general underestimation of gross primary productivity in the forest sites by both models, the carbon assimilation in forests located in boreal and temperate climates tends to be better reproduced than that of Mediterranean ecosystems. The GPP underestimation could be a consequence of the choice of using only the main tree species to describe the whole ecosystem, and assuming a full coverage, so no low vegetation or understory are included. Another possibility is that the prescribed LAI, adopted from ECMWF's procedures from MODIS imagery, is too low due to smoothing procedures (Values shown in Appendix D).

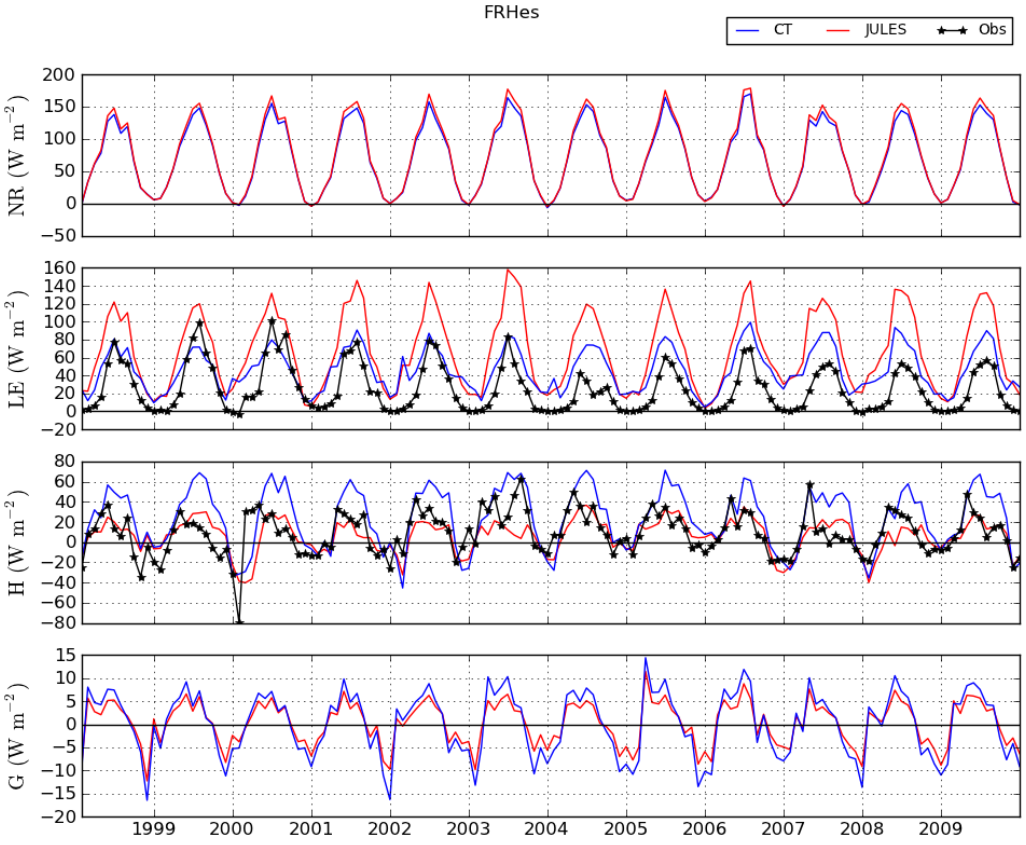

(a) Energy fluxes

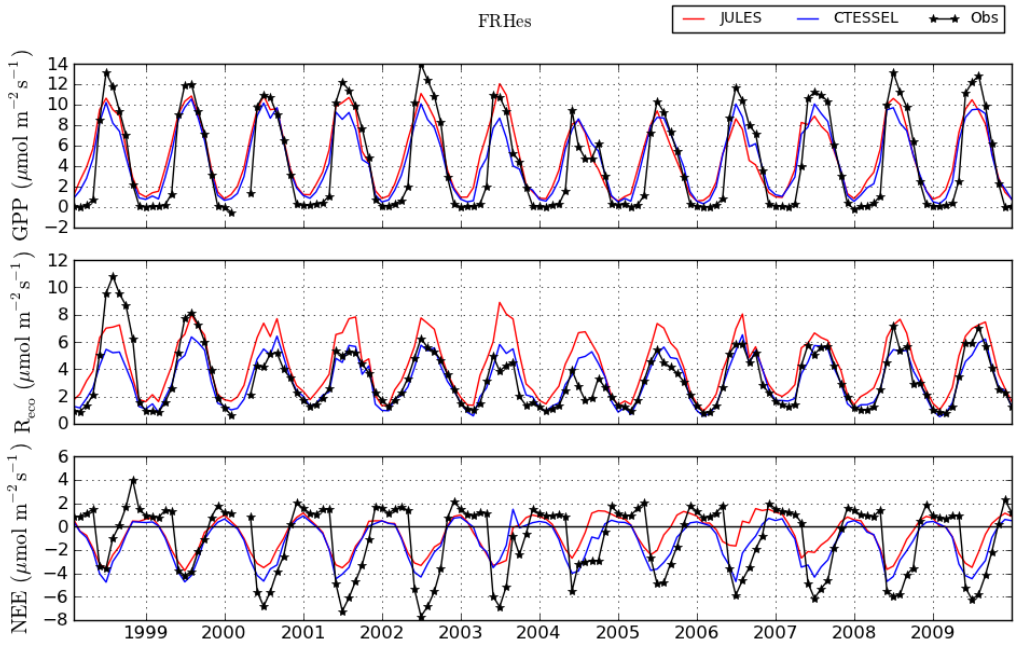

(b) Carbon fluxes

Figure 4.2: Flux monthly means for the full simulation period, Hesse Forest-Sarrebourg, France. Broadleaf forest in temperate climate.

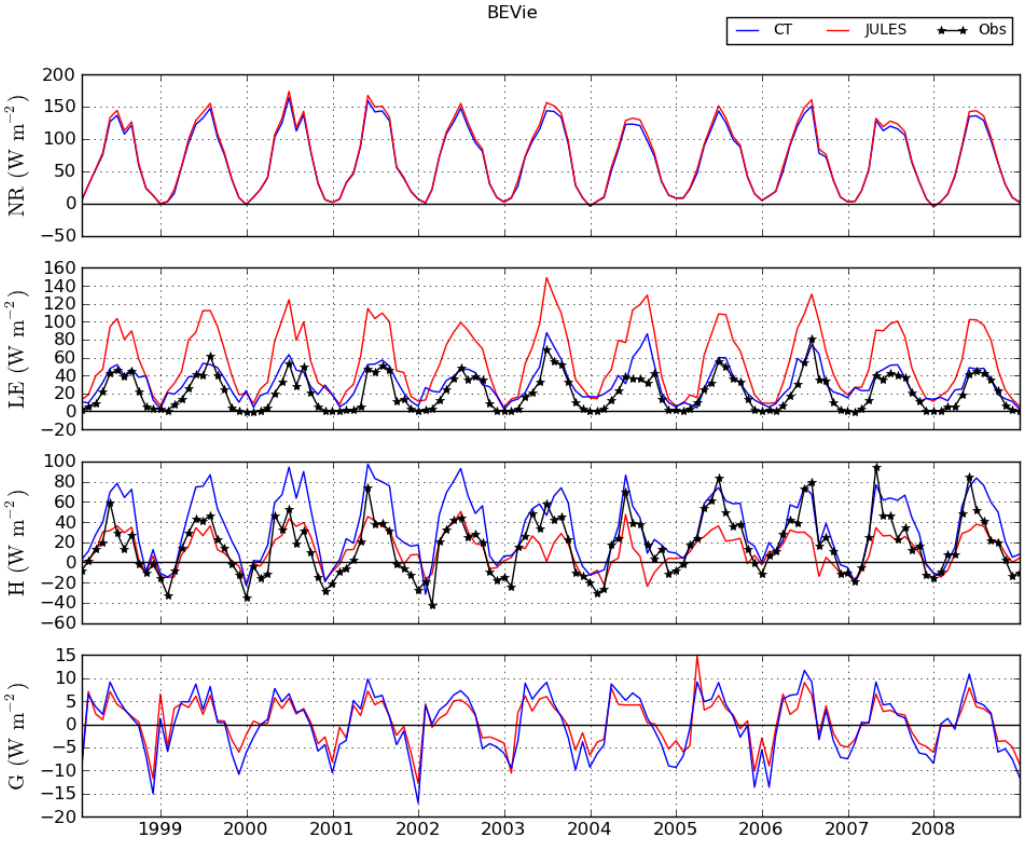

(a) Energy fluxes

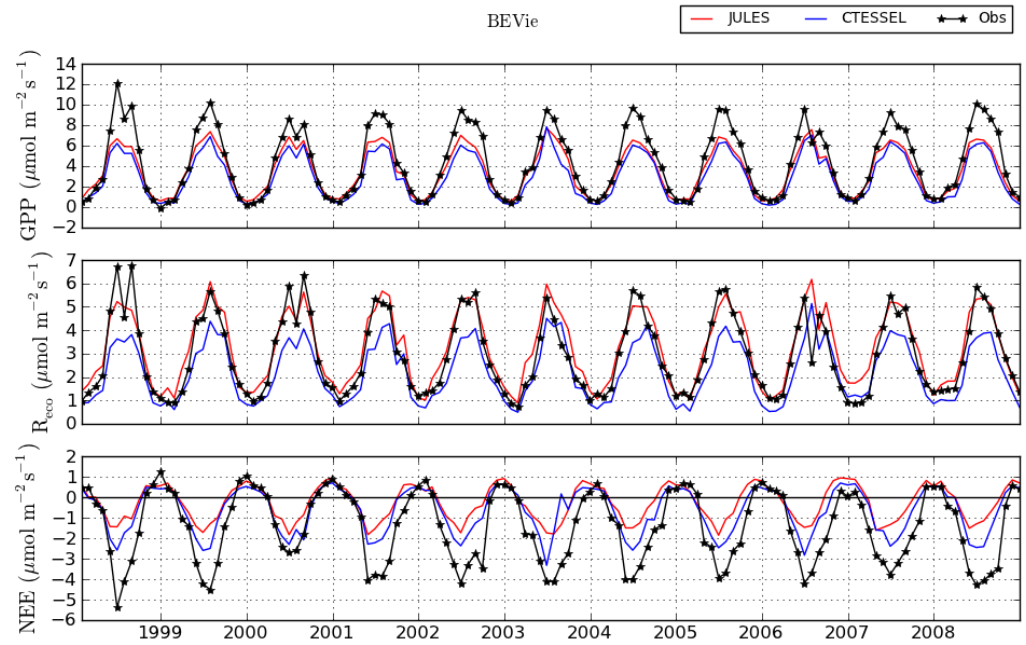

(b) Carbon fluxes

Figure 4.3: Flux monthly means for the full simulation period, Vielsalm, Belgium. Broadleaf forest in temperate climate.

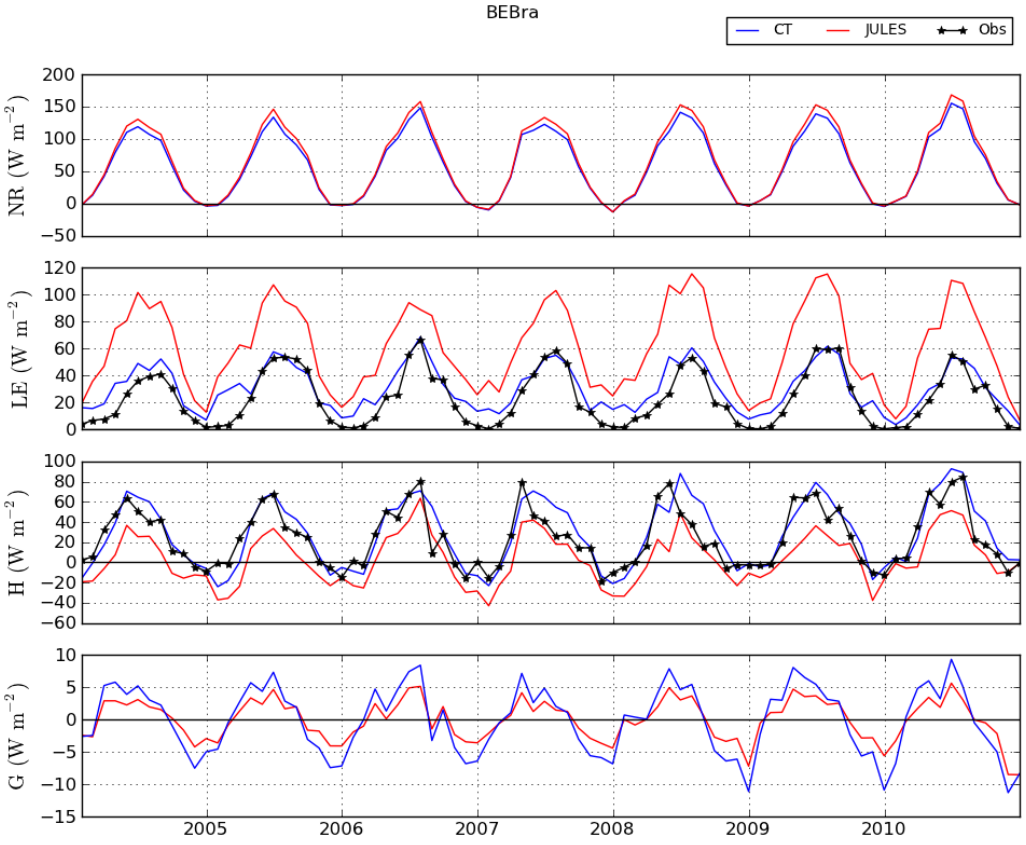

(a) Energy fluxes

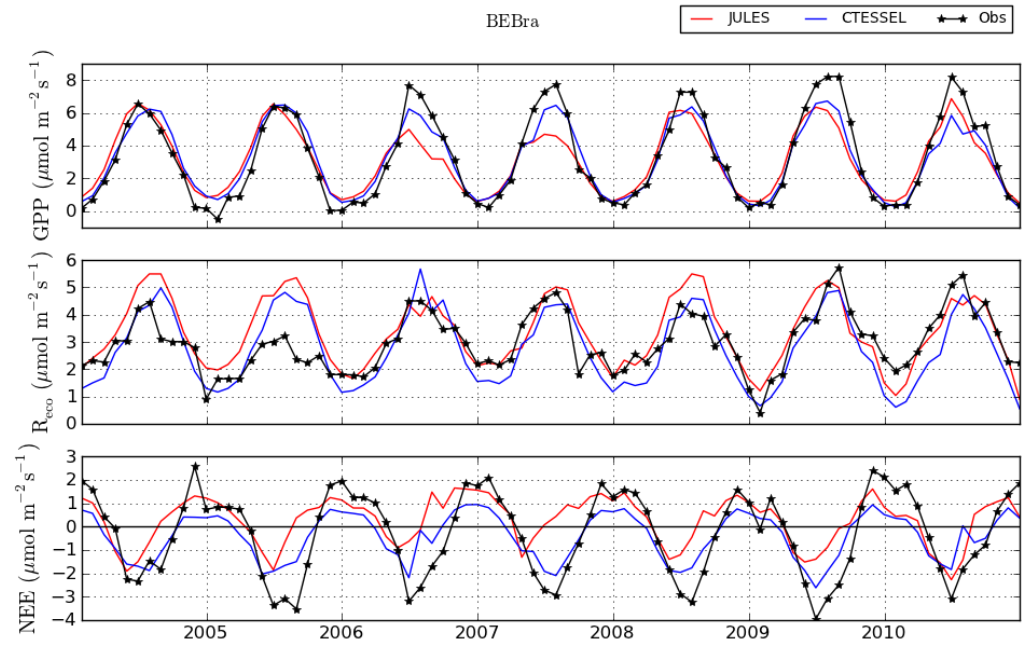

(b) Carbon fluxes

Figure 4.4: Flux monthly means for the full simulation period, Brasschaat, Belgium. Broadleaf forest in temperate climate.

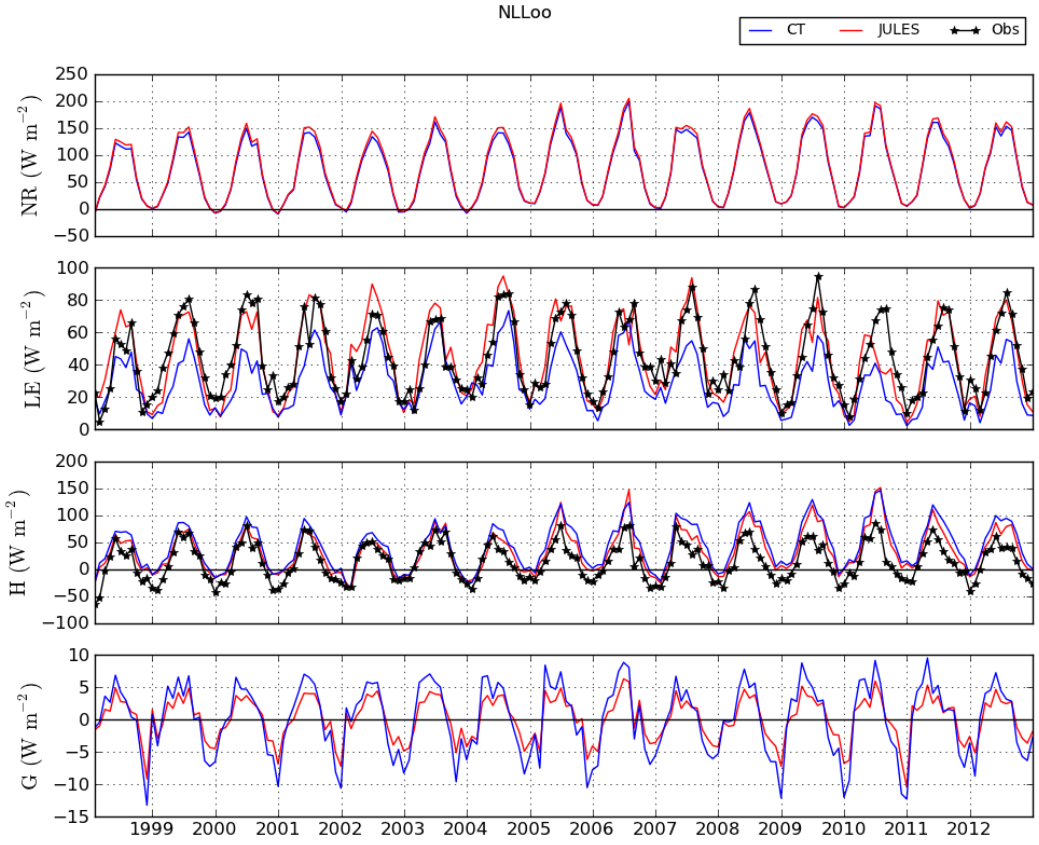

(a) Energy fluxes

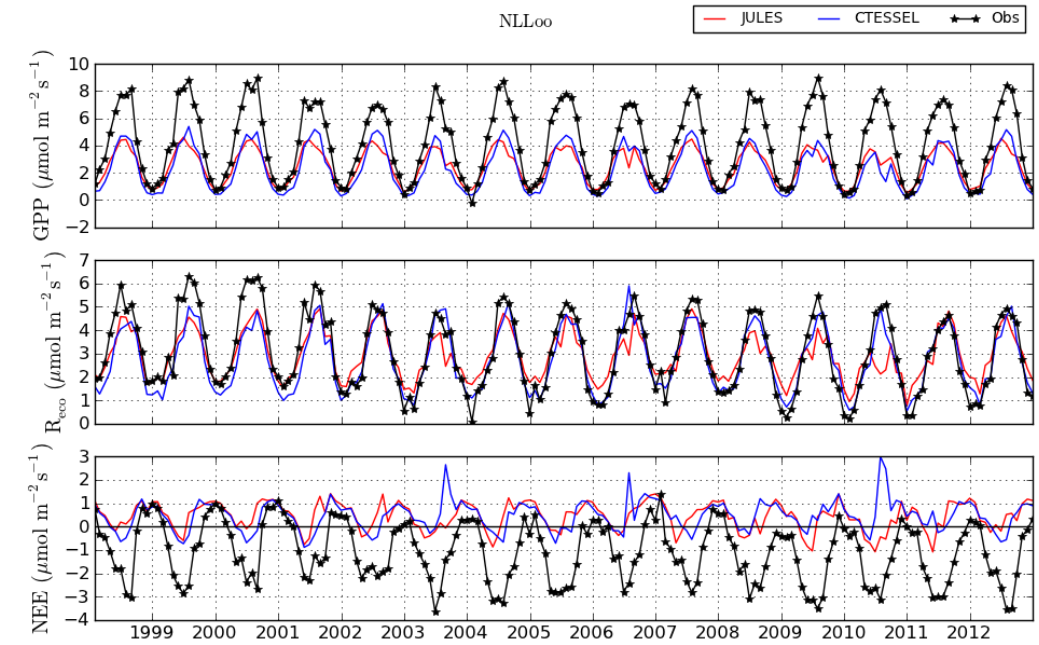

(b) Carbon fluxes

Figure 4.5: Flux monthly means for the full simulation period, Loobos, The Netherlands. Needle leaf forest in temperate climate.

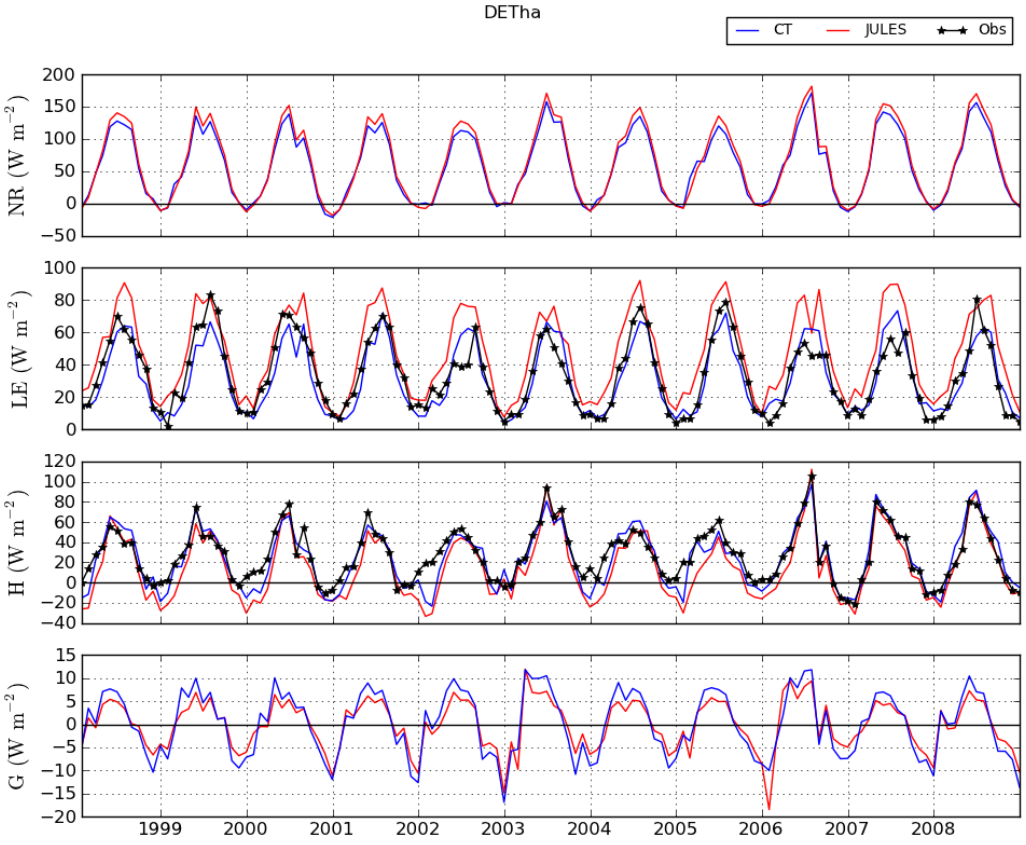

(a) Energy fluxes

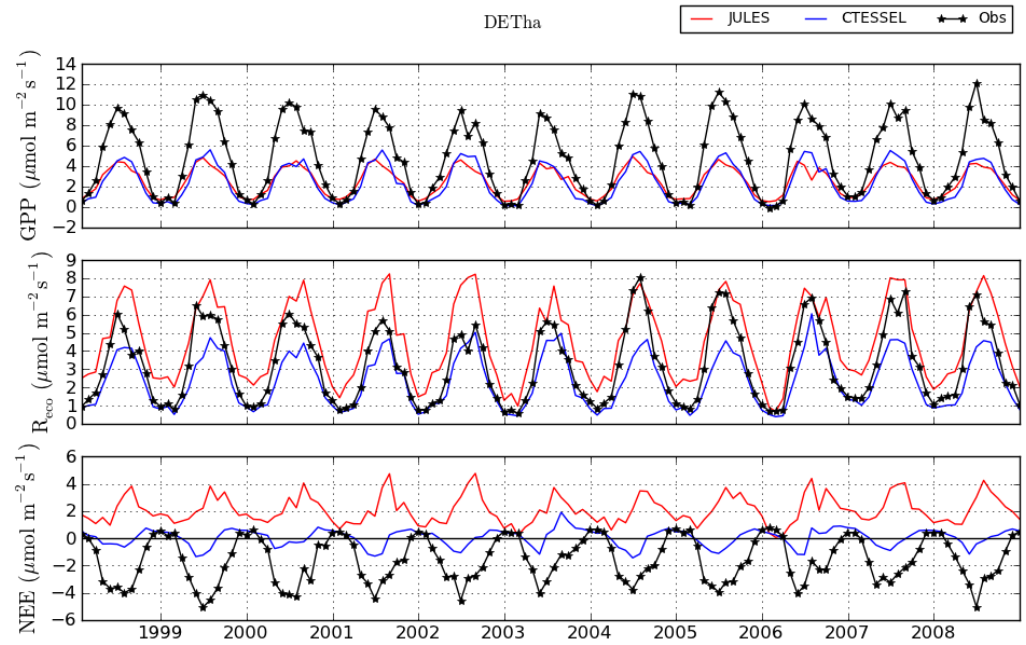

(b) Carbon fluxes

Figure 4.6: Flux monthly means for the full simulation period, Tharandt, Germany. Needle leaf forest in temperate climate.

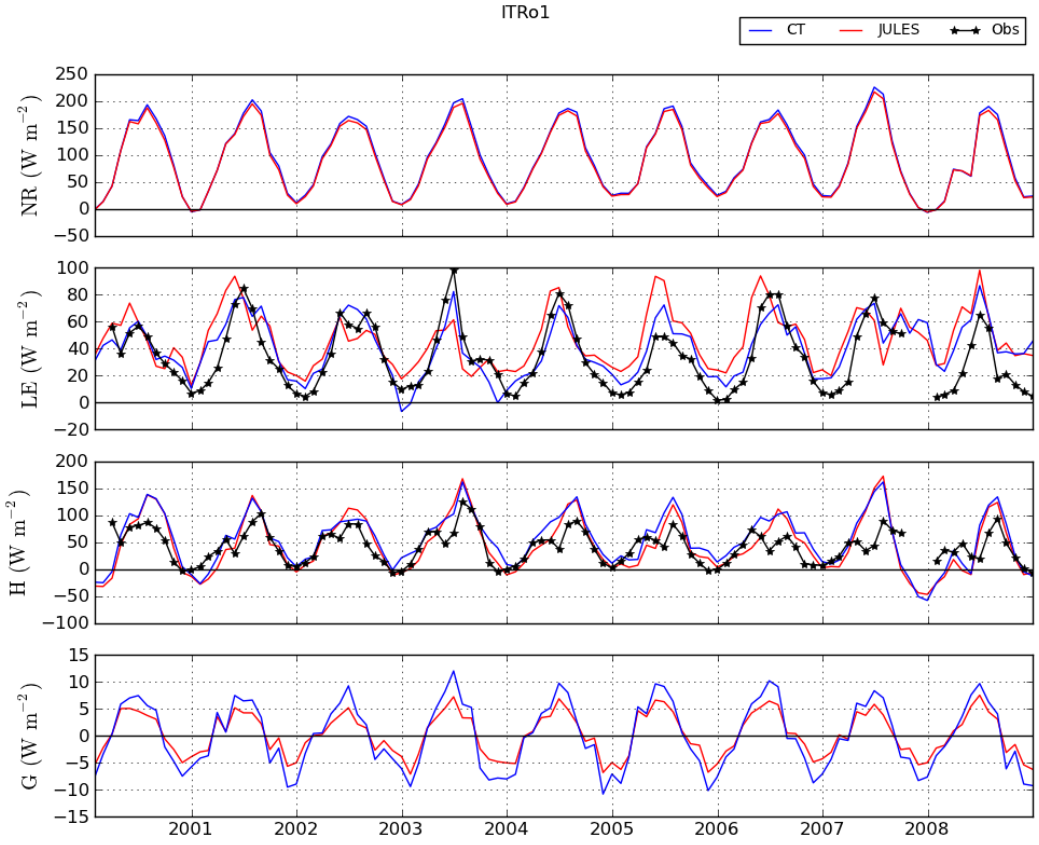

(a) Energy fluxes

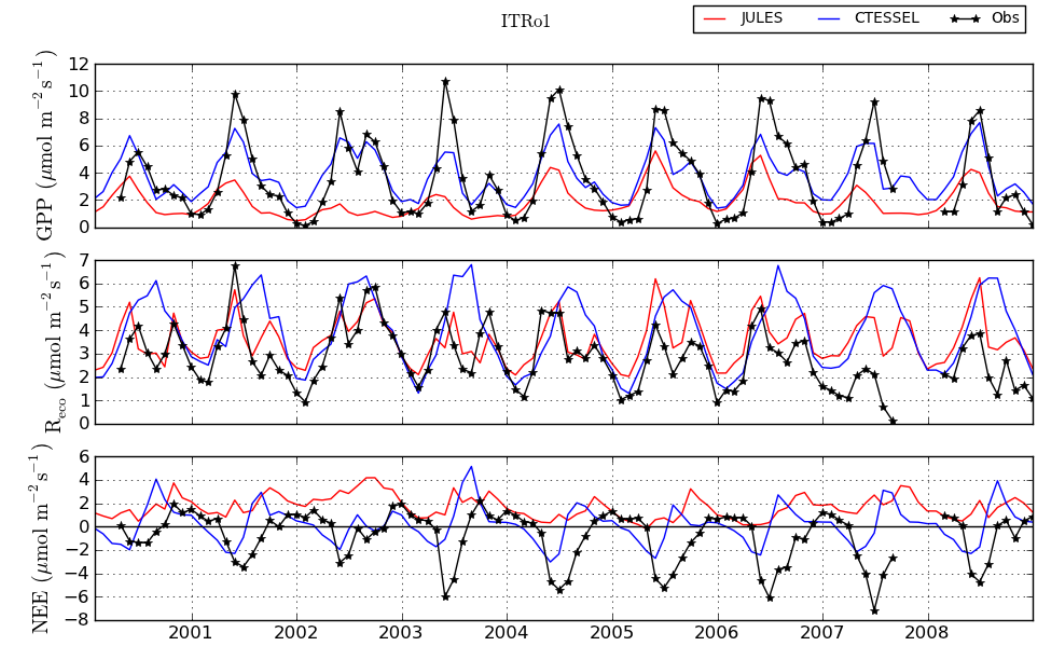

(b) Carbon fluxes

Figure 4.7: Flux monthly means for the full simulation period, Roccarespampani, Italy. Broadleaf forest in Mediterranean climate.

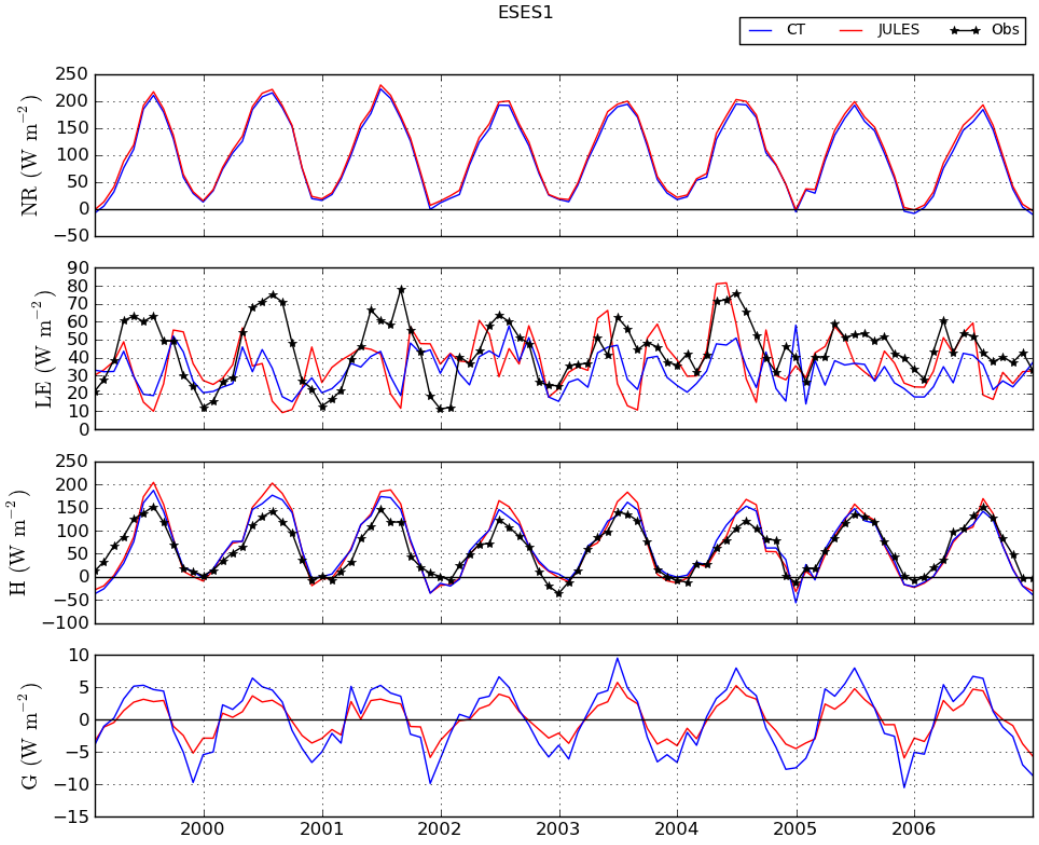

(a) Energy fluxes

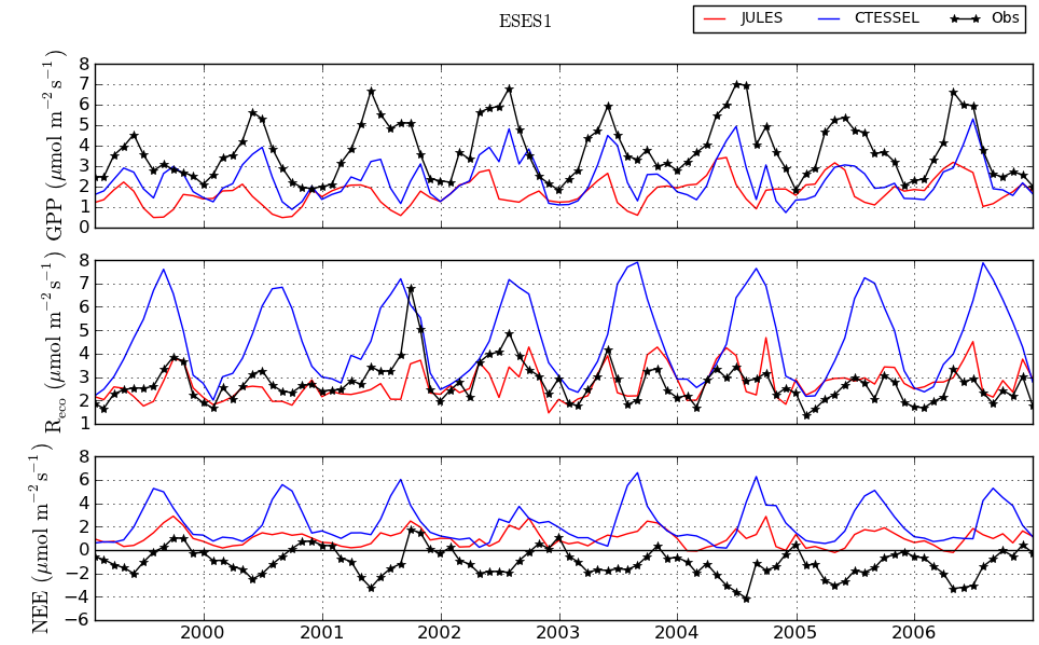

(b) Carbon fluxes

Figure 4.8: Flux monthly means for the full simulation period, El Saler, Spain. Needle leaf forest in Mediterranean climate.

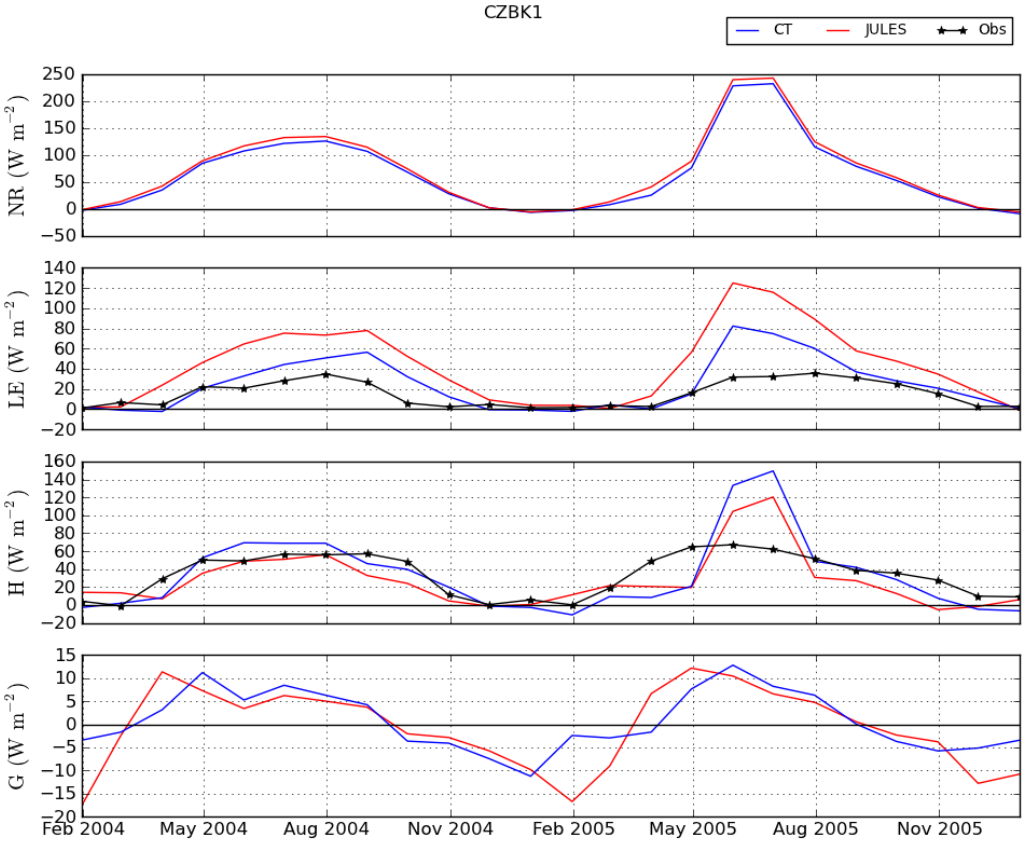

(a) Energy fluxes

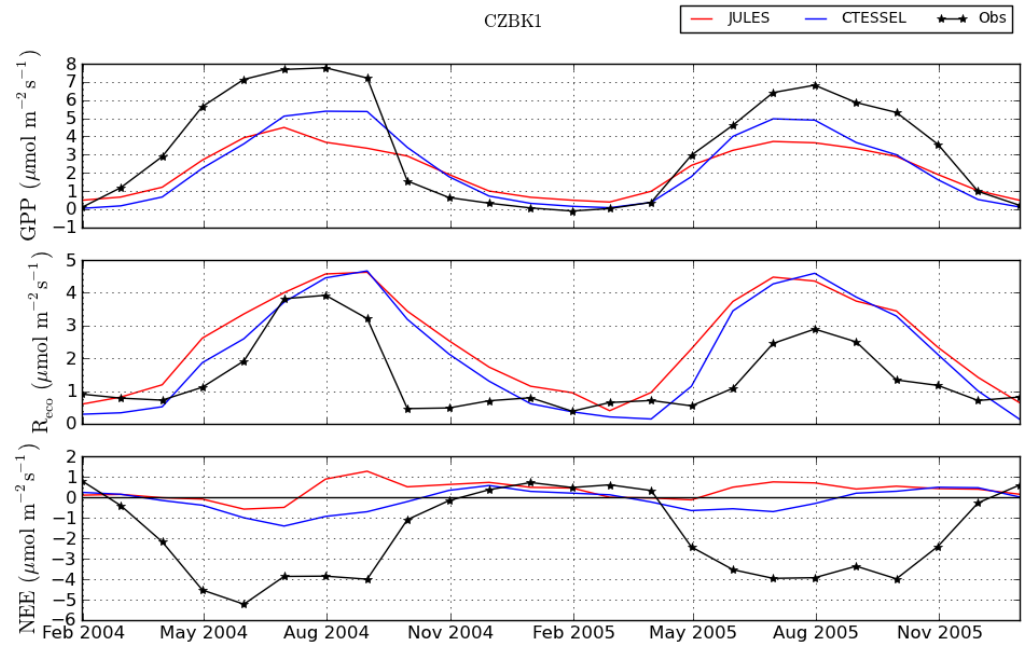

(b) Carbon fluxes

Figure 4.9: Flux monthly means for the full simulation period, Bily Kriz, Czech Republic. Needle leaf forest in cold climate.

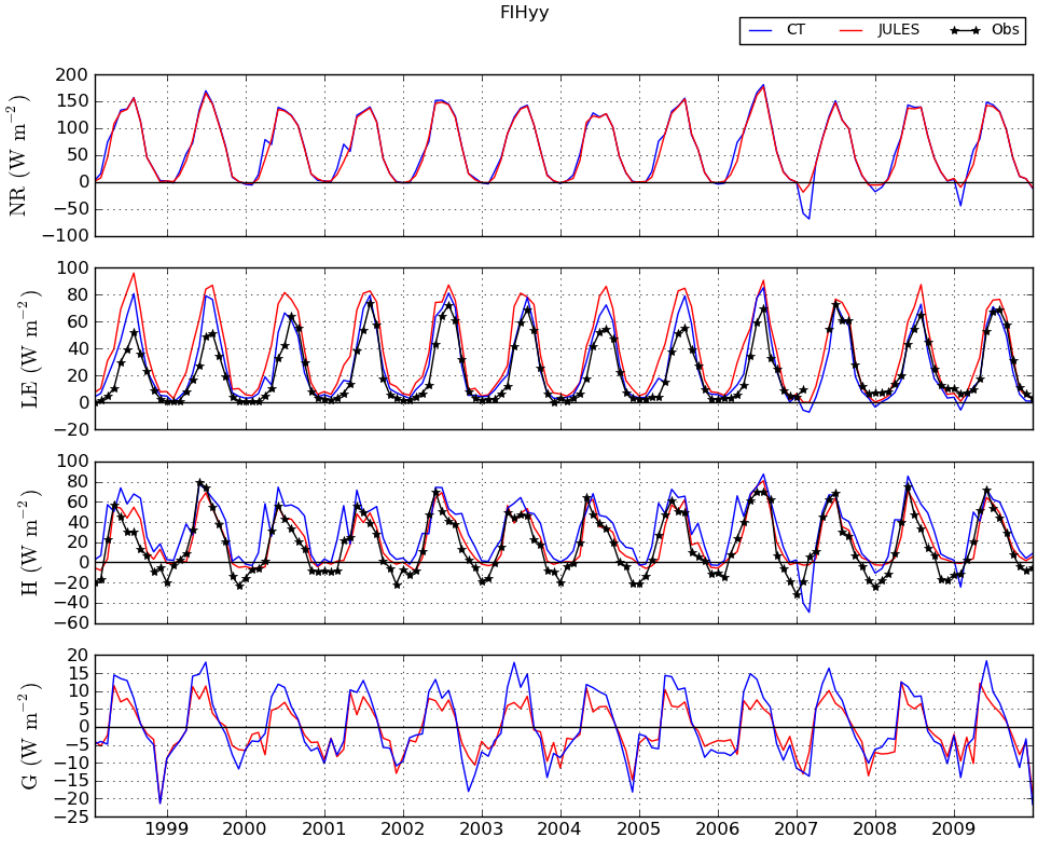

(a) Energy fluxes

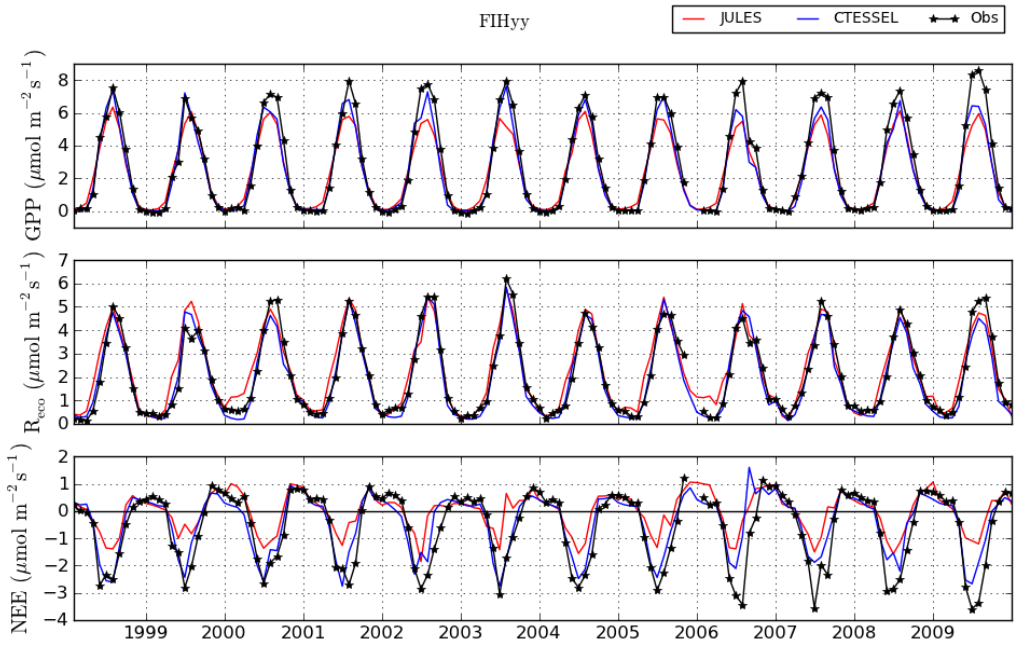

(b) Carbon fluxes

Figure 4.10: Flux monthly means for the full simulation period, Hyytiälä, Finland. Needle leaf forest in boreal climate

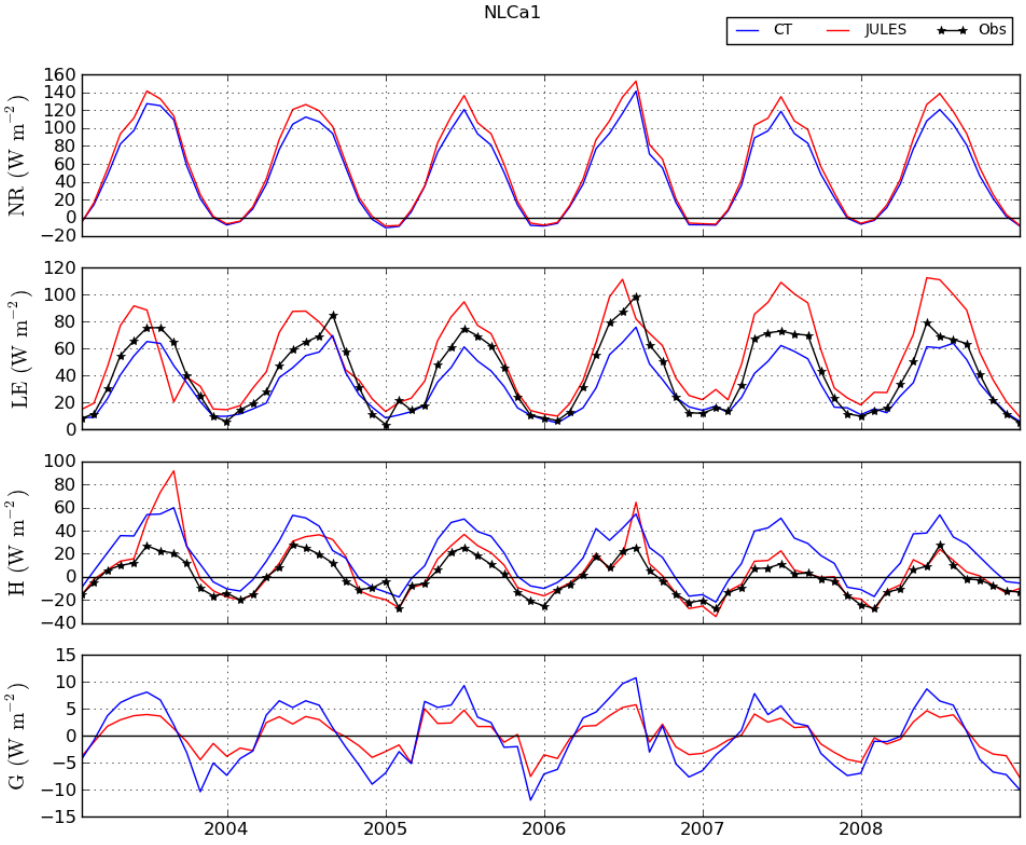

(a) Energy fluxes

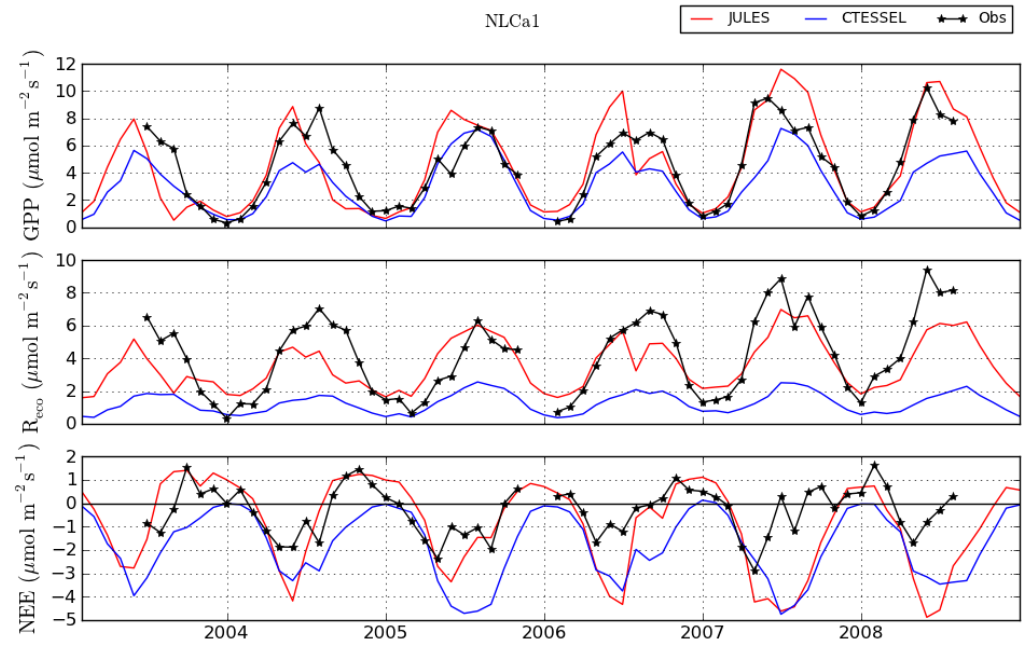

(b) Carbon fluxes

Figure 4.11: Flux monthly means for the full simulation period, Cabauw, The Netherlands. Grass site in temperate climate.

4.4.1.1 Soil moisture content

Each model was initialised with values of soil moisture derived from the spin up process. For all sites the equilibrium soil moisture content for JULES is lower than for CTESSEL. The precipitation is the same in both cases and both models use Van Genuchten (1980) hydraulic scheme with equal parameters where possible (Table 4.4). As an example, the volumetric soil moisture content for each soil layer at two of the simulated sites is shown in Figure 4.12. Each panel corresponds to each of the four soil layers. The different time scale of variations in soil moisture content can be appreciated at each layer. The soil moisture content in the top layer varies more quickly following the precipitation signal. As depth increases, the soil moisture content variability decreases. The evolution of the soil moisture content of the fourth layer in JULES presents an annual cycle with a larger amplitude than in the case of CTESSEL. The larger evapotranspiration seen in JULES may explain this difference. The lower water content has implications as it restricts GPP quite strongly. The JULES soil moisture factor for these two and all other sites is shown in Figure 4.13.

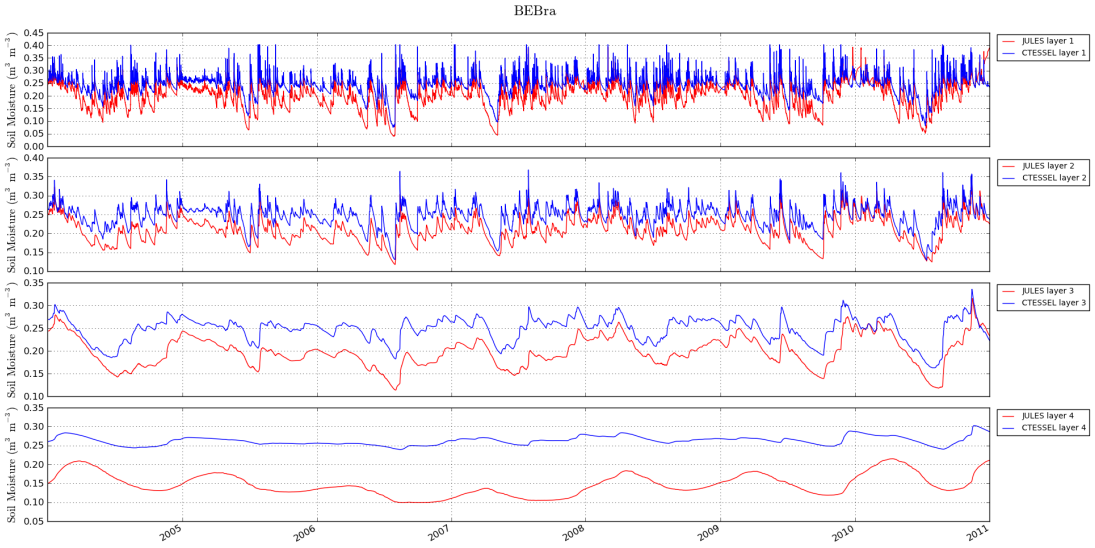

(a)

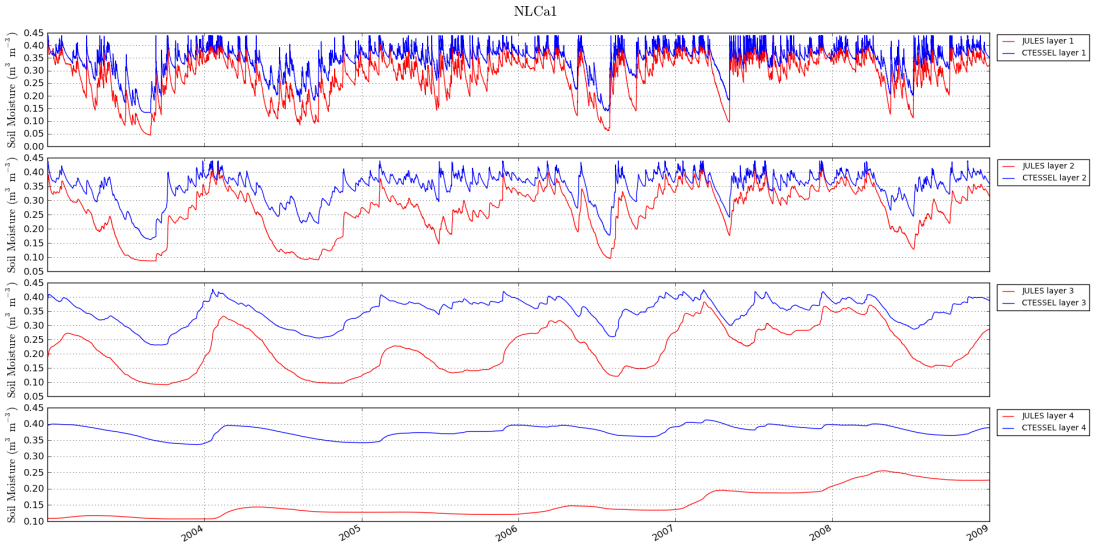

(b)

Figure 4.12: Volumetric soil moisture at each soil layer as reproduced by both models for two sites: BE-Bra forest site (a) and NL-Ca1 grass site (b). For JULES, it can be noted how for BE-Bra the deepest layer has a strong role in determining the soil moisture stress on photosynthesis, as seen by the low soil moisture content in years 2006 and 2007 matching the low values of β in Figure 4.13c; whereas in NL-Ca1, the uppermost layer determines the soil moisture stress, as seen by the low soil moisture content in years 2003, 2004 and 2006 matching the low values of β in Figure 4.13j.

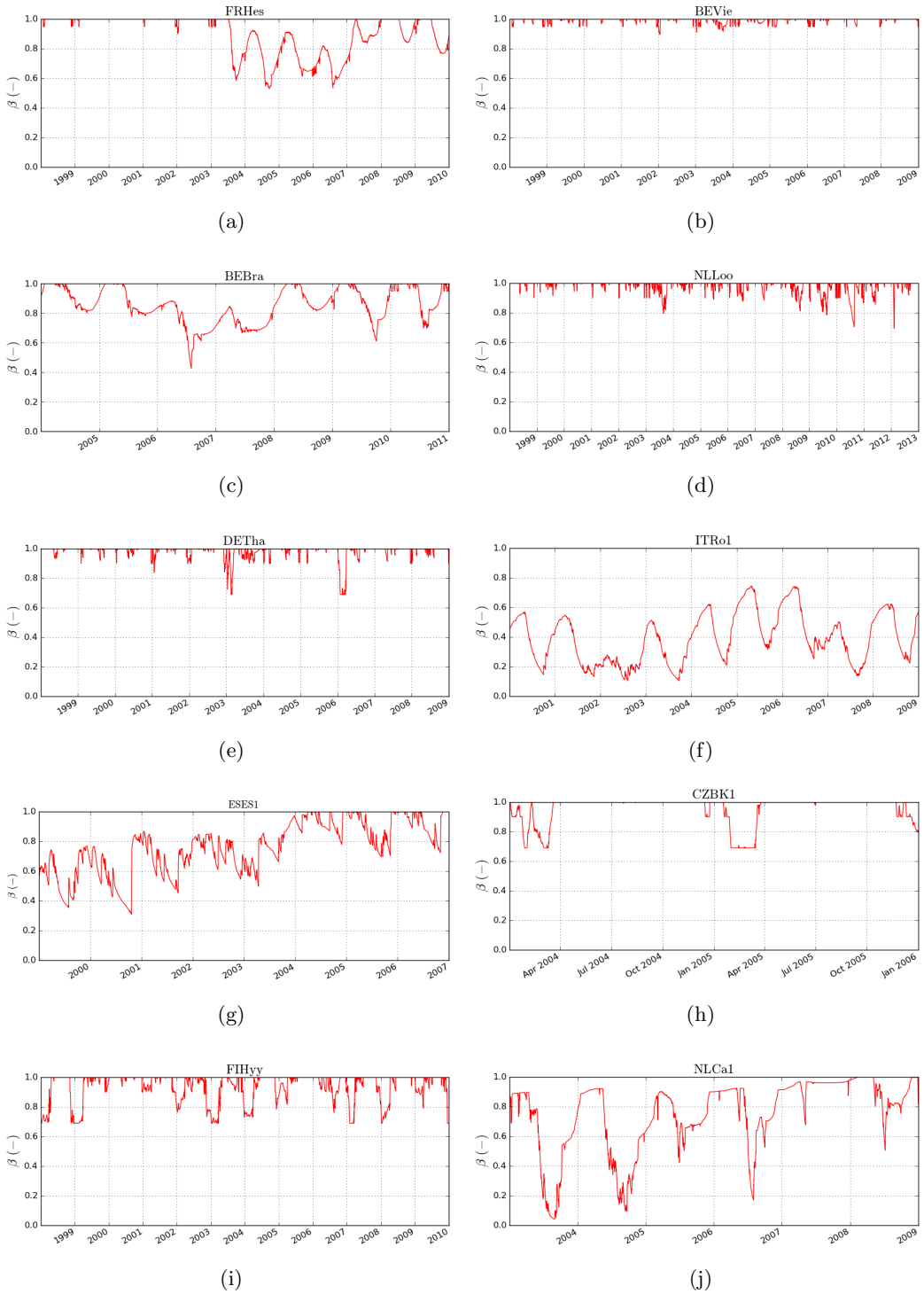

Figure 4.13: JULES soil moisture stress factor (β) for each site.

4.4.1.2 Seasonal means and ecosystem water use efficiency

The monthly means of GPP and LE of all modelled years have been averaged together for a better illustration of the seasonal variation at each site (first two columns in Figure 4.14). In the third column, the ratio between carbon assimilation and latent heat is presented ($WUE = GPP/LE$). It must be noted that the latent heat in the denominator includes evaporative flux from soil and direct evaporation from the canopy interception as well as stomatal transpiration, while other definitions of WUE relate the GPP to only the transpired water. This extended calculation can be compared against observations, as the GPP/LE ratio can be derived from the measured fluxes. The units of WUE calculated in this manner are μmol of carbon per unit of evaporative energy. In winter, due to the small magnitude of both fluxes, the WUE values are more variable and should not be considered, in Figure 4.14h some values of CTESSEL were removed.

As already discussed, GPP is typically underestimated by both models, while LE is overestimated by JULES. Figure 4.14 summarises this result and also highlights how similar the models' estimates of GPP are; while more variability arises for the latent heat fluxes, with JULES typically predicting higher LE values. This was already seen in the model-to-model errors shown in Tables 4.5 and 4.7. The similarity in GPP is more evident for the sites located in temperate climate. For the Mediterranean sites (Figures 4.14f and 4.14g) and the grass site NL-Ca1 (Figure 4.14j) the differences in carbon assimilation are larger. This is partly due to differences in the soil moisture stress parameterization and the actual soil moisture content.

In terms of WUE, it can be seen that the ecosystem WUE derived from the observed fluxes is generally higher than that of the models. Between the models, JULES has the lowest WUE, due to its higher LE flux. The model disagreement in latent heat fluxes can be disentangled at two levels: at the leaf level and at the ecosystem level. At the leaf level, both models present different sensitivity of stomatal pores to air humidity. Leaf level analysis in Section 3.5.2 showed how for relative humidities above 30% stomatal conductance in JULES was larger than in CTESSEL (Figure 3.24). This effect was reflected in the lower intrinsic WUE (A_n/g_s) in JULES (Figure 3.23). In those leaf level experiments, the aerodynamic conductance was fixed to the same high value in both models, ensuring good coupling between vegetation and the atmosphere and thus little or no disturbance on

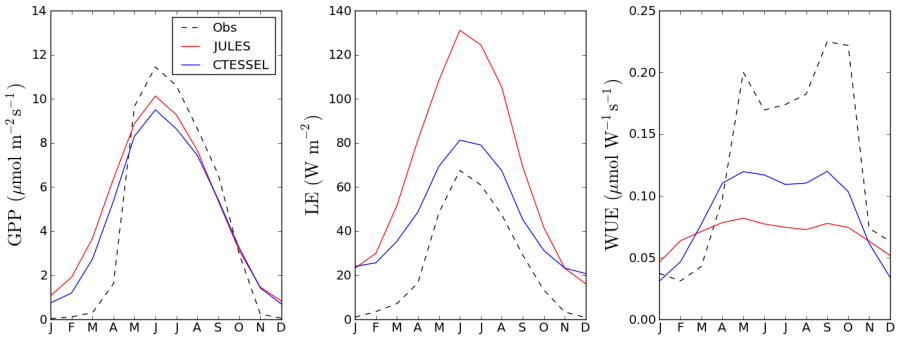

(a) FR-Hes

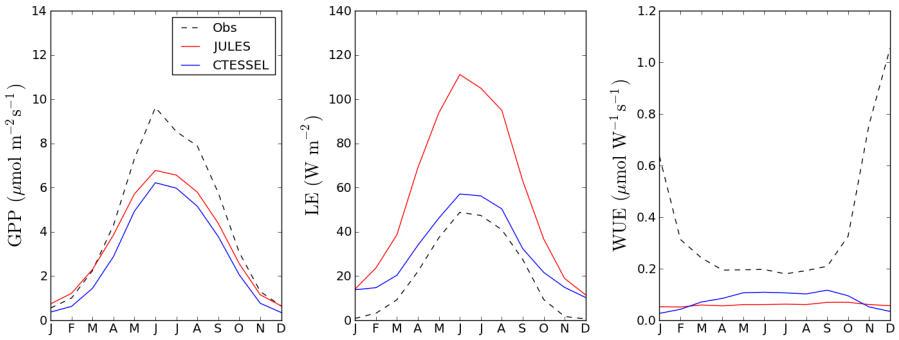

(b) BE-Vie

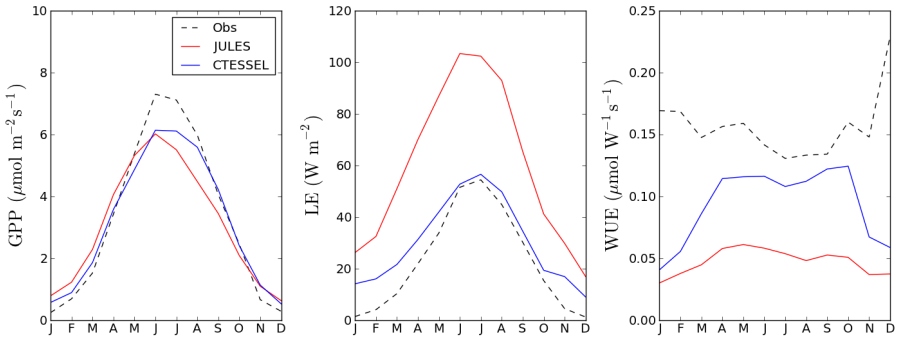

(c) BE-Bra

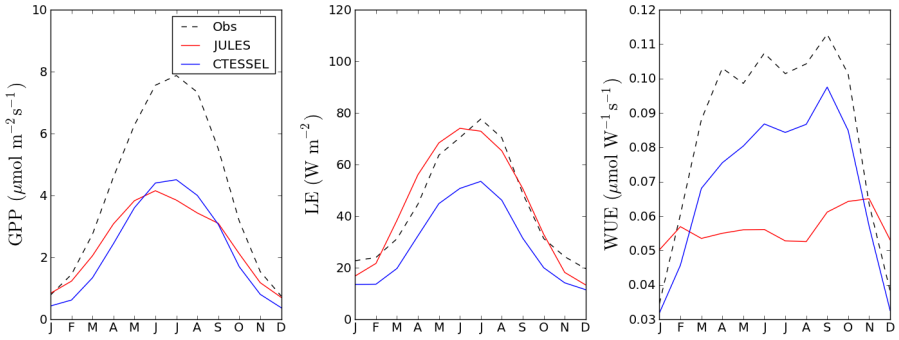

(d) NL-Loo

Figure 4.14: Seasonal average of GPP, LE and WUE = GPP/LE

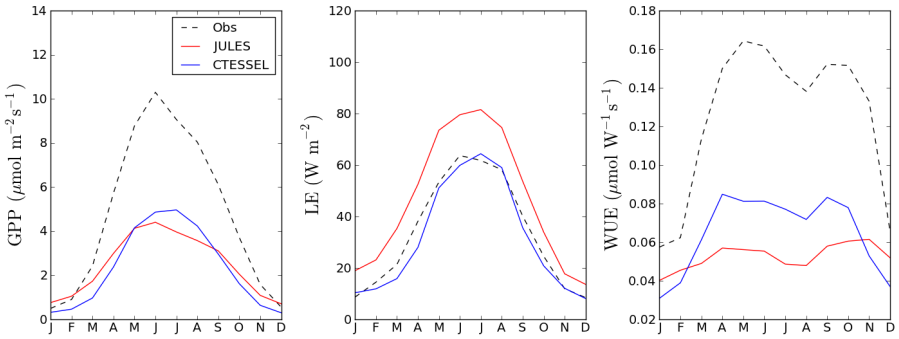

(e) DE-Tha

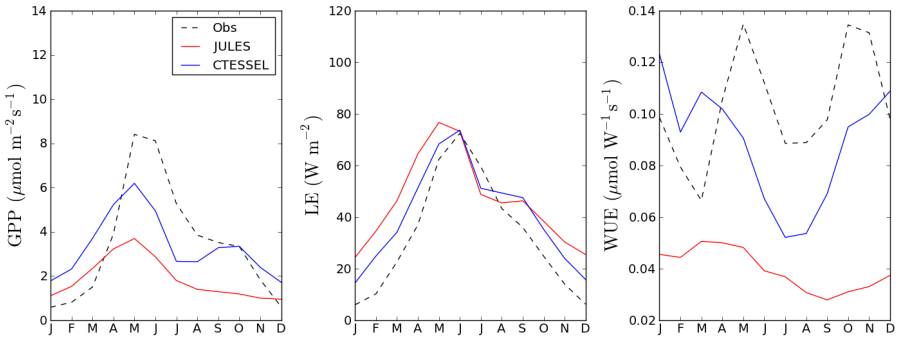

(f) IT-Ro1

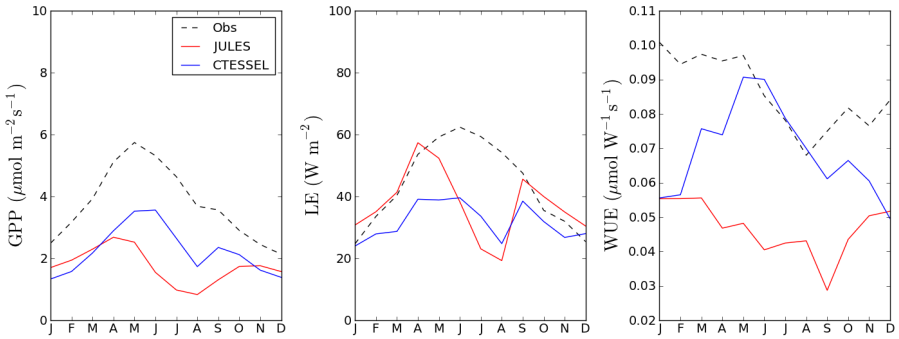

(g) ES-ES1

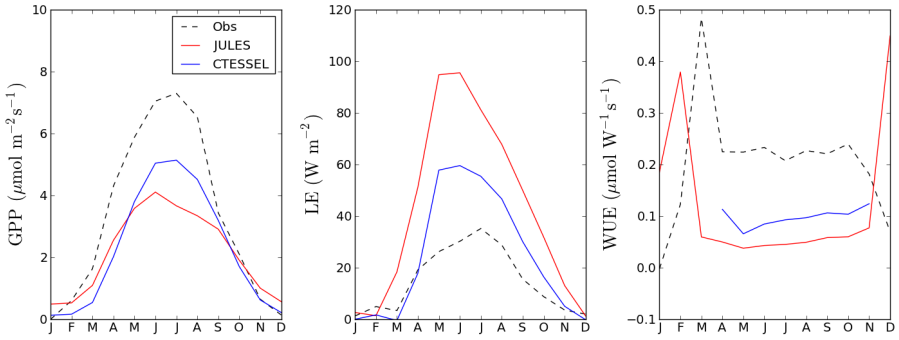

(h) CZ-BK1

Figure 4.14: (Cont.) Seasonal average of GPP, LE and WUE = GPP/LE

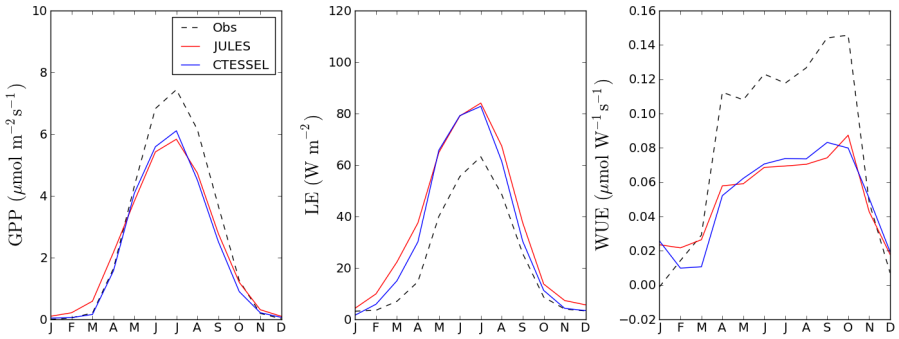

(i) FI-Hyy

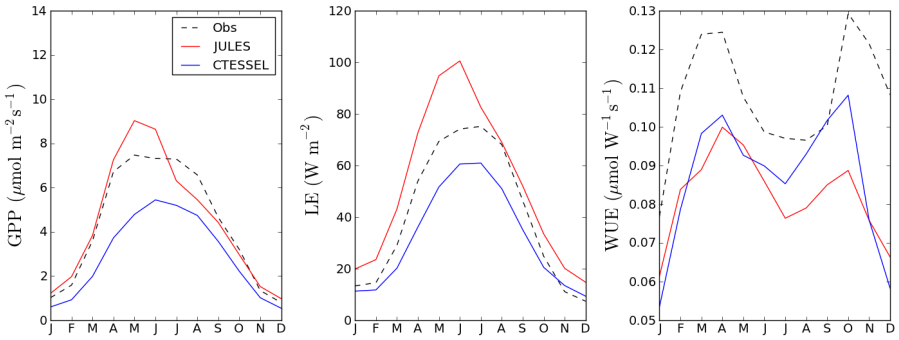

(j) NL-Ca1

Figure 4.14: (Cont.) Seasonal average of GPP, LE and WUE = GPP/LE

g_s. However when dealing with the ecosystem as a whole, the degree of coupling between canopy and atmosphere affects WUE (De Kauwe et al., 2013). The degree of coupling increases as the ratio of boundary layer conductance to stomatal conductance increases; the canopy becomes decoupled when boundary layer conductance is low or when stomatal conductance is high (Jarvis and McNaughton, 1986). The boundary layer between the forest and the atmophere affects the calculation of g_s, and reduces the effect of stomatal conductance on tranpiration. In the studied models the boundary layer conductance is represented by the aerodynamic conductance, determined by surface windspeed and the surface exchange coefficents, which are a function of roughness length and the surface layer stability. Therefore the aerodynamic conductance, and consequently the degree of canopy-atmosphere coupling, is a source of model discrepancy that could affect the differences in latent heat, as well as affecting the stomatal conductance.

4.4.2 Diurnal validation

The analysis is further extended to the diurnal evolution of fluxes. The 30 minute values of GPP and LE were averaged daily for the winter months (DJF: December-January-February) and summer months (JJA: June-July-August). Figures 4.15, 4.16, 4.17 and 4.18 show the diurnal cycles at four of the modelled sites.

GPP is better reproduced in the morning and evening than in the middle of the day, corresponding to low levels of radiation, and hence photosynthesis being light limited. The relation between models' skill in reproducing GPP and the limiting factor for photosynthesis will be discussed in Section 4.4.4. The diurnal amplitude of GPP in JJA is lower than observed at all sites, in accordance to the underestimation seen at the seasonal time scale. In winter, however, the diurnal amplitude modelled by JULES is higher than observed at some temperate sites, for instance Braaschat (Figure 4.15).

JULES presents a midday depression of CO_2 uptake during the summer months for many of the studied sites (the two Mediterranean sites, ES-ES1, IT-Ro1; the two continental, FI-Hyy, CZ-BK1 and one of the temperate sites, NL-Loo). The dip in GPP can be appreciated for IT-Ro1 and NL-Loo in Figures 4.17 and 4.16. It is caused by midday stomatal closure driven by the low air humidity. However, in the majority of sites it is not seen in the the eddy covariance data nor is it reproduced by the other model. The only exception is IT-Ro1, where CTESSEL also develops a depression for both fluxes and the observations show a slight reduction (Figure 4.17). Overall, however, the behaviour is associated with the JULES model. Section 3.5.2 showed that JULES had higher sensitivity than CTESSEL to relative humidity (Figure 3.24). However the strong reduction in g_s was not translated into a strong reduction in A_n (Figure 3.25). In the full model simulations, the midday depression occurs more often in GPP than in LE. In fact, the midday stomatal closure only affects the latent heat flux in the case of the Mediterranean sites, as can be seen for IT-Ro1 in Figure 4.17, whereas at the other sites latent heat does nor reflect the stomatal closure (as seen in NL-Loo, Figure 4.16). This seems to show that g_s is not determining the evaporative flux, due to the canopy being decoupled from the atmosphere or transpiration not being the main component of the total evaporation.

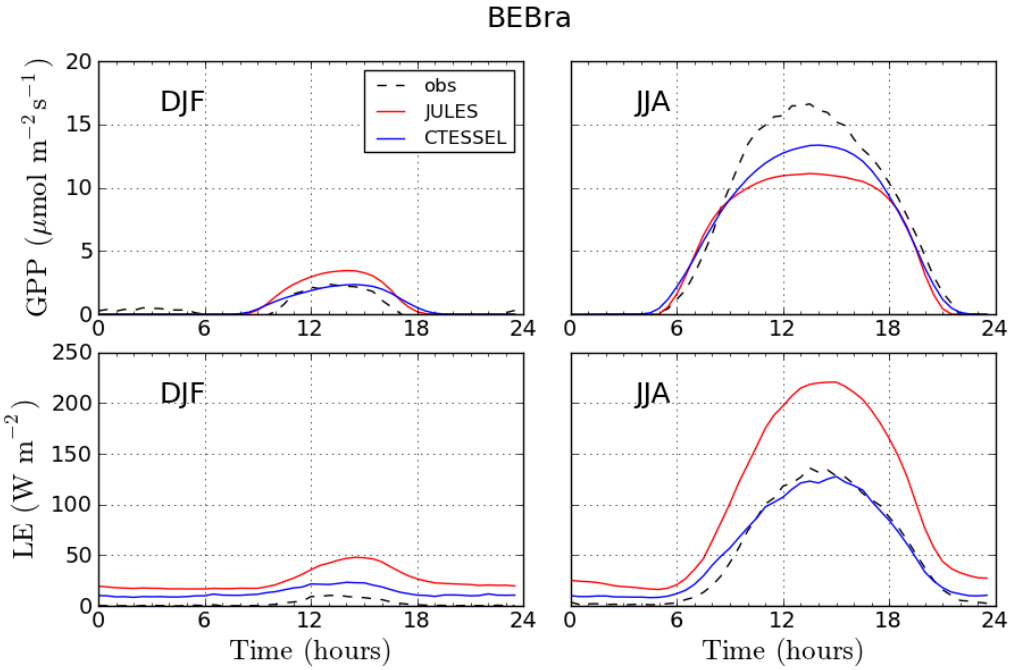

Figure 4.15: Mean diurnal GPP and *LE* for December-January-February (DJF) and June-July-August (JJA)

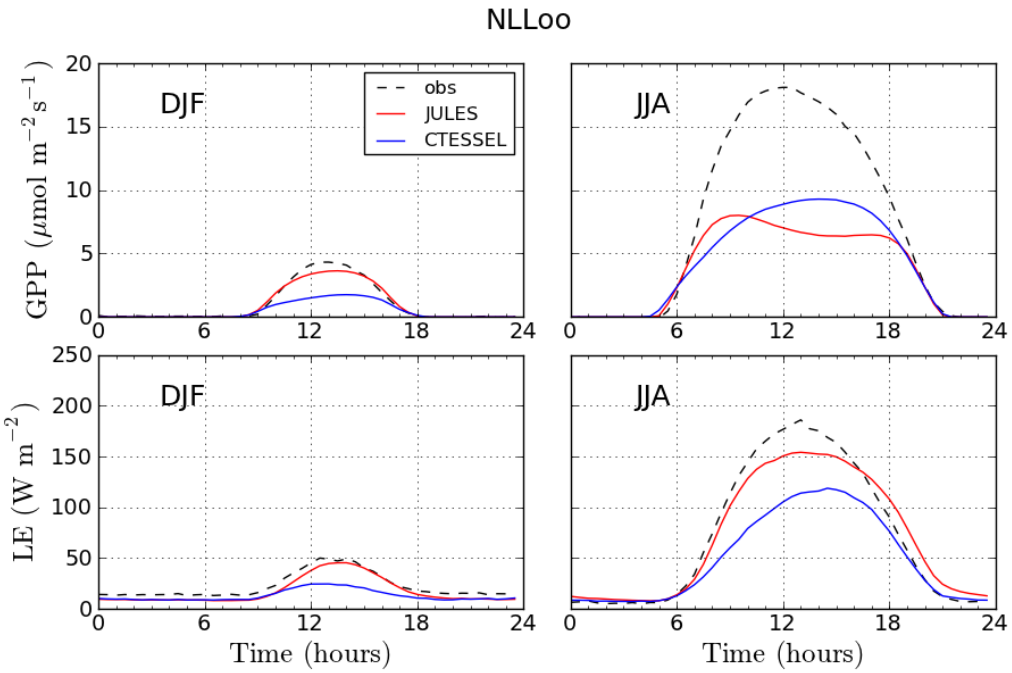

Figure 4.16: Mean diurnal GPP and *LE* for December-January-February (DJF) and June-July-August (JJA)

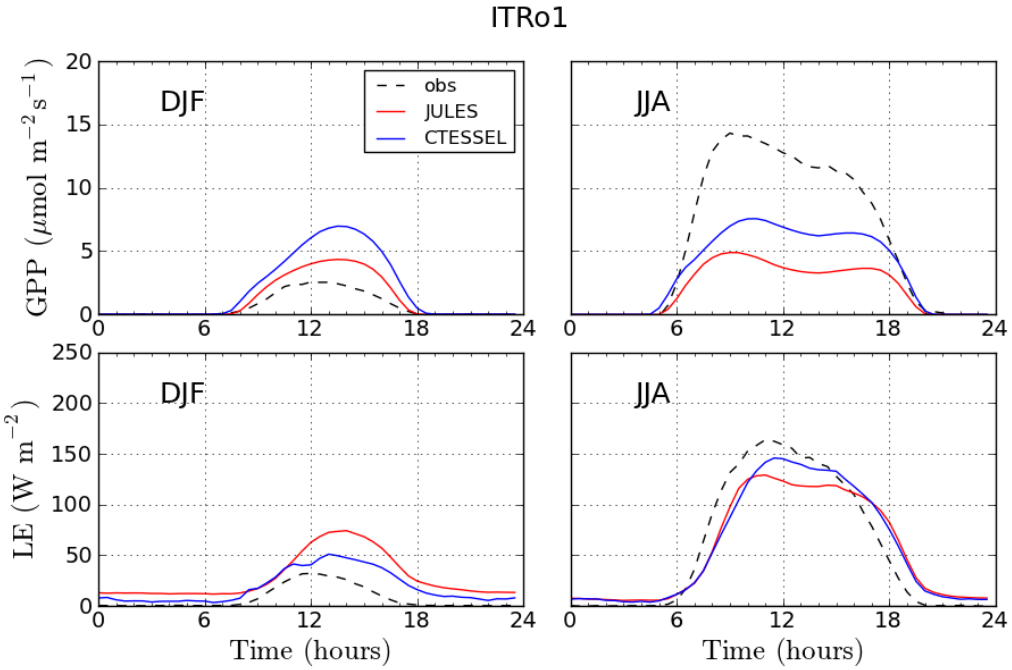

Figure 4.17: Mean diurnal GPP and *LE* for December-January-February (DJF) and June-July-August (JJA)

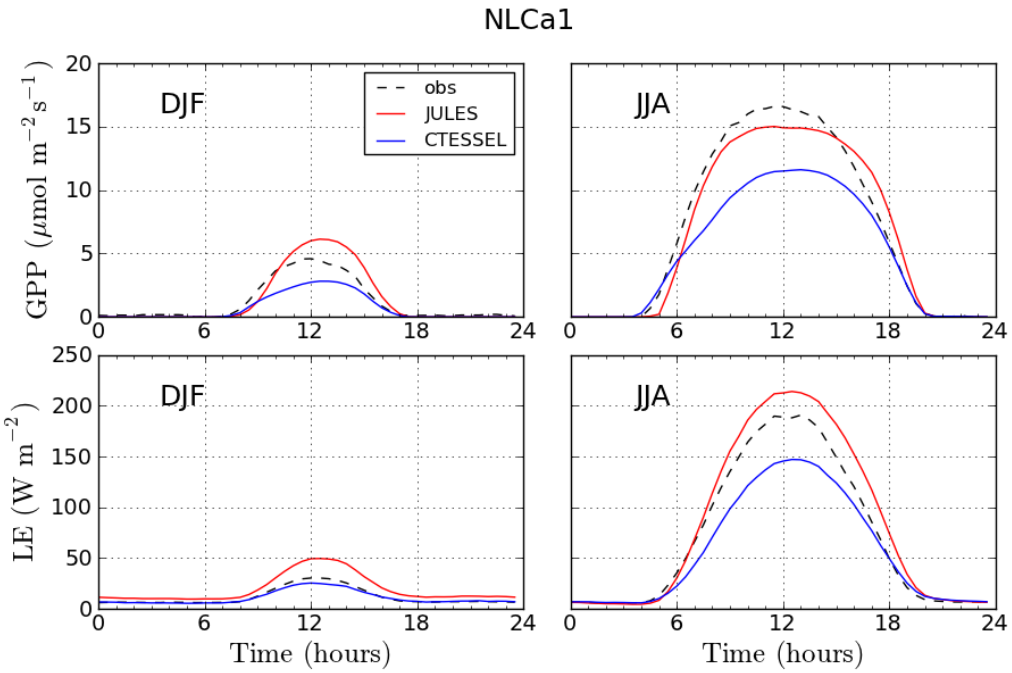

Figure 4.18: Mean diurnal GPP and *LE* for December-January-February (DJF) and June-July-August (JJA)

4.4.3 Interannual variability

In this section the interannual variability in the observed GPP is analysed for each site. Furthermore, the interannual variability in the studied models is also analysed, in order to determine the ability of the models to reproduce the interannual variations in GPP. Two metrics are used: the annual coefficient of variation (ACV) for year to year variations in the annual mean and monthly scaled anomalies to address the interannual variability for each particular month. These statistics were calculated for all sites that had more than two years worth of data.

4.4.3.1 Annual coefficient of variation

The annual coefficient of variation (ACV) is computed as the ratio of the standard deviation of the mean annual GPP of all available years to the long-term mean annual.

$$ACV = \frac{stdev(GPP(yr))}{\overline{GPP(yr)}} \tag{4.4}$$

where GPP(yr) is the mean GPP flux for year yr. The higher ACV, the more variation is found in the annual mean form year to year. The values of ACV calculated for the eddy covariance data, JULES simulated GPP and CTESSEL simulated GPP are presented in Figure 4.19. For the forest sites located in temperate climates (FR-Hes, Be-Vie, BE-Bra, NL-Loo, DE-Tha) the models tend to produce less year to year variability than observed (except CTESSEL at NL-Loo). On the other hand, at the Mediterranean sites both models exaggerate the variability, with JULES showing the highest ACV. At IT-Ro1 JULES's ACV is particularly high, due to the excessive soil moisture stress at some years.

It is interesting that the largest coefficient of variation is found for the grass site NL-Ca1, possibly due to the effect of dry years on short grass. Both models reproduce well the variability, coinciding in high ACV at this site.

4.4.3.2 Monthly scaled anomalies

As an additional measure of interannual variability, the monthly scaled anomaly is calculated for the measurements and both models. Each month of each year is attributed an

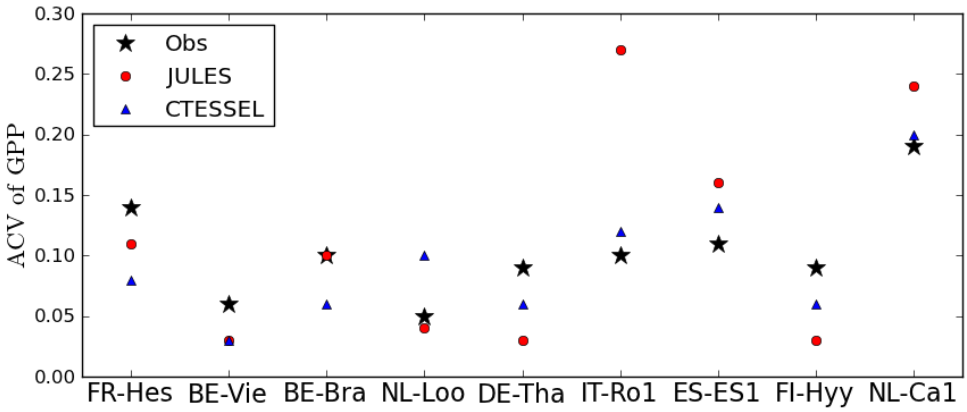

Figure 4.19: Annual coefficient of variation (ACV) of GPP. High coefficients indicate high interannual variation.

anomaly value, based on the average GPP for that month over all available years. The monthly anomalies are calculated as:

$$Ano_{GPP}(m, yr) = \frac{GPP(m, yr) - \overline{GPP(m, :)}}{stdev(GPP(m, yr) - \overline{GPP(m, :)})} \tag{4.5}$$

where m represents each month and yr each year. This metric informs how a monthly mean of a particular year stands compared to the average value of that month across all years scaled by the standard deviation. The values are shown by the mesh plots in Figure 4.20. Each box represents one month: green colours indicate positive anomaly (GPP above the average of the considered years) and brown colours indicate negative anomaly (GPP below the average of the considered years). Note that the number of years varies for each site. The comparison is fair between models and observations for a specific site but not across sites.

The effects of the 2003 heatwave can be attributed to the lower GPP at some sites: FR-Hes, DE-Tha and NL-Loo. In FR-Hes, the lowest GPP is found during the summer of 2004. Models reproduce this reduction; however, in JULES the negative anomaly is propagated into 2007, due to a water depletion in lower layer in the subsoil. In DE-Tha 2003 heatwave effects can also be identified both in the eddy covariance data and the observations. In BE-Bra, both models do not show the high GPP anomaly seen in observations in the two first years. Later, JULES shows negative GPP anomaly in 2006 and 2007, years which the model wrongly had soil moisture stress affecting GPP (Figure 4.2b). In ES-ES1 and

NL-Ca1 there is a progressive greening towards the last years of each data set and seems to be reproduced by the models.

To assess the interannual variability of the whole timeseries, the monthly anomalies were put end to end and a Pearson correlation coefficient was calculated for the whole timeseries, between models and observations. The significant correlations (p values < 0.05) are shown in Table 4.8. Also the correlation coefficient between the two models was computed. None of the models show a clear advantage over the other one in terms of reproducing the observed GPP monthly variability. CTESSEL has slightly higher coefficients for the forest the sites (except ES-ES1), and JULES shows better correlation for the grass site. In fact for the sites where the best correlations were found, both models showed similar skill (DE-Tha and NL-Loo).

The correlations between both models are higher than those of the models with the observations (except for IT-Ro1, where CTESSEL correlates better with the observations). This indicates that both models represent the interannual variation in a similar fashion which does not always agree with the eddy covariance data. The higher correlations were found for the sites located in temperate climate, except Brasschaat where no significant correlation was found for any model. At these sites, the correlation coefficients between each model and the observations were very similar to each other. Lower correlations were found for the Mediterranean sites and the boreal site.

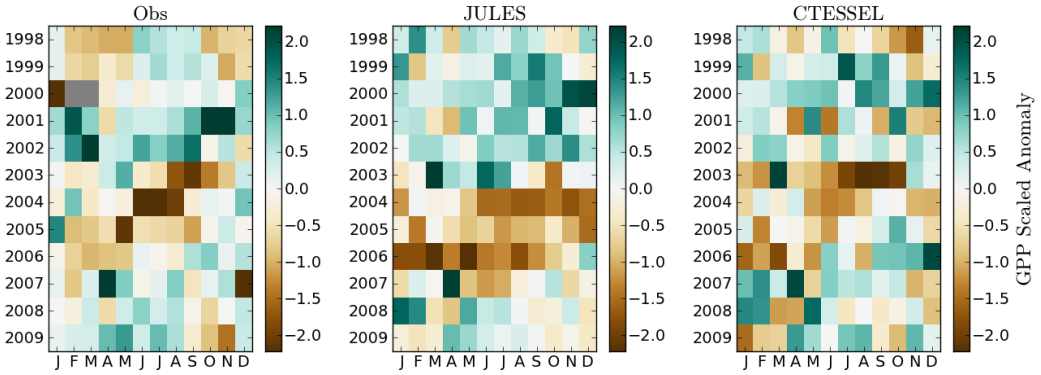

(a) FR-Hes

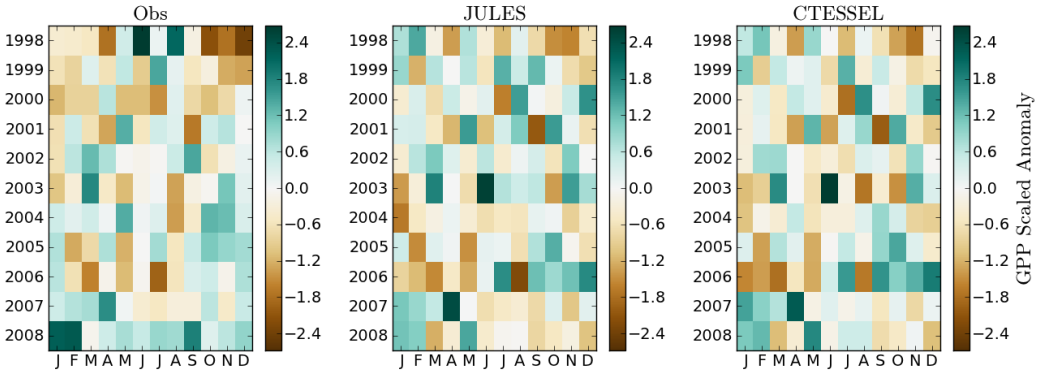

(b) BE-Vie

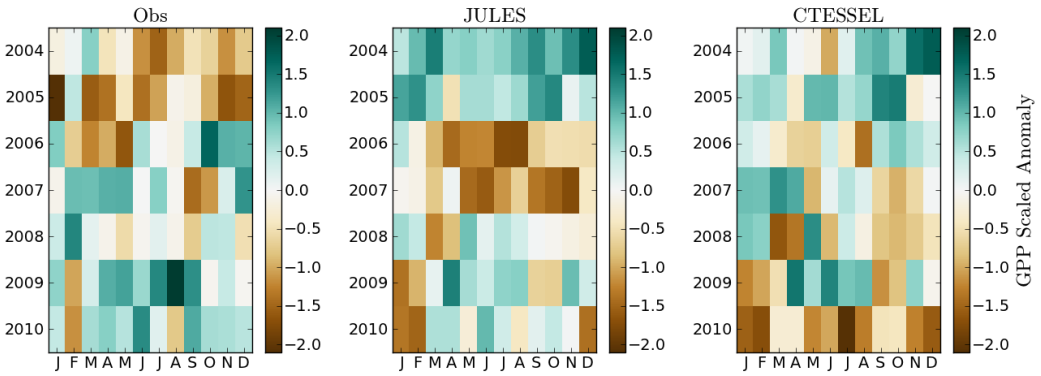

(c) BE-Bra

Figure 4.20: Scaled GPP monthly anomalies. Units are dimensionless and correspond to standard deviations.

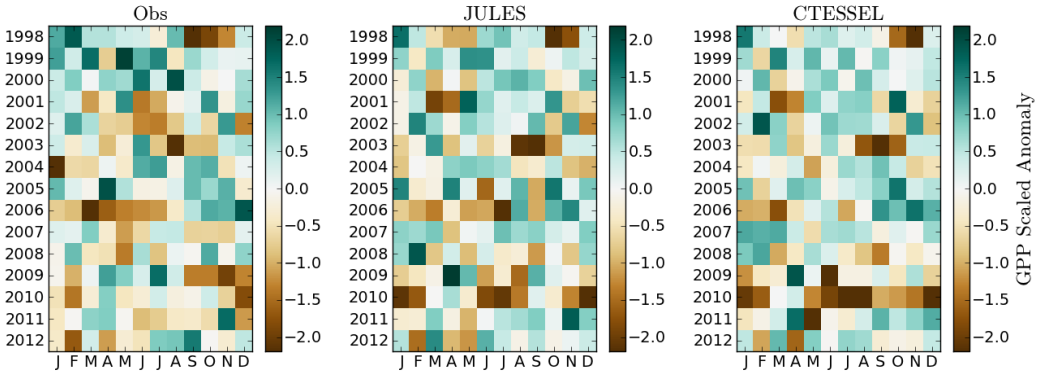

(d) NL-Loo

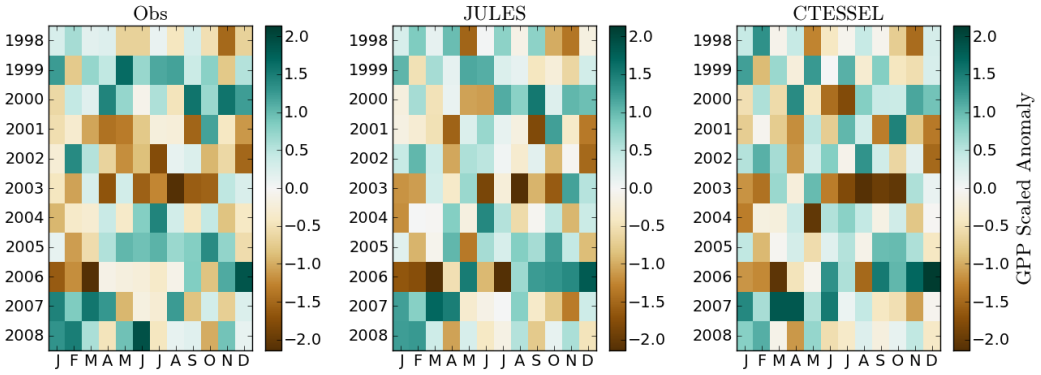

(e) DE-Tha

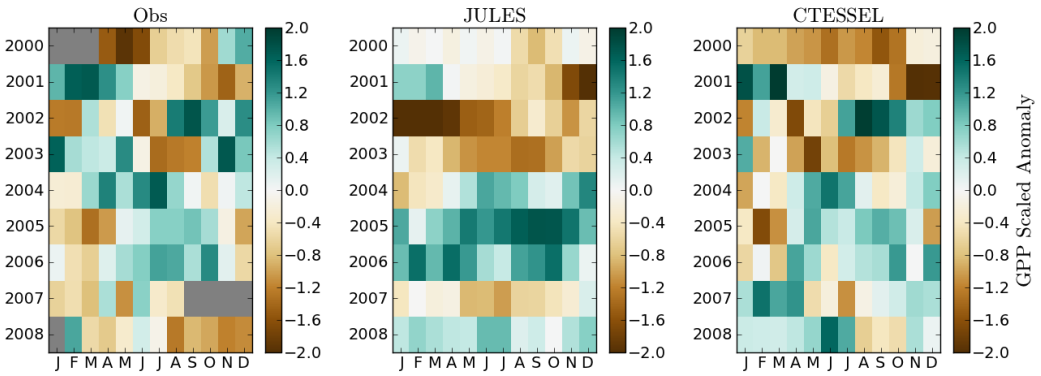

(f) IT-Ro1

Figure 4.20: (Cont.) Scaled GPP monthly anomalies. Units are dimensionless and correspond to standard deviations.

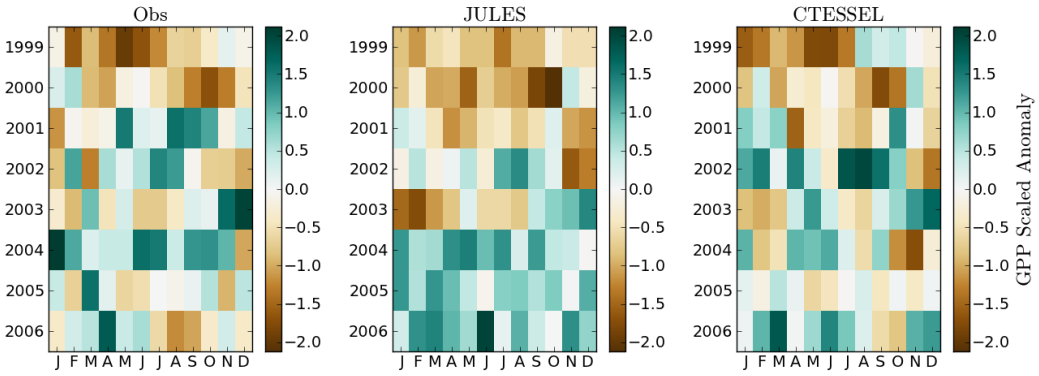

(g) ES-ES1

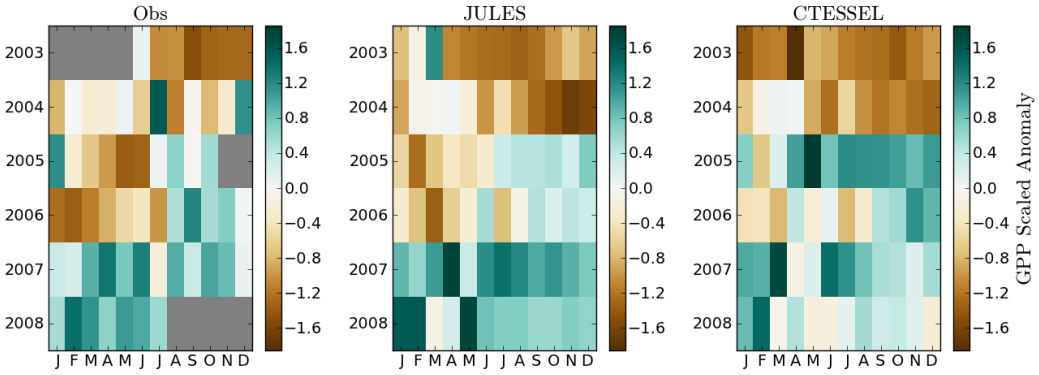

(h) NL-Ca1

Figure 4.20: (Cont.) Scaled GPP monthly anomalies. Units are dimensionless and correspond to standard deviations.

Table 4.8: Pearson correlation coefficient of the GPP scaled monthly anomaly correlations. Only coefficients for significant correlations are shown

Site	Obs-JULES	Obs-CTESSEL	JULES-CTESSEL
FR-Hes	0.39	0.41	0.58
BE-Vie	0.45	0.46	0.92
BE-Bra	-	-	0.61
NL-Loo	0.50	0.50	0.73
DE-Tha	0.69	0.68	0.71
IT-Ro1	0.29	0.56	0.49
ES-ES1	0.53	0.44	0.67
FI-Hyy	0.39	0.47	0.61
NL-Ca1	0.59	0.37	0.68

4.4.4 Photosynthesis limiting regimes in JULES

In this section carbon assimilation by the canopy is analysed in the context of the limiting regimes. For each model timestep the computation of the leaf level photosynthesis rate as the co-limited rate from the three limiting regimes is performed for each of the 10 vertical canopy layers. Then the values are averaged and upscaled to canopy level using the LAI (See Section 2.4.7). Therefore the limitation on photosynthesis is not unique but varies within the canopy (e.g. the upper layers in a dense forest canopy maybe be carbon limited while the lower layers are light limited if the penetrating radiation is sufficiently attenuated). To be able to associate one limiting regime for each timestep, the dominant limitation on photosynthesis throughout the whole canopy was determined as the regime that limited the maximum number of layers at each given timestep. The separation into limiting regimes was only performed for timesteps with net leaf level photosynthesis above zero, corresponding to daytime.

In Figure 4.21, the carbon uptake at the canopy level represented by GPP is related to the limitation on photosynthesis at the leaf level. GPP has been used because it is the model output variable linked more closely with photosynthesis. From the point of view of observations, the assumptions made in the partitioning process add some uncertainty to

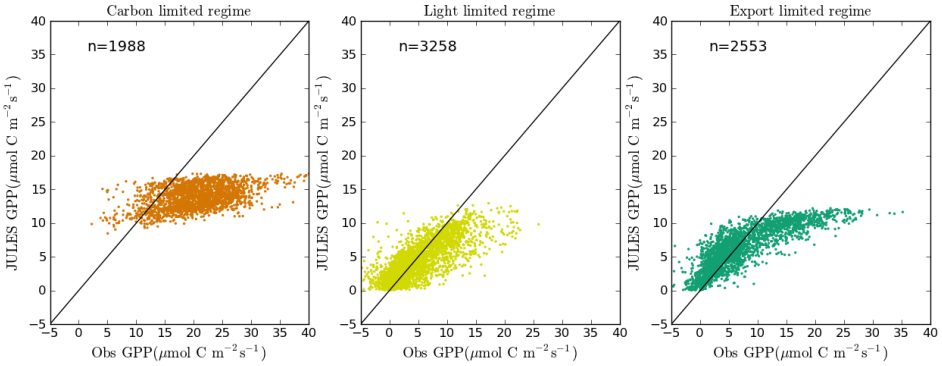

(a) BE-Vie, year 1998

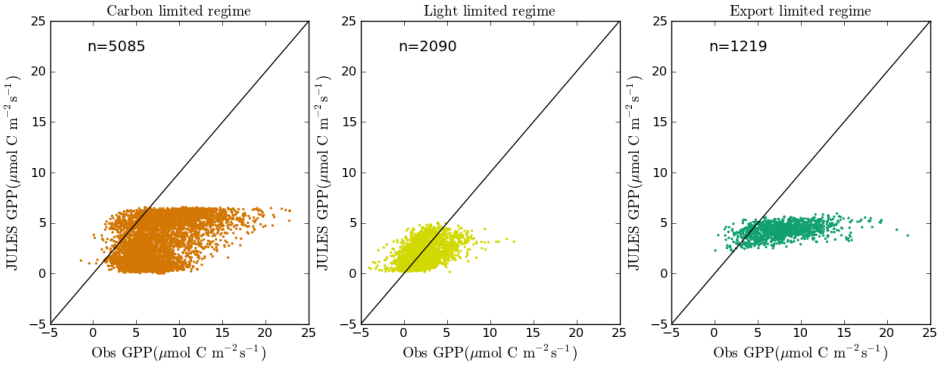

(b) ES-ES1, year 1999

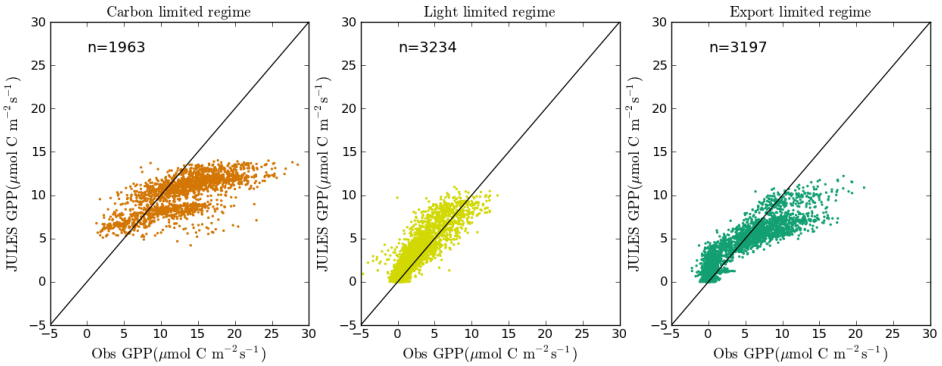

(c) FI-Hyy, year 1998

Figure 4.21: Correlation between JULES and observed GPP for one simulated year during daytime. GPP values have been binned according to the dominating limiting regime across the 10 canopy layers. (a) BE-Vie, broadleaf forest in a temperate climate, (b) ES-ES1 needle leaf forest in a Mediterranean climate and (c) FI-Hyy needle leaf forest in a boreal climate.

observed GPP. In Figure 4.21 GPP modelled by JULES is correlated with measured GPP. For each site, GPP values have been binned into three groups, according to the regime that was limiting photosynthesis (or was the dominant limitation). Carbon limited points are shown in orange in the left plot, light limited points are shown in yellow in the middle plot and export limited points are shown in green in the right plot. Each point corresponds to one timestep (Δt = 30 min) during one year of simulation. Only three representative sites are shown: (a) BE-Vie, broadleaf forest in a temperate climate, (b) ES-ES1, needle leaf forest in a Mediterranean climate (c) FI-Hyy, needle leaf forest in a boreal climate.

The best match between modelled and observed GPP occurs for light limited photosynthesis. From these correlations it emanates that the negative biases in GPP (Table 4.7) are mostly related to situations when carbon (rubisco activity) or export (triose phosphate consumption) are limiting the photosynthesis process in the leaves. JULES' limitations on photosynthesis from carbon and export are too strict and constrain photosynthesis to values that are lower than observed. On the top left hand corner of each figure, the number of points that are limited by that particular regime is indicated: the total number varies from site to site and is about half of timesteps in a year, because only cases with positive net leaf photosynthesis are considered, corresponding to daytime. From this distribution it can be derived how often each limiting regime occurs at each site. El Saler in Spain is mainly carbon limited, while at Vielsalm light is the principal limitation. At the boreal site, both light and export play an important role.

The relative occurrence of each limiting regime during the one year period for these and all the other sites is shown in Table 4.9. The distribution over a year of carbon, light and export regime is well balanced (each regime limits for at least 12% of the time and no more than 63% of the time at each site). As can be seen from these distributions, the apparent irrelevance of the export limiting regime found in the leaf level validation with grapevine data in Section 3.3.3.1 was in fact due to the time of the year being July. The fraction of export limitation is larger at the sites located in cold climates, boreal Hyytiälä and mountainous Bily Kriz-Beskidy forest. At Hyytiälä photosynthesis is limited roughly equally by export and light. At Tharandt, the export limitation also has a significant presence. Carbon is the dominant factor at the Mediterranean sites (IT-Ro1 and ES-ES1), followed by light and slightly by export during the colder months, especially at the beginning of the growing season. Note that these percentages represent the fraction

of time spent in each regime, not the fraction of carbon assimilated under each regime. Typically the highest rates of CO_2 are assimilated when photosynthesis is carbon limited. In the next section the temporal distribution of the limiting regimes at the seasonal and daily scales is shown as well as the relative importance of each regime based on the amount of carbon assimilated by vegetation.

Table 4.9: Relative occurrence of the limiting regimes during a year, calculated at 30 minutes temporal resolution and aggregating canopy layers. The percentages indicate the fraction of time spent on each regime and are calculated for daytime only, determined as the timesteps with positive net leaf photosynthesis.

Site	**Carbon limitation**	**Light limitation**	**Export limitation**
FR-Hes (1998)	25 %	63 %	12 %
BE-Vie (1998)	25 %	42 %	33 %
BE-Bra (2004)	38 %	36 %	26 %
NL-Loo (1998)	32 %	37 %	31 %
DE-Tha (1998)	33 %	31 %	36 %
IT-Ro1 (2000)	50 %	30 %	20 %
ES-ES1 (1999)	61 %	24 %	15 %
CZ-BK1 (2004)	29 %	35 %	36 %
FI-Hyy (1998)	23 %	39 %	38 %
NL-Ca1 (2005)	35 %	42 %	23 %

4.4.4.1 Temporal analysis of the limiting regimes

The competition between limiting regimes is highly dependent on the temperature and the level of radiation; consequently, the limiting factor for photosynthesis varies throughout the year and throughout the day. The fraction corresponding to each limiting regime has been derived by determining the dominant factor at each timestep across the 10 canopy layers for the cases with positive net photosynthesis (daytime). Then each fraction is scaled by the accumulated net photosynthesis, so instead of representing time spent in each regime (as in Table 4.9), they represent the amount of carbon that was assimilated

under each limiting regime accounting for all canopy layers. Figure 4.22 shows the monthly means of daytime leaf net photosynthesis. Each bar is divided into the fractions to show the contribution to assimilated carbon from photosynthesis limited by each regime. Four representative sites are shown, FR-Hes, IT-Ro1, FI-Hyy, NL-Ca1.

A common pattern emerges across all sites. During winter, photosynthesis is only limited by light or export, which is in line with the analysis performed in Section 3.4.4, where export limitation was associated to low temperatures. Then, between February and March, associated with the beginning of the growing season, photosynthesis begins to be carbon limited. The carbon limitation becomes progressively more dominant towards the summer months, and the export limitation declines. In the case of the Mediterranean sites, export limitation is negligible in the middle of summer. The light limitation on photosynthesis occurs during the whole year, but its importance varies across sites, with FR-Hes (Figure 4.22a) presenting larger fractions of light limited photosynthesis especially towards late summer early autumn.

In Figure 4.23 the same partition into limiting regimes is shown for the same sites but this time at the daily timescale and aggregated by seasons. Positive values of leaf net photosynthesis rate were averaged in three hours blocks. The export limitation occurs mainly in the mornings during growing period (MAM and JJA). It is associated with colder temperatures found in the mornings, due to the soil's thermal inertia after the cool nights. In the hours around midday carbon becomes the most important limitation during the growing period. For the continental sites (FI-Hyy (Figure 4.22c), CZ-BK1 (not shown)) in spring (MAM), the export limitation predominates over carbon during the rest of the day as well. This is also the case in NL-Loo (not shown). Photosynthesis is limited by light when the radiation levels are low, hence the hours close to dawn and sunset. The attenuation of radiation at high zenith angles as well as the increased attenuation within the canopy reduces the incident radiation reaching the leaves. The larger influence of radiation seen for FR-Hes (Figure 4.22a) can now be associated to the afternoons 15:00-18:00 (Figure 4.23a).

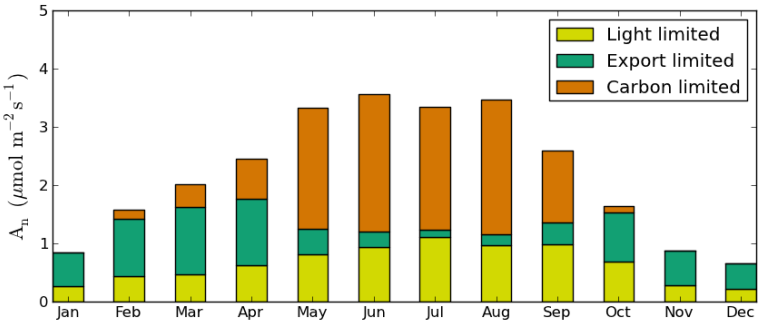

(a) FR-Hes, year 1998

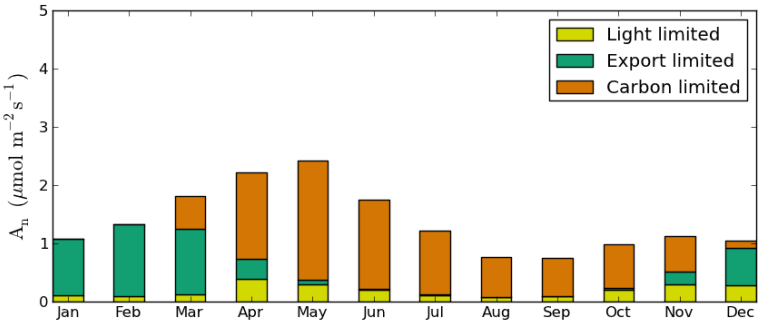

(b) IT-Ro1, year 2000

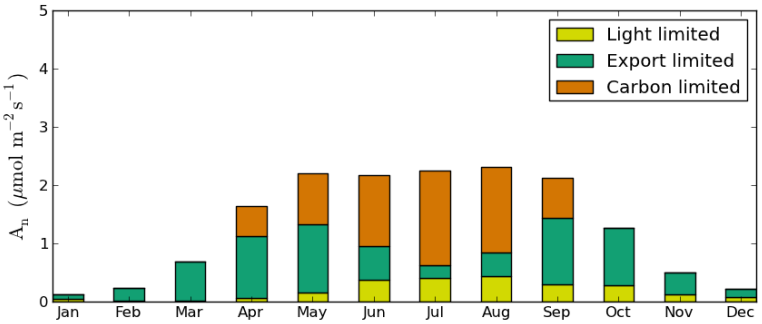

(c) FI-Hyy, year 1998

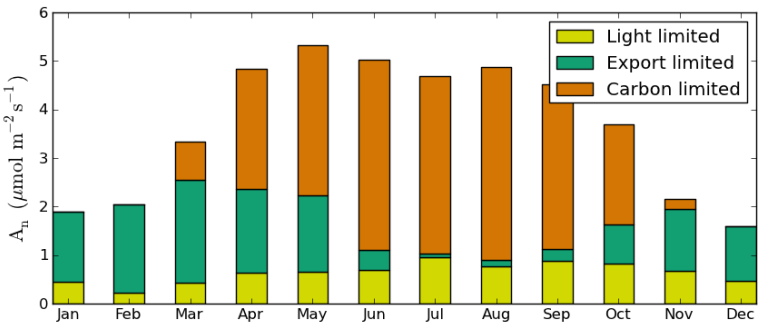

(d) NL-Ca1, year 2005

Figure 4.22: Monthly averaged net leaf level photosynthesis divided according to the limiting regimes

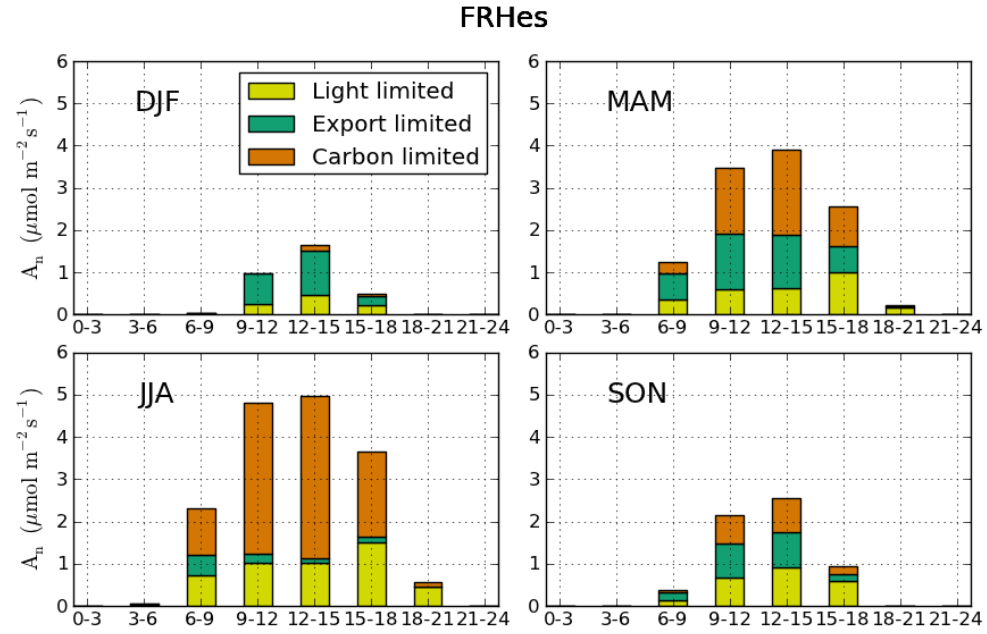

(a)

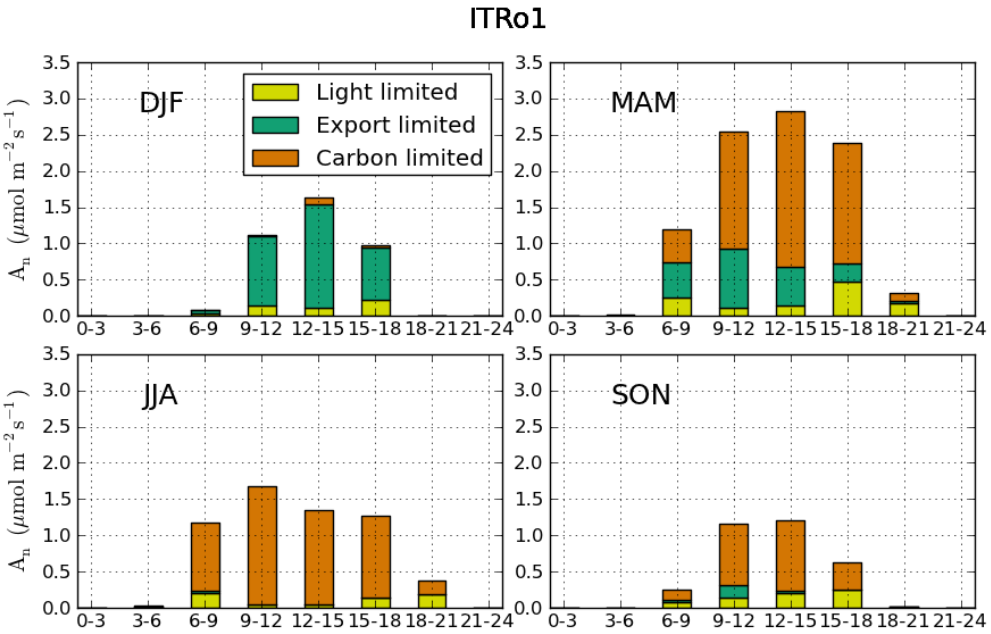

(b)

Figure 4.23: Mean diurnal rate of leaf net photosynthesis averaged in 3 hour blocks for each season: December-January-February (DJF), March-April-May (MAM), June-July-August (JJA) and September- October-November (SON). Times are local. The colours indicate the fraction of assimilated carbon under each limiting regime.

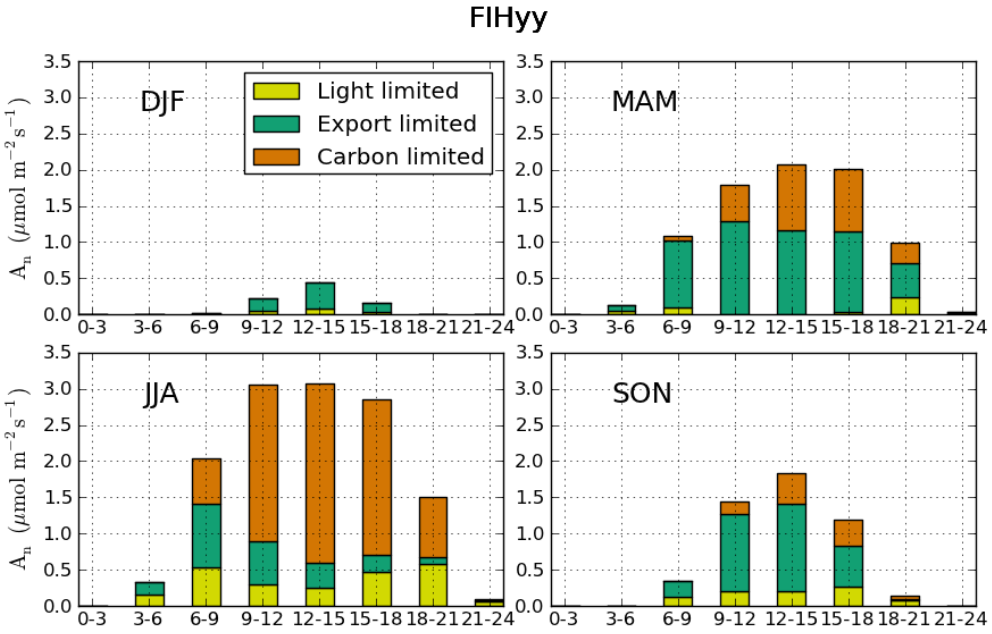

(c)

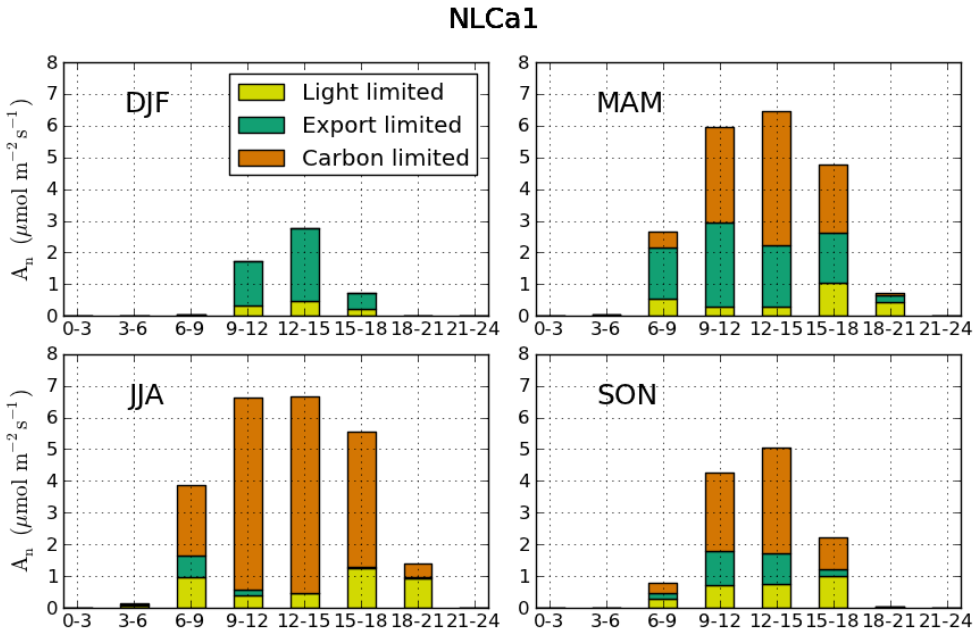

(d)

Figure 4.23: (Cont.) Mean diurnal rate of leaf net photosynthesis averaged in 3 hour blocks for each season: December-January-February (DJF), March-April-May (MAM), June-July-August (JJA) and September- October-November (SON). Times are local. The colours indicate the fraction of assimilated carbon under each limiting regime.

4.5 Conclusions and discussion

In this chapter both models were tested for 10 European sites from the FLUXNET network. The model settings were specified to be as similar as possible to provide a fair model comparison on how models reproduce the energy and carbon fluxes. A monthly climatology of LAI was prescribed, hence all differences in seasonal cycle can attributed to the models' response to external variables. The emphasis was put on carbon assimilation but also in how GPP and LE are linked. Using JULES simulations, the extent to which each limiting regime controls photosynthesis at each site has been exposed, as well as the temporal evolution. The conditions under which each regime is favoured were already analysed under a theoretical framework in Chapter 3, however the FLUXNET sites widen the research, providing realistic scenarios, with specific climates and plant types.

Despite differences in photosynthesis formulation, both models predictions of GPP were shown to be similar. The carbon assimilation produced by both models was lower than the one derived from measurements. However eddy covariance towers measure NEE directly, and GPP has to be derived, opening possibilities to some error in its estimates. The main differences in GPP between models were caused by the soil moisture stress. JULES' restriction on GPP due to the unavailability of moisture was at times too strong. Moreover, the equilibrium soil moisture content in JULES was lower than in CTESSEL.

Although GPP estimates from both models were similar, this was not the case for LE estimates. JULES consistently predicted larger LE than CTESSEL. This could in part be explained by larger g_s shown by JULES at the leaf level but also due to the differences the aerodynamic conductances of both models that control the turbulent exchange in the models. The ratio between both conductances determines the degree of coupling between canopy and atmosphere, which has already been identified as a source of model discrepancy (De Kauwe et al., 2013). Furthermore, the excessive evaporation contributes to the stronger drying of soils seen in JULES, exacerbating the soil water stress on GPP.

The GPP diurnal cycle was well reproduced by both models (despite the underestimation in the amplitude). Radiation is an important driver of GPP at the diurnal time scale. It is of vital importance that the radiative scheme provides the photosynthesis scheme an appropriate profile of solar radiation within the canopy. CTESSEL's big leaf approach

combined with Beer's law has proved to perform just as well as JULES' multilayer scheme by which the canopy is divided into 10 layers combined with the 2-stream radiative scheme. The key in the success of CTESSEL's simpler parameterization is that the attenuation coefficient used in Beer's attenuation law varies with the angle of incidence of the solar radiation. Radiation is attenuated more efficiently (by scattering and absorption within the canopy) when the solar beams enter the canopy with a high inclination.

JULES GPP during summer months suffered from midday stomatal closure, which was not justified by the observations. This feature can be related to an exaggerated stomatal sensitivity to water vapour pressure deficit, but there must be another canopy level mechanism exacerbating it. At the leaf level, although g_s was found to be more sensitive in JULES than in CTESSEL, this was not translated into high sensitivity in net photosynthesis, therefore cannot completely explain the observed midday stomatal closure.

In terms of interannual variability, both models showed less variability than the observations at most sites. The exception was found at the Mediterranean sites, where the excessive variability was attributed to soil moisture changes from year to year. The correlation of monthly anomalies between each model and the observations was quite similar for each site, particularly at the temperate sites.

The distribution of the photosynthesis limitations in JULES was well balanced in terms of time spent in each of the three regimes. Export and light limitations occur during the whole year. Export is most important during spring. Carbon limitation starts in spring and lasts until autumn. It becomes the main limitation during the growing season, reducing the limitation from the other regimes. Some similarities could be extracted for the sites belonging to the same climate. Continental sites had more export limitation, associated to the colder temperatures. Mediterranean sites on the other hand were mostly limited by carbon, with export limitation being negligible during the peak of summer. Because carbon limitation controls photosynthesis when the assimilation rate is greater, the carbon dioxide assimilated under carbon limitation is the largest at most sites.

Chapter 3 showed how the dominant limiting regime controlling the photosynthesis reaction affects the degree of leaf level CO_2 fertilisation. Therefore, the fact that sites located in different climates have more or less limitation through a certain regime, will have an

impact in JULES estimates of CO_2 fertilisation effect. At the same time, the varying environmental conditions may modify the distribution of limiting regimes found for the present conditions. The next chapter explores the effects of increased levels of CO_2 and temperature on GPP fluxes for both JULES and CTESSEL, as well as the derived changes in limiting regimes in JULES.

Chapter 5

Effect of climate change at FLUXNET sites

5.1 Introduction

In this chapter both models are tested for an idealised climate change scenario. The results are interpreted in the light of the findings of Chapter 3; providing insight into the origin of some model discrepancies in climate modelling studies. The effect of climate change in the limiting regimes is also analysed.

Anthropogenic greenhouse gas emissions have increased since the pre-industrial era, leading to increases in the atmospheric carbon dioxide, methane (CH_4) and nitrous oxide (N_2O) concentrations (Figure 5.1). About half of the emitted CO_2 is removed from the atmosphere by the ocean sink and the vegetation biomass in roughly equal parts, while the rest remains in the atmosphere (Le Quéré et al., 2013). Although both the ocean and land CO_2 sinks have taken up more CO_2 since the 1960s (Le Quéré et al., 2013), the airborne CO_2 that remains in the atmosphere is still increasing. In fact, the atmospheric CO_2 concentration increased at an average rate of 2.0 ppm yr^{-1} during the period 2002-2011 IPCC 2013 (Stocker et al., 2013).

The effects of the greenhouse gases, together with those of other anthropogenic drivers are 'extremely likely' to be the dominant cause of the observed warming since the mid-

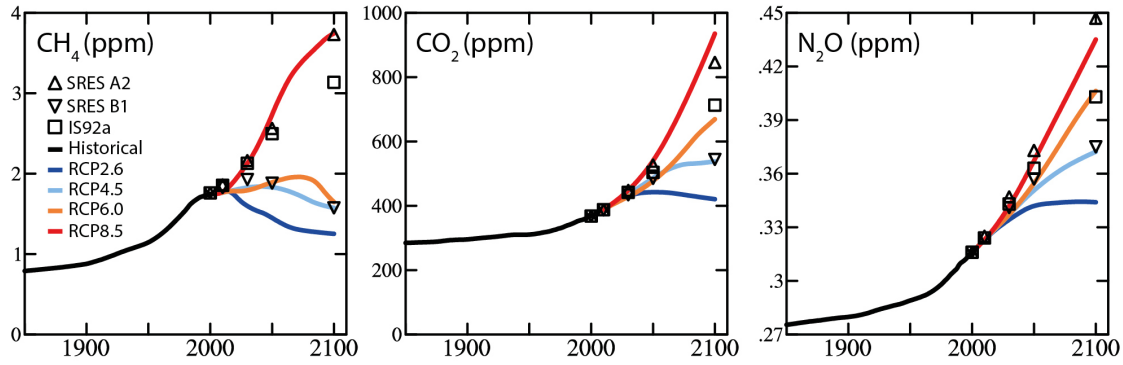

Figure 5.1: Global averaged concentrations for methane (CH_4), carbon dioxide (CO_2) and nitrous oxide N_2O for each RCP (Representative Concentration Pathway) in AR5, SRES (Special Report on Emissions Scenarios) from AR4 are also indicated for reference. Figure from (Stocker et al., 2013) based on (Meinshausen et al., 2011).

20th century IPCC 2013 (Stocker et al., 2013). The effects of climate change on terrestrial ecosystem carbon sink still remain poorly understood. Global climate models (GCMs) predict an increase in the biomass sink when changing CO_2 alone but the effect is weakend when the climate change effect on the carbon cycle is included, and there is considerable disagreement in the magnitude of this effect (Friedlingstein et al., 2006). The main uncertainty is related to the the response of modelled NPP to climate change (Cramer et al., 2001), whose main term is GPP. In this Chapter, the effect that a doubling of atmospheric CO_2 (800 ppm) has on GPP, as represented by LSM JULES and CTESSEL, is assessed, as well as the joint impact of an associated rise in air temperature. This CO_2 concentration corresponds approximately with the projected concentration for the end of the century according to the most pessimistic pathway (RCP8.5 in Figure 5.1). The LSMs are run in offline mode and therefore vegetation-atmosphere feedbacks are not reproduced, as there is no interaction with the atmosphere. Thus, the aim of this analysis is to contrast the responses of both photosynthesis parameterization in LSMs rather than make predictions about plant behaviour as a response to climate change.

The analysis of the photosynthesis schemes at the leaf level in Chapter 3 already highlighted a stronger CO_2 fertilisation effect in CTESSEL due to the lack of export limiting regime. Now, the impact of the photosynthesis scheme within the full LSM is analysed by running the same simulations conducted in Chapter 4 at FLUXNET sites but with altered ambient conditions. In the case of JULES, the effect that climate change (through CO_2

increase and temperature increase) has on the relative importance of each limiting regime is analysed.

5.2 Increase in atmospheric CO_2 and air temperature

An increase in the number of CO_2 molecules in the atmosphere enhances the absorption of outgoing longwave radiation from the surface and its re-emission toward the Earth, which alters the net radiative balance, inducing a positive radiative forcing and resulting in more energy stored in the system. Radiative forcing is defined as the change in net downward radiative flux, hence a positive forcing causes global warming. The atmospheric concentration of CO_2 was the largest contributor to the positive anomaly in radiative forcing on the climate system for the period 1750-2011 (Stocker et al., 2013). The projected increase in global surface temperature by CMIP5 models until the end of the century for the different representative concentration pathways (RCPs) is shown in Figure 5.2. Given the direct implications that an increase in accumulated CO_2 have on global temperature, the effect of increased temperature was also considered in the experiments, especially since temperature was found to be a key factor for the photosynthesis reaction, shown by the global sensitivity analysis of the photosynthesis models (Section 3.6). An adequate temperature increase, coherent with a doubling of atmospheric CO_2, was selected as 4°C, which corresponds to the projected temperature increment for RCP8.5 by 2100 (Figure 5.2). The temperature field was increased evenly by adding ΔT=4°C to the air temperature variable, at all times, for all sites.

All other driving variables are left unchanged and the observed values are used. One special case is the air humidity because of its connection to temperature. An increase in air temperature with constant atmospheric water vapour content would result in an increase in the water vapour pressure deficit, due to the higher saturated water vapour at higher temperatures. Because the increase is exponential, the effect is larger at higher temperatures. Increased evaporative demand can have a detrimental effect on photosynthesis, via stomatal closure, as well as a distortion of latent heat flux. To avoid these effects and maintain a consistent equilibrium between temperature and humidity, it is assumed that the water vapour pressure deficit is maintained constant while air temperature rises. The

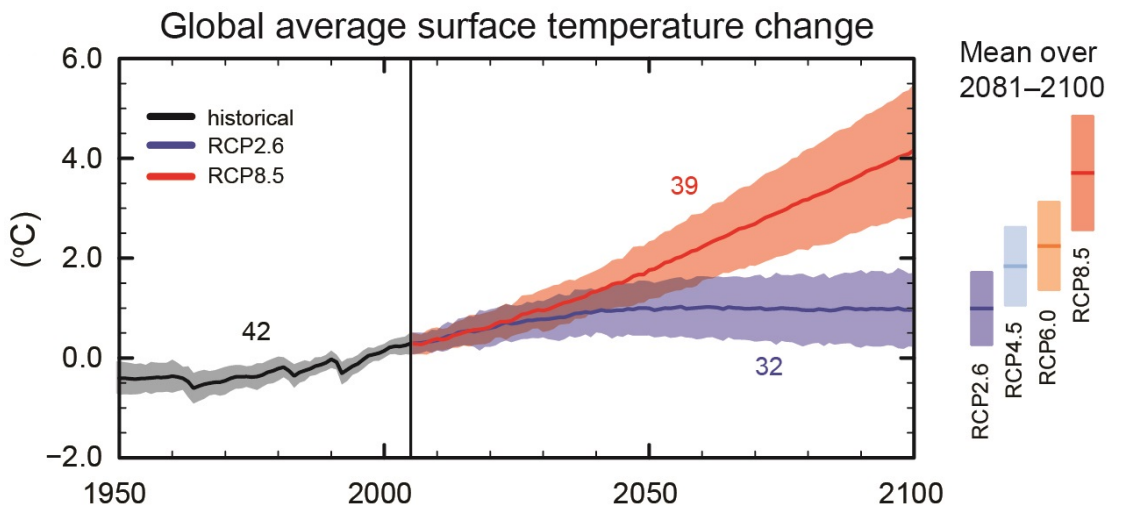

Figure 5.2: CMIP5 multi-model simulated time series of global average surface temperature change from 1950-2100 for scenarios RCP2.6 and RCP8.5. The shading indicates a measure of uncertainty. The black line is the modelled historical evolution using historical reconstructed forcings. The number of CMIP5 models used to calculate the multi-model mean is indicated.

specific humidity is calculated ensuring that the vapour pressure deficit measured at the FLUXNET sites is kept constant. This implies an increase in specific humidity with respect to the values used to drive the models in Chapter 4. Other studies maintain relative humidity constant instead of vapour pressure deficit, both variables are related as shown by Eq. 2.40.

It could be argued that, for consitency with the hydrological cycle, an increase in the specific humidity should be accompanied by an increase in precipitation. In this study, however, the precipitation field has been left unchanged to focus on how each model reproduces the effect of CO_2 and temperature on GPP.

5.3 Model runs

Both models were run offline at the same FLUXNET sites modelled in Chapter 4, for a hypothetical scenario where CO_2 is increased to 800 ppm and temperature and spe-

Table 5.1: Year for the climate change experiments

Site	**Year**
FR-Hes	1998
BE-Vie	1998
BE-Bra	2004
NL-Loo	1998
DE-Tha	1998
IT-Ro1	2000
ES-ES1	1999
CZ-BK1	2004
FI-Hyy	1998
NL-Ca1	2005

cific humidity rise. To be able to characterise separately the effects of enhanced CO_2 and temperature on GPP, two experiments were conducted. In the first one only atmospheric CO_2 is increased, keeping all other driving variables to their 'present climate' values (FLUXNET observations). In the second one a temperature increment $\Delta T = 4°C$ is added to the air temperature variable. The FLUXNET sites were described in Section 4.2.2. Models settings are the same as described in Section 4.3. The simulations were run for a full year at each site. This period is long enough to analyse the effects of CO_2 and temperature at all stages of the vegetation cycle. The LAI plays no role in these experiments as it is prescribed by a monthly climatology for all runs (Appendix D).

5.4 Results

Annual changes for gross primary productivity, ecosystem respiration and net ecosystem exchange are presented. However, because the studied LSMs don not represent a complete carbon cycle, results of R_{eco} and NEE are only illustrative of the most direct effect of CO_2 and temperature and should be taken with caution. The focus is on the induced changes on GPP. The divergences found between models are analysed in the light of the findings of Chapter 3.

5.4.1 Annual changes in carbon fluxes

Changes in the carbon fluxes have been expressed by comparing the results from the climate change runs against the values from 'present climate' simulation of the same year performed in Chapter 4. The annual means of the difference for carbon fluxes at each site are shown in Figure 5.3 for (a) gross primary productivity, (b) ecosystem respiration and (c) net ecosystem exchange. Each colour bar represents the difference between the annual averaged flux from a climate change run, either CO_2 increase alone (800 ppm) or both CO_2 increase and temperature increase (800 ppm $+\Delta T$), and the annual averaged flux from the 'present climate' run. A positive increment in GPP reflects an increase in the assimilated carbon with respect to 'present climate' values. A positive increment in R_{eco} reflects an increase in released CO_2. A negative increment in NEE indicates that more carbon is stored in the ecosystem as a result of the alterations, regardless if the site was a net source or sink of carbon. For all sites and in both models when doubling CO_2 alone there is a fertilisation effect of enhanced GPP (Fig. 5.3a). The modelled fertilisation effects on GPP of increased CO_2 are stronger in CTESSEL than in JULES, coinciding with the findings at the leaf level in Section 3.4. The stronger CO_2 fertilisation effect in CTESSEL was associated to the lack of export limiting regime, which in JULES becomes increasingly the determining factor on the photosynthesis reaction as CO_2 levels rise. The temperature increase combined with CO_2 increase in most cases produces a synergy, enhancing the GPP increase with different degrees of strength. In JULES especially, it can be seen how for broadleaf forests (FR-Hes, BE-Vie, BE-Bra, IT-Ro1) the effect of temperature is more evident, while for needle leaf trees (NL-Loo, DE-Tha, CZ-BK1, FI-Hyy) the increase is subtle, even resulting in a reduction of the CO_2 fertilisation effect for ES-ES1. These differences are caused by differences in the optimum temperature for photosynthesis between these tree species and will be further discussed in Section 5.4.2.

In terms of respiration (Fig. 5.3b), the doubling in carbon increases the R_{eco} via an increase in plant respiration proportional to the GPP increase, thus it is stronger in CTESSEL. The main increase in R_{eco} is driven by the temperature change, as it enhances soil respiration as well. However, it should be noted that these estimates do not account for any changes in the soil carbon pool.

Changes in NEE are the combination of the induced changes in GPP and R_{eco} (Fig. 5.3c).

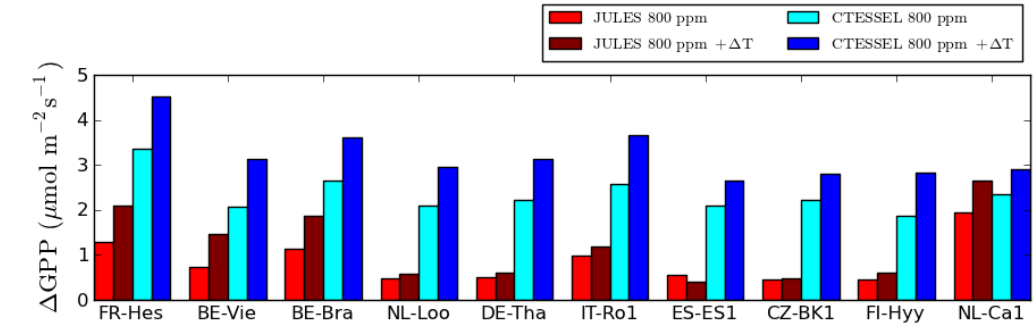

(a) GPP

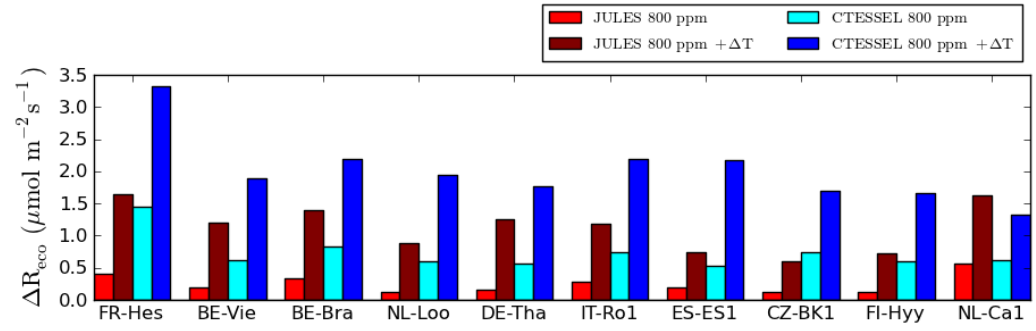

(b) R_{eco}

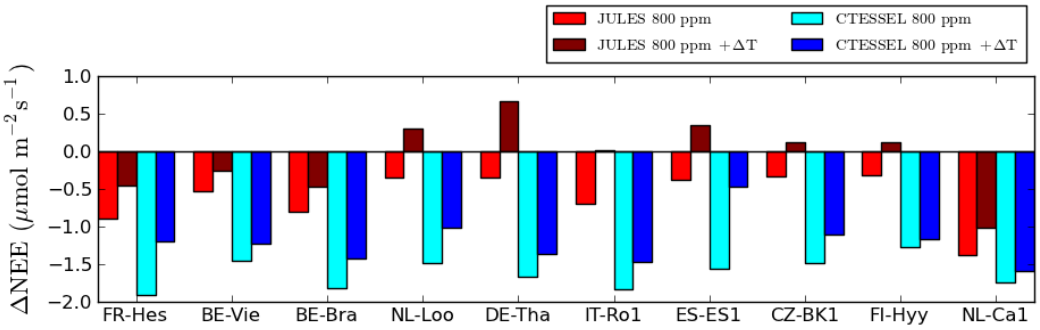

(c) NEE

Figure 5.3: Change in the annual average of (a) GPP, (b) R_{eco} and (c) NEE for each site, for the runs with double CO_2 concentration alone and the runs with double CO_2 concentration and temperature increase.

For all sites, a doubling in carbon alone always results in an increase in the net carbon sink, since the increases in GPP exceed the increases in R_{eco}. The combined effect of a doubling in CO_2 and increased temperature is also of an increase in the carbon sink for CTESSEL simulations. For JULES, however, at some sites the temperature effect results in a net decrease in the carbon sink, notably at the needle leaf forest sites (NL-Loo, DE-Tha, ES-ES1, CZ-BK1, FI-Hyy). This result is a consequence of the lower optimum temperature in JULES for this species and is further explained in the next section.

5.4.2 Monthly changes in Gross Primary Productivity

For the monthly analysis only some sites representative of each PFT are presented. The changes in the monthly averages are shown for two broadleaf forests in Figure 5.4, for two needle leaf forests in Figure 5.6 and for the grass site in Figure 5.8. Each colour bar shows the difference in the GPP monthly average due to increased CO_2 alone (800 ppm) and due to the combined effect of increased CO_2 and increased temperature (800 ppm + ΔT). For all sites and in both models when doubling CO_2 alone there is a fertilisation effect of enhanced GPP. The effect on GPP of an accompanying increase in air temperature depends on the PFT and time of the year.

For the two broadleaf forests in Figure 5.4 the effects of the CO_2 doubling in both models are towards an increase in GPP. At Be-Vie (Figure 5.4a), when also the air temperature is increased, GPP increases even more for all months in both models. At this site, increases in temperature enhance photosynthetic activity by drawing the air temperature closer to the optimum temperature for photosynthesis. The optimum temperature for broadleaf trees is $T_{opt} = 27°C$ for JULES and $T_{opt} = 31°C$ for CTESSEL. These values were derived from the photosynthesis models for PPFD = 1000 μmol photon m^{-2} s^{-1} and 400 ppm (Section 3.4.2.1, Table 3.6). In the case of CO_2 levels increasing to 800 ppm, the optimum temperature was found to increase by 2°C in JULES due to the effects of increased CO_2 on the limiting regimes distribution. In CTESSEL no change was found in T_{opt} for high vegetation. In Figure 5.5a the distribution of 'present climate' air temperature for the year of the simulation is shown by the green histogram, while the increase in 4°C in the temperature field is depicted by the pink histogram. The vertical lines indicate the optimum temperatures for photosynthesis as inferred from both models, with a second

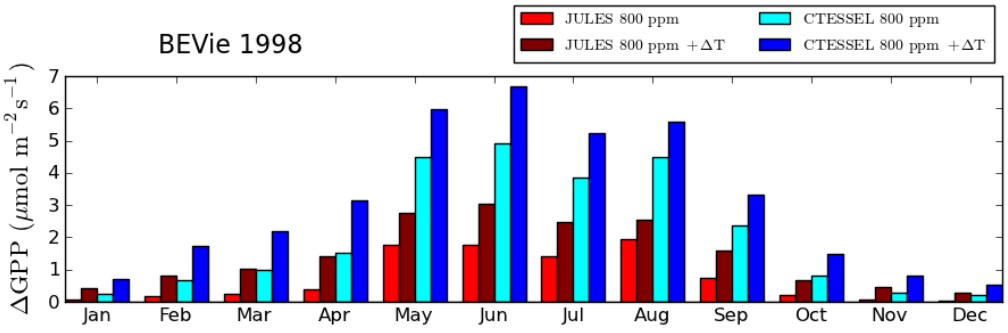

(a)

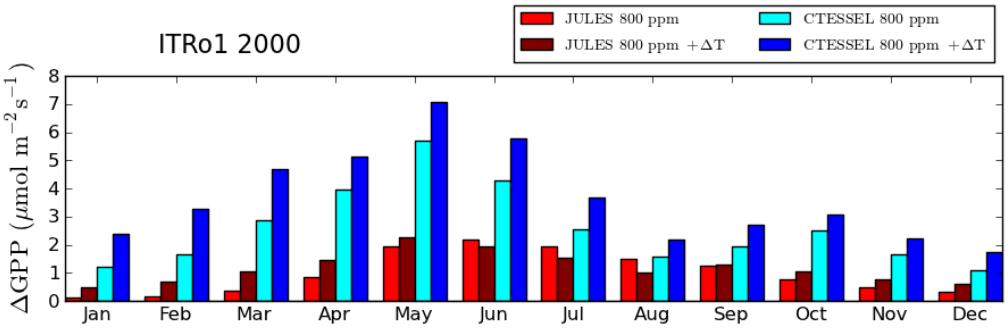

(b)

Figure 5.4: Change in monthly average GPP with double atmospheric CO_2 with and without temperature increase as modelled by JULES and CTESSEL for two broadleaf forest sites.

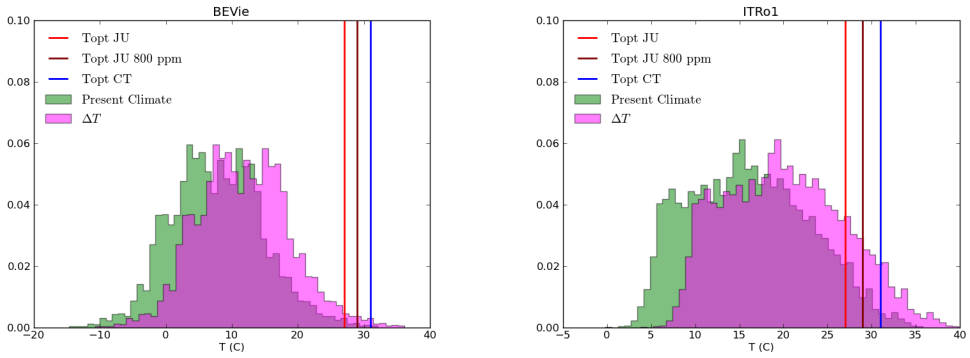

(a) (b)

Figure 5.5: Histogram of the air temperatures for present climate and the idealised scenario with increased temperature $\Delta T = 4°C$. The optimum temperature for photosynthesis for broadleaf trees in present climate conditions is indicated by vertical lines, in the case of JULES the optimum temperature increases under double CO_2 conditions and is indicated by T_{opt} 800 ppm.

value for JULES at double CO_2 concentration. Despite the increase in the optimum temperature, the air temperature values associated to the CO_2 doubling (pink) stay mainly below the optimum. This explains why the increase in temperature amplifies the increase in GPP.

On the other hand, at IT-Ro1 site, located in a Mediterranean region with higher baseline temperatures, an increase in temperature does not always enhance GPP in JULES. Again, the effect of $C_a = 800$ ppm alone is of an increase in GPP for both models and all months (Figure 5.4b). However, when the accompanying increase in temperature is included, the response is mixed. In CTESSEL, the same effect seen in BE-Vie occurs, and CO_2 fertilisation is reinforced by the temperature increase. However, in JULES, during the summer months (June, July and August) the temperature increase results in a decrease in the fertilisation compared to when only CO_2 was changed. The net effect with respect to present climate is still positive, but the change in ΔGPP is reduced. The reduction in the fertilisation effect due to the temperature rise is a consequence of the summer temperatures surpassing the optimum temperature for broadleaf trees (Figure 5.5b). The higher T_{opt} in CTESSEL (blue line in Figure 5.5b) results in no temperature driven reduction in photosynthesis.

Figure 5.6 shows the response of GPP for two needle leaf forests. For this species the optimum temperature for photosynthesis in both models differs by 10°C. While in CTESSEL it is the same value as for broadleaf trees (31°C), in JULES $T_{opt} = 20$°C, shifting to 21°C at 800 ppm. At Hyytiälä forest in Finland, the fertilisation effect of doubling CO_2 is significantly stronger in CTESSEL; and an increase in temperature enhances this effect. When increasing temperature in JULES, fertilisation is reinforced for most months, except June when the change is negligible and July, when fertilisation is in fact reduced due to the high temperatures. Figure 5.7a shows the temperature histograms, with the tail of the distribution surpassing JULES's T_{opt}. For temperatures above T_{opt} the fertilisation effect is reduced. At this site the temperature never reaches CTESSEL's T_{opt}, therefore the temperature effect in CTESSEL is always of enhanced fertilisation. In the case of the warmer needle leaf forest located at the east coast of Spain, ES-ES1 (Figure 5.6b) the combination of higher temperatures and needle leaf tree results in a stronger divergence between the models. In the case of JULES, the temperature distribution and the T_{opt} presented in Figure 5.7b reveal that, for a large portion of the time, air temperature is above

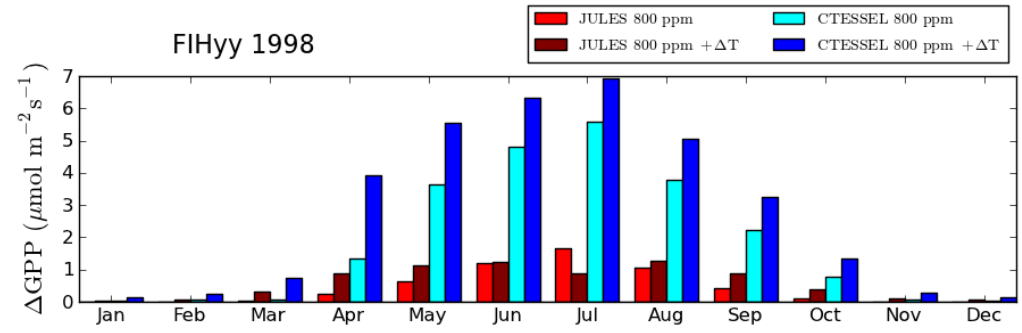

(a)

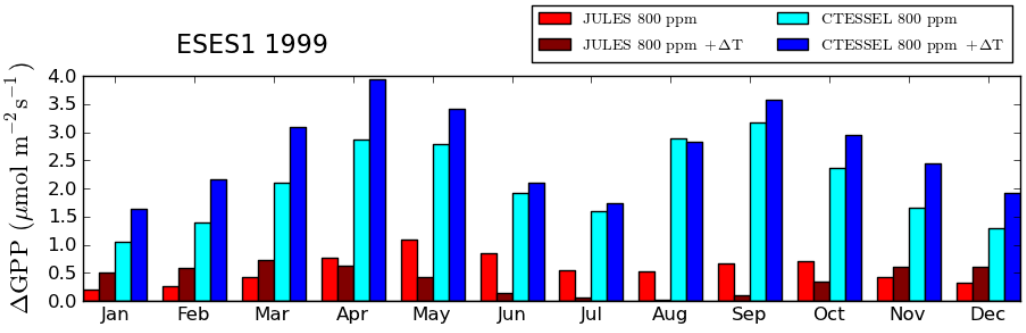

(b)

Figure 5.6: Change in monthly average GPP with double atmospheric CO_2 with and without temperature increase as modelled by JULES and CTESSEL for two needle leaf forest sites.

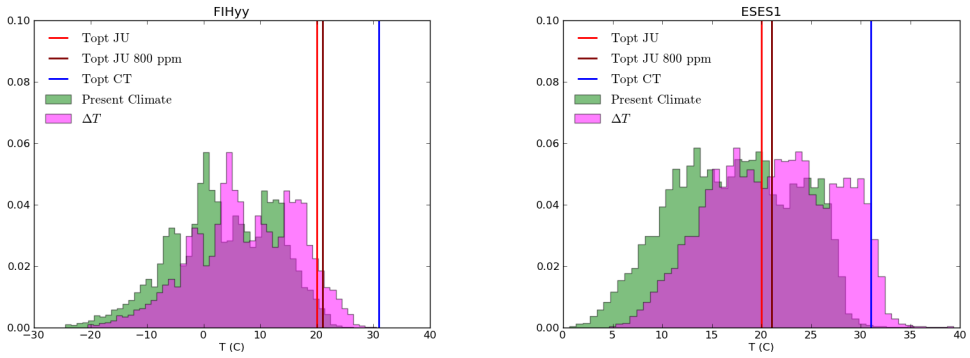

(a) (b)

Figure 5.7: Histogram of the air temperatures for present climate and the idealised scenario with increased temperature $\Delta T = 4°C$. The optimum temperature for photosynthesis for needle leaf trees in present climate conditions is indicated by vertical lines, in the case of JULES the optimum temperature increases under double CO_2 conditions and is indicated by T_{opt} 800 ppm.

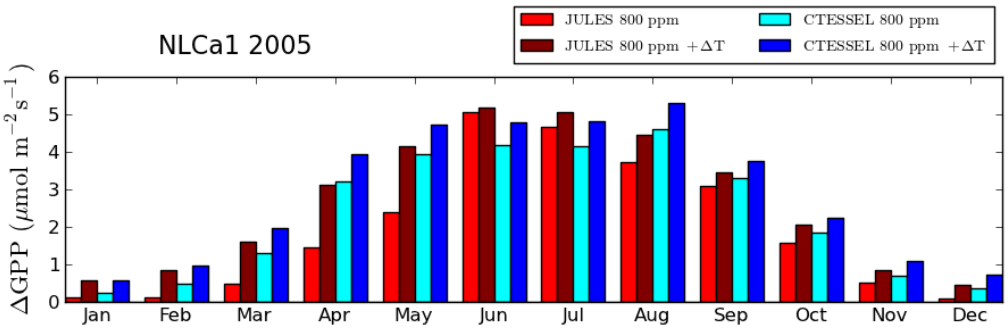

Figure 5.8: Change in monthly average GPP with double atmospheric CO_2 with and without temperature increase as modelled by JULES and CTESSEL for NL-Ca1, C_3 grass.

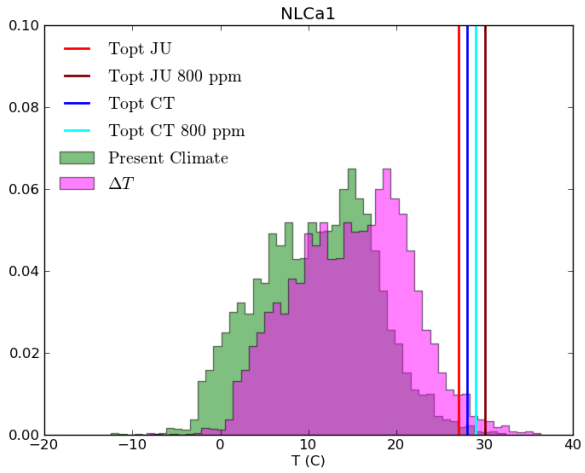

Figure 5.9: Histogram of the air temperatures for present climate and the idealised scenario with increased temperature $\Delta T = 4°C$. The optimum temperature for photosynthesis for C_3 grasses for each model in present climate conditions and under double CO_2 conditions is indicated by the vertical lines.

the optimum, hence the fertilisation effect is partly counteracted by increased temperature (April-October in Figure 5.6b). For this site, also CTESSEL shows a temperature driven reduction in fertilisation in August, but of smaller magnitude due to the higher T_{opt}.

Finally, the effects of the idealised climate change runs are shown for the grass site, Cabauw, in Figure 5.8. In this case, contrarily to the forest sites, the fertilisation effect in CTESSEL is not significantly higher than in JULES, with both models showing similar increments in GPP. For this plant type (C_3 grass), the optimum temperature shift due to the doubling in CO_2 occurs in CTESSEL as well as in JULES. The increase is from 27°C to 30 °C in JULES and from 28°C to 29°C in CTESSEL. The 3°C shift for grasses is the highest implicit acclimation found in JULES and results in no reduction effects of temperature in GPP at this site.

5.4.3 Changes in limiting regimes in JULES

The increased levels of CO_2 concentration and high temperatures have a direct impact on the limitations controlling the photosynthesis reaction. The limiting regimes were already analysed at the leaf level for JULES 5 PFTs in Chapter 3 Section 3.4.4, where the effects of CO_2 and temperature on the limiting regimes distribution were revealed and at the stand level for the FLUXNET sites in Chapter 4 Section 4.4.4, where the seasonal and diurnal partitioning was shown. In this section, the changes induced by the idealised climate change on the amount of limitation imposed by each regime are analysed as well as the changes in the temporal evolution of each limitation.

In Figure 5.10 the annual average of day leaf photosynthesis for each FLUXNET site has been divided into photosynthesis limited by carbon, light and export regimes and is shown separately across the three rows. This allows to compare how the fraction of photosynthesis that is dominated by each regime varies under the idealised climate change scenario. The y-axis indicates the annual averaged contribution to the leaf net photosynthesis from each regime accumulated across the ten canopy layers. The averaged annual diurnal net leaf photosynthesis is the sum of the 3 bars of each regime along the same column. For each site and regime, the first bar illustrates the contribution of that regime in present climate conditions, the second bar is the result of the model run with $[CO_2] = 800$ ppm, and the

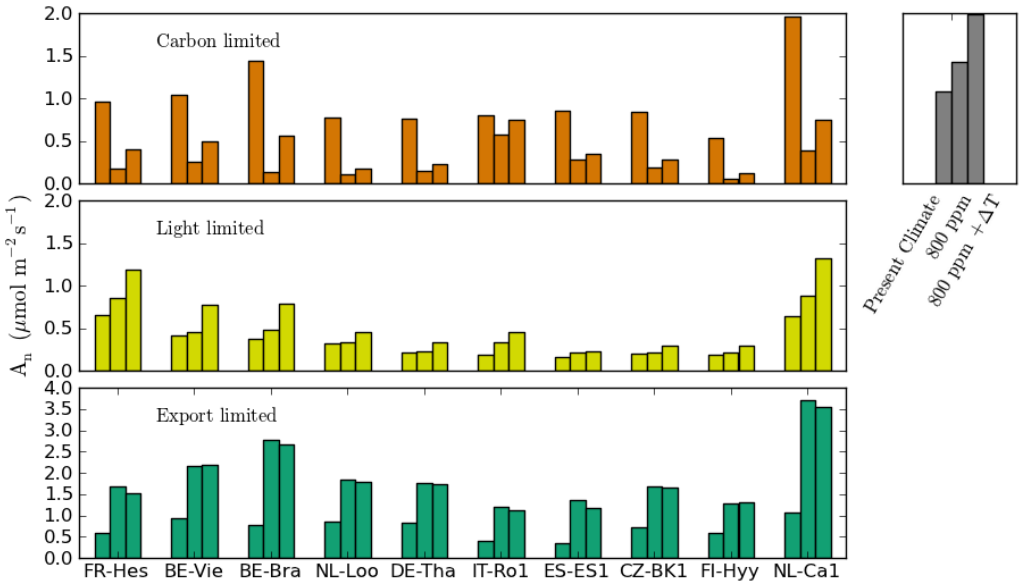

Figure 5.10: Annual averages in daytime leaf net photosynthesis for each photosynthesis regime, as modelled by JULES. For each site, the first bar represents present climate conditions, the second bar the result of a raise in atmospheric CO_2 to 800 ppm, and the third bar the result of also adding a temperature increase.

third bar is the result of the model run when both [CO_2] and temperature are increased. The procedure to characterise the limiting regimes is the same as in previous chapters (i.e. the regime with the minimum photosynthetic rate is considered the limiting factor, and the prevailing regime in the ten canopy layers is considered limiting).

The changes in the dominating regime found in the offline runs at FLUXNET sites are in line with the predictions derived from the photosynthesis scheme alone (Section 3.4.4). The main effect of the enhanced atmospheric CO_2 is a reduction in the carbon (or rubisco) limited photosynthesis in favour of the export and light limitations. The effect of also increasing temperature is to return some dominance to carbon limitation and increase even more the light limitation.

The increases in export and light limitations due to elevated CO_2 are directly related to the changes in the distribution of limiting regimes at the leaf level depicted in Figure 3.20. Two main consequences of a doubling in CO_2 were highlighted as: (i) the increase

in the temperature threshold between export and carbon limitations and (ii) the increase of the radiation threshold between light saturation and carbon. In graphical terms, the boundaries surrounding the carbon region in Figure 3.20 are being pushed to the right from the export region and upwards from the light region with increasing levels of CO_2. The leaf level results are effectively translated into a reduction of carbon regime dominance and increased importance of export and light regimes in the full LSM runs. These results apply for all PFTs and climates, as can be seen in Figure 5.10.

Although, at the leaf level, the effect of CO_2 increasing light saturating levels of radiation was more subtle than the change in the threshold between export and light, the consequences are equally apparent in the LSM runs, with light limitation becoming noticeably more important with enhanced CO_2 and under climate change. Needle leaf species, however, showed no change in the light saturating radiation. In Figure 5.10 the needle leaf sites (NL-Loo, DE-Tha, ES-ES1, CZ-BK1 and FI-Hyy) show the smallest gain of light limiting regime, and it is due to the temperature increase rather than the CO_2 change.

The shift towards more export limitation indicates that, because of enhanced photosynthesis activity as a result of the doubling in atmospheric CO_2, the physiological limitation of the plant is being reached more frequently. When photosynthesis is limited by export limited regime, the carbon assimilation becomes independent of CO_2 levels and radiation and is only affected by temperature and physiological characteristics such as nitrogen content via the V_{cmax} parameter.

5.4.3.1 Monthly distribution of changes

The seasonal distribution of the climate effect on the photosynthesis limiting regimes is similar across all sites. Figure 5.11 shows the monthly changes for one of the sites, BE-Vie, as an illustration. The top panel corresponds to present climate conditions (same as Figure 4.22 reproduced here for the sake of comparison). During the summer months carbon limitation is the dominant regime, so it is in this period when the shift from carbon to other limitation occurs. The increased atmospheric CO_2 also reduces the duration of the carbon dominated period from February-October to May-August. The temperature effect regains carbon limitation especially in April as well and increases light limitation for

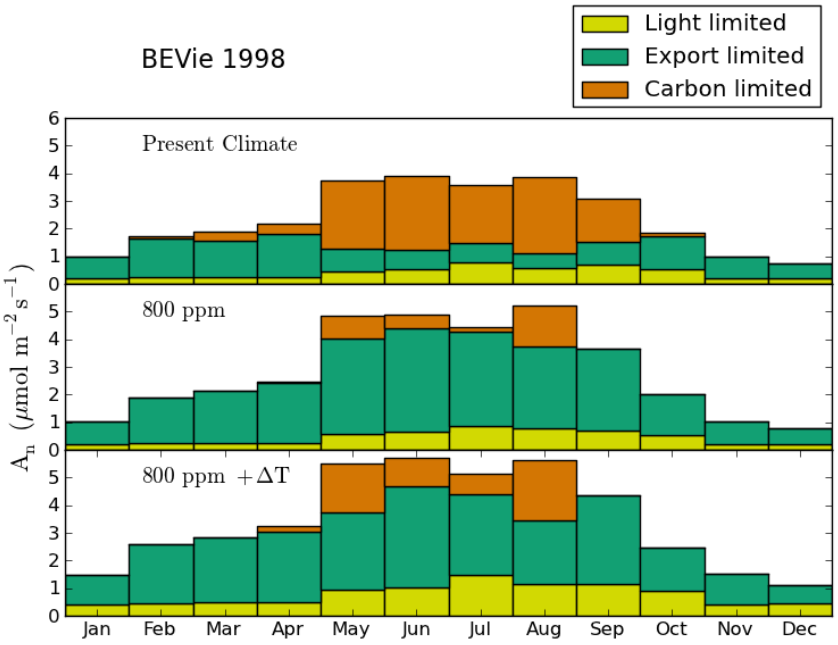

Figure 5.11: Change in the monthly distribution of limiting regimes in daytime leaf net photosynthesis, as modelled by JULES for present climate conditions (top panel), with increased atmospheric CO_2 (middle panel) and when also imposing a increase in temperature (bottom panel).

all months. The total effect is a net enhancement of photosynthesis due to carbon alone (CO_2 fertilisation) and a further increase due to the temperature effect, resulting in the changes in GPP shown in Figure 5.4a. These results suggest that summer months have more potential to increase photosynthesis based on CO_2 fertilisation (carbon limited), while spring months have more potential to increase photosynthesis based on temperature effects (export limitation).

5.5 Conclusions and discussion

The experiments presented in this chapter reproduce the effect of a doubling in atmospheric CO_2 and associated temperature increase (as a proxy for climate change) in carbon fluxes as modelled by JULES and CTESSEL. The LSMs were run in offline mode for the FLUXNET sites studied in Chapter 4, with (i) atmospheric $[CO_2]$ = 800 ppm and (ii) atmospheric $[CO_2]$ = 800 ppm with an associated increase of 4°C in the driving air temperatures. The air humidity was assumed to increase to meet the enhanced evaporative demand due to the increased temperature. This way the water vapour pressure deficit was kept constant and the changes can be attributed to temperature changes. The validity of this assumption depends on the availability of moisture supply. For the Northern Hemisphere air humidity is expected to increase driven by increased temperature, however in areas of the Southern Hemisphere soil moisture limitation has reduced the evapotranspiration trend (Jung et al., 2010). Stomata are very responsive to low air humidity, so the fluxes could be affected.

Although CTESSEL was not designed to perform model projections of future climate, it has provided a baseline for comparison, helping to identify the effect of the export limiting or lack thereof. In addition, with the constant increase of atmospheric CO_2, it seems appropriate to include a limitation to avoid unrealistic increase of GPP in the model.

A widespread enhancement of GPP was found for double atmospheric CO_2. The effect was stronger for CTESSEL than for JULES, in agreement with the larger CO_2 fertilisation effect found at the leaf level (Section 3.4). The effect of also increasing the air temperature, although it was generally of an intensification of the CO_2 enhancement, was found to be more diverse, varying across months and plant species. In particular, JULES presented a

marked difference between the sites of the two tree species. The effect of temperature in enhancing GPP in JULES was weaker for the needle leaf sites, with one of them reducing the carbon assimilation due to carbon alone (ES-ES1). A decisive element in determining the temperature effect was the optimum temperature for photosynthesis, a value that is plant specific. In JULES there is a 10°C difference between the optimum temperature for broadleaf forests and needle leaf forests, which causes marked differences in the response to temperature of these PFTs. The lower needle leaf optimum temperature was surpassed more easily in the warmer climate, resulting in a negative effect for plant productivity especially in the summer months of needle leaf forests (ES-ES1).

The optimum temperature for photosynthesis is not a model parameter *per se*, but the result of the temperature dependence of several model parameters involved in the biochemistry of photosynthesis. The optimum values for the two studied models were derived in Chapter 3 and presented in Table 3.6. In JULES the main temperature dependent photosynthesis parameters are: maximum velocity of carboxylation V_{cmax}, Michaelis-Menten parameters K_c K_o and CO_2 compensation point Γ. From these, only V_{cmax} has a temperature dependence that varies for each PFT following Eq. 2.47 and controlled by PFT specific parameters T_{low} and T_{upp}. Moreover, the intercellular carbon C_i which also controls the photosynthetic rate, varies slightly with temperature ,via changes in air humidity. Finally, because of the co-limitation amongst the three limiting photosynthetic rates, the optimum temperature is not a straight forward derivable value. Similarly, in CTESSEL the temperature dependence relies on three model parameters, the maximum light saturated photosynthetic rate $A_{m,max}$ (Eq. 2.62), mesophyll conductance g_m (Eq. 2.61) and CO_2 compensation point Γ (Eq. 2.60). The fist two have a temperature dependence regulated by the parameters $T_{1Am,max}$, $T_{2Am,max}$, T_{1gm} and T_{2gm}, which have specific values for C_3 and C_4 plants. However, not all C_3 species have the same optimum temperature, most likely because of the influence of temperature driven variations of C_i. Overall, JULES presents more diversity amongst plant types resulting in greater variance in their optimum temperatures for photosynthesis (Table 3.6) both at present and doubled CO_2 concentrations.

The LSMs simulations performed in this chapter are run offline, with no carbon cycle, the effect of climate is only represented by an increase in air temperature, and the spatial scope limited to specific sites. Nevertheless, the collection of sites comprises different climates

and ecosystems with and without soil moisture stress. The value of this analysis lies in the interpretation of the sign of the temperature feedback on GPP in terms of the optimum temperature of photosynthesis. These results can help understand more comprehensive studies that use global dynamic global vegetation models (DGVMs) to identify the effects of increased CO_2 and climate on the carbon cycle (Cox et al., 2000; Cramer et al., 2001; Friedlingstein et al., 2006; Hemming et al., 2013). Models agree that the effect of increased CO_2 is of an increase in the terrestrial carbon sink due to the fertilisation of vegetation. However the effect of climate change is to reduce the efficiency of the sink, but there is large variability in the predicted responses. The results presented here highlight the optimum temperature as a key element determining the response of vegetation to climate change in models. Although precipitation was not varied, a proportional increase in this field would not affect significanty the results. More precipitation would increase the soil moisture content and would allow a larger fertilisation effect. In experiments that study land-atmosphere interactions coupled to an atmospheric model, where the variation in precipitation can be both positive and negative, variations in precipitation may be decisive. In fact, a decrease in soil moisture content can mitigate the fertilisation effects (Gray et al., 2016).

In terms of the factors limiting the photosynthesis reaction, JULES' runs show that the increase in CO_2 produces a shift from carbon limited photosynthesis to both light and export. The increase in temperature reduces the export limitation with respect to CO_2 alone. The behaviour is similar across all sites: no differences were attributed to specific PFTs. The results are in line with findings at the leaf level (Section 3.4.4). At the leaf level the only PFT that showed no variation in limiting regimes due to changes in temperature was C_4. The increased limitation from the export limiting regime represents a physiological limit to the capacity of vegetation to increase carbon assimilation. It could represent an acclimation or downregulation of photosynthesis to elevated CO_2. There are other external limitations that can limit or reduce the fertilisation effect from increasing indefinitely, like the lack of nutrients (Zaehle et al., 2010).

Chapter 6

Conclusions

In this thesis the research questions presented in Chapter 1 have been explored by analysing the representation of vegetation processes in two land surface models, JULES and CTESSEL. The analysis has consisted of two levels: first a detailed analysis of the leaf level representation of photosynthesis in both models, and then the implications for carbon and energy fluxes at the canopy level, using the full LSMs at 10 European FLUXNET sites. Due to its importance for climate change projections, the response of photosynthesis to elevated atmospheric CO_2 and temperature rise were analysed in both models, at the leaf level and at the FLUXNET sites. This chapter presents the main findings, summarises how the research questions have been addressed and concludes with some recommendations for future work.

6.1 Main findings

The main differences in the leaf level parameterization of photosynthesis in the two models studied are the representation of the soil moisture stress on photosynthesis and the absence of export limiting regime in CTESSEL. The difference in soil moisture stress had consequences for present day simulations while the lack of export limiting regime influenced the response of photosynthesis to increased CO_2 and is therefore primarily relevant when considering climate changes.

The comparison of the LSMs at the FLUXNET sites revealed that, despite the differences in parameterization, both models reproduced similar GPP fluxes for present day conditions. The main dissimilarities in GPP were related to JULES overly restricting photosynthesis due to excessive soil moisture stress, which was in disagreement with the GPP flux observations. The GPP reproduced by both models was too low compared to the eddy covariance measurements. More discrepancy was found in the turbulent fluxes reproduced by both models, especially latent heat. JULES latent heat flux was generally higher than that of CTESSEL. The higher sensitivity of JULES stomatal conductance to humidity can be partly responsible for a larger contribution from leaf transpiration, but the differences in the degree of canopy-atmosphere coupling, which depends on the magnitude of the aerodynamic resistance, related to the surface exchange coefficients, may also play a role.

Under conditions of elevated CO_2 both models exhibited an increase of carbon assimilation, both at the leaf level and at the canopy level for C_3 species. The CO_2 fertilisation effect in JULES levelled off at high CO_2 concentrations, as a consequence of the photosynthesis reaction being hampered by the export limiting regime. In the case of CTESSEL, which does not include an equivalent limitation on photosynthesis, the CO_2 fertilisation showed a linear increase. The increase in photosynthesis rate meant that the reaction was more often controlled by the export limiting regime in JULES, observed both at leaf level and ecosystem level. This result is a direct consequence of the export limiting rate for photosynthesis not being a function of C_i. Unlike the other photosynthetic limitations, the export limited photosynthetic rate does not increase with atmospheric CO_2, and therefore slows the process of photosynthesis. Both land surface models use a photosynthesis scheme based on the relationship between photosynthesis and stomatal conductance, showing an increase in the intrinsic water use efficiency (A/g_s) for elevated CO_2 concentrations.

The consequences of doubling atmospheric CO_2 from 400 ppm to 800 ppm in JULES leaf level photosynthesis scheme on limiting regimes were: (i) an increase of the temperature threshold between export and carbon limitations and (ii) an increase of the radiation threshold between light and carbon limitations. The changes in the temperature threshold generated a shift in the optimum temperature for photosynthesis, which increased a few degrees due to the doubling in CO_2. The changes in radiation threshold translate in a higher radiation for light saturation. A shift of optimum temperature for photosynthesis

was also found in CTESSEL's scheme for grasses and shrubs albeit of a lower magnitude.

The optimum temperature for photosynthesis was found to be a key parameter in determining the effect of temperature on GPP. JULES optimum temperatures are lower than the ones in CTESSEL, in particular needle leaf trees has a value about 10°C lower. These low values were responsible for a more frequent reduction of GPP due to increased temperatures in JULES compared to CTESSEL.

6.2 Research questions

The research questions can be now addressed as follows:

RQ1. When do the limiting regimes determining photosynthetic activity occur?
To answer RQ1, concerning the photosynthesis limiting regimes and the conditions under which they occur, the JULES photosynthesis scheme was tested both at the leaf level in a theoretical framework and at the canopy level for the 10 FLUXNET sites. In Chapter 3, analysis of the isolated JULES photosynthesis model indicated that carbon is the main limitation at moderate temperatures and high radiation. For C_3 species, the export limitation is reached at temperatures below approximately 18°C depending on the PFT. Light was found to be limiting for radiation levels below approximately 300 μmol photons m^{-2} s^{-1}. In Chapter 4, RQ1 is tackled for a set of realistic settings, ten sites located in different climatic regions and using the the full LSMs. Results agreed with the findings at the leaf level, with particularities related to the specific climate. Carbon limitation only occurs during the growing season (March-October depending on sites), while export and light limitations occur throughout the year. Continental sites were more limited by the export regime due to the lower temperatures. On the other hand, Mediterranean sites were mostly carbon limited, with export limitation being negligible. At the daily timescale, carbon limitation occurs during the middle of the day while light limitation is associated with the hours around dawn and sunset. The export limiting regime was predominantly found in the mornings as a result of the cooler temperatures.

In the case of C_4 plants, the analysis was only performed at the leaf level because the study sites were located in Europe. Photosynthesis was limited either by carbon (rubisco)

or by light, with the radiation threshold between them being dependent on temperature. The export limitation (PEP carboxylase) is only effective at very low intercellular CO_2 concentrations, below the levels analysed.

RQ2. What are the most important driving variables and model internal parameters during each regime?

The global sensitivity analysis in Chapter 3 revealed that leaf temperature and soil moisture stress factor are the most important factors for leaf photosynthesis. However, when the analysis was targeted to JULES photosynthetic rate, as limited by each regime separately, some specific results emerged. For carbon limited photosynthesis, leaf temperature is the main factor, followed by the leaf nitrogen content (parameter determining the magnitude of V_{cmax}). For light limited photosynthesis, it is the photosynthetic photon flux density (PPFD) that mainly determines the photosynthetic rate, with the parameter that determines the quantum efficiency next. For export limited photosynthesis, again, leaf temperature is the main factor, followed by T_{upp}, a parameter that defines the temperature dependence of V_{cmax}

RQ3. What differences are there in the carbon uptake-water use relation in models?

Water use efficiency represents the carbon gain per unit of water lost and is related to the vegetation's strategy for present and future climate. JULES has been found to present lower water use efficiency, both at the leaf level and at the canopy level. The lower intrinsic water use efficiency (A_n/g_s) found for JULES in Chapter 3, was ascribed to larger stomatal conductances predicted by JULES. In Chapter 4 the ratio between GPP and LE was found to be generally lower in JULES than in CTESSEL, as caused by larger LE. GPP/LE calculated from eddy covariance observations were higher than those found from the models.

RQ4. How well do models capture the interannual variability in vegetation fluxes?

Due to the availability of several years of data, it was possible to analyse year to year variations in observations and the ability of models to reproduce it, it was decided to focus on GPP. For the temperate sites models underestimated the variability. At the Mediterranean sites models overestimated the variability due (in the case of JULES) to incorrect excessive soil moisture stress. It was found that the correlations in monthly anomalies were more similar between models than either model with the observations,

revealing that there are causes of year to year variation that are not represented by models.

RQ5. What are the assumptions in photosynthesis models that mainly affect their response to CO_2 increase and associated changes in climate change?
The main factor affecting the CO_2 fertilisation effect is the export regime limitation on photosynthesis, as found in the leaf level analysis in Chapter 3 and further confirmed by the climate change model experiments in Chapter 5. The absence of this limitation in CTESSEL produced an almost linear response of photosynthesis to increasing levels of CO_2, resulting in larger CO_2 fertilisation effects in the climate change experiments. This limitation introduces physiological constraints on the photosynthesis reaction. This aspect will be further discussed in Section 6.3. In addition, the treatment of soil moisture stress is also likely to condition model projections. Finally, the response of the LSMs to increased temperature was conditioned by the specific values of the optimum temperature for photosynthesis, which also will be further discussed in Section 6.3.

6.3 Discussion

The photosynthesis reaction is equally limited by each regime (carbon, light and export) for present climatic conditions, as derived from the analysis of 10 European ecosystems. However, the enhancement of the photosynthetic rate driven by increased atmospheric CO_2 concentrations will augment the limitation exerted by the export regime. The export limitation on the photosynthesis process is of an internal nature, and reveals the physiological limitations in plants. It occurs because, although environmental conditions are favourable (i.e. no carbon or light limitation), the plant is not able to process the triose phosphate into the final carbon compounds and it is accumulated instead. This results in a metabolic imbalance between triose phosphate production and triose phosphate utilization by the plant's organs. Modelling the vegetation response at this regime requires a deep understanding of the different plant strategies and vegetation's capacity for adaptation.

When forcing vegetation models with unprecedented extreme conditions, a frontier is reached between the mechanistic processes that characterised plant behaviour under current conditions and what nature can achieve by biological changes via acclimation. Due to the complexity of the living organisms and the myriad of coping strategies, it becomes

inviable to model in an explicit processed-based approach all the ecosystem processes, at least at the global scale. It is in this context that new approaches are emerging, advocating a holistic approach for ecosystem modelling that can benefit from advances in the fields of ecology and evolutionary biology. These efforts include identifying and exploiting physical and biological constraints by explicitly including them in models (Prentice et al., 2014).

An example of the application of a biophysical constraint in vegetation modelling is the stomatal optimisation theory, based on the hypothesis by Cowan and Farquhar (1977) that stomata behave in such a way to maximise the carbon gain while minimising the water loss. The optimisation has been developed mathematically combining photosynthesis and transpiration formulations to yield an expression for the stomatal conductance (Katul et al., 2010; Medlyn et al., 2011; Prentice et al., 2014). The stomatal optimisation theory has been implemented in LSMs: CLM (Bonan et al., 2014) and CABLE (De Kauwe et al., 2015), providing comparable results to the previous schemes. The functional dependencies derived through the optimisation are equivalent to the A-g_s relationship already employed by models using gas exchange formulations based on Ball et al. (1987), and in particular the two LSMs analysed in this thesis. However, it is argued that this mathematical derivation allows for a direct interpretation of the parameter that relates A-g_s (g_1 in Medlyn et al. (2011)). The factor g_1 is inversely related to the intrinsic water use efficiency and can be linked to plant traits across the globe (Lin et al., 2015). Moreover, because the relationships are derived from an optimisation theory rather than empirically, there is greater confidence when applying the model in novel situations like increased CO_2 concentrations. However, the main flaw of the optimisation theory at the moment is a discrepancy in the predicted stomatal response to ambient CO_2, which varies depending on whether photosynthesis is assumed to be limited by carbon (or rubisco) or by light (RuBP regeneration)(Medlyn et al., 2013). The inconsistency arises due to the different response of carbon and light limited photosynthesis to CO_2. If photosynthesis is carbon limited, it responds strongly to increased CO_2, thus the optimal response is for the stomata to open because the benefit of increased carbon assimilation outweights the loss of water. This response contradicts the observations of stomata closure with increased CO_2 (Morison, 1998). Conversely, if photosynthesis is assumed to be light limited, the slope of A-C_a curve is less steep, so the carbon gain is not sufficient to justify the the loss of water and consequently the stomata close, in accordance to the observed behaviour. To overcome this

inconsistency, Medlyn et al. (2011) argue that the stomata optimise as if photosynthesis was light limited. Another interpretation proposed by Katul et al. (2010) is to consider that the marginal cost of water (λ) is not constant, but increases with C_a. The marginal cost of water represents the plants water use efficiency, thus there is potential to link this factor to water availability. The optimisation theory is a sound approach to resolve the stomatal gas exchange by understanding the strategy adopted by plants. However, the optimisation theory is not a substitute for a robust photosynthesis model. The results presented here suggest that the limitations on photosynthesis will most likely arise from the physiological capacity of plants. This aspect is only included in the stomatal optimisation theory via the photosynthetic rate derived from the photosynthesis scheme.

Furthermore, the idea of exploiting ecophysiological constraints can be applied to the spatial distribution of vegetation as well as the plant physiology. The adequacy of classifying vegetation diversity into a handful of plant functional types with fixed model parameters to define their traits is being challenged. Analysis of a global database of plant characteristics revealed that although PFTs captured a substantial fraction of the observed variation, for several traits most variation occurs within PFTs (Kattge et al., 2011). This evidence calls for a shift from PFTs to a trait-based approach to characterise vegetation in a more flexible way. Pavlick et al. (2013) introduced a model that resolves subgrid-scale trait variability using functional trade-offs filtered by environmental selection.

The models analysed in this study do not account for nutrient availability, which could become an important limitation on vegetation growth (Zaehle et al., 2010). It is not represented in most models, due to its complexity. Its implementation requires good understanding of nitrogen and carbon interactions. The most important nutrient is nitrogen, whose abundance in the soil could decrease due to reduced mineralization of nitrogen in the soil driven by warm temperatures (Mcguire et al., 1995).

The models analysed have fixed characteristics for each plant type, therefore do not contemplate any change in the plant's response to its environment (neither acclimation nor adaptation). However, the shift in the optimum temperature for photosynthesis under conditions of double CO_2 resembles an acclimation strategy. The reason behind the shift in JULES is the heterogeneous response of the three limiting regimes to CO_2 rising concentration, producing changes in the intersection point between limitations. This shift has

arisen implicitly from the co-limitation formulation. The same feature occurred in CTESSEL, although to a lesser extent. The increase in T_{opt} can be regarded as an acclimation to temperature, but it is a consequence of the change in CO_2. This result is a consequence derived from assumptions that are implicit in the construction of the models, therefore could be regarded as supporting evidence of the model ability to represent realistic vegetation behaviour. However it is difficult to determine whether it is indeed the skill of the schemes that is driving the change in T_{opt}. The fact that the shift was recognised in both photosynthesis schemes with different formulations supports this idea.

As climate change modifies the environment, some of the elements that drive the photosynthesis process, CO_2 and temperature, are increased, favouring the carbon assimilation. The direct effect of leaf level fertilisation was reproduced by both models, although with different magnitudes. The fertilisation was greater in CTESSEL, with photosynthesis showing an almost linear response, due to the lack of physiological limitation, such as the export limiting regime in JULES. Although CTESSEL is a LSM embedded in a medium range weather forecasting system and its design is not intended for climate model projections, the comparison between both models has allowed the identification of the effect of the lack of a physiological limitation on photosynthesis. In accordance with the greater CO_2 fertilisation at the leaf level, the experiments at the FLUXNET sites with double CO_2 resulted in a stronger fertilisation effect at the canopy level. The fertilisation effects studied here could be amplified by the use of a prognostic LAI, that would increase due to the larger biomass generated by larger assimilation rates.

The fertilisation effect produces a negative feedback on the carbon cycle by increasing the terrestrial carbon sink, with vegetation growing more vigorously due to increased carbon assimilation. However, the effect of a climate feedback in the carbon cycle is a source of divergence amongst models, as illustrated by a number of modelling studies (Cox et al., 2000; Cramer et al., 2001; Friedlingstein et al., 2006; Hemming et al., 2013). This study has highlighted the optimum temperature for photosynthesis as a determining element in the sign and strength of the climate feedback.

Cramer et al. (2001) analysed the response of 6 DGVMs to increasing CO_2 and associated change in climate variables separately and combined. They found that all models showed an increase in the terrestrial sink driven by the rise in atmospheric CO_2, while the response

of the net ecosystem production (NEP) to climate change was more divergent amongst models, due to differences in the models' parameterizations of vegetation processes. In northern mid-latitudes the effect of climate was to enlarge the carbon sink (as for most sites of this study) while in southern mid-latitudes and tropics the effect was reversed. Globally, in their experiments the negative effect of climate change dominates and by 2100 the CO_2 fertilisation is considerably weakened.

In Friedlingstein et al. (2006) the climate feedback on the carbon cycle is analysed with regards to the CMIP4 models. Models were run with coupled climate-carbon cycle and in uncoupled mode to quantify the effect of climate in weakening the carbon sink. The model that showed the highest positive climate-carbon cycle feedback was HadCM3LC. It even predicted the land carbon sink to become a source by 2050. HadCM3LC uses the dynamic global vegetation model, Top-Down Representation of Interactive Foliage and Flora including Dynamics (TRIFFID) coupled to the land surface scheme, Met Office Surface Exchange Scheme (MOSES), which is the precursor of JULES. Some hypotheses for the large positive feedback listed by Friedlingstein et al. (2006) are the Amazon dieback (Cox et al., 2004, 2013), the choice of $Q_{10} = 2$ for soil respiration (Jones et al., 2003), the use of a single carbon pool (Jones et al., 2005), the parameterization of plant respiration (Huntingford et al., 2004). The results shown here suggest that the low optimum temperatures for photosynthesis found in JULES could also in part explain the reduction in the terrestrial land carbon sink under climate change predicted by HadCM3LC.

6.4 Recommendations for future work

1. *Photosynthesis measurements.*

   (a) The physiological limitation to the transport of photosynthetic products (export limiting regime) has been found to become increasingly limiting for photosynthesis with rising levels of atmospheric CO_2, and yet it is poorly understood and oversimplified or neglected by models. There is a need for measurements of photosynthesis when plants are under the triose phosphate limitation to better understand and characterise this limitation.

   (b) Photosynthesis observations are taken mainly over short periods of time and

for present day climate conditions. Observations over longer periods of time would help to understand plant behaviour and potential changes under varying CO_2 concentrations, temperature and humidity. In this direction, the Free-Air Carbon Dioxide Enrichment experiments can provide useful data.

2. *Leaf temperature.* Leaf temperature has been found to be a key variable determining photosynthesis. Photosynthesis model estimates would benefit from an accurate value of the temperature in the canopy, either from a dedicated energy balance or from satellite data in the case of forecasting purposes.

3. *Satellite data.* The lack of skill in predicting interannual variability (Chapter 4) shows that there are aspects of vegetation growth that models still do not capture. The use of satellite observations of vegetation related parameters (LAI, fraction of absorbed PAR) or environmental related variables (canopy temperature) can help with the representation of vegetation processes, by using data assimilation techniques as well as serve as a tool for model validation and development of parameterizations.

4. *PFTs vs trait-based approach.* The representation of vegetation classes with PFTs has been shown to introduce some specifications on plant types that result in important differences in plant responses (e.g. the optimum temperature determining the effect of temperature increase on the carbon sink, Chapter 5). A trait-based approach that takes into account the climatic conditions where vegetation grows will provide better representation of plant behaviour at the ecosystem level.

5. *Optimisation theory.* There is a potential to develop vegetation models based on biophysical constraints but the new generation of vegetation models should acknowledge the internal physiological limitations based on experimental results.

Appendix A

Photosythesis subroutines

A.1 JULES

The photosynthesis subrotines for JULES were extracted from version 3.3. Subroutine `leaf_limits_jls.F90` calculates the three potential photosynthetic rates corresponding to carbon limited regime, light limited regime and export limited regime for the leaf conditions of temperature, humidity, atmospheric pressure. The plant specific model parameters are declared in the module `pftparm.F90` and defined in the namelist `pft_params.nml`. An estimate of the intercellular carbon (C_i) is first made using Jacobs (1994) closure equation, based on specific humidity deficit (D_s) and the carbon dioxide concentration outside the leaf (taken as atmospheric CO_2 concentration, C_a). The values of D_s and C_i will be later updated with the change in humidity due to the leaf transpiration as determined by stomatal conductance. The temperature dependencies of the parameters are accounted for in this subroutine. The leaf temperature is fixed and equal to the skin temperature calculated in the surface energy balance of the full model, there is not a further adjustment at the leaf environment due to photosynthesis processes as happens with humidity. The three potential photosynthesis rates are then passed to subroutine `leaf_jls.F90` which is where the gross leaf photosynthesis is calculated by combining the three rates in the colimitation equation. Then the leaf dark respiration is subtracted to obtain the net carbon flux. This magnitude is multiplied by the soil moisture factor, which is if the soil moisture is below the critical point. At this point leaf stomatal conductance for carbon is is calculated by

dividing the net carbon flux by the difference in CO_2 across the stomata (C_a-C_i). The leaf stomatal conductance for humidity derived from the stomatal conductance for carbon and used to recalculate the leaf level humidity and intercellular carbon. This process is iterated 3 times to achieve a consistency between the stomata, carbon and water vapour flux. For the purpose of the leaf level analysis, only these subroutines are run, providing as output variables the intercellular carbon dioxide, the three potential leaf-level photosynthetic rates, the gross and net leaf level photosynthesis, leaf dark respiration and stomatal conductance. In the full model, these two subroutines are called from `sf_stom_jls.F90`, which is the one that calculates the canopy level quantities. The leaf level calculus is done once for the big-leaf approach and then scaled by radiative profile. If canopy is divided in multiple layers then the leaf level subroutines are called once for each layer and the biochemical properties, and radiation is specified at each level.

A.2 CTESSEL

In CTESSEL, the main leaf-level computations are performed in subroutine `cotwo_mod.F90`. The plant type dependent parameters are initialised in the module `sucotwo_mod.F90`. The parameters that vary with temperature (CO_2 compensation point, mesophyll conductance and maximum photosynthetic capacity $A_{m,max}$) are adjusted for temperature in the canopy level subroutine `cotworesterss_mod.F90` before `cotwo_mod.F90` is called. Further adjustments to parameters include the derivation of D_{max} from g_m for low vegetation and the derivation of f_0 from g_m for high vegetation, based on Calvet (2000); Calvet et al. (2004). All these parameters are introduced to `cotwo_mod.F90`, where first C_i is estimated from Jacobs (1994) closure from the humidity deficit and outside carbon dioxide concentration; also including a term accounting for some CO_2 flux through the cuticule when stomata are closed. A maximum photosynthetic rate for high radiation intensities (A_m) is derived from internal carbon and carbon related parameters. This value is only attained at high radiations, and grants an asymptotic value for the photosynthesis light dependence. The actual photosynthesis is scaled by the absorbed radiation (I_a) and quantum efficiency (ϵ) and has the dark respiration subtracted. With the net leaf photosynthesis known, stomatal conductance for carbon is derived and from it the stomatal conductance for humidity. The

stomatal transpiration is then used in an iterative process to account for the interaction of CO_2 and water vapour molecules as they cross the stomata, and stomatal conductance is recalculated.

Appendix B

Photosynthesis for the different vegetation types

B.1 A-C_i curves

The response of CO_2 assimilation to intercellular CO_2 concentration is one of the main diagnostic tools in the study of photosynthesis (Von Caemmerer, 2000) (see Figure 2.2). Although atmospheric CO_2 (C_a) has been used in Chapter 3 as the main variable to represent the CO_2 fertilization effect, A-C_i curves relate the models to physiological studies. The A-C_i curve describes the demand of CO_2 of the photosynthetic system. The A-C_i response curve provides a platform for model validation, the shape of the curve defines many key parameters used in the description of photosynthesis. The intercept of the curve with the x-axis represents the CO_2 compensation point, i.e. the intercellular CO_2 at which the leaf dark respiration equals the gross CO_2 intake, giving a null net assimilation. The slope of the curve is determined by different parameters depending on the limiting regime of photosynthesis. For low intercellular concentrations, when photosynthesis is limited by rubisco, the slope of the curve is controlled by the parameter V_{cmax} (in JULES) or mesophyll conductance (in CTESSEL). For higher C_i, if the irradiance is low, the RuBP regeneration limits the photosynthesis. In this case, the incoming radiation is the limiting factor via the actual irradiance directly (in JULES) or by means of the electron transport (in CTESSEL). Figure B.1 shows the A-C_i curves for the five studied plant types and both

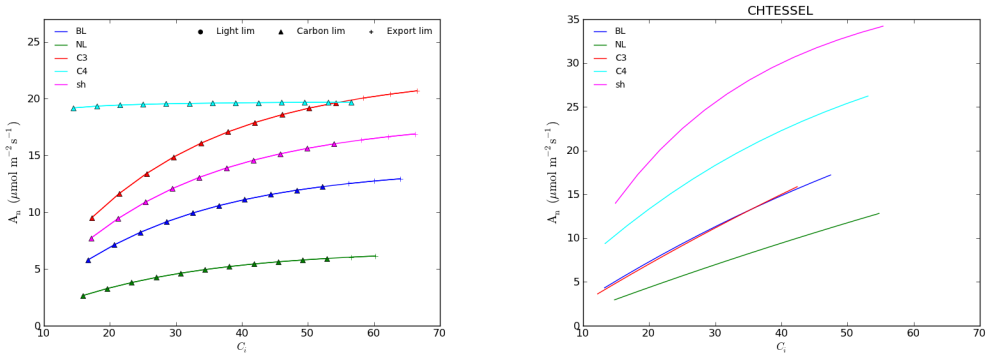

(a) JULES (b) CTESSEL

Figure B.1: CO_2 response curve for 5 PFTs (BL: Broadleaf trees, NL: needle leaf trees, C3: C3 grasses, C4: C4 grasses, sh: shrubs), leaf T =24°C, PAR=1600 μmol photon m^{-2} s^{-1}.

photosynthesis models.

B.2 *A*-temperature

Figures B.2a and B.2b illustrate the temperature dependence of leaf level photosynthesis for each of the selected plant types, in JULES and CTESSEL respectively at current carbon dioxide concentration (400 ppm). The radiation has been set to 1000 μmol photon m^{-2} s^{-1}, which corresponds to light saturated conditions for all the the PFTs except for C_4, which still has potential for higher A_n if radiation was to be increased. JULES dependence on leaf temperature is dominated by V_{cmax} temperature dependence (See Figure 2.5) for the regions where carbon is limiting (triangles). The optimum temperatures for photosynthesis are a few degrees lower than those found for V_{cmax}, except for C_4 vegetation which is the same. At low temperatures, where export is the limiting regime, there appears to be a linear increase with temperature, this is a result of the co-limitation amongst regimes.

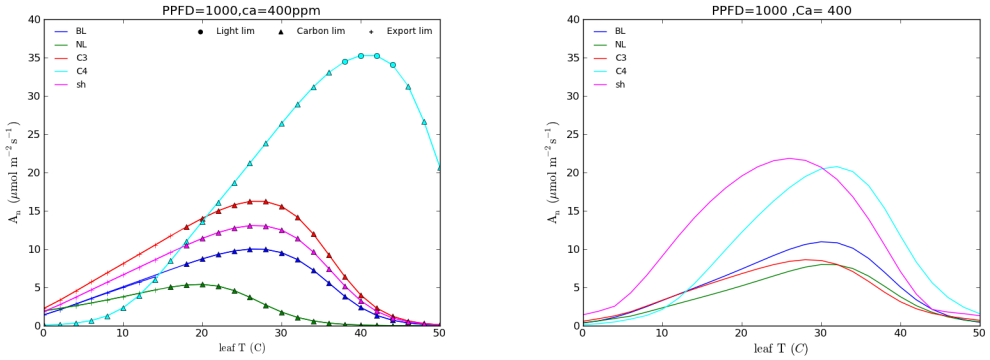

(a) JULES (b) CTESSEL

Figure B.2: Leaf level photosynthesis as a function of leaf temperature for the 5 plant functional types; PPFD=1000μmol photon m^{-2} s^{-1} , C_a=400 ppm.

B.3 *A*-radiation

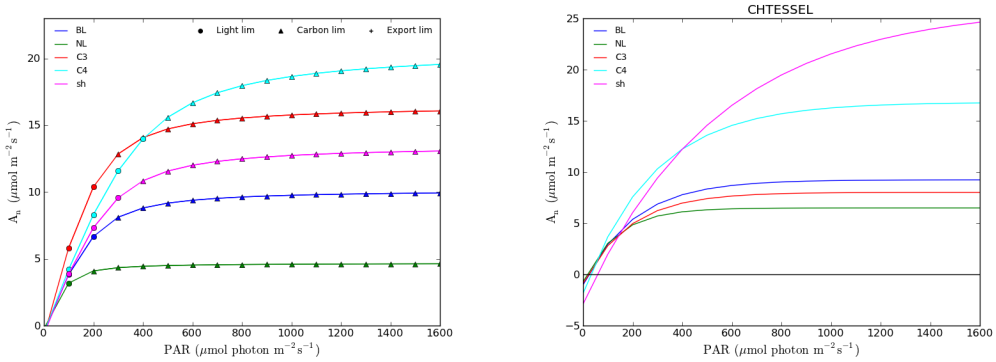

(a) JULES (b) CTESSEL

Figure B.3: Leaf level photosynthesis as a function of PAR irradiance for 5 plant functional types; leaf T = 24°C, Ca = 400 ppm.

Appendix C

FAST method for Global Sensitivity Analysis

The Fourier Amplitude Sensitivity Test (FAST) was developed in the 70s for uncertainty and sensitivity analysis of non linear and non monotonic systems (Cukier et al., 1973, 1975, 1978). The mechanism of FAST (or any quantitative methods for sensitivity analysis) is shown in the schematic in Figure 3.26 extracted from Saltelli et al. (1999). The system or model f returns an output y for a given set of n input parameters x_i:

$$y = f(x_1, x_2, ...x_n) \tag{C.1}$$

Each of the input parameters is sampled from its characteristic probability distribution. Each combination of n values of the input parameters yields a random vector $\mathbf{x} = (x_1, x_2, ...x_n)$ with an assumed pdf $p(\mathbf{x}) = p(x_1, x_2, ...x_n)$. The vector $\mathbf{x}$ represents a point in the n dimensional input parameter space. The rth noncentral moment of model output y is expressed as:

$$E(y^r) = \int_{K^n} f^r(x_1, x_2, ...x_n) p(x_1, x_2, ...x_n) \tag{C.2}$$

which is a multidimensional integral over the parameters space, K^n. The purpose of the sensitivity analysis is to ascertain how much of the variance of the output is attributable to the variance of each input parameter (x_i). The main effect of each parameter on the

output, sometimes called 'importance measure' is represented by:

$$\frac{Var_X[E(Y|X)]}{Var(Y)} \tag{C.3}$$

The FAST method performs a Fourier decomposition of f on each of the input parameters, and calculates the variances from the decomposition making use of properties of the Fourier series. The parameter space is sampled using a search curve $x_i(s) = G_i(sin\omega_i s)$, for $i = 1, 2, ...n$ in s, where s is a scalar ranging from $-\infty < s < \infty$. The key of this transformation is that the n-dimensional integral in Eq. C.2 over all the uncertain model inputs is converted to a one-dimensional integral in s. The ω_i are a set of frequencies associated to each input parameter that need to be properly selected. As s varies, all factors change simultaneously along a curve that systematically explores K^n. Each parameter x_i oscillates periodically with its particular frequency ω_i, the perturbation is defined by the transformation function G_i.

Then the model output is computed for a large number of input samples ($\mathbf{x}$). The output y will contain the different periodicities combined. If the ith factor has a strong influence on the output, the oscillation of y will show a high amplitude for frequency ω_i. The sensitivity indices are computed from the Fourier coefficients related to each frequency and its harmonics. The Fourier expansion of $f(s)$ is:

$$y = f(s) = \sum_{j=-infty}^{\infty} (A_j cos(js) + B_j sin(js)) \tag{C.4}$$

where the Fourier coefficients are given by:

$$\begin{aligned} A_j &= \frac{1}{2\pi} \int_{-\pi}^{\pi} f(s) cos(js) ds \\ B_j &= \frac{1}{2\pi} \int_{-\pi}^{\pi} f(s) sin(js) ds \end{aligned} \tag{C.5}$$

Over the domain of integer frequencies j in $\mathbb{Z}$. The output variance can be expressed as:

$$Var(y) = \frac{1}{2\pi} \int_{-\pi}^{\pi} f^2(s) ds - \Big[\frac{1}{2\pi} \int_{-\pi}^{\pi} f(s) ds\Big]^2 \tag{C.6}$$

Making use of the Fourier expansion and properties (Saltelli et al., 1999), the total output variance is approximated as:

$$Var(y) \approx 2 \sum_{j=1}^{\infty} (A_j^2 + B_j^2) \tag{C.7}$$

The contribution to the total variance by parameter x_i is represented by the terms of the summation associated to the parameters frequency ω_i and harmonics $p\omega_i$:

$$Var_i(y) \approx 2\sum_{p=1}^{\infty}(A^2_{p\omega_i} + B^2_{p\omega_i}) \tag{C.8}$$

The main effect of x_i on y is determined by the fraction of the individual contribution (Eq C.8) divided by the total variance (Eq C.7) and it is characterised by the index S_i:

$$S_i = \frac{Var_i(y)}{Var(y)} \tag{C.9}$$

The computation of the first order indices requires the evaluation of the function or model f at a number of points in K^n to calculate the Fourier coefficients A_j and B_j. The number of points for evaluation is determined by the sample size N_s, which is in practice the number of terms in the integrals C.5. See Saltelli et al. (1999) for discussion on the choice of frequencies ω_i and the search curve $G_i(s)$.

FAST first order indices have been shown to be equivalent to those computed with Sobol's method (Saltelli and Bolado, 1998).

Saltelli et al. (1999) proposed some modifications to FAST in a method known as extended FAST. A new search curve with random phase shift and resampling was designed to better cover the input parameter space, improving the accuracy of the classic FAST. The sample size is determined by:

$$N_s = (2M\omega_{max} + 1)N_r \tag{C.10}$$

where M is the interference factor (typically 4), ω_{max} is the largest of the ω_is and N_r is related to resampling procedure.

Moreover, Saltelli et al. (1999) developed a technique to derive the effect of the interactions amongst parameters, by making use of the set of frequencies not contained by the harmonics of the analysed parameter. This residual variance contains information about the parameter interactions not apparent in the first order or main indices. FAST extended method allows the computation of total sensitivity indices S_{Ti} that provide a measurement of the contribution to the output variable of the parameter taking into account its interactions with the other input parameters. The indices are computed similarly to Sobol' (2001), by subtracting the variance related to the complementary set:

$$S_{Ti} = Var(y) - Var_{(\sim i)}(y) \tag{C.11}$$

where $Var_{(\sim i)}$ includes all effects of any order that do not include factor x_i. Although this calculation comes at an increased computational cost, the effect of interactions amongst paramaters in complex systems can be crucial (Chan et al., 1997). An input factor is considered 'very important' if its S_{Ti} is above 0.8 , 'important' if 0.8 $>S_{Ti}$ >0.5, 'unimportant' if 0.5 $>S_{Ti}$ >0.3 and 'irrelevant' if less than 0.3.

Appendix D

LAI

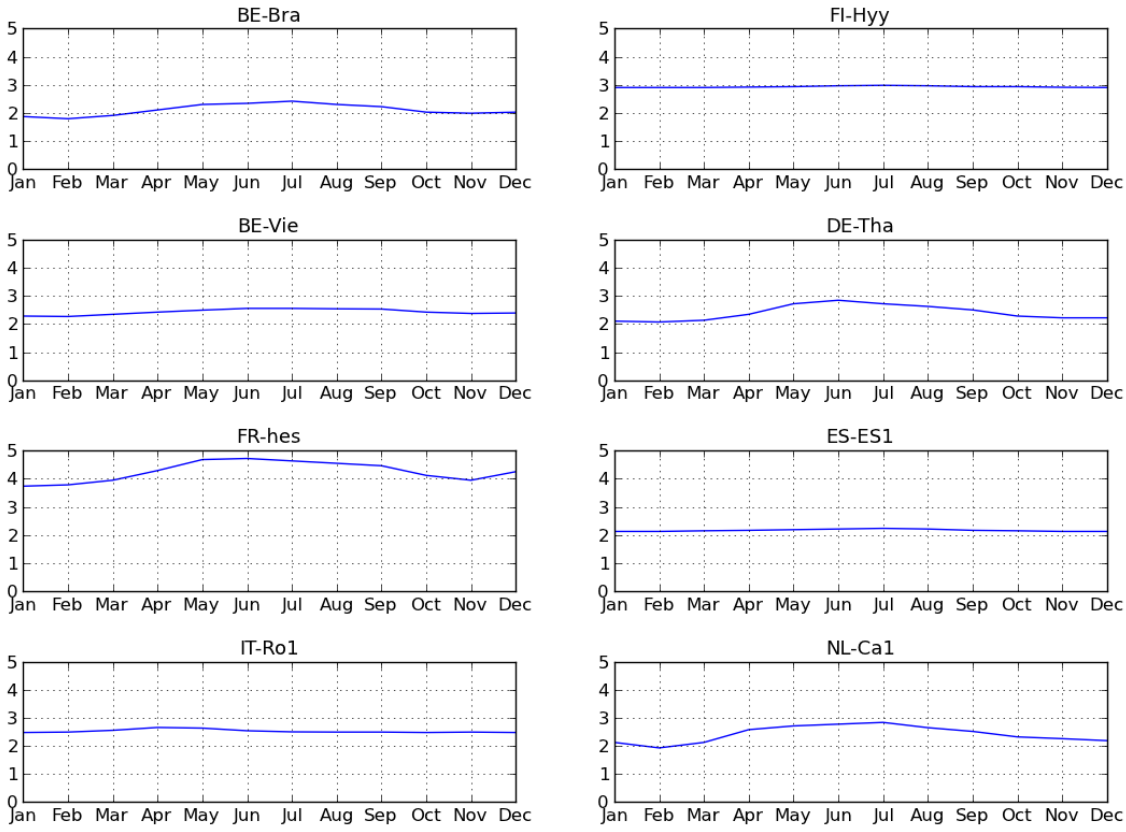

Figure D.1: LAI from ECMWF's climate package from MODIS imagery

Bibliography

A. Agustí-Panareda, S. Massart, F. Chevallier, S. Boussetta, G. Balsamo, A. Beljaars, P. Ciais, N. M. Deutscher, R. Engelen, L. Jones, R. Kivi, J.-D. Paris, V.-H. Peuch, V. Sherlock, A. T. Vermeulen, P. O. Wennberg, and D. Wunch. Forecasting global atmospheric CO_2. *Atmospheric Chemistry and Physics*, 14(21):11959–11983, 2014.

P. Alton, L. Mercado, and P. North. A sensitivity analysis of the land-surface scheme JULES conducted for three forest biomes: Biophysical parameters, model processes, and meteorological driving data. *Glob. Biogeochem. Cycles*, 20, 2007.

O. K. Atkin. Leaf Respiration of Snow Gum in the Light and Dark. Interactions between Temperature and Irradiance. *Plant Physiol.*, 122(3):915–924, 2000.

O. K. Atkin, J. R. Evans, and K. Siebke. Relationship between the inhibition of leaf respiration by light and enhancement of leaf dark respiration following light treatment. *Aust. J. Plant Physiol.*, 25(4):437, 1998.

M. Aubinet, A. Grelle, A. Ibrom, and Ü. Rannik. *Estimates of the annual net carbon and water exchange of forests: the EUROFLUX methodology.* 2000.

M. Aubinet, T. Vesala, and D. Papale. Eddy Covariance: A Practical Guide to Measurement and Data Analysis. 2012.

M. Badger and T. Andrews. Effects of CO2, O2 and temperature on a high-affinity form of ribulose diphosphate carboxylase-oxygenase from spinach. *Biochem. Biophys. Res. Commun.*, 60(1):204–210, 1974.

M. Badger and G. J. Collatz. Studies on the kinetic mechanism of ribulose-1, 5-bisphosphate carboxylase and oxygenase reactions, with particular reference to the effect of temperature on. *Year B. Leo. Baeck. Inst.*, 1977.

D. Baldocchi. Assessing the eddy covariance technique for evaluating carbon dioxide exchange rates of ecosystems : past , present and future. (October 2002):479–492, 2003.

D. Baldocchi, E. Falge, L. H. Gu, R. Olson, D. Hollinger, S. Running, P. Anthoni, C. Bernhofer, K. Davis, R. Evans, J. Fuentes, A. Goldstein, G. Katul, B. Law, X. H. Lee, Y. Malhi, T. Meyers, W. Munger, W. Oechel, K. T. P. U, K. Pilegaard, H. P. Schmid, R. Valentini, S. Verma, T. Vesala, K. Wilson, S. Wofsy, U. K. T. Paw, K. Pilegaard, H. P. Schmid, R. Valentini, S. Verma, T. Vesala, K. Wilson, and S. Wofsy. FLUXNET: A New Tool to Study the Temporal and Spatial Variability of Ecosystem-Scale Carbon Dioxide, Water Vapor, and Energy Flux Densities. *Bull. Am. Meteorol. Soc.*, 82(11): 2415–2434, 2001.

J. T. Ball, I. E. Woodrow, and J. Berry. A model predicting stomatal conductance and its contribution to the control of photosynthesis under different environmental conditions. *Prog. Photosynth. Res.*, (953), 1987.

G. Balsamo, P. Viterbo, A. C. M. Beljaars, B. van den Hurk, M. Hirschi, A. K. Betts, K. Scipal, P. Viterbo, B. van den Hurk, M. Hirschi, and A. K. Betts. A Revised Hydrology for the ECMWF Model: Verification from Field Site to Terrestrial Water Storage and Impact in the Integrated Forecast System. *J. Hydrometeorol.*, 10(3):623–643, 2009.

M. Balzarolo, S. Boussetta, G. Balsamo, A. Beljaars, F. Maignan, J.-C. Calvet, S. Lafont, A. Barbu, B. Poulter, F. Chevallier, C. Szczypta, and D. Papale. Evaluating the potential of large-scale simulations to predict carbon fluxes of terrestrial ecosystems over a European Eddy Covariance network. *Biogeosciences*, 11:2661–2678, 2014.

C. J. Bernacchi, E. L. Singsaas, C. Pimentel, A. R. Portis Jr, and S. P. Long. Improved temperature response functions for models of Rubisco-limited photosynthesis. *Plant, Cell Environ.*, 24(2):253–259, 2001.

C. J. Bernacchi, A. R. Portis, H. Nakano, S. Von Caemmerer, and S. P. Long. Temperature response of mesophyll conductance. Implications for the determination of Rubisco enzyme kinetics and for limitations to photosynthesis in vivo. *Plant Physiol.*, 130(4): 1992–8, 2002.

J. Berry and O. Bjorkman. Photosynthetic response and adaptation to temperature in higher plants. *Annu. Rev. Plant Physiol.*, 1980.

J. A. Berry and G. D. Farquhar. The CO2 concentrating function of C4 photosynthesis: a biochemical model. *Photosynthesis*, 77:119–131, 1978.

M. Best. Jules technical documentation. *Met Office, Joint Centre for Hydrometeorological Research, Wallingford, UK*, 2009.

M. Best, M. Pryor, D. B. Clark, G. G. Rooney, R. L. H. Essery, C. B. Ménard, J. M. Edwards, M. a. Hendry, a. Porson, N. Gedney, L. M. Mercado, S. Sitch, E. Blyth, O. Boucher, P. M. Cox, C. S. B. Grimmond, and R. J. Harding. The Joint UK Land Environment Simulator (JULES), model description Part 1: Energy and water fluxes. *Geosci. Model Dev.*, 4(3):677–699, 2011.

R. A. Betts, O. Boucher, M. Collins, P. M. Cox, P. D. Falloon, N. Gedney, D. L. Hemming, C. Huntingford, C. D. Jones, D. M. H. Sexton, and M. J. Webb. Projected increase in continental runoff due to plant responses to increasing carbon dioxide. *Nature*, 448 (7157):1037–41, 2007.

E. Blyth, R. Harding, and R. Essery. A coupled dual source gcm svat. *Hydrology and Earth System Sciences Discussions*, 3(1):71–84, 1999.

E. Blyth, J. Gash, A. Lloyd, M. Pryor, G. P. Weedon, and J. Shuttleworth. Evaluating the JULES Land Surface Model Energy Fluxes Using FLUXNET Data. *J. Hydrometeorol.*, 11(2):509–519, 2010.

H.-J. Bolle, J.-C. Andre, J. L. Arrue, H. K. Barth, P. Bessemoulin, A. Brasa, H. A. R. De Bruin, J. Cruces, G. Dugdale, E. T. Engman, D. L. Evans, R. Fantechi, F. Fiedler, A. Van De Griend, A. C. Imeson, A. Jochum, P. Kabat, T. Kratzsch, J.-P. Lagouarde, I. Langer, R. Llamas, E. Lopez-baeza, J. M. Miralles, L. S. Muniosguren, F. Nerry, J. Noilhan, H. R. Oliver, R. Roth, S. S. Saatchi, J. Sanchez Diaz, M. De Santa Olalla, W. J. Shuttleworth, H. Søgaard, H. Stricker, J. Thornes, M. Vauclin, and D. Wickland. EFEDA: European Field Experiment in a Desertification-threatened Area. *Ann. Geophys.*, 11(2-3):173–189, 1993.

B. Bonan, P. J. Lawrence, K. W. Oleson, S. Levis, M. Jung, M. Reichstein, D. M. Lawrence, and S. C. Swenson. Improving canopy processes in the Community Land Model version

4 (CLM4) using global flux fields empirically inferred from FLUXNET data. *J. Geophys. Res.*, 116(G2):G02014, 2011.

G. Bonan, M. Williams, R. Fisher, and K. Oleson. Modeling stomatal conductance in the earth system: linking leaf water-use efficiency and water transport along the soil–plant–atmosphere continuum. *Geoscientific Model Development*, 7(5):2193–2222, 2014.

S. Boussetta, G. Balsamo, A. Beljaars, T. Kral, and L. Jarlan. Impact of a satellite-derived leaf area index monthly climatology in a global numerical weather prediction model. *Int. J. Remote Sens.*, 34(9-10):3520–3542, 2013a.

S. Boussetta, G. Balsamo, A. C. M. Beljaars, A.-A. Panareda, J.-C. Calvet, C. Jacobs, B. van den Hurk, P. Viterbo, S. Lafont, E. Dutra, L. Jarlan, M. Balzarolo, D. Papale, and G. van der Werf. Natural land carbon dioxide exchanges in the ECMWF integrated forecasting system: Implementation and offline validation. *J. Geophys. Res. Atmos.*, 118(12):5923–5946, 2013b.

R. H. Brooks and A. T. Corey. Hydraulic properties of porous media and their relation to drainage design. *Transactions of the ASAE*, 7(1):26–0028, 1964.

H. T. Brown and F. Escombe. Researches on some of the Physiological Processes of Green Leaves, with Special Reference to the Interchange of Energy between the Leaf and Its Surroundings, 1905.

J.-C. Calvet. Investigating soil and atmospheric plant water stress using physiological and micrometeorological data. *Agric. For. Meteorol.*, 103(3):229–247, 2000.

J.-C. Calvet, J. Noilhan, J.-L. Roujean, P. Bessemoulin, M. Cabelguenne, A. Olioso, and J.-P. Wigneron. An interactive vegetation SVAT model tested against data from six contrasting sites. *Agric. For. Meteorol.*, 92(2):73–95, 1998.

J.-C. Calvet, V. Rivalland, C. Picon-Cochard, and J. Guehl. Modelling forest transpiration and CO2 fluxes - Response to soil moisture stress. *Agric. For. Meteorol.*, 124(3-4):143–156, 2004.

K. Chan, A. Saltelli, and S. Tarantola. Sensitivity analysis of model output. In *Proc. 29th Conf. Winter Simul. - WSC '97*, pages 261–268, New York, New York, USA, 1997. ACM Press. ISBN 078034278X.

R. Clapp and G. Hornberger. Empirical equations for some soil hydraulic properties. *Water Resour. Res*, 1978.

D. B. Clark, L. M. Mercado, S. Sitch, C. D. Jones, N. Gedney, M. J. Best, M. Pryor, G. G. Rooney, R. L. H. Essery, E. Blyth, O. Boucher, R. J. Harding, C. Huntingford, and P. M. Cox. The Joint UK Land Environment Simulator (JULES), model description Part 2: Carbon fluxes and vegetation dynamics. *Geosci. Model Dev.*, 4(3):701–722, 2011.

G. J. Collatz, J. A. Berry, G. D. Farquhar, and J. Pierce. The relationship between the rubisco reaction mechanism and models of photosynthesis. *Plant, Cell & Environment*, 13(3):219–225, 1990.

G. J. Collatz, J. T. Ball, C. Grivet, and J. Berry. Physiological and environmental regulation of stomatal conductance, photosynthesis and transpiration: a model that includes a laminar boundary layer. *Agric. For. Meteorol.*, 54(2-4):107–136, 1991.

G. J. Collatz, M. Ribas-Carbo, and J. Berry. Coupled Photosynthesis-Stomatal Conductance Model for Leaves of C4 Plants. *Aust. J. Plant Physiol.*, 19(5):519, 1992.

D. Collins and R. Avissar. An Evaluation with the Fourier Amplitude Sensitivity Test (FAST) of Which Land-Surface Parameters Are of Greatest Importance in Atmospheric Modeling. *J. Clim.*, 7:681–703, 1994.

B. J. Cosby, G. M. Hornberger, R. B. Clapp, and T. R. Ginn. A Statistical Exploration of the Relationships of Soil Moisture Characteristics to the Physical Properties of Soils. *Water Resour. Res.*, 20(6):682–690, 1984.

I. R. Cowan and G. D. Farquhar. Stomatal function in relation to leaf metabolism and environment. *Symp. Soc. Exp. Biol.*, 31:471–505, 1977.

P. M. Cox, C. Huntingford, and R. J. Harding. A canopy conductance and photosynthesis model for use in a GCM land surface scheme. *J. Hydrol.*, 212-213:79–94, 1998.

P. M. Cox, R. A. Betts, C. B. Bunton, R. L. H. Essery, P. R. Rowntree, and J. Smith. The impact of new land surface physics on the GCM simulation of climate and climate sensitivity. *Clim. Dyn.*, 15(3):183–203, 1999.

P. M. Cox, R. A. Betts, C. D. Jones, S. A. Spall, and I. J. Totterdell. Acceleration of global warming due to carbon-cycle feedbacks in a coupled climate model. *Nature*, 408 (6809):184–187, 2000.

P. M. Cox, R. Betts, M. Collins, P. Harris, C. Huntingford, and C. Jones. Amazonian forest dieback under climate-carbon cycle projections for the 21st century. *Theoretical and applied climatology*, 78(1-3):137–156, 2004.

P. M. Cox, D. Pearson, B. B. Booth, P. Friedlingstein, C. Huntingford, C. D. Jones, and C. M. Luke. Sensitivity of tropical carbon to climate change constrained by carbon dioxide variability. *Nature*, 494(7437):341–4, 2013.

W. Cramer, A. Bondeau, F. I. Woodward, I. C. Prentice, R. A. Betts, V. Brovkin, P. M. Cox, V. Fisher, J. A. Foley, A. D. Friend, C. Kucharik, M. R. Lomas, N. Ramankutty, S. Sitch, B. Smith, A. White, and C. Young-Molling. Global response of terrestrial ecosystem structure and function to CO2 and climate change: Results from six dynamic global vegetation models. *Glob. Chang. Biol.*, 2001.

R. I. Cukier, C. M. Fortuin, K. E. Shuler, A. G. Petschek, and J. H. Schaibly. Study of the sensitivity of coupled reaction systems to uncertainties in rate coefficients. I Theory. *J. Chem. Phys.*, 1973.

R. I. Cukier, J. H. Schaibly, and K. E. Shuler. Study of the sensitivity of coupled reaction systems to uncertainties in rate coefficients. III. Analysis of the approximations. *J. Chem. Phys.*, 63(3):1140, 1975.

R. I. Cukier, H. B. Levine, and K. E. Shuler. Nonlinear sensitivity analysis of multiparameter model systems. *J. Comput. Phys.*, 26(1):1–42, 1978.

P. S. Curtis, P. J. Hanson, P. Bolstad, C. Barford, J. Randolph, H. Schmid, and K. B. Wilson. Biometric and eddy-covariance based estimates of annual carbon storage in five eastern North American deciduous forests. *Agric. For. Meteorol.*, 113(1-4):3–19, 2002.

M. G. De Kauwe, B. E. Medlyn, S. Zaehle, A. P. Walker, M. C. Dietze, T. Hickler, A. K. Jain, Y. Luo, W. J. Parton, I. C. Prentice, B. Smith, P. E. Thornton, S. Wang, Y.-P. Wang, D. Wårlind, E. Weng, K. Y. Crous, D. S. Ellsworth, P. J. Hanson, H. Seok Kim, J. M. Warren, R. Oren, and R. J. Norby. Forest water use and water use efficiency

at elevated CO2 : a model-data intercomparison at two contrasting temperate forest FACE sites. *Glob. Chang. Biol.*, 19(6):1759–79, 2013.

M. G. De Kauwe, J. Kala, Y.-S. Lin, A. J. Pitman, B. E. Medlyn, R. A. Duursma, G. Abramowitz, Y.-P. Wang, and D. G. Miralles. A test of an optimal stomatal conductance scheme within the CABLE land surface model. *Geosci. Model Dev.*, 8(2):431–452, 2015.

D. G. G. De Pury and G. D. Farquhar. Simple scaling of photosynthesis from leaves to canopies without the errors of big-leaf models. *Plant, Cell Environ.*, 20(5):537–557, 1997.

J. Deardorff. Efficient prediction of ground surface temperature and moisture, with inclusion of a layer of vegetation. *Journal of Geophysical Research: Oceans*, 83(C4): 1889–1903, 1978.

C. V. den Hoof, P. L. Vidale, A. Verhoef, and C. Vincke. Improved evaporative flux partitioning and carbon flux in the land surface model jules: Impact on the simulation of land surface processes in temperate europe. *Agricultural and Forest Meteorology*, 181: 108 – 124, 2013.

J. C. I. Dooge. Sensitivity of Runoff to Climate Change: A Hortonian Approach. *Bull. Am. Meteorol. Soc.*, 73(12):2013–2024, 1992.

E. Dutra, G. Balsamo, P. Viterbo, P. M. Miranda, A. Beljaars, C. Schär, and K. Elder. An improved snow scheme for the ecmwf land surface model: description and offline validation. *Journal of Hydrometeorology*, 11(4):899–916, 2010a.

E. Dutra, V. M. Stepanenko, G. Balsamo, P. Viterbo, P. Miranda, D. Mironov, and C. Schär. An offline study of the impact of lakes in the performance of the ecmwf surface scheme. *Boreal environment research*, 15(2), 2010b.

ECMWF. IFS Documentation. Part IV. Technical report, 2015.

G. Egea, A. Verhoef, and P. L. Vidale. Towards an improved and more flexible representation of water stress in coupled photosynthesis stomatal conductance models. *Agric. For. Meteorol.*, 151(10):1370–1384, 2011.

J. R. Ehleringer, T. E. Cerling, and B. R. Helliker. C4 photosynthesis, atmospheric CO2, and climate. *Oecologia*, 112(3):285–299, 1997.

J. R. Ehleringer, T. E. Cerling, and T. Munn. C3 and C4 Photosynthesis . 2:186–190, 2002.

J. L. Ehman, H. P. Schmid, C. S. B. Grimmond, J. C. Randolph, P. J. Hanson, C. A. Wayson, and F. D. Cropley. An initial intercomparison of micrometeorological and ecological inventory estimates of carbon exchange in a mid-latitude deciduous forest. *Glob. Chang. Biol.*, 8(6):575–589, 2002.

J. R. Evans and S. Von Caemmerer. Carbon Dioxide Diffusion inside Leaves. *Plant Physiol.*, 110(2):339–346, 1996.

E. Falge, D. Baldocchi, R. Olson, P. Anthoni, M. Aubinet, C. Bernhofer, G. Burba, R. Ceulemans, R. Clement, H. Dolman, A. Granier, P. Gross, T. Grünwald, D. Hollinger, N.-O. Jensen, G. Katul, P. Keronen, A. Kowalski, C. T. Lai, B. E. Law, T. Meyers, J. Moncrieff, E. Moors, J. Munger, K. Pilegaard, Ü. Rannik, C. Rebmann, A. Suyker, J. Tenhunen, K. Tu, S. Verma, T. Vesala, K. Wilson, and S. Wofsy. Gap filling strategies for defensible annual sums of net ecosystem exchange. *Agric. For. Meteorol.*, 107(1): 43–69, 2001.

E. Falge, D. Baldocchi, J. Tenhunen, M. Aubinet, P. Bakwin, P. Berbigier, C. Bernhofer, G. Burba, R. Clement, K. J. Davis, J. a. Elbers, A. H. Goldstein, A. Grelle, A. Granier, J. Gumundsson, D. Hollinger, A. S. Kowalski, G. Katul, B. E. Law, Y. Malhi, T. Meyers, R. K. Monson, J. Munger, W. Oechel, K. T. Paw U, K. Pilegaard, Ü. Rannik, C. Rebmann, A. Suyker, R. Valentini, K. Wilson, and S. Wofsy. Seasonality of ecosystem respiration and gross primary production as derived from FLUXNET measurements. *Agric. For. Meteorol.*, 113(1-4):53–74, 2002.

G. D. Farquhar and T. D. Sharkey. Stomatal conductance and photosynthesis. *Annu. Rev. Plant Physiol.*, 1982.

G. D. Farquhar and S. C. Wong. An Empirical Model of Stomatal Conductance. *Aust. J. Plant Physiol.*, 11(3):191, 1984.

G. D. Farquhar, S. von Caemmerer, and J. Berry. A Biochemical Model of Photosynthetic CO2 Assimilation in Leaves of C3 Species. *Planta*, 90:78–90, 1980.

J. Flexas, M. Ribas-Carbo, A. Diaz-Espejo, J. Galmes, and H. Medrano. Mesophyll conductance to co2: current knowledge and future prospects. *Plant, Cell & Environment*, 31(5):602–621, 2008.

H. H. Franssen, R. Stöckli, I. Lehner, E. Rotenberg, and S. Seneviratne. Energy balance closure of eddy-covariance data: A multisite analysis for European FLUXNET stations. *Agric. For. Meteorol.*, 150(12):1553–1567, 2010.

P. Friedlingstein, P. Cox, R. Betts, L. Bopp, W. Von Bloh, V. Brovkin, P. Cadule, S. Doney, M. Eby, I. Fung, G. Bala, J. John, C. Jones, F. Joos, T. Kato, M. Kawamiya, W. Knorr, K. Lindsay, H. D. Matthews, T. Raddatz, P. Rayner, C. Reick, E. Roeckner, K.-G. Schnitzler, R. Schnur, K. Strassmann, A. J. Weaver, C. Yoshikawa, and N. Zeng. ClimateCarbon Cycle Feedback Analysis: Results from the C 4 MIP Model Intercomparison. *J. Clim.*, 19(14):3337–3353, 2006.

A. D. Friend, A. Arneth, N. Y. Kiang, M. Lomas, J. Ogée, C. Rödenbeck, S. W. Running, J.-D. Santaren, S. Sitch, N. Viovy, F. Ian Woodward, and S. Zaehle. FLUXNET and modelling the global carbon cycle. *Glob. Chang. Biol.*, 13(3):610–633, 2007.

N. Gedney, P. Cox, R. Betts, O. Boucher, C. Huntingford, and P. Stott. Detection of a direct carbon dioxide effect in continental river runoff records. *Nature*, 439(7078): 835–838, 2006.

T. G. Gilmanov, S. B. Verma, P. L. Sims, T. P. Meyers, J. A. Bradford, G. G. Burba, and A. E. Suyker. Gross primary production and light response parameters of four Southern Plains ecosystems estimated using long-term CO 2 -flux tower measurements. *Global Biogeochem. Cycles*, 17(2), 2003.

J. Goudriaan. A simple and fast numerical method for the computation of daily totals of crop photosynthesis. *Agric. For. Meteorol.*, 38(1-3):249–254, 1986.

J. Goudriaan, H. Van Laar, H. Van Keulen, and W. Louwerse. Photosynthesis, CO2 and plant production. In *Wheat growth and modelling*, pages 107–122. Springer, 1985.

S. B. Gray, O. Dermody, S. P. Klein, A. M. Locke, J. M. McGrath, R. E. Paul, D. M. Rosenthal, U. M. Ruiz-Vera, M. H. Siebers, R. Strellner, et al. Intensifying drought eliminates the expected benefits of elevated carbon dioxide for soybean. *Nature Plants*, 2:16132, 2016.

P. C. Harley, R. B. Thomas, J. F. Reynolds, and B. R. Strain. Modelling photosynthesis of cotton grown in elevated CO2. *Plant, Cell Environ.*, 15(3):271–282, 1992.

D. Hemming, R. Betts, and M. Collins. Sensitivity and uncertainty of modelled terrestrial net primary productivity to doubled CO2 and associated climate change for a relatively large perturbed physics ensemble. *Agric. For. Meteorol.*, 170:79–88, 2013.

A. Herold. Regulation of photosynthesis by sink activity-The missing link. *New Phytol.*, 86(2):131–144, 1980.

R. E. Horton. Rainfall Interception. *Mon. Weather Rev.*, 47(9):603–623, 1919.

R. E. Horton. The field, scope, and status of the science of hydrology. *Trans. Am. Geophys. Union*, 12(1):189, 1931.

C. Huntingford, P. P. Harris, N. Gedney, P. M. Cox, R. A. Betts, J. A. Marengo, and J. H. C. Gash. Using a GCM analogue model to investigate the potential for Amazonian forest dieback. *Theor. Appl. Climatol.*, 78(1-3):177–185, 2004.

C. M. J. Jacobs. *Direct impact of atmospheric CO2 enrichment on regional transpiration.* PhD thesis, Wageningen Agricultural University, 1994.

C. M. J. Jacobs, B. M. M. van den Hurk, and H. A. R. de Bruin. Stomatal behaviour and photosynthetic rate of unstressed grapevines in semi-arid conditions. *Agric. For. Meteorol.*, 80(2-4):111–134, 1996.

P. G. Jarvis. The interpretation of the variations in leaf water potential and stomatal conductance found in canopies in the field. *Philosophical Transactions of the Royal Society of London B: Biological Sciences*, 273(927):593–610, 1976.

P. G. Jarvis and K. McNaughton. Stomatal Control of Transpiration: Scaling Up from Leaf to Region. *Adv. Ecol. Res.*, 15:1–49, 1986.

D. Jenkinson, S. Andrew, J. Lynch, M. Goss, and P. Tinker. The turnover of organic carbon and nitrogen in soil [and discussion]. *Philosophical Transactions of the Royal Society of London B: Biological Sciences*, 329(1255):361–368, 1990.

V. Jogireedy, P. M. Cox, C. Huntingford, T. J. Harding, and L. M. Mercado. An improved description of canopy light interception for use in a GCM land-surface scheme: calibra-

tion and testing against carbon fluxes at a coniferous forest. *Hadley Cent. Tech. Note*, (63), 2006.

C. Jones, C. McConnell, K. Coleman, P. Cox, P. Falloon, D. Jenkinson, and D. Powlson. Global climate change and soil carbon stocks; predictions from two contrasting models for the turnover of organic carbon in soil. *Glob. Chang. Biol.*, 11(1):154–166, 2005.

C. D. Jones, P. M. Cox, and C. Huntingford. Uncertainty in climatecarboncycle projections associated with the sensitivity of soil respiration to temperature. *Tellus B*, 2003.

H. G. Jones. *Plants and Microclimate: A Quantitative Approach to Environmental Plant Physiology*. Cambridge University Press, 1992. ISBN 1107511631.

M. Jung, M. Reichstein, P. Ciais, S. I. Seneviratne, J. Sheffield, M. L. Goulden, G. Bonan, A. Cescatti, J. Chen, R. de Jeu, A. J. Dolman, W. Eugster, D. Gerten, D. Gianelle, N. Gobron, J. Heinke, J. Kimball, B. E. Law, L. Montagnani, Q. Mu, B. Mueller, K. Oleson, D. Papale, A. D. Richardson, O. Roupsard, S. Running, E. Tomelleri, N. Viovy, U. Weber, C. Williams, E. Wood, S. Zaehle, and K. Zhang. Recent decline in the global land evapotranspiration trend due to limited moisture supply. *Nature*, 467(7318):951–4, 2010.

J. Kattge, S. Diaz, S. Lavorel, I. Prentice, P. Leadley, G. Bönisch, E. Garnier, M. Westoby, P. B. Reich, I. Wright, et al. Try–a global database of plant traits. *Global change biology*, 17(9):2905–2935, 2011.

G. Katul, S. Manzoni, S. Palmroth, and R. Oren. A stomatal optimization theory to describe the effects of atmospheric CO2 on leaf photosynthesis and transpiration. *Ann. Bot.*, 105(3):431–42, 2010.

T. F. Keenan, D. Y. Hollinger, G. Bohrer, D. Dragoni, J. W. Munger, H. P. Schmid, and A. D. Richardson. Increase in forest water-use efficiency as atmospheric carbon dioxide concentrations rise. *Nature*, 499(7458):324–7, 2013.

P. J. Kramer and J. S. Boyer. *Water Relations of Plants and Soils*. 1995. ISBN 0080924115.

H. Lambers, F. S. Chapin, and T. L. Pons. *Plant Physiological Ecology*. Springer, New York, 1998.

C. Le Quéré, R. J. Andres, T. Boden, T. Conway, R. A. Houghton, J. I. House, G. Marland, G. P. Peters, G. R. Van Der Werf, A. Ahlström, R. M. Andrew, L. Bopp, J. G. Canadell, P. Ciais, S. C. Doney, C. Enright, P. Friedlingstein, C. Huntingford, A. K. Jain, C. Jourdain, E. Kato, R. F. Keeling, K. Klein Goldewijk, S. Levis, P. Levy, M. Lomas, B. Poulter, M. R. Raupach, J. Schwinger, S. Sitch, B. D. Stocker, N. Viovy, S. Zaehle, and N. Zeng. The global carbon budget 1959-2011. *Earth Syst. Sci. Data*, 2013.

R. Leuning. Modelling Stomatal Behaviour and and Photosynthesis of Eucalyptus grandis. *Aust. J. Plant Physiol.*, 17(2):159, 1990.

R. Leuning. A critical appraisal of a combined stomatal-photosynthesis model for C3 plants. *unc.edu*, (18):339–355, 1995.

Y.-S. Lin, B. E. Medlyn, R. A. Duursma, I. C. Prentice, H. Wang, S. Baig, D. Eamus, V. R. de Dios, P. Mitchell, D. S. Ellsworth, et al. Optimal stomatal behaviour around the world. *Nature Climate Change*, 5(5):459–464, 2015.

J. Lloyd and J. A. Taylor. On the Temperature Dependence of Soil Respiration. *Funct. Ecol.*, 8(3):315, 1994.

J. Lloyd, S. Wong, J. Styles, D. Batten, R. Priddle, C. Turnbull, and C. Mcconchie. Measuring and Modelling Whole-Tree Gas Exchange. *Aust. J. Plant Physiol.*, 22(6): 987, 1995.

S. Manabe. Climate and the ocean Circulation 1. The atmospheric circulation and the hydrology of the earth's surface. *Mon. Weather Rev.*, 97(11), 1969.

A. Manrique-Suñén, A. Nordbo, G. Balsamo, A. C. M. Beljaars, and I. Mammarella. Representing Land Surface Heterogeneity: Offline Analysis of the Tiling Method. *J. Hydrometeorol.*, 14(3):850–867, 2013.

T. Mansfield, A. Hetherington, and C. Atkinson. Some current aspects of stomatal physiology. *Annual review of plant biology*, 41(1):55–75, 1990.

W. Massman and X. Lee. Eddy covariance flux corrections and uncertainties in long-term studies of carbon and energy exchanges. *Agric. For. Meteorol.*, 113(1-4):121–144, 2002.

C. R. McClung. Plant circadian rhythms. *Plant Cell*, 18(4):792–803, 2006.

A. D. Mcguire, J. M. Melillo, and L. A. Joyce. The Role of Nitrogen in the Response of Forest Net Primary Production to Elevated Atmospheric Carbon Dioxide. *Source Annu. Rev. Ecol. Syst. Annm Rev. Ecol Syst*, 26(26), 1995.

B. E. Medlyn, R. A. Duursma, D. Eamus, D. S. Ellsworth, I. C. Prentice, C. V. M. Barton, K. Y. Crous, P. De Angelis, M. Freeman, and L. Wingate. Reconciling the optimal and empirical approaches to modelling stomatal conductance. *Glob. Chang. Biol.*, 17(6): 2134–2144, 2011.

B. E. Medlyn, R. A. Duursma, M. G. De Kauwe, and I. C. Prentice. The optimal stomatal response to atmospheric CO2 concentration: Alternative solutions, alternative interpretations. *Agric. For. Meteorol.*, 182-183:200–203, 2013.

H. Meidner and j. a. Mansfield, T. A. (Terence Arthur). *Physiology of stomata*. New York : McGraw-Hill, 1968. ISBN 0070940797. Bibliography: p. 160-169.

M. Meinshausen, S. J. Smith, K. Calvin, J. S. Daniel, M. L. T. Kainuma, J.-F. Lamarque, K. Matsumoto, S. A. Montzka, S. C. B. Raper, K. Riahi, A. Thomson, G. J. M. Velders, and D. P. van Vuuren. The RCP greenhouse gas concentrations and their extensions from 1765 to 2300. *Clim. Change*, 109(1-2):213–241, 2011.

L. M. Mercado, C. Huntingford, J. H. C. Gash, P. M. Cox, and V. Jogireddy. Improving the representation of radiation interception and photosynthesis for climate model applications. *Tellus B*, 59(3):553–565, 2007.

L. M. Mercado, N. Bellouin, S. Sitch, O. Boucher, C. Huntingford, M. Wild, and P. M. Cox. Impact of changes in diffuse radiation on the global land carbon sink. *Nature*, 458 (7241):1014–7, 2009.

J. B. Moncrieff, J. Massheder, H. De Bruin, J. Elbers, T. Friborg, B. Heusinkveld, P. Kabat, S. Scott, H. Soegaard, and A. Verhoef. A system to measure surface fluxes of momentum, sensible heat, water vapour and carbon dioxide. *Journal of Hydrology*, 188: 589–611, 1997.

M. Monsi and T. Saeki. On the factor light in plant communities and its importance for matter production. 1953. *Ann. Bot.*, 95(3):549–67, 2005.

J. I. L. Morison. Stomatal response to increased CO2 concentration. *J. Exp. Bot.*, 49 (Special):443–452, 1998.

K. A. Mott. Do Stomata Respond to CO2 Concentrations Other than Intercellular? *Plant Physiol.*, 86(1):200–203, 1988.

K. A. Mott and D. F. Parkhurst. Stomatal responses to humidity in air and helox. *Plant, Cell Environ.*, 14(5):509–515, 1991.

R. R. Nemani, C. D. Keeling, H. Hashimoto, W. M. Jolly, S. C. Piper, C. J. Tucker, R. B. Myneni, and S. W. Running. Climate-driven increases in global terrestrial net primary production from 1982 to 1999. *Science*, 300(5625):1560–3, 2003.

R. Orth, E. Dutra, and F. Pappenberger. Improving Weather Predictability by Including Land Surface Model Parameter Uncertainty. *Mon. Weather Rev.*, 144(4):1551–1569, 2016.

T. Osborne, J. Gornall, J. Hooker, K. Williams, A. Wiltshire, R. Betts, and T. Wheeler. Jules-crop: a parametrisation of crops in the joint uk land environment simulator. *Geoscientific Model Development*, 8(4):1139–1155, April 2015.

R. Pavlick, D. T. Drewry, K. Bohn, B. Reu, and A. Kleidon. The jena diversity-dynamic global vegetation model (jedi-dgvm): a diverse approach to representing terrestrial biogeography and biogeochemistry based on plant functional trade-offs. *Biogeosciences*, 10: 4137–4177, 2013.

I. C. Prentice, N. Dong, S. M. Gleason, V. Maire, and I. J. Wright. Balancing the costs of carbon gain and water transport: testing a new theoretical framework for plant functional ecology. *Ecol. Lett.*, 17(1):82–91, 2014.

S. Rahman, M. Khallat, and Z. Salameh. Characterization of insolation data for use in photovoltaic system analysis models. *Energy*, 13(1):63–72, 1988.

R. Raj, N. A. S. Hamm, C. van der Tol, and A. Stein. Variance-based sensitivity analysis of BIOME-BGC for gross and net primary production. *Ecol. Modell.*, 292:26–36, 2014.

M. Reichstein, E. Falge, D. Baldocchi, D. Papale, M. Aubinet, P. Berbigier, C. Bernhofer, N. Buchmann, T. Gilmanov, A. Granier, T. Grunwald, K. Havrankova, H. Ilvesniemi, D. Janous, A. Knohl, T. Laurila, A. Lohila, D. Loustau, G. Matteucci, T. Meyers, F. Miglietta, J.-M. Ourcival, J. Pumpanen, S. Rambal, E. Rotenberg, M. Sanz, J. Tenhunen, G. Seufert, F. Vaccari, T. Vesala, D. Yakir, and R. Valentini. On the separation

of net ecosystem exchange into assimilation and ecosystem respiration: review and improved algorithm. *Glob. Chang. Biol.*, 11(9):1424–1439, 2005.

L. A. Richards. Capillary conduction of liquids through porous mediums. *Physics (College. Park. Md).*, 1(5):318, 1931.

L. F. Richardson. *Weather Prediction by Numerical Process*. Cambridge University Press, 2007. ISBN 0521680441.

E. Rodríguez-Camino and R. Avissar. Comparison of three land-surface schemes with the Fourier amplitude sensitivity test (FAST), 1998.

R. J. Ronda, H. A. R. de Bruin, and A. A. M. Holtslag. Representation of the Canopy Conductance in Modeling the Surface Energy Budget for Low Vegetation. *J. Appl. Meteorol.*, 40(8):1431–1444, 2001.

J.-L. Roujean. A tractable physical model of shortwave radiation interception by vegetative canopies. *J. Geophys. Res.*, 101(D5):9523, 1996.

S. Running, D. Baldocchi, D. Turner, S. Gower, P. Bakwin, and K. Hibbard. A Global Terrestrial Monitoring Network Integrating Tower Fluxes, Flask Sampling, Ecosystem Modeling and EOS Satellite Data. *Remote Sens. Environ.*, 70(1):108–127, 1999.

N. Sade, B. J. Vinocur, A. Diber, A. Shatil, G. Ronen, H. Nissan, R. Wallach, H. Karchi, and M. Moshelion. Improving plant stress tolerance and yield production: is the tonoplast aquaporin SlTIP2;2 a key to isohydric to anisohydric conversion? *New Phytol.*, 181(3):651–61, 2009.

N. Sade, A. Gebremedhin, and M. Moshelion. Risk-taking plants: anisohydric behavior as a stress-resistance trait. *Plant signaling & behavior*, 7(7):767–770, 2012.

R. F. Sage, T. D. Sharkey, and J. R. Seemann. Regulation of Ribulose-1,5-Bisphosphate Carboxylase Activity in Response to Light Intensity and CO2 in the C3 Annuals Chenopodium album L. and Phaseolus vulgaris L.'. *Plant Physiol*, 94:1735–1742, 1990.

A. Saltelli and R. Bolado. An alternative way to compute Fourier amplitude sensitivity test (FAST). *Comput. Stat. Data Anal.*, 26:445–460, 1998.

A. Saltelli, S. Tarantola, and .-S. Chan. A Quantitative Model-Independent Method for Global Sensitivity Analysis of Model Output. *Technometrics*, 41(1):39–56, 1999.

A. Saltelli, M. Ratto, S. Tarantola, and F. Campolongo. Sensitivity analysis practices: Strategies for model-based inference, 2006.

M. Saurer, R. T. Siegwolf, and F. H. Schweingruber. Carbon isotope discrimination indicates improving water-use efficiency of trees in northern eurasia over the last 100 years. *Global Change Biology*, 10(12):2109–2120, 2004.

C. B. Schaaf, F. Gao, A. H. Strahler, W. Lucht, X. Li, T. Tsang, N. C. Strugnell, X. Zhang, Y. Jin, J.-P. Muller, P. Lewis, M. Barnsley, P. Hobson, M. Disney, G. Roberts, M. Dunderdale, C. Doll, R. P. D'Entremont, B. Hu, S. Liang, J. L. Privette, and D. Roy. First operational BRDF, albedo nadir reflectance products from MODIS. *Remote Sens. Environ.*, 83(1):135–148, 2002.

H. Schmid. Source areas for scalars and scalar fluxes. *Boundary-Layer Meteorol.*, 1994.

H. R. Schultz. Differences in hydraulic architecture account for near-isohydric and anisohydric behaviour of two field-grown Vitis vinifera L. cultivars during drought. *Plant, Cell Environ.*, 26(8):1393–1405, 2003.

P. J. Sellers and L. Bounoua. Comparison of radiative and physiological effects of doubled atmospheric CO2 on climate. *SCIENCE-NEW YORK THEN WASHINGTON-*, 1996.

P. J. Sellers, J. A. Berry, G. J. Collatz, C. B. Field, F. Hall, and E. G. Hall. Canopy reflectance, photosynthesis, and transpiration. III. A reanalysis using improved leaf models and a new canopy integration scheme. *Remote Sens. Environ.*, 42(3):187–216, 1992.

P. J. Sellers, D. A. Randall, G. J. Collatz, J. A. Berry, C. B. Field, D. A. Dazlich, C. Zhang, G. D. Collelo, and L. Bounoua. A Revised Land Surface Parameterization (SiB2) for Atmospheric GCMS. Part I: Model Formulation. *J. Clim.*, 9(4):676–705, 1996.

T. D. Sharkey. Photosynthesis in Intact Leaves of C3 Plants: Physics, Physiology and Rate Limitations. *Bot. Rev.*, 1985.

T. D. Sharkey, C. J. Bernacchi, G. D. Farquhar, and E. L. Singsaas. Fitting photosynthetic carbon dioxide response curves for C3 leaves. *Plant. Cell Environ.*, 30(9):1035–40, 2007.

I. Sobol'. Global sensitivity indices for nonlinear mathematical models and their Monte Carlo estimates. *Math. Comput. Simul.*, 2001.

G. J. Steeneveld. On photosynthesis parameters for the A-gs surface scheme for high vegetation. (March):1–79, 2002.

T. Stocker, D. Qin, G. Plattner, M. Tignor, S. Allen, A. Boschung, Y. X. Nauels, V. B. (eds.), and P. Midgley. *IPCC, 2013: Climate change 2013: The physical science basis. Contribution of Working Group I to the Fith Assesment Report of the Intergovernmental Panel on Climate Change*. Cambridge University Press, Cambridge, United Kingdom and New York, NY, USA, 2013.

M. Sulaiman, W. Oo, M. Wahab, and A. Zakaria. Application of beta distribution model to Malaysian sunshine data. *Renew. energy*, 1999.

F. Tardieu, J. Zhang, N. Katerji, O. Bethenod, S. Palmer, and W. J. Davies. Xylem ABA controls the stomatal conductance of field-grown maize subjected to soil compaction or soil drying. *Plant, Cell Environ.*, 15(2):193–197, 1992.

F. Tardieu, B. Parent, C. F. Caldeira, and C. Welcker. Genetic and physiological controls of growth under water deficit. *Plant Physiol.*, 164(4):1628–35, 2014.

M. Van Genuchten. A closed-form equation for predicting the hydraulic conductivity of unsaturated soils. *Soil Sci. Soc. Am. J.*, 1980.

A. Verhoef and S. Allen. A svat scheme describing energy and co 2 fluxes for multi-component vegetation: calibration and test for a sahelian savannah. *Ecological Modelling*, 127(2):245–267, 2000.

A. Verhoef and G. Egea. Modeling plant transpiration under limited soil water: Comparison of different plant and soil hydraulic parameterizations and preliminary implications for their use in land surface models. *Agric. For. Meteorol.*, 191:22–32, 2014.

J. Verrelst, J. P. Rivera, C. Van Der Tol, F. Magnani, G. Mohammed, and J. Moreno. Global sensitivity analysis of the SCOPE model: What drives simulated canopy-leaving sun-induced fluorescence? *Remote Sens. Environ.*, 166:8–21, 2015.

P. Viterbo. A review of parametrization schemes for land surface processes. In *Train. Course Lect. Ser. ECMWF*, pages 1–49. 2002.

P. Viterbo and A. C. M. Beljaars. An Improved Land Surface Parameterization Scheme in the ECMWF Model and Its Validation. *J. Clim.*, 8(11):2716–2748, 1995.

P. Viterbo, A. C. M. Beljaars, J.-F. Mahfouf, and J. Teixeira. The representation of soil moisture freezing and its impact on the stable boundary layer. *Quarterly Journal of the Royal Meteorological Society*, 125(559):2401–2426, 1999.

S. Von Caemmerer. *Biochemical models of leaf photosynthesis*. Csiro publishing, 2000. ISBN 064306379X.

K. Wilson, A. Goldstein, E. Falge, M. Aubinet, D. Baldocchi, P. Berbigier, C. Bernhofer, R. Ceulemans, H. Dolman, C. Field, A. Grelle, A. Ibrom, B. Law, A. Kowalski, T. Meyers, J. Moncrieff, R. Monson, W. Oechel, J. Tenhunen, R. Valentini, and S. Verma. Energy balance closure at FLUXNET sites. *Agric. For. Meteorol.*, 113(1-4):223–243, 2002.

S. C. Wong, I. R. Cowan, and G. D. Farquhar. Leaf Conductance in Relation to Assimilation in Eucalyptus pauciflora Sieb. ex Spreng: Influence of Irradiance and Partial Pressure of Carbon Dioxide. *Plant Physiol.*, 62(4):670–674, 1978.

S. C. Wong, I. R. Cowan, and G. D. Farquhar. Stomatal conductance correlates with photosynthetic capacity. *Nature*, 282(5737):424–426, 1979.

J. Wösten, A. Lilly, A. Nemes, and C. Le Bas. Development and use of a database of hydraulic properties of european soils. *Geoderma*, 90(3):169–185, 1999.

W. Yamori, K. Noguchi, and I. Terashima. Temperature acclimation of photosynthesis in spinach leaves: analyses of photosynthetic components and temperature dependencies of photosynthetic partial reactions. *Plant, Cell Environ.*, 28(4):536–547, 2005.

S. Zaehle, P. Friedlingstein, and A. D. Friend. Terrestrial nitrogen feedbacks may accelerate future climate change. *Geophysical Research Letters*, 37(1), 2010.

M. Zhao and S. W. Running. Drought-induced reduction in global terrestrial net primary production from 2000 through 2009. *science*, 329(5994):940–943, 2010.